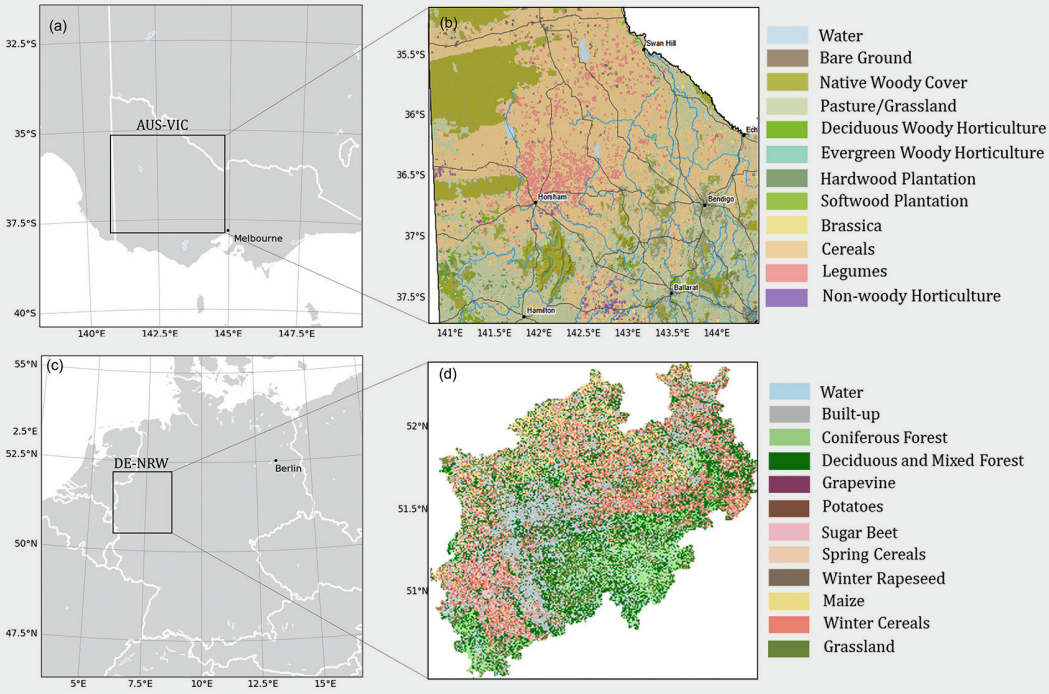

Advancing the representation of agricultural systems in Land Surface Models: systematic model evaluations and technical model developments

Theresa Sophie Boas

Energie & Umwelt / Energy & Environment
Band / Volume 640
ISBN 978-3-95806-777-6

Mitglied der Helmholtz-Gemeinschaft

JÜLICH
Forschungszentrum

Schriften des Forschungszentrums Jülich
Reihe Energie & Umwelt / Energy & Environment Band / Volume 640

Forschungszentrum Jülich GmbH
Institut für Bio- und Geowissenschaften (IBG)
Agrosphäre (IBG-3)

Advancing the representation of agricultural systems in Land Surface Models: systematic model evaluations and technical model developments

Theresa Sophie Boas

Schriften des Forschungszentrums Jülich
Reihe Energie & Umwelt / Energy & Environment Band / Volume 640

ISSN 1866-1793 ISBN 978-3-95806-777-6

Bibliografische Information der Deutschen Nationalbibliothek.
Die Deutsche Nationalbibliothek verzeichnet diese Publikation in der
Deutschen Nationalbibliografie; detaillierte Bibliografische Daten
sind im Internet über http://dnb.d-nb.de abrufbar.

Herausgeber und Vertrieb:	Forschungszentrum Jülich GmbH Zentralbibliothek, Verlag 52425 Jülich Tel.: +49 2461 61-5368 Fax: +49 2461 61-6103 zb-publikation@fz-juelich.de www.fz-juelich.de/zb
Umschlaggestaltung:	Grafische Medien, Forschungszentrum Jülich GmbH
Druck:	Grafische Medien, Forschungszentrum Jülich GmbH
Copyright:	Forschungszentrum Jülich 2024

Schriften des Forschungszentrums Jülich
Reihe Energie & Umwelt / Energy & Environment, Band / Volume 640

D 82 (Diss. RWTH Aachen University, 2024)

ISSN 1866-1793
ISBN 978-3-95806-777-6

Vollständig frei verfügbar über das Publikationsportal des Forschungszentrums Jülich (JuSER)
unter www.fz-juelich.de/zb/openaccess.

Abstract

Global climate change, with its projected increase in weather extremes and drought risk, presents global and regional agriculture with vulnerability and new challenges. It is crucial to gain a comprehensive understanding and accurate quantification of the intricate dynamics of agricultural land cover and its role within the terrestrial system, especially in the context of climate change. Land surface models play a central role for the research on climate change effects on the Earth's surface and hold particular value in examining the influence of weather patterns on agricultural land at larger spatial scales. The incorporation of a comprehensive crop module in land surface models offers the possibility to study the effect of agricultural land use and land management changes on the terrestrial water, energy and biogeochemical cycles. It may help to improve the simulation of biogeophysical and biogeochemical processes on regional and global scales and thus to study climate change impacts on terrestrial ecosystem as well as the significance of human land cover changes for climate change. Land surface models simulate the complex interactions at the terrestrial land surface in response to atmospheric states, based on land cover and soil type information. In combination with data from different sources, like seasonal weather forecasts, land surface models can potentially provide useful information for water resources or agricultural planning.

In this thesis, a systematic evaluation of the state-of-the-art land surface model, the Community Land Model version 5.0 (CLM5), was conducted from point to regional scales in combination with data from a multitude of sources, e.g. from remote sensing, numerical predictions and field observations. A special focus was placed on the representation of arable land and its feedback to weather related factors in the context of climate change.

In the first part of this thesis, the performance of the crop module of CLM5 was evaluated at point scale with site specific field data focussing on the simulation of seasonal and inter-annual variations in crop growth, planting and harvesting cycles, and crop yields as well as water, energy and carbon fluxes. In order to better represent agricultural sites, the model was modified by (1) implementing the winter wheat subroutines after Lu et al. (2017) in CLM5; (2) implementing plant specific parameters for sugar beet, potatoes and winter wheat, thereby adding the two crop functional types (CFT) for sugar beet and potatoes to the list of actively managed crops in CLM5; (3) introducing a cover cropping subroutine that allows multiple crop types on the same column within one year. The latter modification allows the simulation of cropping during winter months before usual cash crop planting begins in spring, which is an agricultural management technique with a long history that is regaining popularity to reduce erosion, improve soil health and carbon storage, and is commonly used in the regions evaluated in this study. In comparison with field data, the crop specific parameterizations, as well as the winter wheat subroutines, led to a significant simulation improvement in terms of energy fluxes (RMSE reduction for latent and sensible heat by up to 57 % and 59 %, respectively), leaf area index (LAI), net ecosystem exchange and crop yield (up to 87 % improvement in winter wheat yield prediction) compared with default model results. The cover cropping subroutine yielded a substantial improvement in representing field conditions after harvest of the main cash crop (winter season) in terms of LAI magnitudes and seasonal cycle of LAI, and latent heat flux (reduction of winter time RMSE for latent heat flux by 42 %). Our modifications significantly improved model simulations and should therefore be applied in future studies with CLM5 to improve regional yield predictions and to better understand large-scale impacts of agricultural management on carbon, water and energy fluxes.

These model improvements were then ported to the regional scale and tested in combination with sub-seasonal and seasonal weather forecasts in the second part of this thesis. Long-range weather forecasts provide predictions of atmospheric, ocean and land surface conditions that can potentially be used in land surface and hydrological models to predict the water and energy status of the land surface or in crop growth models to predict yield for water resources or agricultural planning. However, the coarse spatial and temporal resolutions of available forecast products have hindered their widespread use in such modelling applications, which usually require high-resolution input data. In this study, we applied sub-seasonal (up to 4 months) and seasonal (7 months) weather forecasts from the latest European Centre for Medium-Range Weather Forecasts (ECMWF) seasonal forecasting system (SEAS5) in a land surface modelling approach using the Community Land Model version 5.0 (CLM5). Simulations were conducted for 2017-2020 forced with sub-seasonal and seasonal weather forecasts over two different domains with contrasting climate and cropping conditions: the German state of North Rhine-Westphalia (DE-NRW) and the Australian state of Victoria (AUS-VIC). We found that, after pre-processing of the forecast products (i.e. temporal downscaling of precipitation and incoming short-wave radiation), the simulations forced with seasonal and sub-seasonal forecasts were able to provide a model output that was very close to the reference simulation results forced by reanalysis data (the mean annual crop yield showed maximum differences of 0.28 and 0.36 t/ha for AUS-VIC and DE-NRW, respectively). Differences between seasonal and sub-seasonal experiments were insignificant. The forecast experiments were able to satisfactorily capture recorded inter-annual variations of crop yield. In

addition, they also reproduced the generally higher inter-annual differences in crop yield across the AUS-VIC domain (approximately 50 % inter-annual differences in recorded yields and up to 17 % inter-annual differences in simulated yields) compared to the DE-NRW domain (approximately 15 % inter-annual differences in recorded yields and up to 5 % in simulated yields). The high- and low-yield seasons (2020 and 2018) among the 4 simulated years were clearly reproduced in the forecast simulation results. Furthermore, sub-seasonal and seasonal simulations reflected the early harvest in the drought year of 2018 in the DE-NRW domain. However, simulated inter-annual yield variability was lower in all simulations compared to the official statistics. While general soil moisture trends, such as the European drought in 2018, were captured by the seasonal experiments, we found systematic overestimations and underestimations in both the forecast and reference simulations compared to the Soil Moisture Active Passive Level-3 soil moisture product (SMAP L3) and the Soil Moisture Climate Change Initiative Combined dataset from the European Space Agency (ESA-CCI). These observed biases of soil moisture and the low inter-annual differences in simulated crop yield indicate the need to improve the representation of these variables in CLM5 to increase the model sensitivity to drought stress and other crop stressors.

While extensive research is dedicated to investigating the impacts of changing climate conditions on global food security, the specific implications for regional inter-annual yield variability remain largely uncertain. In the final part of this thesis, the model's ability to represent the inter-annual variability of crop yield in comparison to recorded yield variability was evaluated in multi-decadal simulations (1999-2019) that were forced with the WFDE5 reanalysis. Additionally, synthetic experiments were performed for both regional domains, AUS-VIC and DE-NRW, and forced with a reduced precipitation rate (50% of the reanalysis precipitation), allowing for a more detailed analysis of crop water stress regimes and correlations between seasonal rainfall and crop yields. Overall, the simulation results were able to reproduce the total annual crop yields of certain crops, with RMSE values between 0.52 t/ha to 1.76 t/ha in AUS-VIC and 0.61 t/ha and 1.58 t/ha in DE-NRW, while also capturing the differences in total yield magnitudes between the domains. However, the simulations showed limitations in correctly capturing inter-annual differences of crop yield compared to official yield records, in particular for winter crops, which resulted in relatively low correlations (maximum correlation coefficients of 0.39 in AUS-VIC and 0.42 in DE-NRW). Specifically, the mean absolute anomaly of simulated winter wheat yields was up to 4.6 times lower compared to state-wide records from 1999 to 2019. Our results suggest the following limitations of CLM5 in predicting inter-annual variability in crop yields: (1) limitations in simulating yield responses from plant hydraulic stress; (2) errors in simulating soil moisture contents compared to satellite-derived data; and (3) errors in the representation of cropland in general, e.g. crop parameterizations, differentiations of crop varieties, and human influences (such as management decisions, fertilizer types, and application techniques).

Zusammenfassung

Der globale Klimawandel stellt die Landwirtschaft auf globaler und regionaler Ebene vor neue Herausforderungen. Insbesondere die prognostizierte Zunahme extremer Wetterbedingungen wie Dürren, Überflutungen, Unwetter und Veränderungen der Saisonalität sind Risikofaktoren, deren Auswirkungen sorgfältig untersucht und quantifiziert werden müssen. Diese Untersuchungen sind von großer Bedeutung, um effektive Anpassungsstrategien entwickeln und die Sicherheit in der Landwirtschaft zu gewährleisten zu können. Während die allgemeinen Auswirkungen des Klimawandels auf die globale Ernährungssicherheit ein viel erforschtes Thema sind, bleiben die Implikationen für saisonale Ertragsschwankung auf regionaler Ebene noch weitgehend nicht quantifiziert.

Landoberflächenmodelle spielen eine zentrale Rolle in der Erforschung der Auswirkungen des Klimawandels auf die Erdoberfläche. Sie berücksichtigen komplexe Wechselwirkungen an der Erdoberfläche in Reaktion auf atmosphärische Bedingungen und können in Kombination mit saisonalen Wettervorhersagen wertvolle Informationen für Risikoabschätzungen (Dürren und Überflutungen), den Wasserhaushalt und die landwirtschaftliche Planung liefern. Um die Auswirkungen der landwirtschaftlichen Landnutzung auf den Wasserkreislauf, den Energiehaushalt und die biogeochemischen Kreisläufe besser zu verstehen, ist die Integration eines umfassenden Pflanzenmoduls in Landoberflächenmodelle von großer Bedeutung. Dies ermöglicht eine verbesserte Simulation biogeophysikalischer und biogeochemischer Prozesse auf regionaler und globaler Ebene und unterstützt die Erforschung der Wechselwirkungen zwischen Klimawandel und landwirtschaftlich genutzten Flächen.

Im Rahmen dieser Doktorarbeit wurde eine systematische Analyse des Landoberflächenmodells Community Land Model Version 5.0 (CLM5) auf lokaler und regionaler Skala durchgeführt. Hierzu wurden Daten aus einer Vielzahl von Quellen, wie Fernerkundung, numerischen Vorhersagen und Feldmessungen verwendet. Ein besonderer Analyseschwerpunkt lag hierbei auf der Darstellung von Ackerland und dessen Wechselwirkung mit wetterbedingten Faktoren im Kontext des Klimawandels.

Im ersten Teil dieser Doktorarbeit wurde die Modell-Performance des neuen Pflanzenmoduls von CLM5 für mehrere Europäische Ackerstandorte mit langen Zeitreihen standortspezifischer und hochaufgelöster Messdaten getestet, angepasst und bewertet. Dabei lag der Fokus auf der Simulation des Pflanzenwachstums und der Ernteerträge spezifischer Nutzpflanzen, sowie der Darstellung von Wasser-, Energie- und Kohlenstoffflüssen. Um landwirtschaftliche Standorte besser abbilden zu können, wurde das Modell durch folgende Änderungen angepasst: (1) Die Ergänzung des Modellcodes durch Algorithmen zur Darstellung von Wintergetreide (unter anderem die Prozesse der Vernalisation, Temperaturresistenz und frostbedingter Schädigungen der Pflanze) basierend auf Lu et al. (2017); (2) die Implementierung von pflanzenspezifischen Parametern für Zuckerrüben, Kartoffeln und Winterweizen (hierbei wurden zwei neue Nutzpflanzen in die Liste der aktiv bewirtschafteten Kulturen in CLM5 aufgenommen) und (3), die Einführung eines neuen Algorithmus für Zwischenfruchtanbau und Fruchtwechsel. Die letzte Modifikation erlaubt die Simulation von Deckfrüchten, die typischerweise zwischen den Vegetationsperioden der Ertragspflanzen während der Wintermonate oder auf länger brachliegenden Feldern angebaut werden. Diese landwirtschaftliche Technik wird häufig in der regenerativen Landwirtschaft genutzt, um Erosion zu reduzieren und die Bodengesundheit sowie Kohlenstoffspeicherung zu verbessern.

Der Vergleich der Simulationsergebnisse mit detaillierten Felddaten ergab, dass sowohl die neuen pflanzenspezifischen Parametrisierungen als auch die Berücksichtigung der wesentlichen phenologischen Prozesse von Winterweizen zu einer signifikanten Verbesserung der Simulationen führten. Verbesserungen ergaben sich bei der Simulation der Energieflüsse auf der Landoberfläche (Reduktion des RMSE für latente und sensible Wärme um bis zu 57 % bzw. 59 %), des Blattflächenindex, des Nettoökosystemaustausches und der Ernteerträge (bis zu 87 % Verbesserung bei der Vorhersage des Winterweizenertrags) im Vergleich zu den Standardeinstellungen des Modells. Zudem führten die technischen Veränderungen des Modellcodes zu einer erheblich verbesserten Darstellung der Feldbedingungen nach der Haupternte, sowohl in Bezug auf den saisonalen Verlauf des Blattflächenindex, als auch auf die Energieflüsse während der Wintermonate (Reduktion des RMSE für latente Wärme um 42 %). Insgesamt haben die Modifikationen die Modellsimulationen signifikant verbessert und sollten in zukünftige Studien mit CLM5 eingebunden werden, um regionale Ernteertragsvorhersagen zu verbessern und die Auswirkungen des landwirtschaftlichen Managements auf Kohlenstoff-, Wasser- und Energieflüsse im großen Maßstab besser untersuchen zu können.

Im zweiten Teil der Doktorarbeit wurden die Modellverbesserungen auf regionaler Skala angewandt. Das Modell wurde für zwei verschiedene landwirtschaftliche Regionen in Kombination mit den aktuellsten saisonalen Wettervorhersagen des European Centre for Medium-Range Weather Forecasts (ECMWF) getestet. Saisonale

Wettervorhersagen bergen ein großes Potenzial für regionale landwirtschaftliche Planung und Entscheidungsfindung, insbesondere in Verbindung mit weiteren Modellanwendungen, die relevante Informationen zu Ernteerträgen bestimmter Feldfrüchte liefern können. Trotz des großen Potenzials saisonaler Vorhersagen werden sie in der Praxis noch nicht weitreichend von Endverbrauchern genutzt. Dies ist hauptsächlich auf unzureichende Daten und das Fehlen benutzerfreundlicher Tools zur Verarbeitung der Rohdaten zurückzuführen. Diese Studie bietet einen ersten Einblick in die Anwendung saisonaler Vorhersageprodukte in der numerischen Modellierung. Simulationen mit saisonalen Wettervorhersagen und einem Referenzdatensatz aus Reanalyse-Wetterdaten wurden für die Anbausaisons (April - Oktober) der Jahre 2017 - 2020 und für zwei Modellgebiete mit unterschiedlichen Klima- und Anbaubedingungen durchgeführt: Ein Modellgebiet, welches das gesamte deutsche Bundesland Nordrhein-Westfalen (DE-NRW) umfasst und ein weiteres, welches sich über große Teile des australischen Bundesstaates Victoria (AUS-VIC) erstreckt. Nach einer umfassenden Aufbereitung der Vorhersagedaten (räumliche Skalierung aller Variablen, sowie zeitliche Skalierung von Niederschlag und einfallender kurzwelliger Strahlung) konnten die Simulationen mit den saisonalen Vorhersagen Ergebnisse erzielen, die sehr nah an denen der Referenzsimulationen lagen. Der mittlere jährliche Ernteertrag zeigte eine maximale Differenz von 0,28 t/ha für AUS-VIC und 0,36 t/ha für DE-NRW zwischen den Modellergebnissen mit saisonalen Vorhersagen und Reanalyse-Wetterdaten. Interessanterweise konnten die Simulationen mit saisonalen Wettervorhersagen die generell höhere interjährliche Ertragsvariabilität in AUS-VIC (ca. 50 % zwischenjährliche Variabilität in offiziellen Aufzeichnungen und bis zu 17 % in den Simulationsergebnissen) im Vergleich zu DE-NRW (mit ca. 15 % zwischenjährliche Variabilität in offiziellen Aufzeichnungen und bis zu 5 % in den simulierten Erträgen) erfassen. Die relativen Hoch- und Niedrigertragsjahre 2020 und 2018 spiegeln sich in den Simulationsergebnissen deutlich wider. Insbesondere die frühe Ernte im Dürrejahr 2018 im deutschen Gebiet konnte mit dem Modell in Verbindung mit saisonalen Wettervorhersagen prognostiziert werden. Während der allgemeine Entwicklungstrend der Bodenfeuchtigkeit, wie beispielsweise die europäische Dürre im Jahr 2018, von den saisonalen Experimenten erfasst wurden, wurden systematische Über- und Unterschätzungen der Bodenfeuchte im Vergleich zu Satelliten-Daten, dem Soil Moisture Active Passive Level-3 Bodenfeuchteprodukt (SMAP L3) und dem Soil Moisture Climate Change Initiative Combined Datensatz der European Space Agency (ESA-CCI), festgestellt. Obwohl das Modell insgesamt dazu in der Lage war die zwischenjährlichen Variationen der Produktivität anzudeuten, waren die Unterschiede zwischen den Jahren quantitativ deutlich geringer als in den offiziellen Erntestatistiken. Dies war sowohl bei den Simulationen mit saisonalen Vorhersagen, als auch bei den Referenzsimulationen der Fall. Insgesamt weisen diese Abweichungen auf die Notwendigkeit hin, die Darstellung dieser Variablen in CLM5 zu verbessern, um die Modellempfindlichkeit gegenüber Trockenstress und anderen Stressfaktoren für Pflanzen zu erhöhen.

Auf diesen Erkenntnissen aufbauend wurden im dritten Teil der Doktorarbeit langjährige Simulationen, von 1999 bis 2019, mit meteorologischen Reanalyse-Wetterdaten für die gleichen Modellregionen durchgeführt. Hierbei wurde insbesondere die Leistung des Modells in Bezug auf die Simulation der jährlichen Ertragsschwankungen regionaler Feldfrüchte sowie die Auswirkungen von Wettertrends auf die simulierten Vegetationsproduktivität analysiert. Um systematische Ungenauigkeiten in den Simulationen bei der Darstellung der Ertragsvariabilität zu identifizieren, wurde der simulierte Ertrag mit der offiziellen Erntestatistiken der jeweiligen Regionen verglichen. Zusätzlich wurde untersucht, welche Variablen (z. B. Temperatur, Niederschlag, Bodenfeuchtegehalt) hauptsächlich für Veränderungen in der von CLM5 vorhergesagten Ertragsvariabilität verantwortlich sind. Darüber hinaus wurden synthetische Experimente durchgeführt, bei denen die Niederschlagsrate um 50% reduziert wurde, um die Beziehung zwischen simuliertem Ertrag und simulierten Bodenfeuchtegehalten genauer bewerten zu können.

Insgesamt waren die Simulationsergebnisse in der Lage, die Gesamterträge bestimmter Kulturen zu reproduzieren, zeigten jedoch Einschränkungen bei der korrekten Erfassung der jährlichen Unterschiede im Ertrag, insbesondere bei Winterkulturen. Die mittlere interjährliche absolute Abweichung der simulierten Winterweizenerträge war 4,6-mal niedriger im Vergleich zu den offiziellen Erntestatistiken von 1999 bis 2019. Die Analyseergebnisse der Studie deuteten auf eine unzureichende Modellsensitivität gegenüber Trockenstress hin. Mögliche Ursachen für die Ungenauigkeiten bei den Ertragssimulationen und ihrer interjährlichen Variabilität konnten im Rahmen dieser Studie diskutiert werden: (1) ein Mangel an Sensitivität gegenüber Trockenstress und bei der Darstellung der Pflanzenhydraulik; (2) Ungenauigkeiten bei der Simulation des Bodenfeuchteregimes im Vergleich zu satellitengestützten Daten; und (3) ein fehlendes Einbeziehen weitere wichtiger Faktoren, die interjährliche Ernteertragsschwankungen beeinflussen können, wie menschliche Einflüsse (z. B. Managemententscheidungen, Düngertypen und Anwendungstechniken), weitere Umweltfaktoren (z.B. Krankheiten, Schädlingsbefall, Überflutungen) sowie Ungenauigkeiten in der Parametrisierung der entsprechenden Nutzpflanzen.

Declaration

I declare that this thesis comprises only my original work towards the degree of Doctor of Philosophy / Doctor rerum naturalium. Due acknowledgement has been made in the text to all other material used. The thesis is less than 100,000 words in length, exclusive of tables, bibliographies and appendices.

Theresa Sophie Boas

Eidestattliche Erklärung

Ich erkläre hiermit eidesstattlich, dass ich die Dissertation selbstständig verfasst, alle in Anspruch genommenen Hilfen in der Dissertation angegeben habe und die schriftliche und elektronische Fassung übereinstimmen. Des Weiteren erkläre ich, dass durch die Veröffentlichung meiner Dissertation keine Betriebsgeheimnisse oder Patente der Forschungszentrum Jülich GmbH verletzt werden.

Theresa Sophie Boas

Preface

This thesis is based on several peer-reviewed publications that are listed below in the actual publication status.

Boas, T., Bogena, H., Grünwald, T., Heinesch, B., Ryu, D., Schmidt, M., Vereecken, H., Western, A., and Hendricks Franssen, H.-J.: Improving the representation of cropland sites in the Community Land Model (CLM) version 5.0, Geosci. Model Dev., 14, 573–601, https://doi.org/10.5194/gmd-14-573-2021, 2021.

Boas, T., Bogena, H. R., Ryu, D., Vereecken, H., Western, A., and Hendricks Franssen, H.-J.: Seasonal soil moisture and crop yield prediction with fifth-generation seasonal forecasting system (SEAS5) long-range meteorological forecasts in a land surface modelling approach, Hydrol. Earth Syst. Sci., 27, 3143–3167, https://doi.org/10.5194/hess-27-3143-2023, 2023.

Boas, T., Bogena, H., Ryu, D., Western, A., and Hendricks Franssen, H.-J.: Multi-decadal soil moisture and crop yield variability – A case study with the Community Land Model (CLM5), Journal of Advances in Modeling Earth Systems, 16(9), https://doi.org/10.1029/2023MS004023, 2024.

Acknowledgements

I gratefully acknowledge my supervisors Harrie-Jan Hendricks-Franssen and Heye Bogena for their great support, their detailed feedback on my work, and encouragements throughout my doctoral studies. I am also grateful to my supervisors Andrew Western and Dongryeol Ryu for their support and their valuable feedback on my work. Our regular online meetings always provided me with fresh insights and perspectives.

I also want to acknowledge my colleagues from the Institute of Bio- and Geosciences at the Jülich Research Center, the head of the institute, Harry Vereecken, and Jan Vanderborght for their valuable feedback, and my fellow PhDs and working group colleagues for our interesting discussions. A special thanks goes to Lukas Strebel, for being an exceptional office mate and for his support, particularly in setting up CLM5 on the supercomputers. I would also like to thank Alexander Graf and Marius Schmidt for sharing their observational datasets for the European cropland sites and the respective site PIs for granting permission to use the data.

I am especially thankful to my friends and colleagues Anneli, Helena and Amirpasha for their encouragements and all the fun times.

Moreover, I acknowledge the JUMPA initiative for partially funding my PhD project and enabling the collaboration between the Research Centre Juelich, the University of Aachen and the University of Melbourne in this joint PhD program.

I also gratefully acknowledge the computing time granted on the supercomputers JURECA and JUWELS at the Jülich Supercomputing Centre (JSC), and the JSC team for their support on high performance computing.

Lastly, I am immensely thankful to my family, my friends and my partner for their encouragements and support, and to my little one, who unknowingly, is the greatest motivation of all.

Contents

List of Tables

List of Figures

List of Abbreviations

AUS-VIC	Simulation domain covering large parts of the state of Victoria, Australia
BE-Lon	Lonzée (test site in Belguim)
CFT	Crop Functional Type
CLM5	Community Land Model, version 5.0
CLM-S	Seasonal experiments forced with 7-month lead time forecasts
CLM-SUB	Sub-seasonal experiments forced with a combined set of forecasts (lead times of 3 and 4 months)
CLM-WFDE5	Reference simulations forced with reanalysis
CRNS	Cosmic-ray neutron sensor for measuring neutron count density, from which soil moisture is estimated
CRUNCEP	Combined dataset of the CRU TS3.2 0.5 x 0.5 degree monthly data covering the period 1901-2002 (Harris et al., 2014) and the NCEP reanalysis 2.5 x 2.5 degree 6-hourly data covering the period 1948-2016 (Viovy, 2018)
DE-Kli	Klingenberg (test site in Germany)
DE-RuS	Selhausen (test site in Germany)
DE-RuM	Merzenhausen (test site in Germany)
DE-NRW	Simulation domain covering the state of North Rhine-Westphalia, Germany
ECMWF	European Centre for Medium-Range Weather Forecasts
ESA-CCI	Soil Moisture Climate Change Initiative Combined dataset from the European Space Agency's (Dorigo et al., 2017)
ESM	Earth System Model
G	soil heat flux
GCM	global climate model
GDD	growing degree day
GPP	gross primary production
H	sensible heat flux
LE	latent heat flux
LSM	land surface model
NEE	Net Ecosystem Exchange of CO_2 between the land surface and the atmosphere
MBE	mean bias error
MAA	mean absolute anomaly
MAD	mean absolute deviation
MADr	mean absolute deviation ratio (simulated/observed)
MetSim	Meteorology Simulator (Bennett et al., 2020)
MODIS	Satellite data product (MCD15A3H version 6) including the LAI product and the MODIS ET/LE (MOD1A2 version 6) product (Myneni et al., 2015; Running et al., 2017)
PFT	Plant Functional Type
r	Pearson correlation coefficient
Rn	Net radiation
RMSE	root mean square error
SEAS5	Fifth-generation seasonal forecasting system from the ECMWF (Johnson et al., 2019)
SMC	Soil moisture content
SMAP L3	Soil Moisture Active Passive Level-3 soil moisture product (Entekhabi et al., 2016)
VLUIS	Victorian Land Use Information System (Morse-McNabb et al., 2015)
WFDE5	Bias-adjusted global reanalysis dataset generated from the ERA5 reanalysis product (Hersbach et al., 2020) using the WATCH Forcing Data (WFD) methodology (Cucchi et al., 2020)

1 Introduction

How can we better understand and quantify the complex dynamics of agricultural land cover and its role within our terrestrial system to improve the accuracy of crop yield predictions in the face of climate change?

Global climate change is expected to have a profound impact on future agriculture, with declining global yield trends and increasing irrigation requirements (Urban et al., 2012; Challinor et al., 2014; Deryng et al., 2014; Rosenzweig et al., 2014; Tai et al., 2014; Levis et al., 2018). New challenges for agricultural planning arise from the climate change related rise in annual average temperatures, changes in global radiation, shifts in seasonality, changing precipitation amounts and temporal distribution, as well as from the increasing number of extreme weather events at higher intensities as predicted in recent climate projections (Urban et al., 2012; Challinor et al., 2014; Deryng et al., 2014; Rosenzweig et al., 2014; Tai et al., 2014; Levis et al., 2018). Understanding and improving predictions of the impact of climate change on food security is crucial for society, as highlighted by several studies (Lobell et al., 2011; Aaheim et al., 2012; Ma et al., 2012; Gosling, 2013; Rosenzweig et al., 2014). The assessment of the inter-annual variability of yield for specific agricultural regions can provide useful information and variables of interest for local stakeholders and policy makers. Furthermore, fluxes of water, energy and organic matter associated with agriculture (use of irrigation and fertilizer, timing of crop growth and fallow periods, etc.) can have implications for local and regional weather (Sacks et al., 2009). Continued research is required to deepen our comprehension of the effects of climate change on terrestrial ecosystems, arable land in particular.

To achieve this, reliable tools are needed to provide accurate predictions of land cover feedback mechanisms in response to weather and climate conditions, and to explore potential mitigation strategies and their implications for society. Land surface models (LSMs) are our primary tool for studying the effects of climate change at larger spatial scales, serving as valuable frameworks for representing the complex interactions within our terrestrial system. LSMs are used in global circulation models for numerical weather forecasting and climate projections and are broadly applied in scientific studies to simulate water, energy and nutrient fluxes in the terrestrial ecosystem (e.g. Baatz et al., 2017; Lu et al., 2017; Chang et al., 2018; Han et al., 2018; Lawrence et al., 2018, 2019; Naz et al., 2019; Fisher and Koven, 2020; Lombardozzi et al., 2020). LSMs have become increasingly complex to address a range of key questions, spanning multiple disciplines (Fisher and Koven, 2020). Continuous model development and thorough performance analyses are vital in enhancing the reliability and accuracy of these models. An accurate representation of agriculture in LSMs can provide valuable insights into the interplay between climate change and anthropogenic land use, which represents a key gap in current models. In combination with a comprehensive crop module, LSMs have the potential to predict changes in water and energy cycles and crop production in response to climate, environmental, and land use changes, thereby improving the simulation of biogeophysical and biogeochemical processes on regional and global scales (Kucharik and Brye, 2003; Lobell et al., 2011; Lawrence et al., 2018; Lombardozzi et al., 2020). However, incorporating a sophisticated representation of agricultural land cover into LSMs is a complex task due to the large variety of crop types and the complexity of agricultural management decisions, and thus, remains an ongoing challenge. Recent efforts to integrate detailed crop modules in LSMs have resulted in significant improvements in the simulation of vegetation properties and fluxes, such as

leaf area index, net ecosystem exchange, and gross primary production. For instance, the representation of temperate crop varieties in the Simple Biosphere model (SiB) led to improved simulation of leaf area index and net ecosystem exchange (NEE) (Lokupitiya et al., 2009). In addition, the Joint UK Land Environment Simulator (JULES) was extended to include a global representation of crops (Osborne et al., 2015), and the latest versions of the Community Land Model (CLM) were extended with a prognostic crop module from the Agro-Ecosystem Integrated Biosphere Simulator (Agro-IBIS) (Kucharik and Brye, 2003). These developments have yielded significant improvements in simulation results over arable land (e.g. Twine and Kucharik, 2009; Levis et al., 2012; Webler et al., 2012; Osborne et al., 2015; Xu et al., 2016). Despite recent advancements in the field, the complexity of simulating a wide range of crop varieties and management practices poses significant challenges for current state-of-the-art LSMs. The main challenges stem from the complex parameterization of simulated crop varieties due to their distinct phenology in combination with the scarcity of available data, as well as the incorporation of human management decisions such as cover cropping, fertilizer types and application techniques, and political influences on agricultural decision-making. To ensure LSMs benefit a wider audience, it is crucial to test and validate their applicability for different ecosystems, incorporating more flexible management practices. The current scientific literature lacks comprehensive analyses of LSM performance for agricultural land across different regions and biomes. Further development of LSMs requires thorough testing across various biomes and reviewing the complex parameterizations and interconnected processes. Comprehensive plant-specific parameters need to be provided and potentially calibrated. Therefore, there is a continuous demand for performance analysis research in the land surface and crop modelling community.

A central goal of this PhD research was to systematically evaluate and improve the performance of the latest Community Land Model, version 5.0 (CLM5), with specific emphasis on the model's representation of arable land. This involved identifying key limitations and potential uncertainties within the model, and validating model results against validation datasets from a variety of data sources. The Community Land Model is an open source model continuously being developed by a large user community and maintained by the National Center for Atmospheric Research (NCAR). Its latest version, CLM5, features an interactive crop module that includes a fertilizer and irrigation scheme, as well as eight actively managed crop types (temperate soybean, tropical soybean, temperate corn, tropical corn, spring wheat, cotton, rice, and sugarcane), and irrigated and unirrigated unmanaged crops. Additionally, CLM5 includes a new representation of plant hydraulic stress that explicitly models plant water stress and the transport of water within the soil-root-leaf system. CLM5 also considers root hydraulic redistribution in the soil and contains an updated calculation of stomatal conductance compared to earlier model versions based on the Medlyn et al. (2011) approach (Lawrence et al., 2019). Ongoing efforts also focus on the expansion of the CLM5 crop module to include more varieties of crops through parameterization and model developments e.g. perennial bioenergy crops (Cheng et al., 2020), crop trees (Dombrowski et al., 2022), and winter crops (Lu et al., 2017). These recent developments in CLM5 have made it one of the most sophisticated LSMs in representing cropland and plant hydraulics.

However, detailed assessments of CLM5's performance with high-resolution validation data, particularly at the point or regional scale, are still scarce (e.g. Chen et al., 2015; Sulis et al., 2015; Lu et al., 2017; Chen et al., 2018; Dombrowski et al., 2022; Sheng et al., 2018). The performance of land surface models can vary significantly depending on the specific characteristics of the area being simulated, including soil type, vegetation cover, anthropogenic influences, and weather patterns. Comparing the results of point-scale simulations with high-

resolution field observations allows in-depth analysis on how well the model captures the physical processes and interactions that govern the land surface. High-resolution point-scale settings also enable the validation and testing of technical model developments and set the basis for subsequent regional simulations. This study aimed at evaluating and improving the model performance at point scale for multiple European cropland sites, which encompassed the addition of crop specific parameters for several important cash crops at these sites (winter wheat, sugar beet, and potatoes).

The primary aim of this research was to improve our understanding of how arable land is represented in LSMs and to provide valuable insights for the effective utilization of LSMs in different contexts. A specific focus was placed on investigating the performance and capabilities of CLM5 in representing arable land dynamics. The central objectives of this PhD work were to:

- Provide a comprehensive overview of the CLM5 model's performance over agricultural land with a focus on crop phenology, plant hydraulic stress representation, yield predictions and the soil moisture regime;
- Improve the performance of the state-of-the-art land surface model CLM5 for cropland sites, which is an important prerequisite for accurately simulating regional agricultural fluxes;
- Develop algorithmic procedures to include options for cover cropping and more flexible crop rotation scenarios on the technical model level;
- Evaluate the feasibility of using seasonal weather forecasts in a land surface model, such as CLM5, for the prediction of regional crop productivity and soil moisture;
- Identify key limitations of the model and provide recommendations for future model improvements.

In the course of this thesis, the model was extended to consider an algorithmic representation of cover cropping and crop rotations. At this stage, the CLM5 model structure does not allow for a rotation of crop types on the same land column within the same year. A large part of global cropland is cultivated with rotations of different non-perennial cash crops, and with multiple cropping cycles within one year in certain regions. Cover cropping is a land management practice where certain crops, such as legumes and grasses, are grown during fallow periods to prevent soil erosion and nutrient depletion (Basche et al., 2016; Kaye and Quemada, 2017; Lombardozzi et al., 2018; Möller and Reents, 2009; Quintarelli et al., 2022). Cover cropping offers additional benefits such as weed suppression, pest and disease control, improved biodiversity, and organic fertilization of the soil, making it an important strategy for sustainable agriculture and a common practice in many agricultural regions worldwide (Kaye and Quemada, 2017; Quintarelli et al., 2022). Including a representation of cover cropping in land surface simulations is a crucial factor to accurately represent land surface and vegetation fluxes over agricultural areas, particularly outside of the main cropping season. The natural fertilization that is achieved by ploughing of cover crops into the soil before planting of the next cash crop influences the carbon cycle and overall nutrient budget of the soils and needs to be considered in the simulation of carbon and nitrogen budgets over agricultural areas (Lombardozzi et al., 2018; Kollas et al., 2015). In this work, an algorithmic procedure was developed and embedded in the model code that enables the model to simulate multiple cropping cycles within a single year and the rotation between different crop types. Additionally, the new model development considers the allocation of carbon from cover crops to the soil carbon pool instead of the grain carbon pool, representing the natural fertilization effect. The new parameterizations and model developments were tested for multiple European sites, using high-resolution field observations as validation data, and then ported to the regional scale.

Another major aspect to the relevance of land surface model applications for society, for agricultural planning and decision making in particular, is the combination with seasonal weather forecasts. The effectiveness of such a combination is based on two main pillars: the quality and skill of the land surface model, as well as the applicability, efficacy and skill of the forecast. Reliable high-resolution seasonal weather forecasts can provide crucial information for weather-sensitive sectors like agriculture, water management, and risk management. Knowledge of seasonal rainfall and temperature trends can help in making informed agricultural decisions and mitigating drought-related yield losses. Despite significant progress in numerical weather prediction over the past decade, particularly for short-term forecasts with improved models and data assimilation techniques and the precise characterization of initial conditions, achieving accurate seasonal predictions remains a challenging task. Integrating boundary conditions from various sources, including ocean, land surface (soil moisture and temperature), and stratosphere (downwelling propagation) data, is essential for enhancing predictive capability beyond short-term forecasts. However, current advancements in seasonal weather prediction, especially in temperate regions, are limited, with notable progress primarily observed in regions strongly influenced by El Niño-Southern Oscillation (ENSO). As a consequence of these existing limitations, the adoption of seasonal forecasting products in farming and politics remains low (Parton et al., 2019). Another reason is the lack of available data supporting their usefulness for the respective sectors, in particular for specific regions and management types (i.e., crop varieties) and limited user-friendly communication and data processing tools and services (Hansen et al., 2006; Meza et al., 2008; Coelho and Costa, 2010; Bauer et al., 2015; Monhart et al., 2018; Parton et al., 2019; Klemm and McPherson, 2017). Furthermore, there is often a mismatch between the temporal and spatial resolutions of the forecasting products and the modelling applications that can be forced by these products to predict variables of interest for stakeholders, such as crop yield and flooding risks. This is further exacerbated by the lack of available services for temporal and spatial downscaling of the forecasts. This study aims to explore the feasibility and application of seasonal forecasts within a land surface model, contributing to the understanding and utilization of these forecasts in practice. Given that agricultural practices vary widely among countries and states, influenced by both climatological factors and the political context, regional simulations for areas with available high-resolution land cover and land use information as input for the model and official agricultural statistics as validation data for the simulation results can be used to assess the model performance at larger scales. Thus, regional simulations were conducted with CLM5 for two domains with different climate regimes and agricultural characteristics, one covering the state of North Rhine-Westphalia in Germany (DE-NRW), and one covering large parts of Victoria in Australia (AUS-VIC). Seasonal weather forecasts for multiple cropping seasons from one of the most sophisticated forecasting systems, ECMWFs latest seasonal forecasting system SEAS5 (Johnson et al., 2019), were used as atmospheric input for the simulations. By addressing the challenges mentioned above, this research aimed at enhancing our understanding of the potential benefits and limitations of utilizing seasonal forecasts in land surface modelling.

In addition to evaluating the forecasting product's suitability for LSMs, the assessment also aimed at analysing the model's response to seasonal weather changes. A comparison between simulations forced with seasonal forecasts and reference simulations using reanalysis data can help understand the model's performance in capturing the impacts of seasonal weather variations on soil moisture, crop productivity, and inter-annual crop yield variability. It is critical that LSMs used in coupled climate models realistically represent land surface responses to drought, particularly in light of the anticipated increase in drought risk associated with climate change. While there is growing research on integrating irrigation and human water use in LSMs and hydrological models (e.g. Pokhrel et

al., 2016, 2012; Shah et al., 2019; Yassin et al., 2019; Xia et al., 2022), challenges remain in accurately representing rain-fed agricultural systems in global climate models (GCMs) and LSMs. These challenges stem from the complex interactions between soil, plants, and the atmosphere, including root water uptake, plant responses to environmental stress, land use and land cover changes, spatial heterogeneity in soil properties, vegetation cover, topography, and uncertainties in model parameterizations (Huntzinger et al., 2013; Franks et al., 2018; Trugman et al., 2018; Sulis et al., 2019; Dagon et al., 2020; Fisher and Koven, 2020; Lombardozzi et al., 2020; Blyth et al., 2021; Sabot et al., 2022). Moreover, LSMs often oversimplify the human influences on land use and land cover, such as agricultural practices and management decisions, limiting their ability to capture the impacts of land use change on biogeochemistry and hydrology.

Adequately capturing vegetation responses to changes in precipitation and the corresponding soil moisture conditions in global LSMs is crucial to their performance, particularly in rain-fed areas. This requires an accurate and detailed representation of plant hydraulics and plant responses to environmental stress, which needs further investigation and improvements in global LSMs (De Kauwe et al., 2015b; Franks et al., 2018; Sulis et al., 2019; Sabot et al., 2022). The role of root water uptake in rain-fed agricultural systems is crucial and its representation in global LSMs is often simplified (De Kauwe et al., 2015b; Sulis et al., 2019). Many LSMs, including earlier versions of CLM, employ soil moisture stress parameterizations where water stress is determined based on the plant wilting factor, which is calculated using the soil water matric potential relative to plant-specific parameters for fully open and fully closed stomata. This simplified representation of plant hydraulics can impact the simulated vegetation growth, productivity, and water use efficiency of plants (De Kauwe et al., 2015b; Sulis et al., 2019). Additionally, the selection of stomatal conductance model and the role of roots in redistributing water within the soil profile have been found to be relevant for atmospheric processes, carbon cycling, and nutrient cycling (Li et al., 2012; Tang et al., 2015; Ryel et al., 2002; Zheng and Wang, 2007; Yan and Dickinson, 2014; De Kauwe et al., 2015b; Sulis et al., 2019; Sabot et al., 2022). The latest version of CLM5 includes a new plant hydraulic stress scheme as well as an updated algorithm for stomatal conductance and hydraulic redistribution of soil water from roots (Lawrence et al., 2019). These new formulations in CLM5 have resulted in enhanced model performance in simulating ecosystem water fluxes, vegetation water stress, and productivity, laying the foundation for more accurate and reliable simulations of plant water use and water stress in future applications of CLM5 (Lawrence et al., 2019). This study aimed at assessing the model's effectiveness in capturing inter-annual yield variability as an indicator of its performance regarding the representation of plant drought stress in two distinct agricultural environments.

Next to an accurate representation of plant hydraulics and plant responses to environmental stress, capturing inter-annual yield variations in LSMs is also closely linked to the simulation of soil moisture. In particular, it is crucial for the model to sufficiently represent changes in the soil moisture regime in response to changes in precipitation amounts, specifically in dominantly rain-fed areas. An accurate soil moisture simulation in LSMs is crucial for studying the hydrological cycle, land-atmosphere interactions, agricultural practices, water resource management, and the impacts of climate change on the terrestrial water budget. Soil moisture plays a direct role in the exchange of water and energy between the land surface and the atmosphere, and it serves as the primary water source for plant roots in the soil, thus influencing plant growth, photosynthesis, and transpiration rates. The accurate simulation of soil moisture is therefore essential for understanding water availability for plants, assessing the effects of drought on agricultural systems and a major source of uncertainty in land surface modelling (Trugman

et al., 2018). In order to validate soil moisture simulations, satellite derived products such as the Soil Moisture Active Passive Level-3 soil moisture product (SMAP L3), which provides daily soil moisture retrievals at a 9 km spatial resolution (Entekhabi et al., 2016), can be used. In addition, combined soil moisture products such as the Soil Moisture Climate Change Initiative Combined dataset from the European Space Agency's (ESA-CCI) (Dorigo et al., 2017; Gruber et al., 2017, 2019; Preimesberger et al., 2021), which provides global daily volumetric soil moisture data at a spatial resolution of 0.25 degrees from 1978 to 2019, offer valuable tools for model validation. Furthermore, field observations from cosmic ray neutron sensors can be used to validate simulation results. Cosmic ray neutron sensors detect these secondary neutrons, and their count rate is inversely related to soil moisture content. Cosmic ray neutron sensors offer a non-invasive method of measuring soil moisture, providing valuable insights into soil moisture conditions in the uppermost soil layer at larger horizontal scales (several hectares) compared to invasive measurements (Bogena et al., 2013; Schrön et al., 2017; Bogena et al., 2018).

By investigating the performance and applicability of LSMs in agricultural settings and addressing both the model's skill and limitations in predicting long-term variations in annual crop productivity and soil moisture levels, this research aims to contribute to the advancement and future use of these models and to highlight specific areas in need for further investigation.

In summary, this thesis is structured as follows:

- Chapter 2 provides a theoretical background on the materials and methods used in this study. In section 2.1, the underlying assumptions of the Community Land Model and its representation of crop phenology and plant hydrology are briefly summarized. Major parts of this PhD project were dedicated to extensive data acquisition and processing, as well as the initial compiling and testing of CLM5 in the high-performance supercomputing environment of the Juelich supercomputers JURECA and JUWELS. Section 2.2 presents an overview of the use of computational resources on high-performance systems for numerical simulation experiments with CLM5.
- Chapter 3 is dedicated to detailed performance evaluations and technical model developments of CLM5 at the point scale. The performance of CLM5 was evaluated for four European cropland sites with long records of high-quality field observations. To improve the representation of crop growth and energy fluxes on agricultural fields at the point scale, several modifications were made within the code and parameter configuration of the crop module. The model was enhanced by implementing winter wheat subroutines, plant-specific parameters for sugar beet, potatoes, and winter wheat, and a cover-cropping subroutine that allows multiple crop types on the same column within one year. The main objective of this study was to evaluate and improve the model as a basis for subsequent regional simulations.
- In chapter 4, the modified model is applied at the regional scale and tested in combination with state-of-the-art seasonal weather forecasts from the latest European Centre for Medium-Range Weather Forecasts (ECMWF) seasonal forecasting system (SEAS5). Simulations were conducted for 2017-2020 forced with sub-seasonal and seasonal weather forecasts over two different domains with contrasting climate and cropping conditions: the German state of North Rhine-Westphalia and the Australian state of Victoria. This chapter evaluates and discusses the applicability of the seasonal forecast product for land surface modelling and provides a first impression of the overall skill and potential of this combination. The primary objective was to assess the feasibility of utilizing one of the most sophisticated seasonal forecast

product in conjunction with a land surface model for seasonal crop predictions, and to determine the potential of this combination at the current stage.

- Chapter 5 focuses on the evaluation of the inter-annual variability of crop yield simulated with CLM5. Multi-decadal simulation results for two domains in different climate zones were compared to official crop statistics for the respective regions. To identify potential limitations in the model's sensitivity to drought stress and uncertainties in soil moisture simulation, synthetic experiments with reduced precipitation rates were carried out for the same regions and timescales. This study provides an assessment of the key factors that influence crop yield variability in the model, including precipitation, temperature, and soil moisture content, and serves as a foundation for future discussions on possible techniques for model performance improvements.
- Finally, chapter 6 provides a summary of the main results, and chapter 7 concludes with final remarks and an outlook for future research based on the findings and developments of this thesis. Additional results corresponding to the respective chapters are provided in the appendix.

2 Materials and Methods

2.1 The Community Land Model version 5.0

In this PhD project, land surface simulations and model developments were carried out with the latest version of the Community Land Model version 5.0 (CLM5), the land component of the Community Earth System Model (CESM), which is developed by the National Centre for Atmospheric Research (NCAR) (Kucharik and Brye, 2003; Lawrence et al., 2019). The model is comprised of multiple components related to the hydrologic cycle, biogeochemistry, ecosystem dynamics, land biogeophysics and human dimensions that together represent several aspects of the land surface (Figure 2.1). CLM5 is structured hierarchically on a grid cell structure, where each grid cell can have varying numbers of land units, columns, and patches allowing for the representation of subgrid-scale heterogeneity. Land units, such as glacier, lake, urban, vegetated, and crop, further delineate spatial patterns, while columns capture variability in soil and snow variables within a land unit. For example, the urban land unit has different columns for roof, walls, and canyon floor and the glacier land units are divided into elevation classes. The patch level defines the different vegetation categories, plant functional types (PFTs) and bare ground for vegetated and crop functional types (CFTs) for crop land units. Fluxes and vegetation state variables are defined at the PFT/CFT level and the physics and fluxes within the columns operate with weighted averages across PFTs/CFTs.

CLM5 contains several improvements and updates compared to earlier versions of CLM such as an extended hydrology and snow features, an expanded river model, plant hydraulics and hydraulic redistribution, revised nitrogen cycle, expansion of number of crop types, time dependent irrigated areas and fertilization rates and an improved urban building energy model and carbon isotopes (Lawrence et al., 2018). Previous versions of CLM (e.g. 3.5, 4.0) represented the human influence on land cover outside of urban areas by natural vegetation types, such as grass and cultivated forest areas. As a result, the representation of interactive crop management, such as irrigation, fertilization, planting, and harvesting, was insufficient. For this purpose, the representation of human land management was extended with a prognostic crop module in the latest version of CLM5, which provides a more accurate and broader approach to human land management, allowing for the exploration of economic challenges and questions related to land use changes and agriculture (Lombardozzi et al., 2020; Lawrence et al., 2018, 2019).

2.1.1 Hydrology

The total water balance of the system is described as the relationship between the water stored in the system (e.g. canopy water, canopy snow water, surface water, canopy snow water, soil liquid water, soil ice and water in the unconfined aquifer) and the water that enters the system and water that is drained from the system (e.g. liquid and solid precipitation, evapotranspiration from vegetation and surface, surface runoff, sub-surface drainage, liquid and solid runoff from glaciers and/or lakes and variable surfaces covered by snow and/or ice) (Figure 2.1) (Lawrence et al., 2018).

Liquid and solid precipitation that enter the system are either intercepted by the canopy, or reach the snow or soil surface directly or by dripping off the vegetation. Additionally the unloading of previously intercepted snow is

considered for solid precipitation. The moisture input at the surface from liquid precipitation (throughfall and canopy drip) and the meltwater from snow, is then distributed among surface runoff, surface water storage, and infiltration into the soil.

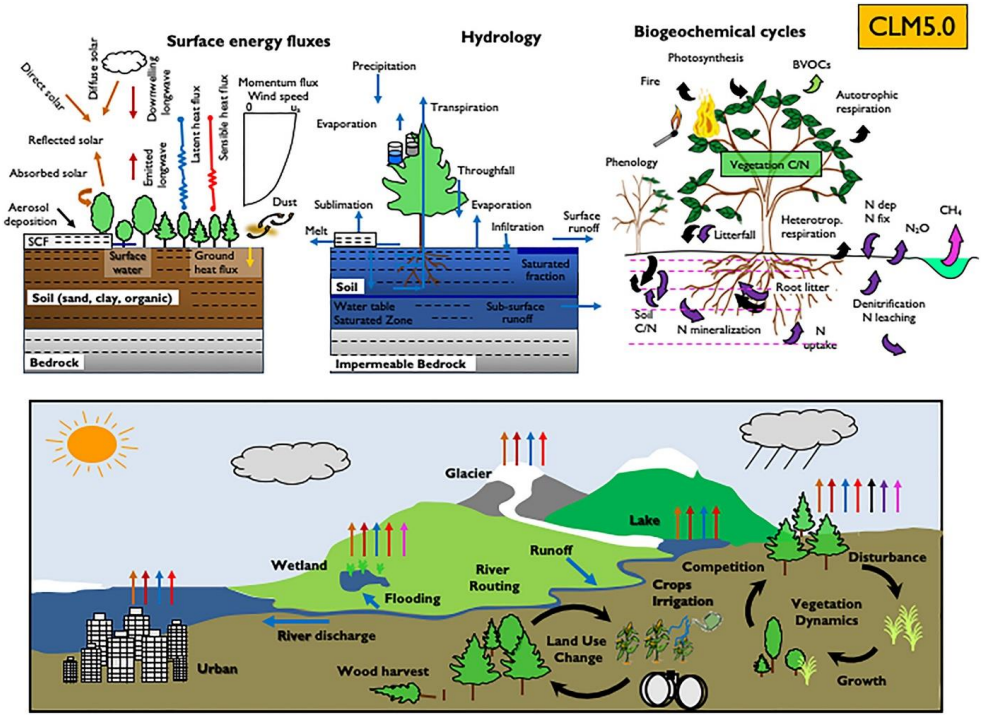

Figure 2.1: Schematic representation of primary land biogeophysical, biogeochemical, and landscape processes simulated by CLM5. Figure adapted from Lawrence et al. (2019).

Surface runoff is described within the system with the runoff model SIMTOP (Niu et al., 2005) that is based on the TOPMODEL (Beven and Kirkby, 1979). Depending on the topographic characteristics and the soil moisture state of a grid cell, surface runoff will be induced by the saturation excess mechanism. Lateral sub-surface runoff is initiated when the soil column reaches saturated soil moisture conditions. Surface water storage and outflow are functions of the microtopography of each grid cell and each sub-grid scale water body, thus being related to the height of the surface water. After the surface runoff has been removed, the surface moisture flux is partitioned into water building up on the surface and water infiltrating into the soil. Once the maximum infiltration capacity of the soil is reached, infiltration excess runoff is generated (Lawrence et al., 2018).

The vertical transport of soil moisture is governed by various processes, including surface and sub-surface runoff, infiltration, gravity, and canopy transpiration through root extraction. The one-dimensional vertical water flow in soils is solved numerically by dividing the soil column into multiple vertical layers and integrating downward over each layer.

The vertical water flow in a soil layer is given by the one-dimensional Richards equation:

$$\frac{\partial \theta}{\partial t} = \frac{\partial}{\partial z}\left[k\left(\frac{\partial \psi}{\partial z} + 1\right)\right], \tag{2.1}$$

where θ is the volumetric soil water content [mm^3/mm^3], t is time [s], z is the vertical distance from the soil surface to the point in the soil column (depth of the soil layer) [mm], k is the hydraulic conductivity [mm/s], and ψ is the soil water potential [mm].

The hydraulic conductivity and the soil water potential for each layer vary with volumetric soil water and soil texture. The soil water retention and permeability curves are determined according the sand and clay contents using the pedotransfer functions by Clapp and Hornberger (1978) and Cosby et al. (1984), and organic properties based on Lawrence and Slater (2008) (Lawrence et al., 2018, 2019).

2.1.2 Plant hydraulics and stomatal conductance

In CLM5, the soil moisture stress function from earlier model versions was replaced by a new plant hydraulic stress routine. The new routine adapts the vegetation water potential according to water supply with transpiration demand (or plant water demand). It simulates water transport through the vegetation based on Darcy´s Law for porous media flow and influenced by Williams et al. (1996), Sperry et al. (1998), Chuang et al. (2006), Bonan et al. (2014), and Sperry and Love (2015) (Lawrence et al., 2018, 2019). Additionally, a plant-mediated vertical hydraulic redistribution of soil water from wet to dry soil layers through either positive or negative soil-to-root fluxes depending on the water potential gradients was implemented (Lawrence et al., 2018, 2019).

The new plant hydraulic stress routine models both plant water supply and demand as function of vegetation water potential and iteratively finds the vegetation water potential that ensures continuity between non-linear water supply and demand. The water supply is discretised into soil-to-root, root-to-stem and stem-to-leaf. Water fluxes in the soil-root-stem-leaf system are modeled as water potential gradients at each time step as follows (Lawrence et al., 2018, 2019):

$$q = kA\,(\psi_1 - \psi_2), \tag{2.2}$$

where q is the flux of water spanning the segment between ψ_1 and ψ_2 [mmH_2O/s], ψ_1 - ψ_2 is the gradient in water potential across the segments [mmH_2O], k is the hydraulic conductance [s^{-1}] and A is the area basis [m^2/m^2].

The hydraulic stress of plants is represented as the segments resistance to hydraulic stress, with hydraulic conductance decreasing as water potentials decrease (Lawrence et al., 2018):

$$k = k_{max} \cdot 2^{-\left(\frac{\psi_1}{p50}\right)^{c_k}}, \tag{2.3}$$

where k_{max} is the maximum segment conductance [s^{-1}], p_{50} is the water potential at 50 % loss of conductivity [mmH_2O], ψ_1 is the water potential of the lower part of the plant segment [mmH_2O] and c_k is the vulnerability curve shape-fitting parameter [-].

In this equation, the maximum segment conductance is multiplied by a sigmoidal function that accounts for the percentage loss of conductivity using the water potential at 50% loss of conductivity (p_{50}) and a shape parameter

(c_k). The parameters k_{max}, p_{50} and c_k control the modelled plant hydraulic stress and thus determine the capability of the plant to extract water from the soil and to resist hydraulic stress. These parameters were derived from the Kennedy et al. (2019) parameterization and are the same for all crop functional types in CLM5 (Figure 2.2).

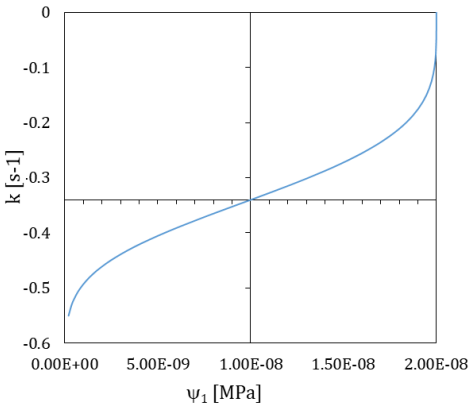

Figure 2.2: Sigmoidal vulnerability curve with water potential (ψ) and segment conductance (k) for CLM5 crop physiology.

The vegetation water demand is simulated as the leaf transpiration which is calculated based on maximum transpiration regulated by the leaf water potential for shaded and sunlit leaves separately (Lawrence et al., 2019). The maximum transpiration is calculated using the maximum stomatal conductance, thus plant water demand depends on stomatal conductance (Lawrence et al., 2019).

The sunlit and shaded leaf stomatal conductance and leaf photosynthesis are modelled based on the approaches of Medlyn et al. (2011), and Farquhar et al. (1980) for C_3 plants and Collatz et al. (1992) for C_4 plants (Lawrence et al., 2019). Adapted from Medlyn et al. (2011), the leaf stomatal resistance is calculated using the net leaf photosynthesis, the vapor pressure deficit and the CO_2 concentration at the leaf surface with plant-specific slope parameters based on de Kauwe et al. (2015a) and Lin et al. (2015) as follows (Lawrence et al., 2019):

$$\frac{1}{r_s} = g_s = g_o + 1.6\left(1 + \frac{g_1}{\sqrt{D}}\right)\frac{A_n}{c_s/P_{atm}}, \tag{2.4}$$

where r_s is leaf stomatal resistance [s m^2/µmol], g_o is the minimum stomatal conductance [µmol/m^2/s], A_n is leaf net photosynthesis [µmolCO_2/m^2/s], g_1 is the plant dependent slope parameter [-] (for a full parameter table see Lawrence et al. (2018)), c_s is the CO_2 partial pressure at the leaf surface [Pa] and P_{atm} is the atmospheric pressure [Pa] and D is the vapor pressure deficit at the leaf surface [kPa].

The ratio of stomatal conductance of the leaf transpiration relative to maximum stomatal conductance corresponding to maximum transpiration is then used to calculate plant water stress, for shaded and sunlit leaves separately (Lawrence et al., 2018):

$$E = E_{max} \cdot 2^{-\left(\frac{\psi}{p50_e}\right)^{ck}}, \tag{2.5}$$

$$\beta_t = \frac{g_s}{g_{s,max}}, \tag{2.6}$$

where E is leaf transpiration [mm/s], E_{max} is the leaf transpiration absent water stress [mm/s], β_t is the transpiration water stress [-], where β_t =1 is no water stress and β_t < 1 is the relative transpiration water stress, g_s is the stomatal conductance of water corresponding to leaf transpiration [µmol/m^2/s], and $g_{s,max}$ is the stomatal conductance of water corresponding to maximum transpiration [µmol/m^2/s].

The calculated transpiration water stress is then used for the attenuation of photosynthesis. In CLM5, photosynthetic capacity is calculated in a mechanistic model of Leaf Utilization of Nitrogen for Assimilation, LUNA (Ali et al., 2016), and represented by two key parameters, the maximum rate of carboxylation at 25 °C and the maximum rate of electron transport at 25 °C (Lawrence et al., 2019). LUNA iteratively solves for attenuated photosynthesis and stomatal conductance until convergence is reached by adjusting these two parameters with the transpiration beta factor β_t:

$$V_{c,max25,i} = V_{c,max25,i-1} \cdot \beta_t, \tag{2.7}$$

$$J_{max25,i} = J_{max25,i-1} \cdot \beta_t, \tag{2.8}$$

where $V_{c,max25}$ is the maximum rate of carboxylation at 25 °C and J_{max25} is the maximum rate of electron transport at 25 °C at the current time step i and the previous step i-1 respectively.

2.1.3 Crop module and plant physiology

CLM5 includes a prognostic crop model based on Agro-IBIS, a process-based ecosystem model with options to simulate dynamic vegetation and crop management (Kucharik, 2003; Kucharik and Brye, 2003). The CLM5 crop model introduces several new developments compared to earlier model versions: (1) additional crop functional types, (2) active management of all crop areas, (3) updated fertilization and irrigation schemes, and (4) the capability to simulate changing distributions of crops and crop management due to dynamic land units (conserving carbon, nitrogen, water, and energy during all transitions) (Lombardozzi et al., 2020). While it is based on the same plant physiology as natural vegetation, the crop module uses crop specific plant parameters, phenology and allocation as well as the possibility of interactive fertilizer and irrigation (Lawrence et al., 2018, 2019; Lombardozzi et al., 2020). The parameterizations for the interactive crop management were derived from combining earlier versions of CLM with Agro-IBIS (Lombardozzi et al., 2020).

In order for interactive crop management to take place without affecting natural vegetation, vegetated land units are separated into natural vegetation and crop land unit with only one CFT on each soil column, thus allowing CFT specific land management techniques to be applied (Lawrence et al., 2018). A total number of 78 plant and crop functional types are included in CLM5 including an irrigated and unirrigated unmanaged C3 crop, eight actively managed crop types - spring wheat, temperate and tropical corn, temperate and tropical soybean, cotton, rice and sugarcane and twenty-three crop types without specific crop parameters associated. For the simulation of those crop types, the specific crop parameters of the spatially closest and most similar out of the eight active crop types are used (Lawrence et al., 2018).

The crop phenology and CN cycling processes in CLM 5.0 adopt the crop phenology algorithm from Agro-IBIS that consists of three phases – phase 1 from planting to leaf emergence, phase 2 from leaf emergence to beginning of grain fill and phase 3 from beginning of grain fill to maturity and harvest (Lawrence et al., 2018). The progression of these phases is influenced by growing-degree-day threshold values (percentages of the crop-specific

number of growing degree days (GDD) necessary for the crop to mature). Harvesting takes place once maturity is reached or the crop-specific maximum number of days for crop growths is exceeded (Lawrence et al., 2018).

Allocation of assimilated carbon as well as the allocation to leaf, stem, root and reproductive pools is linked to the crop phenology phases and ends with harvest of the crop. The total amount of assimilated carbon is regulated by availability of soil nitrogen. The allocation of nitrogen is based on the specific C/N ratios in plant tissue (varying for roots, stem, leaves, reproductive pools) that vary throughout the growing season and are therefore also related to crop phenology phases (Lawrence et al., 2018). For crops, food C and N are allocated to a grain product pool, where they decay to the atmosphere over one year. Additionally, a crop seed pool is filled with C and N from the grain product pool for the following year (Lawrence et al., 2018). The annual grain yield can be calculated from the annual amount of C that is allocated to the food C pool (GRAINC_TO_FOOD) by accounting for the proportion of C in the dry crop weight and under the assumption that harvest efficiency is typically about 85 % (Lawrence et al., 2018):

$$Grain\ yield = \frac{\sum(GRAINC\_TO\_FOOD)\cdot 0.85}{C_{dry}}, \tag{2.9}$$

where GRAINC_TO_FOOD [gC/m^2/s] is the CLM5 history field that is calculated on the CFT level and C_{dry} [g/m^2] is the proportion of C in the dry crop weight of the respective crop.

Each crop type has an irrigated and an unirrigated CFT that can coexist on a land unit but are on individual soil columns. This allows the simulation of irrigated cropland areas which are dynamically connected to simulated soil moisture conditions (Lawrence et al., 2018). The irrigation algorithm initializes water supply through irrigation to the soil, once a specified threshold of available soil water is reached, based on the principle of Ozdogan et al. (2010). With irrigated and rain-fed crops on separate soil columns, runoff between two neighboring soil columns with irrigated and rain-fed crop areas is not considered.

Besides water availability from irrigation and rain, crop yields and food productivity greatly depend on nutrient availability in the soil and additional fertilization. In CLM 5.0, fertilization is carried out by adding nitrogen directly to the soil mineral pool. Fertilization dynamics depend on the crop functional types and vary spatially and yearly based on the Land Use Model Intercomparison Project (Lawrence et al., 2016) land use and land cover change time series. Land fractions of natural vegetation are not influenced by fertilizer application. Manure nitrogen is applied at slower rates to prevent rapid denitrification rates that were observed in earlier CLM versions and more uptake by the plant. Industrial fertilizer application starts during the leaf emergence phase of crop growth and continues for 20 days (Lawrence et al., 2018, 2019).

2.2 Simulation experiments on high performance computing systems

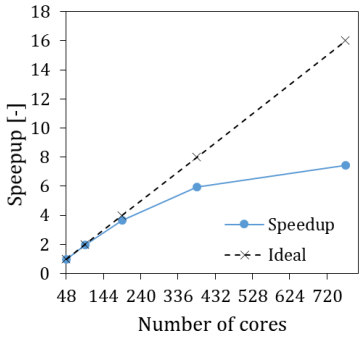

Figure 2.3: Scaling behavior of CLM5 on JUWELS. Corresponding data is listed in Table 2.1.

All simulation experiments were conducted on the high performance computers JURECA and JUWELS from the Juelich Supercomputing Centre (JSC). The CLM5 code runs on Central Processing Units (CPU) and is parallelized with pure Message Passing Interface (MPI) which is a message-passing standard for parallel computing architectures. We conducted scaling studies prior to computationally expensive production simulations to analyse the scaling behaviour on the supercomputers. The example below shows a scaling study performed for CLM5 on JUWELS with a problem size of 300 x 300 x 20 grid cells that indicated a relatively good scalability up to 384 cores (Table 2.1, Figure 2.3). Further large scale simulations were then conducted in accordance with effective usage of computational resources.

Table 2.1: Scaling behavior of CLM5 on JUWELS. This test was performed a problem size of 90.000 cells, absolute timings per time step and relative speedup normalized to 48 cores are given.

Number of cores	Absolute timing [s]	Speedup	Performance per core [MFLOPS/s] x efficiency
48	2583	1.00	800x1.00
96	1311	1.97	800x0.98
192	710	3.64	800x0.91
384	434	5.95	800x0.74
768	348	7.42	800x0.46

3 Improving the representation of cropland sites in CLM5

Adapted from: Boas, T., Bogena, H., Grünwald, T., Heinesch, B., Ryu, D., Schmidt, M., Vereecken, H., Western, A., and Hendricks-Franssen, H.-J.: Improving the representation of cropland sites in the Community Land Model (CLM) version 5.0, Geoscientific Model Development, 14, 573–601, https://doi.org/10.5194/gmd-14-573-2021, 2021.

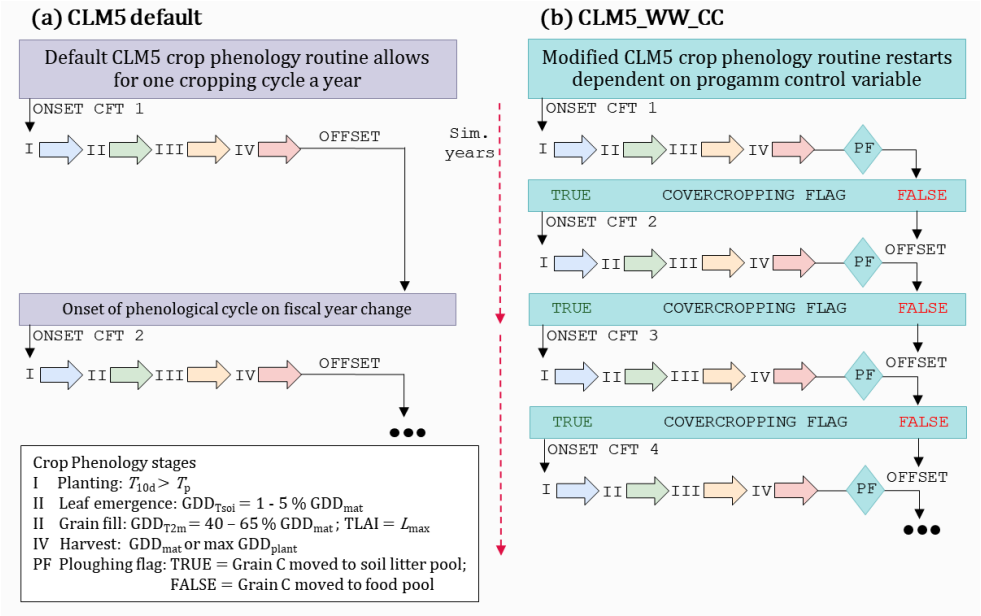

Figure 3.1: Schematic of the CLM5 phenology routine in (**a**) the default CLM5 model and (**b**) the modified CLM5_WW_CC model source code. The default crop phenology routine allows for one cropping cycle a year that is dependent on the fiscal year change on the first of January, while the modified crop phenology routine is constraint by a program control flag (covercropping flag). Additionally, an organic fertilizer option was implemented (PF) that imitates the common practice of ploughing cover crops into the soil, by moving the carbon (C) from the grain pool to the soil litter pool instead of the food pool. The phenology stages are indicated in roman numbering and corresponding thresholds are listed in the legend. Planting starts after an accumulated temperature of 10 consecutive days (T_{10d}) is met within a planting window (T_p), the start of the leaf emergence stage is based on heat accumulated in the top soil layers (GDD_{Tsoi}) equal to 1-5 % of the maximum growing degree days needed for maturity of the crop (GDD_{mat}), the grain fill stage commences based on heat accumulated since leaf emergence (GDD_{T2m}), or when the leaf area index (TLAI) has reached its maximum (L_{max}), and finally the crop is harvested once GDD_{mat} is reached or the maximum days for crop growth (GDD_{plant}) are exceeded.

3.1 Introduction

Global climate change is widely believed to have an important impact on future agriculture and consequently food security under changing climate is an important research topic (Lobell et al., 2011; Aaheim et al., 2012; Ma et al., 2012; Gosling, 2013; Rosenzweig et al., 2014). With a trend of declining crop yield and increasing uncertainty in yields in many parts of the world (Urban et al., 2012; Challinor et al., 2014; Deryng et al., 2014; Rosenzweig et al., 2014; Tai et al., 2014; Levis et al., 2018), understanding the impact of climate change on crop production and improving its prediction at local to global scales is a research topic of great importance to society. Also, agricultural expansion and management practices exert strong influences on physical and biogeochemical properties of terrestrial ecosystems that need to be considered in model simulations of the terrestrial system. Thus, the evaluation and improvement of integrated modelling approaches, including through incorporation of improved crop phenology, to simulate realistic land management and crop yield in response to climate conditions are the focus of many studies (Stehfest et al., 2007; Olesen et al., 2011; Van den Hoof et al., 2011; Rosenzweig et al., 2014).

Nevertheless, the sophisticated representation of agricultural land cover in Earth system models (ESMs) remains an ongoing challenge due to the complexity of agricultural management decisions and the variety of different crop types and their respective phenologies. In many land surface models (LSMs) and land components of ESMs, the representation of crops is limited to simplistic schemes lacking the representation of management (e.g. irrigation and fertilization) or to surrogate representation by natural grassland (Betts, 2005; Elliott et al., 2015; McDermid et al., 2017). In recent studies there is a trend towards the incorporation of a comprehensive crop module in LSMs. These modules offer improved potential to study changes in water and energy cycles and crop production in response to climate, environmental, land use, and land management changes. This may help to improve the simulation of biogeophysical and biogeochemical processes on regional and global scales (Kucharik and Brye, 2003; Lobell et al., 2011; Lokupitiya et al., 2009; Levis et al., 2012; Osborne et al., 2015; McDermid et al., 2017; Lawrence et al., 2018; Lombardozzi et al., 2020). For example, the Simple Biophere model (SiB) incorporated a crop module to represent a number of temperate crop varieties which resulted in improved simulated LAI and net ecosystem exchange (NEE) (Lokupitiya et al., 2009). Also, the Joint UK Land Environment Simulator (JULES) was extended to a global representation of crops which improved simulated LAI and gross primary production (GPP) (Osborne et al., 2015).

Recent versions of CLM (i.e. 4.0, 4.5 and 5.0) have adopted the prognostic crop module from the Agro-Ecosystem Integrated Biosphere Simulator (Agro-IBIS) (Kucharik and Brye, 2003), which has the ability to simulate the soil-vegetation-atmosphere system including crop yields, and has been evaluated in multiple studies (e.g. Twine and Kucharik, 2009; Webler et al., 2012; Xu et al., 2016). Even the simplified version of the Agro-IBIS crop scheme that was implemented in CLM4 led to improved simulation of climate-crop interactions and more comprehensive ecosystem balances than previous CLM versions (Levis et al., 2012). Evaluation studies of CLM4 by Levis et al. (2012) and Chen et al. (2015) revealed significant sensitivities of energy and carbon fluxes to biases in crop phenology, especially for the seasonality of the NEE for managed crop sites where the flux is governed by planting and harvest times. In its latest version, CLM (CLM5) has been extended with an interactive crop module that represents crop management. It includes eight actively managed crop types (temperate soybean, tropical soybean, temperate corn, tropical corn, spring wheat, cotton, rice, and sugarcane), as well as irrigated and non-irrigated unmanaged crops (Lombardozzi et al., 2020). CLM5 is to date the only land surface model that includes time-varying spatial distributions of major crop types and their management (Lombardozzi et al., 2020). Despite these

improvements over earlier versions of CLM, the few studies that evaluated CLM5 at point and regional scale suggest inaccurate phenology and crop yield estimates for specific crops (Chen et al., 2018; Sheng et al., 2018). In summary, current crop modules in LSMs are limited by their ability to represent many different crop types and important management practices such as cover cropping, flexible fertilizer application types and amounts, etc. The main challenges are related to the complex parameterization of simulated crop varieties due to their distinct phenology in combination with information scarcity, as well as the complexity of human interaction through management decisions and biogeochemical processes. In addition to irrigation and fertilizer application, crop rotations and cover cropping are important management practices and their consideration is a crucial factor to accurately represent energy fluxes and crop phenology of agricultural sites (or areas) over longer time scales.

In Western Europe, a large proportion of arable land is cultivated with rotations of different non-perennial cash crops (Kollas et al., 2015; Eurostat, 2018). The most important cash crops grown in the European Union (EU) are cereals such as wheat (mostly winter wheat varieties in Western Europe), barley and maize, root crops such as sugar beet and potatoes, and oilseed crops such as rape, turnip rape, and sunflower (Eurostat, 2018). Cereals account for the majority of all crop production in the EU, contributing up to 12 % to global cereal grain production (Eurostat, 2018). The EU production of sugar beet accounts for about half of the global production (Eurostat, 2018). The use of cover crops is a common agricultural management practice to reduce soil erosion, soil compaction, and nitrogen leaching as well as to increase agricultural productivity by nitrogen fixation (Sainju et al., 2003; Lobell et al., 2006; Basche et al., 2014; Plaza-Bonilla et al., 2015; Tiemann et al., 2015; Kaye and Quemada, 2017). The biogeochemical effects and benefits of cover crops as well as their potential to mitigate climate change are the focus of many studies (e.g. Sainju et al., 2003; Lobell et al., 2006; Groff, 2015; Plaza-Bonilla et al., 2015; Basche et al., 2016; Carrer et al., 2018; Lombardozzi et al., 2018; Hunter et al., 2019). Despite recent development efforts, the representation of these management practices has not yet been included in CLM5. Furthermore, in a previous study by Lu et al. (2017) the default representation of winter cereals performed poorly in simulating the phenology of winter wheat.

In this study, we evaluate and enhance the performance of the crop module of CLM5 focusing on the representation of seasonal and inter annual variations in crop growth, planting and harvesting cycles, and crop yields as well as energy and carbon fluxes. First, we have transferred the modified vernalization and cold tolerance routine by Lu et al. (2017) to the CLM5 code to simulate winter cereal in a more meaningful way. Secondly, new crop specific parameter sets for winter wheat, sugar beet and potatoes that were gathered from the literature and from observation data were added to the default parameter scheme. Finally, we extended CLM5 by adding a new crop rotation and cover cropping subroutine that models the growth of winter cover crops and the rotation from a summer to a winter crop within the same year. All modification were tested at point scale at four cropland reference sites of the ICOS (Integrated Carbon Observation System) and TERENO (Terrestrial Environmental Observatory) networks in central Europe.

3.2 Materials and Methods

3.2.1 Community Land Model

Land surface models such as CLM5 are broadly applied in scientific studies to simulate water, energy and nutrient fluxes in the terrestrial ecosystem (Niu et al., 2011; Han et al., 2014; Lawrence et al., 2018; Naz et al., 2019). CLM5 represents the latest version of the land component in the Community Earth System Model (CESM)

(Lawrence et al., 2018; 2019). In CLM5, simulated land surface fluxes such as latent and sensible heat are driven by atmospheric/meteorological input variables in combination with soil and vegetation states (e.g. soil moisture and LAI) and parameters (e.g. hydraulic conductivity, land cover) (Oleson et al., 2010; Lawrence et al., 2018). The new biogeochemistry and crop module of CLM5 (BGC-Crop) adopted the prognostic crop module from the Agro-Ecosystem Integrated Biosphere Simulator (Agro-IBIS) (Kucharik and Brye, 2003). This incorporation of agriculturally managed land cover may help to improve the general representation of biogeochemical processes on the global scale to better address challenges from land use changes and agriculture practices (e.g. Lobell, Bala, and Duffy, 2006). The CLM5 crop module includes new crop functional types, updated fertilization rates and irrigation triggers, a transient crop management option as well as some adjustments to phenological parameters. Also extensive modifications have been made to the grain C and N pool, e.g. C for annual crop seeding comes from the grain C pool and initial seed C for planting is increased from 1 to 3 gCm^{-2} (Lawrence et al., 2018, 2019; Lombardozzi et al., 2020).

Vegetated land units are separated into natural vegetation and crop land units, with only one crop functional type (CFT) on each soil column, including irrigation as a CFT specific land management technique (Lawrence et al., 2018; Lombardozzi et al., 2020). A total of 78 plant and crop functional types are included in CLM5 including an irrigated and unirrigated unmanaged C3 crop, eight actively managed crop types - spring wheat, temperate and tropical corn, temperate and tropical soybean, cotton, rice and sugarcane and 23 crop types without specific crop parameters associated that are merged to the most closely related and parameterised CFTs (Lombardozzi et al., 2020). For the simulation of those inactive crop types, the specific crop parameters of the spatially closest and most similar out of the eight active crop types are used. Irrigation is simulated dynamically for defined irrigated CFTs in response to soil moisture conditions and is partly based on the implementation of Ozdogan et al. (2010) (Leng et al., 2013; Lawrence et al., 2018).

Besides water availability from irrigation and precipitation, crop yield and food productivity greatly depends on fertilization. In CLM5-BGC-Crop, fertilization is represented by adding nitrogen directly to the soil mineral pool (Lawrence et al., 2018). Fertilization dynamics and annual fertilizer amounts depend on the crop functional types and vary spatially and yearly based on the land use and land cover change time series derived from the Land Use Model Intercomparison Project (Lawrence et al., 2016). In CLM5, land fractions with natural vegetation are not influenced by fertilizer application. In cropping units, mineral fertilizer application starts during the leaf emergence phase of crop growth and continues for 20 days. Manure nitrogen is applied at slower rates (0.002 kg N m^{-2} per year by default) to prevent rapid denitrification rates that were observed in earlier CLM versions so that more uptake by the plant is achieved (Lawrence et al., 2018).

CLM5-BGC-Crop is fully prognostic with regards to carbon and nitrogen in the soil, vegetation and litter at each time step. The crop phenology as well as the carbon and nitrogen cycling processes follow three phenology phases: phase (1) from planting to leaf emergence, phase (2) from leaf emergence to beginning of grain fill and phase (3) from beginning of grain fill to maturity and harvest. These phenology phases are governed by temperature thresholds and the percentage of Growing Degree Days (GDD) required for maturity of the crop with harvest occurring when maturity is reached (Lombardozzi et al., 2020).

The first phenology stage, planting, starts when crop specific 10-day mean temperature thresholds (of both the daily 2-m air temperature T_{10d} and the daily minimum 2-m air temperature $T_{min,10d}$) are met. The transition from planting to leaf emergence (phase 2) begins when the growing degree-days of soil temperature at 0.05 m depth

(GDD_{Tsoi}) reaches 1 - 5 % of the GDD required for maturity (GDD_{mat}), depending on a crop specific base temperature for the GDD_{Tsoi}. Grain fill (phase 3) starts with either the simulated 2-m air temperature (GDD_{T2m}) reaching a heat unit threshold (h) of 40 – 65 % of GDD_{mat} or when the maximum leaf area index (L_{max}) is reached. The crop is harvested in one time step when 100 % GDD_{mat} is reached or when the crop specific maximum number of days past planting is exceeded. The LAI is dependent on the specified specific leaf area (SLA) and the calculated leaf C. The SLA as well as the maximum LAI are specified for each crop in the parameter file (Table A2).

The allocation of carbon and nitrogen also follows the phenology phases. During the leaf emergence phase, carbon from the seed carbon pool is transferred to the leaf carbon pool. Nitrogen is supplied through the soil mineral nitrogen pool. During the grain fill phases, nitrogen from the leaf and stem of the plant is translocated to the grain pool. Allocation ends upon harvest of the crop where grain carbon and nitrogen are transferred from the grain pool to the grain product pool and, a small amount of 3g C m^{-2}, to the seed carbon pool for the next planting (Lawrence et al., 2018; Lombardozzi et al., 2020).

The total amount of assimilated carbon and nitrogen is regulated by availability of soil nitrogen, among other resources, and also depends on crop specific target C/N ratios in the plant tissue (varying for roots, stem, leaves, reproductive pools) (Lawrence et al., 2018; Lombardozzi et al., 2020). For a detailed technical description of the model and all its features, the reader is referred to the technical documentation and description of new features in CLM5 (Lawrence et al., 2018, 2019; Lombardozzi et al., 2020).

3.2.2 Model modifications

In the course of this study, three main limitation of CLM5 for the intended simulation of agricultural sites in Western Europe at point scale were identified: (1) the default CLM5-BGC-Crop code and parameterization yielded a very poor representation of crop growth of winter wheat and other winter crops, (2) the default plant parameter dataset lacks specific parameterization for several important cash crops (here especially sugar beet and potatoes), and (3) CLM5-BGC-Crop does not allow a second crop growth onset or a second CFT to be grown on the same field within one year. These limitations were met by modifications to the code structure and parameterization of the CLM5-BGC-Crop module described below.

3.2.2.1 Winter cereal representation

Winter wheat is an important crop for global food production and covers a significant fraction of the European croplands. (Chakraborty and Newton, 2011; Vermeulen et al., 2012). In general, winter wheat is exposed to a different range of environmental stresses compared to summer crops such low temperatures. In regions with sufficiently cold winters, the main processes that allow a successful cultivation of winter wheat during the colder months are vernalization and cold tolerance (Barlow et al., 2015; Chouard, 1960). Vernalization represents the process that an exposure to a period of non-lethal low temperatures is required to enter the flowering stage for winter crops. In general, the vernalization process ensures that the reproductive development of plants growing over winter (winter crops and also natural vegetation) does not start in late summer or autumn but rather in late winter or spring. The other process, cold tolerance, ensures that the crop can acclimate to low temperatures and thus survive cold temperatures and even freeze-thaw cycles. However, cold damage to the crop can occur when the crop is exposed to low temperatures at a certain development stage. These damages have been documented to have significant impacts in crop yield (Lu et al., 2017). Lu et al. (2017) introduced a new vernalization, as well as

a cold tolerance and frost damage subroutine in CLM4.5 to better simulate the phenology of winter cereal. For this, they adapted the winter wheat vernalization model from Streck et al. (2003). Streck et al. (2003) evaluated their vernalization algorithm for a wide range of winter wheat cultivars for the purpose of being used in crop model approaches. Furthermore, Lu et al. (2017) implemented a cold tolerance scheme including frost damage representation using the approaches after Bergjord et al. (2008) and Vico et al. (2014). In this study, their modifications were ported to the newer version of the model, CLM5, and tested for several study sites.

Vernalization and cold tolerance are cumulative processes that operate in a certain optimum temperature ranges (that can be different for different crop types and cultivars). The vernalization process starts after leaf emergence and ends before flowering (Streck et al., 2003) and is dependent on the crown temperature (T_{crown}) (see Equation A1). The crown is the connecting tissue between the roots and the shoots at the base of the plant. For winter wheat, the crown node is located at about 3 – 5 cm soil depth (Aase and Siddoway, 1979). The daily vernalization dependence is calculated based on T_{crown} and the optimum vernalization temperature (T_{opt}), limited to times when the crown temperature lies within the minimum to maximum vernalization temperature (T_{min} and T_{max}) range:

$$vd = \sum fvn(T_{crown}), \tag{3.1}$$

$$fvn(T_{crown}) = \frac{2(T_{crown}-T_{min})^{\alpha}(T_{opt}-T_{min})^{\alpha}-(T_{crown}-T_{min})^{2\alpha}}{(T_{opt}-T_{min})^{2\alpha}}, \tag{3.2}$$

$$\alpha = \frac{ln2}{ln\,[(T_{max}-T_{min})/(T_{opt}-T_{min})]}, \tag{3.3}$$

$$vf = \frac{vd^5}{22.5^5+vd^5}, \tag{3.4}$$

where *vd* [-] is the sum of the sequential vernalization days, *fvn* [-] is the daily vernalization rate, *vf* [-] is the vernalization factor, T_{crown} [K] is the crown temperature, T_{opt} [K], T_{max} [K] and T_{min} [K] are the optimum, maximum and minimum vernalization temperatures respectively.

The vernalization factor can range between 0 (not vernalized) and 1 (fully vernalized). It is multiplied with the GDD during the phenology phase after planting and the grain carbon allocation coefficient which leads to a reduced growth rate in the beginning of the phenology cycle until the plant is fully vernalized. The vernalization factor is further used in the cold tolerance subroutine to assess the cumulative cold hardening of the plant and the dehardening process when exposed to higher temperatures (see below). Lu et al. (2017) introduced a scheme to quantify the impacts of frost damage based on the approaches after Bergjord et al. (2008) and Vico et al. (2014). The damage from low temperatures is quantified by three main variables: the temperature at which 50 % of the plant is damaged (LT_{50}), the survival probability (f_{surv}) and winter killing degree days (WDD) (Bergjord et al., 2008; Lu et al., 2017; Vico et al., 2014). A detailed description of these approaches can be found in Bergjord et al. (2008) and Vico et al. (2014).

The temperature at which 50 % of the plant is damaged (LT_{50}) is calculated interactively at each time step ($LT_{50,t}$) depending on the previous time step ($LT_{50,t-1}$) and on several accumulative parameters. These parameters are the exposure to near-lethal temperatures ($rate_s$), the stress due to respiration under snow ($rate_r$), the cold hardening or low temperature acclimation (contribution of hardening – $rate_h$) and the loss of hardening due to the exposure to a

period of higher temperatures (dehardening – $rate_d$) that are each functions of the crown temperature (Lu et al., 2017 and references therein) (see Equations A2-A11).

The survival rate (f_{surv}) is then calculated as a function of LT_{50} and the crown temperature. The probability of survival is a function of T_{crown} in time (t). It increases once T_{crown} is higher than LT_{50} or decreases when it is lower (Vico et al., 2014):

$$f_{surv}(T_{crown}, t) = 2^{-\frac{T_{crown}}{LT_{50}}^{\alpha_{surv}}}, \quad (3.5)$$

where α_{surv} is a shape parameter of 4.

The winter killing degree day (WDD) is calculated as a function of crown temperature and survival probability, where the maximum function limits the integration to the potentially damaging periods, when the air temperature (T) is lower than the base temperature (T_{base}) of 0°C (Vico et al., 2014):

$$WDD = \int_{winter} max\,[(T_{base} - T_{crown}),0]\,[1 - f_{surv}(T_{crown}, t)]dt, \quad (3.6)$$

Lower LT_{50} indicate a higher frost tolerance and would result in higher survival rates, smaller WDD and less cold damage to the plant. Thus, when the survival probability and crown temperature are low, the WDD will be high (Vico et al., 2014).

Lu et al. (2017) also implemented a relationship between frost damage described above and the subsequent growth or carbon allocation of the plant. Whenever the survival factor is less than 1, a small amount of leaf carbon (5 g C m^{-2} per model time step) as well as a small amount of leaf nitrogen (scaled by the prescribed C/N target ratios, Table 3.1 and Table A2) are transferred to the soil carbon and nitrogen litter pool thus simulating a reduction in growth and/or damage of small/young leaves and seedlings. Additionally, in order to simulate more drastic and instantaneous damage or death of the plant due to a longer duration of lethal temperatures (most likely to occur in spring when the plant has emerged and is close to or already fully vernalized), a second frost damage function is implemented. When WDD > 1° days the frost damage function is triggered, leading to crop damage by transferring leaf carbon (amount scaled by the survival probability (1 -f_{surv})) to the soil carbon litter pool. A more detailed description of these routines can be found in the source literature Lu et al. (2017) and references therein.

3.2.2.2 Crop specific parameterization

In order to yield a reasonable representation of agricultural areas on the regional scale in future studies, the default parameter set was extended with specific crop parameters for sugar beet, potatoes, and winter wheat based on the characteristics of our study sites to better fit the observed plant phenology and energy fluxes at the simulation sites.

The CTFs sugar beet and potatoes are merged to the spring wheat CFT on the default parameter scheme due to the lack of crop specific parameters for these crops. For winter wheat there is a pre-existing default parameter set available in CLM5. However, this default parameterization performed poorly in representing the crop phenology for the evaluated study sites in this study. This was also reported in an earlier study by Lu et al. (2017). Thus, crop specific parameters were added for sugar beet, potatoes and winter wheat. The parameters to be modified were selected taking into account the sensitivity analysis and parameter estimation studies by Post et al. (2017) (for version 4.5), Cheng et al. (2020) and Fisher et al. (2019) (for version 5.0). Key parameters as identified by previous

studies (Sulis et al., 2015; Post et al., 2017; Lu et al., 2017; Fisher et al., 2019; Cheng et al., 2020) are listed in Table 3.1. These parameters were added with values from the literature or site-specific observations to match observed values. General phenology parameters such as the maximum canopy height, planting temperatures, maximum LAI, maximum and minimum planting dates and days for growing were adjusted according to field data including planting and harvest dates. A list of plant types, planting and harvest dates is provided in Table A1. C/N ratios in leaves and roots for wheat and sugar beet were adapted from Whitmore and Groot (1997), Gan et al. (2011), Sánchez-Sastre et al. (2018) and Zheng et al. (2018). The specific leaf area (slatop) and the fraction of leaf N in Rubisco (flnr) for sugar beet and winter wheat were taken from Sulis et al. (2015) and references therein and adopted also for potatoes. Table A2 provides a full list of default and newly added crop specific parameters for the CFTs temperate corn, spring wheat, sugar beet, potatoes and winter wheat.

Table 3.1: CFT specific phenology and CN allocation parameters.

Parameter	CLM variable name	Units
Phenology		
Minimum planting date for the Northern Hemisphere	min_NH_planting_date	MMDD
Maximum planting date for the Northern Hemisphere	max_NH_planting_date	MMDD
Average 5 day daily temperature needed for planting	planting_temp	K
Average 5 day daily minimum temperature needed for planting	min_planting_temp	K
Minimum growing degree days	gddmin	°days
Maximum number of days to maturity	mxmat	Days
Growing Degree Days for maturity	hygdd	°days
Base Temperature for GDD	baset	°C
Maximum Temperature for GDD	mxtmp	°C
Percentage of GDD for maturity to enter phase 3	lfemerg	% GDDmat
Percentage of GDD for maturity to enter phase 4	grnfill	% GDDmat
Canopy top coefficient	ztopmax	M
Maximum Leaf Area Index	laimx	m^2/m^2
Specific Leaf Area	slatop	m^2/gC
CN ratios and allocation		
Leaf C/N	leafcn	gC/gN
Minimum leaf C/N	leafcn_min	gC/gN
Maximum leaf C/N	leafcn_max	gC/gN
Fine root C/N	frootcn	gC/gN
Grain C/N	graincn	gC/gN
Fraction of leaf N in Rubisco	flnr	$fraction/gNm^{-2}$

3.2.2.3 Cover cropping and crop rotation scheme

The effect of cover crops on the physical and biogeochemical properties of the land surface alters latent heat flux, albedo and soil carbon and nitrogen storage and can potentially impact local and regional climate (Sainju et al., 2003; Lobell et al., 2006; Möller and Reents, 2009; Plaza-Bonilla et al., 2015; Basche et al., 2016; Carrer et al., 2018; Lombardozzi et al., 2018; Hunter et al., 2019).

In the default BGC phenology, the growth algorithm starts in the beginning of each year, when the crop is not alive on the specific patch. Furthermore, the CLM structure does not allow multiple CFTs to coexist on the same column so that multiple planting phases related to cover cropping over winter months or crop rotations with winter and

summer crops, both being very common practices in Europe and worldwide, cannot be accounted for. This might also be an issue when representing ecosystems where agricultural management practices involve multiple sowing and harvest cycles in accordance with the monsoon season (e.g. India). Therefore, a cover cropping subroutine was implemented in the BGC phenology module that affects the onset/offset (crop cycle/fallow) algorithm to allow a second onset period (crop cycle) on the same column.

A cover crop flag was introduced in the parameter file and in the source code. This flag can be set for any CFT in the parameter file and calls the cover-cropping subroutine when it is set to true (covercrop_flag ≠ 0). This allows a flexible handling of this option as well as an application on a larger scale. With this modification, the onset period can start again within one simulation year for another (or the same) CFT. For example, when the maturity of the crop is reached and it has been harvested, the model would by default switch to the next stage (phase 4) where the crop is not alive and the offset (fallow) period begins. The next onset period and GDD accumulation for planting would then start in the subsequent simulation year. In our modified CLM5 version, the cover-cropping subroutine is called before entering into the offset period when the cover-crop flag for the current CFT is set to true. In the cover-cropping subroutine, the CFT is then changed according to a predefined rotation scheme and another onset period and GDD accumulation for planting is initialized.

A common practice is to plough the cover crops into the soil instead of removing their biomass from the field. We simulated this by relocating the biomass of the crop into the litter pool instead of the grain product pool upon harvest using the use_grainproduct flag described below (Figure 3.2).

Individual crop rotation schemes were customized within the code and depend on the currently planted crop type. For example, if a simulation starts with a crop coverage of spring wheat specified in the surface file, the new subroutine is called after harvest of the crop (Figure 3.1). Within the subroutine, the CFT is then changed to the next crop, e.g. sugar beet. Again, after the harvest of this crop, e.g. sugar beet, the CFT is again changed to the next crop and so on. When the CFT is changed back to spring wheat, the rotation cycle starts again. This rotation is defined in a repetitive sequence based on the harvested CFT and its harvest date (Figure 3.2).

The actual rotation of crop types can be user-customized by defining the variables hd and $crop_x$ in a list (e.g. hd_1 = 150 [day of year], $crop_1$ = spring wheat, etc.). By including the harvest date as a dependency, it is also possible to simulate the planting of cover crops based on harvest date thresholds. A user-defined maximum harvest date for any specific cash crop can define whether a cover crop would be planted or not. This technique can be beneficial to study the effects of conceptual cover cropping scenarios on regional scales. The possibility to change the CFT within the same year represents a significant improvement in flexibility, as CLM5 only permitted land use changes at the beginning of every year. In order to simulate cover cropping at our study site DE-RuS, we implemented a new CFT for a greening mix cover crop (or $covercrop_1$).

$$
\begin{aligned}
&if\ \ harvdate\,(p) \geq \mathrm{hd}_1\ \ and\ \ ivt\,(p) = crop_1\ \ then\\
&\qquad ivt\,(p) = crop_2\\
&\qquad croplive\,(p) = false\\
&\qquad idop\,(p) = not\_planted\\
&\qquad use\_grainproduct = true\\
&else\ \ if\ \ harvdate\,(p) \geq \mathrm{hd}_2\ \ and\ \ ivt\,(p) = crop_2\ \ then\\
&\qquad ivt\,(p) = crop_3\\
&\qquad croplive\,(p) = false\\
&\qquad idop\,(p) = not\_planted\\
&\qquad use\_grainproduct = true
\end{aligned}
$$

Figure 3.2: This figure illustrates the key variables and parameters involved in the definition of crop rotation within the new subroutine, written in Fortran code. Harvdate is the harvest day of the current simulation year and hd is the customizable harvest date of the respective CFT, p is the simulated patch on the model grid, ivt is the simulated CFT, $crop_{1\text{-}3}$ represent the user-specified CFTs to the rotated, idop is the planting day and use_grainproduct is a flag to define whether the grain carbon of simulated crop is to be harvested into the food pool or not. If this flag is set to false, the plant carbon and nitrogen are transferred to the soil litter pool and not allocated to the food product pool upon harvest of the crop.

3.2.3 Study sites and validation data

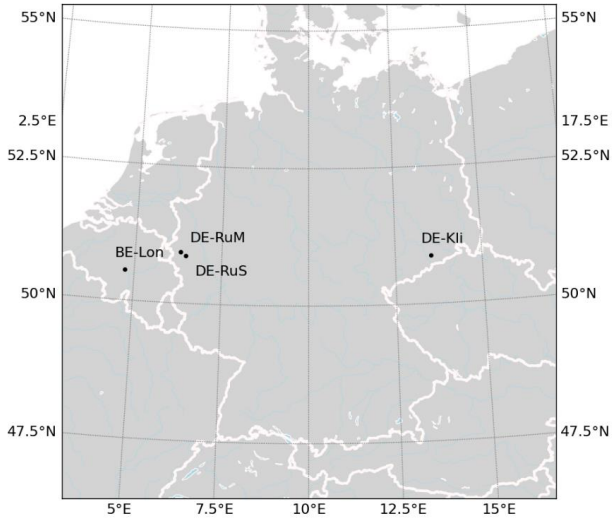

Figure 3.3: ICOS and TERENO cropland study sites Selhausen (DE-RuS), Merzenhausen (DE-RuM), Klingenberg (DE-Kli) and Lonzée (BE-Lon)

The CLM5 model was set up for four European cropland sites: Selhausen, Merzenhausen, Klingenberg and Lonzée (Figure 3.3). These sites were selected mainly for their excellent continuous measurements of surface energy fluxes. Selhausen (50.86589°N, 6.44712°E) is part of the TERENO Rur Hydrological Observatory (Bogena at al., 2018) as well as the Integrated Carbon Observation System (ICOS, 2020). The test site covers an area of approximately 1 km x 1 km and is located in the catchment of the Rur river (Bogena et al., 2018). Selhausen had

a crop rotation of sugar beet (Beta vulgaris), winter wheat (Triticum aestivum) and winter barley (Hordeum vulgare), fewer times also rapeseed (Brassica napus) and potatoes (Solanum tuberosum) from 2015 to 2019. Cover crops such as oilseed radish or cover crop mixes are planted occasionally between two main crop rotations. Continuous records of meteorological variables, soil specific observations, as well as greenhouse gas and energy fluxes are available for Selhausen since 2011. Regular LAI measurements are available since 2016 (Ney and Graf, 2018).

Merzenhausen (50.93033°N, 6.29747°E) is located at approximately 14 km from Selhausen and is also part of the TERENO Rur Hydrological Observatory. The crop rotation of the site includes sugar beet (*Beta vulgaris*), winter wheat (*Triticum aestivum*), winter barley (*Hordeum vulgare*), rape seed (*Brassica napus*) and occasionally catch cover crop mixes. For Merzenhausen, continuous records of meteorological variables, soil specific observations and energy fluxes are available since 2011 and LAI measurements from 2016 – 2018.

Klingenberg (50.89306°N, 13.52238°E) is an ICOS cropland site located in the mountain foreland of the Erzgebirge that is operated by the Technical University Dresden (TU Dresden) (ICOS, 2020; Prescher et al., 2010). The site is characterized as managed cropland with a 5-year planting rotation of rapeseed (*Brassica napus*), winter wheat (*Triticum aestivum*), maize (*Zea mays*), spring and winter barley (*Hordeum vulgare*) (Kutsch et al., 2010). Since 2004, data on ecosystem fluxes (including net ecosystem and net biome productivity), meteorological variables and soil observations are collected. Furthermore, biomass observations and agricultural management information are available for this site.

The cropland site Lonzée (50.553°N 4.746°E) in Belgium is also part of ICOS (Buysse et al., 2017). It has been planted in a four-year rotation cycle with sugar beet (*Beta vulgaris*), winter wheat (*Triticum aestivum*), potato (*Solanum tuberosum*) since 2000 with Mustard as a cover crop after winter wheat harvest (Moureaux, 2006; Moureaux et al., 2008). For Lonzée, continuous records of meteorological variables, EC flux data and LAI (GLAI and GAI) measurements are available from 2004 onwards. General information on the ICOS study sites such as climatic conditions, soil types etc. is provided on the ICOS Carbon Portal under the respective site codes (ICOS, 2020).

At all sites, the application of mineral fertilizer and herbicides/pesticides as well as occasional application of organic fertilizer is regular management practice. Station data required to force CLM, i.e. meteorological variables (see following section), were measured as block averages over 10 minutes or at higher resolutions, gap-filled using linear statistical relations to nearby stations where possible (Graf, 2017), or otherwise, by marginal distribution sampling within the software package REddyProc (Wutzler et al., 2018). Fluxes required for model validation (i.e. net ecosystem CO_2 exchange (NEE), latent heat flux (LE), sensible heat flux (H), soil heat flux (G) and gross primary production (GPP)) and net radiation (Rn), were either measured (G and R_n) or computed from turbulent raw measurements (frequency $\geq 10\ s^{-1}$) using the eddy-covariance method, for 30-minute block averages by the site PIs. Subsequently, gaps were filled and GPP estimated from NEE using REddyProc (Wutzler et al., 2018). More details on quality control, filling of longer gaps and by nearby stations, correction of soil heat flux and energy balance closure analysis are given in Graf et al. (2020) and specifically for DE-RuS and DE-RuM including LAI measurements in Reichenau et al. (2020). The long-term annual energy balance closures of the sites DE-RuS, DE-Kli and BE-Lon were approximately 79%, 77% and 76%, respectively, according to analyses in Graf et al. (2020) and 76% at DE-RuM according to an earlier study by Eder et al. (2015). All half-hourly meteorological and flux data were aggregated to hourly averages to match our customized CLM forcing time step. Site-specific

measurement records of latent and sensible heat fluxes, net ecosystem exchange (NEE), LAI, soil temperature and soil moisture were used as validation data for the simulation runs. Forcing variables were always used in gap-filled form, while validation variables were used in un-filled, quality-filtered form. Continuous measurements of meteorological variables and land-atmosphere exchange fluxes are available via the respective data portals (Kunkel et al., 2013; ICOS, 2020; TERENO, 2020).

Table 3.2: ICOS and TERENO cropland study site location coordinates and altitude A [msl], soil types, Köppen-Geiger climate classification based on Peel et al. (2007), approximate mean annual temperature T [°C], mean annual precipitation amounts P [mm/a] and corresponding reference. Textural fractions for the top soil layers (up to 50 cm) at each study site are provided in Table A3.

Site/ID	Project	Location	A	Soil type	Climate	T*	P*	Reference
Selhausen DE-RuS	TERENO ICOS	50.865°N 6.447°E	104.5	Luvisol	Cfb - temperate maritime	10	698	Ney and Graf (2018)
Merzenhausen DE-RuM	TERENO	50.930°N 6.297°E	100	Cambisol	Cfb - temperate maritime	10	698	Bogena et al. (2018)
Klingenberg DE-Kli	ICOS	50.893°N 13.522°E	478	Gleysoil	Cfb – suboceanic, subcontinental	8	766	Grünwald (personal communication, 2020)
Lonzée BE-Lon	ICOS	50.553°N 4.746°E	167	Luvisol	Cfb - temperate maritime	10	800	Buysse et al. (2017)

* Reference periods: 1961-2010 for DE-RuS (adapted also for DE-RuM), 2005-2019 for DE-Kli and 2004-2017 for BE-Lon.

3.3 Experimental design and analyses

3.3.1 Model implementation

For the single point study sites, CLM was run in point mode with only one grid cell and forced with site specific hourly meteorological data. The annual fertilization amounts at the single point study sites were adjusted according to documented amounts of applied fertilizer that ranged between 12 and 20 gNm^{-2}. In CLM5, the potential photosynthetic capacity as well as the total amount of assimilated carbon during the phenology stages are regulated by the availability of soil nitrogen (Lawrence et al., 2018). With modern fertilization practices in Europe, nitrogen is not assumed to be a limiting factor for the studied sites.

In order to balance ecosystem carbon and nitrogen pools, gross primary production and total water storage in the system, a spin-up is required (Lawrence et al., 2018). An accelerated decomposition spin-up of 600 years and an additional spin-up of 400 years was conducted for each site with the BGC-Crop module (Lawrence et al., 2018; Thornton and Rosenbloom, 2005). The simulated conditions at the end of the spin-up were then used as initial conditions for the following simulations.

In order to test the winter wheat representation, several simulations were conducted for all winter wheat years at the sites DE-RuS, DE-RuM, DE-Kli and BE-Lon. In a first step, the impact of each modification was assessed individually by simulating one winter wheat year at the site DE-RuS using four different model configurations: (1) the default model and default parameter set (control), (2) the default model with the new parameter set (control + crop specific), (3) the extended winter wheat model with the default parameter set (new routine), and (4) the extended winter wheat model with the new parameter set (new routine + crop specific). Further evaluations for the other study sites and years were conducted for the combined winter wheat modifications CLM_WW (extended

model with winter wheat subroutines and new crop specific parameterization) in comparison to control simulations (default model configuration and default parameterization of winter wheat).

For the evaluation of the crop specific parameter sets for sugar beet and potatoes, simulations were run with the new parameterizations at the sites DE-RuS and BE-Lon over several years. For both sites, control simulations were conducted without the new parameter set, in which both CFTs sugar beet and potatoes are simulated as a spring wheat by default. Furthermore, an evaluation of the default parameterization for the CFT temperate corn at the site DE-Kli is included in the appendix (Figure A1, Table A4).

The cover cropping and crop rotation scheme was tested for two practical cases at DE-RuS. From 2016 to 2017, planting was altered at DE-RuS from barley (here represented by the CFT for spring wheat) in 2016 to sugar beet in 2017 with a greening mix cover crop in between (winter months 2016/2017). In order to simulate this common cover cropping practice, we implemented a new CFT for a greening mix cover crop (or covercrop$_1$). For the years 2017 to 2019 at DE-RuS, the subroutines ability to simulate realistic crop rotation cycles was tested by changing the simulated CFT from sugar beet (2017) to winter wheat (2017-2018) and then to potatoes (2019). In this step, simulations were run with the previously tested crop specific parameterizations for sugar beet, potatoes and winter wheat. Simulation results were again compared to a control simulation run, where a consecutive growth of spring wheat is simulated.

3.3.2 Evaluation of model performance

For statistical evaluation of the model results, the root mean square error (RMSE), the bias (BIAS) and the Pearson correlation (r) were chosen as performance metrics:

$$RMSE = \sqrt{\frac{1}{n}\sum_{i=1}^{n}(x_i - y_i)^2}, \tag{3.7}$$

$$BIAS = \sum_{i=1}^{n}(x_i - y_i) / \sum_{i=1}^{n}(y_i), \tag{3.8}$$

$$r = \frac{\sum(x_i - \bar{x})(y_i - \bar{y})}{(n-1)\sigma_x \sigma_y}, \tag{3.9}$$

where n is the total number of time steps (days or years), x_i and y_i are the simulated and the observed values of a given variable at every time step i, and the overbar represents the mean value, and σ_x and σ_y are the standard deviations of the simulated and observed data respectively.

The statistical evaluation was conducted for daily simulation output and daily observation data for the variables NEE, LE, H and Rn.

3.4 Results

3.4.1 Winter cereal representation

The impact of the new winter wheat specific parameterization and the new winter wheat routine, as well as the combination of both is illustrated in Figure 3.4. Here we show simulated LAI for the default model and default parameter set (control), the default model with the new parameter set (control + crop specific), the extended winter wheat model with the default parameter set (new routines) and the extended winter wheat model with the new parameter set (new routines + crop specific).

Using only the new crop specific parameter set with the default model configuration resulted in slightly higher LAI values compared to the control run but did not reach the observed maximum LAI values and the growth cycle duration. The implementation of the winter wheat subroutines using the default parameter set led to a more realistic reproduction of the growth cycle duration compared to the control run, but did not yield good correspondence with observed LAI magnitudes. The combination of the new crop specific parameter set and the new winter wheat subroutines resulted in the most realistic LAI dynamics (Figure 3.4). As previously described by Lu et al. (2017), the default vernalization routine reaches a factor of 1 (fully vernalized) shortly after planting when the first frost occurs. This induced an unrealistically early commencement of the grain fill stage within two months after planting in the control run (November or December). The default vernalization also resulted in peak LAI occurring too early in the year, leading to significantly lower photosynthesis compared to the observations. This also applies to the implementation of the new crop-specific parameter set, which generally leads to slightly higher LAI values.

In the extended winter wheat model, the adapted vernalization routine produces lower initial vernalization factors which reduce the growing degree days. This leads to later onset of the leaf emergence and grain fill stage and allows a more realistic representation of the LAI cycle and peak in combination with the new crop specific parameterization.

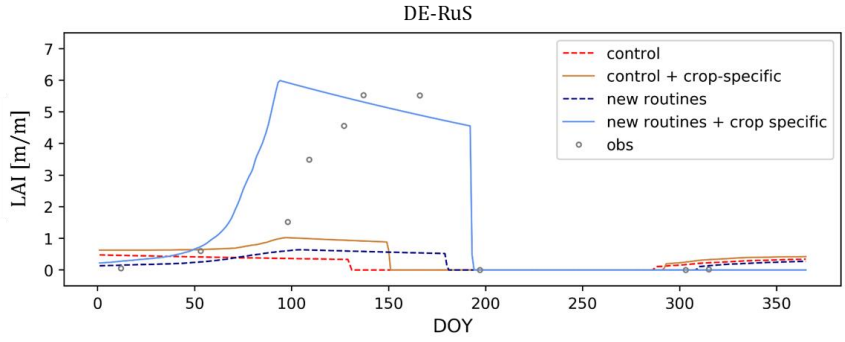

Figure 3.4: Daily simulation results for the LAI, simulated with default model and the default parameter set (control), the default model with new parameter set (control + crop specific), the extended winter wheat model with default parameterization (new routines) and the extended model with the new parameter set (new routines + crop specific), compared to point observations for a winter wheat year at DE-RuS.

In further evaluations, the combined winter wheat package, including the new crop specific parameterization and the extended winter wheat subroutines is implemented in CLM_WW simulations and compared to control runs (Figure 3.5). For all study sites and simulation years, CLM_WW simulations resulted in a much better

representation of the growth cycle and corresponding seasonal LAI variation and magnitudes compared to control simulations (Figure 3.5). Also, the temporal pattern of energy fluxes and NEE were improved with CLM_WW compared to the control run.

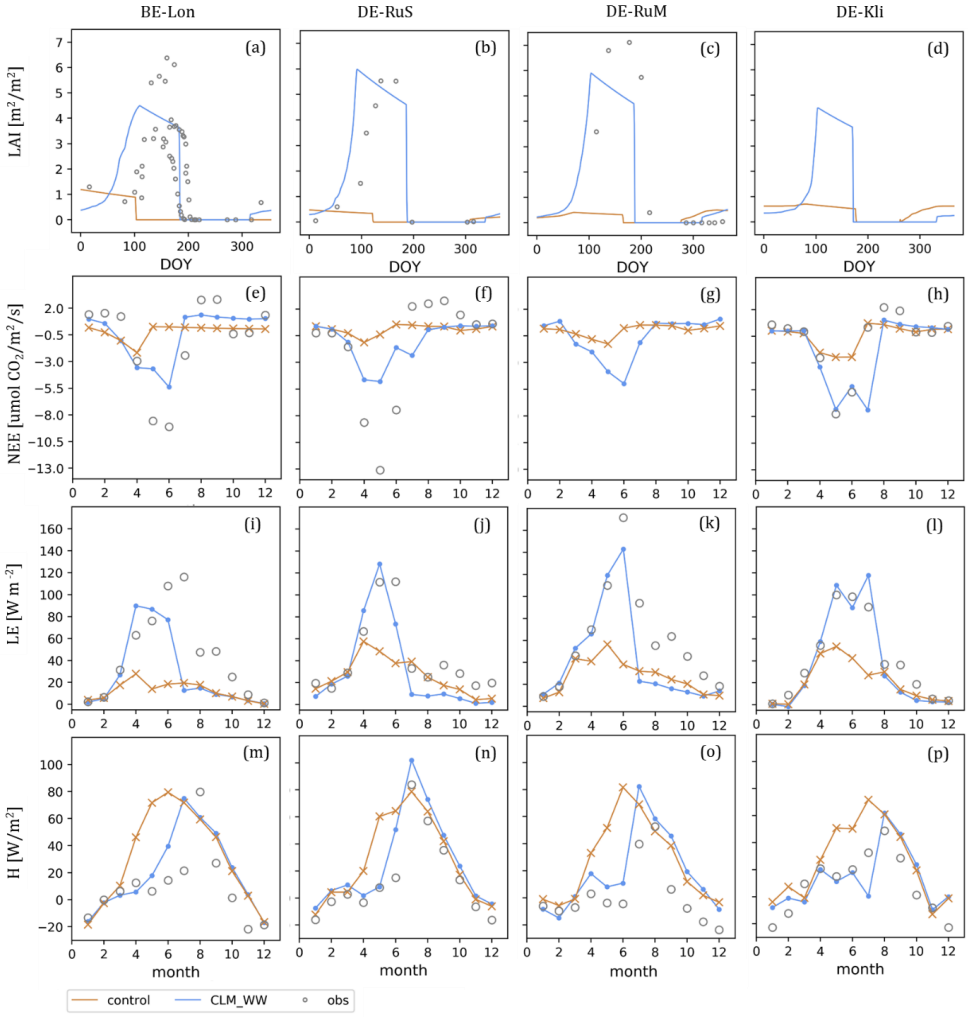

Figure 3.5: Simulation results of (**a-d**) LAI and simulation results averaged for each month of (**e-h**) NEE, (**i-l**) LE, and (**m-p**) H for all winter wheat years (see) at the sites (from left to right) BE-Lon, DE-RuS, DE-RuM and DE-Kli. Simulation results from the new routine with crop specific parameterization – CLM_WW (blue) are compared to control simulations (orange) and available site observations (grey) of LAI (all available point observations plotted) and fluxes (averaged over all respective years and for each month respectively). Corresponding performance statistics for daily simulation results during the crop growth cycle are listed in Table 3.4..

In general, CLM_WW yielded LAI peak magnitudes similar to observations at the sites BE-Lon, DE-RuS and DE-RuM (Figure 3.5). For DE-Kli, site-specific observations of the LAI were not available, but simulated LAI magnitudes for DE-Kli using CLM_WW are similar to those for BE-Lon. For the BE-Lon site, CLM_WW simulated peak LAI magnitudes are close to the observations. An exception is the year of 2015, where CLM_WW

underestimated the unusually high LAI values observed in May and June, which ranged from 5.40 to 6.38 m^2/m^2. For BE-Lon, faster growth was simulated in the early growing stage of winter wheat, resulting in a more gradual increase in LAI compared to the other sites (Figure 3.5). This is related to higher air temperatures at BE-Lon early in the growing stage (especially in February) that enabled more simulated growth compared to the other sites.

Overall, the LAI peak simulated with CLM_WW occurred about one month earlier than observed, suggesting that maturation was reached too early. This is also reflected in the simulated CLM_WW harvest dates that are approximately one month earlier than the recorded dates (Table 3.3). While the planting date is the same for the control run and the CLM_WW simulations, CLM_WW generally resulted in a better match of simulated and recorded harvest dates (1.5 to 2 months later than control run).

The correlation of simulated grain yield and site records was significantly improved by up to 87 % in CLM_WW simulations compared to the control run. At the DE-RuS site, CLM_WW resulted in a grain yield of 9.15 t/ha that is very close to the observed value of 9.2 t/ha, while grain yield is strongly underestimated in the control run (1.17 t/ha). For DE-Kli, the CLM_WW simulated crop yield matched the recorded yield data very well for the year 2016 and was overestimated for 2011 by approximately 16 %. The control run resulted in an underestimation of yield by more than 80 % (Figure 3.6, Table 3.3). For BE-Lon the simulated crop yield is underestimated compared to site harvest records (Figure 3.6, Table 3.3). While CLM_D simulations underestimated the grain yield by approximately 85 – 90 %, CLM_WW underestimated yield by only 18 - 36 % at BE-Lon. The simulated yields by CLM_WW for the individual years show only minimal variations with values from 8.12 to 8.16 t/ha, while the measured yields ranged from 9.92 to 12.88 t/ha, indicating that CLM did not capture the inter-annual yield variation very well (Table 3.3).

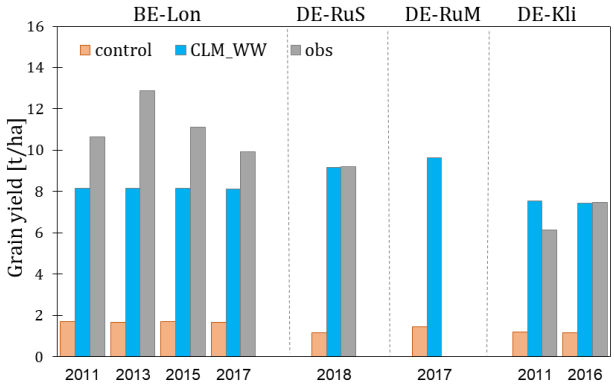

Figure 3.6: Annual grain yield [t/ha] simulated with the control run (orange) and the extended winter wheat model with crop specific parameterization (blue), compared to recorded harvest yields (grey) for all simulated winter wheat years (indicated on the x axis) at the sites BE-Lon, DE-RuS, DE-RuM and DE-Kli.

Table 3.3: Simulated annual planting and harvest dates and grain yield [tDM/ha] by CLM_WW and CLM_D simulations (calculated using the peak daily grain carbon throughout the growth cycle) compared to recorded harvest dates and grain yield (Obs) for all simulated winter wheat years at the sites BE-Lon, DE-RuS, DE-RuM and DE-Kli. For CLM simulation results, grain yield is calculated from grain carbon which is assumed to be 45 % of the total dry weight.

Year	Source	Planting date	Harvest date	Grain Yield [tDM/ha]
BE-Lon				
2010/2011	CLM_D	11.09.2010	10.05.2011	1.71
	CLM_WW	11.09.2010	05.07.2011	8.14
	Obs	*14.10.2010*	*16.08.2011*	*10.64**
2012/2013	CLM_D	12.09.2012	19.04.2013	1.68
	CLM_WW	12.09.2012	25.06.2013	8.16
	Obs	*25.10.2012*	*12.08.2013*	*12.88*
2014/2015	CLM_D	09.09.2014	20.04.2015	1.71
	CLM_WW	09.09.2014	01.07.2015	8.15
	Obs	*15.10.2014*	*02.08.2015*	*11.13*
2016/2017	CLM_D	11.09.2016	02.05.2017	1.68
	CLM_WW	11.09.2016	24.07.2017	8.12
	Obs	*29.10.2016*	*30.07.2017*	*9.92*
DE-RuS				
2017/2018	CLM_D	29.09.2017	17.05.2018	1.17
	CLM_WW	29.09.2017	27.06.2018	9.15
	Obs	*25.10.2017*	*16.07.2018*	*9.2*
DE-RuM				
2016/2017	CLM_D	27.09.2016	15.05.2017	1.45
	CLM_WW	27.09.2016	30.06.2017	9.65
	Obs	*17.10.2016*	*22.07.2017*	-
DE-Kli				
2010/2011	CLM_D	15.09.2009	23.07.2011	1.19
	CLM_WW	15.09.2009	11.08.2011	7.53
	Obs	*02.10.2010*	*22.08.2011*	*6.12*
2015/2016	CLM_D	17.09.2015	24.07.2016	1.17
	CLM_WW	17.09.2015	28.07.2016	7.44
	Obs	*18.09.2015*	*24.08.2016*	*7.48*

*: Grain yield estimated from 18.09 t/ha total biomass (stem and ear) yield according to stem and ear (grain) biomass yield ratios measured for other winter wheat years at the same site.

Overall, the better representation of the winter wheat growing cycle by CLM_WW can also be inferred from the simulated surface energy fluxes (Figure 3.5). In terms of net radiation, both CLM_WW and the control run are very close to the observations (Table 3.4). However, CLM_WW was able to better capture seasonal variations of surface energy fluxes during the growing cycle of the crop (Figure 3.5). The correlation coefficients for the energy fluxes (LE, H and Rn) calculated over the period from planting to harvest date for daily simulation results and daily observation data improved for all sites (Table 3.4). Highest correlations were reached for the sites DE-Kli with r values of 0.62 and 0.71 and for BE-Lon with r values of 0.5 and 0.46 for sensible heat and latent heat flux respectively (Table 3.4). Due to the simulated LAI peak being too early, latent heat flux is underestimated by CLM_WW (Figure 3.5, Table 3.4). The high latent heat fluxes measured at BE-Lon and DE-Kli in the later months of the year (from day 220 onwards) reflect the growth of a cover crop. At both the BE-Lon site as well as at the DE-Kli site, cover crops are typically sown after harvest of winter wheat (mustard at BE-Lon, radish and brassica at DE-Kli), and they strongly affect surface energy fluxes later in the year. In contrast, in the control simulations, as well as in CLM_WW, the crop field were simulated as fallow after the harvest of winter wheat (Figure 3.5). While the correlation of the latent and sensible heat flux during the growing cycle of the crop is generally increased with the CLM_WW model, the overall annual correlation is still relatively poor due to the influence of cover cropping and poor representation of post-harvest field conditions (annual performance metrics are included appendix, Table A5).

Table 3.4: Bias, RMSE and *r* for the control run and CLM_WW simulated daily NEE [umol CO_2 W m^{-2} s^{-1}], LE [W m^{-2}], H [W m^{-2}] and Rn [W m^{-2}] at the sites BE-Lon, DE-RuS, DE-RuM and DE-Kli respectively. Values were calculated over the time period between recorded planting and harvest dates (averaged over all winter wheat years at each site) using simulation output and observation data at daily time step.

CFT	WINTERWHEAT							
Site	BE-Lon		DE-RuS		DE-RuM		DE-Kli	
Year(s)	2010/2011 2012/2013 2014/2015 2016/2017		2017/2018		2016/2017		2010/2011 2015/2016	
Model	*control*	*CLM_WW*	*control*	*CLM_WW*	*control*	*CLM_WW*	*control*	*CLM_WW*
NEE								
Bias	-0.87	-0.37	-1.01	-0.61	-	-	-0.56	0.50
RMSE	6.34	4.96	7.73	7.58	-	-	3.80	3.27
r	-0.13	0.46	0.21	0.33	-	-	0.29	0.56
LE								
Bias	-0.72	-0.13	-0.47	-0.23	-0.55	-0.09	-0.47	-0.77
RMSE	61.96	50.73	52.47	52.65	67.17	48.67	44.64	56.75
r	0.35	0.46	0.21	0.24	0.50	0.67	0.61	0.71
H								
Bias	5.56	1.35	4.24	1.70	-8.49	-2.74	4.99	3.10
RMSE	45.97	27.63	40.93	39.94	47.26	32.81	49.30	35.08
r	0.42	0.50	0.45	0.48	0.21	0.36	0.47	0.63
Rn								
Bias	-0.18	-0.05	-0.17	-0.13	-0.09	0.08	-0.03	-0.09
RMSE	36.11	38.01	47.28	45.15	37.34	46.43	45.17	44.49
r	0.80	0.81	0.68	0.69	0.78	0.97	0.71	0.73

Furthermore, CLM_WW was generally better able to match NEE observations compared to control runs, partly due to the better representation of the seasonal LAI variations (Figure 3.5). During the growing season of winter wheat, the negative peak in NEE, coincides with the peak in LAI. Negative NEE values indicate a carbon sink and happen when the crop gains more carbon through photosynthesis than is lost through respiration. Correlation improved (comparing CLM_WW to the control run) from 0.13 to 0.46 for BE-Lon, from 0.21 to 0.33 for DE-RuS and from 0.29 to 0.56 for DE-Kli. The resulting correlation for CLM_WW simulations is still relatively low due to an underestimation of the cumulative monthly NEE during seasons with high NEE at BE-Lon and DE-RuS. For DE-Kli, CLM_WW was able to match NEE observed at peak LAI very well, but late seasonal NEE (July), shortly before harvest, is overestimated by CLM_WW resulting in a low overall agreement with observation data. Furthermore, post-harvest field observations at BE-Lon, DE-RuS and DE-Kli indicate that heterotrophic respiration from soil organic matter and litter results in a carbon source which is not simulated well in CLM (no GPP, near zero NEE) (Figure 3.5). This poor representation of post-harvest field conditions is reflected in low correlations over the whole year (Table A5).

3.4.2 Crop specific parameterization of sugar beet and potatoes

The crop specific parameter sets were tested for several years with sugar beet and potatoes planting at BE-Lon and DE-RuS respectively. The performance in reproducing seasonal variations and magnitudes of energy fluxes was strongly improved with the crop specific parameterization. Correspondingly, simulations with the crop specific parameter sets for both sugar beet and potatoes were able to reasonably capture seasonal variations and peak values of LAI as well as growth cycle length and harvest time (Figure 3.7 and Figure 3.8). The control run in CLM uses the spring wheat parameterization for these crop types and therefore reproduced the growth cycle and seasonal LAI of spring wheat, while simulations using the crop-specific potato and sugar beet parameterizations better captured harvest date and growth cycle of these crops.

The improved growth cycle representation with crop specific parameters also led to more accurate simulation of energy fluxes. For sugar beet at BE-Lon, the latent heat flux at peak LAI corresponds well with observed values while being underestimated before and after peak LAI and hence the sensible heat flux is overestimated at these times (Figure 3.7). Seasonal variations of energy fluxes and magnitudes were also captured much better in simulations with the new parameterization. The simulations with crop specific parameters show slightly better net radiation correlations for both the sugar beet and potato CFTs at each site, compared to the control run (Table 3.5). The correlation between simulated and observed latent heat flux for sugar beet were strongly improved by changing the parameters (0.11 to 0.55 for DE-RuS and 0.21 to 0.55 for BE-Lon). The same is true for the simulated sensible heat flux for sugar beet (0.04 to 0.76 for DE-RuS and 0.08 to 0.51 for BE-Lon site). The NEE for the sugar beet CFT is underestimated during peak LAI periods in the control run, resulting in poorer correlations compared to latent and sensible heat flux and net radiation (Figure 3.7). Simulations with the crop specific parameter set resulted in a reduction in negative bias for NEE and reached higher correlation compared to the control simulation (0.03 to 0.37 for DE-RuS and 0.05 to 0.64 for BE-Lon).

Similar improvements can be observed for the new potato parameterization while the correlation of simulation results with observation data is generally lower compared to the sugar beet CFT (Figure 3.8, Table 3.5). Seasonal LAI variations, growing cycle length and corresponding energy flux variations are improved in simulations with the new parameter set. Both the latent and the sensible heat flux are strongly improved at DE-RuS with correlation coefficients of 0.54 and 0.45 respectively for CLM_WW simulations. For BE-Lon, the improvement in correlation is slightly lower for both latent and sensible heat flux compared to DE-RuS. The seasonal variation of the NEE at BE-Lon is reasonably captured while monthly sums are overestimated with both parameterizations. Simulations of the NEE using the crop specific parameter set yielded a slightly better correlation of 0.58 compared to the control simulation that resulted in a correlation of 0.43 (Table 3.5).

Table 3.5: Bias, RMSE and *r* for the simulated daily NEE [µmol CO_2 W m^{-2} s^{-1}], LE [W m^{-2}], H [W m^{-2}] and Rn [W m^{-2}]) using the crop specific parameterization (*specific*) for the CFTs sugar beet and potatoes at the sites BE-Lon and DE-RuS respectively. Results are compared to those from the control simulation runs (*control*). Values were calculated over the time period between recorded planting and harvest dates (averaged over all respective CFT years at each site) using simulation output and observation data at daily time step.

CFT	SUGARBEET				POTATOES			
Site	DE-RuS		BE-Lon		DE-RuS		BE-Lon	
Year(s)	2017		2008 2016		2019		2010 2014 2018	
Parameter set	*control*	*specific*	*control*	*specific*	*control*	*specific*	*control*	*specific*
NEE								
Bias	-0.59	-0.75	0.05	-0.05	-	-	19.73	19.56
RMSE	9.1	5.94	6.19	3.75	-	-	5.24	5.21
r	-0.03	0.37	0.05	0.64	-	-	0.43	0.58
LE								
Bias	-0.32	0.01	-0.37	-0.35	-0.28	0.25	0.26	0.09
RMSE	58.44	24.47	60.09	48.31	60.94	50.58	43.41	40.05
r	0.11	0.55	0.21	0.55	0.01	0.54	0.5	0.53
H								
Bias	1.65	0.45	1.73	1.61	1.01	-0.38	0.5	0.22
RMSE	42.77	17.24	39.75	33.45	51.61	29.9	34.06	31.17
r	-0.04	0.76	-0.08	0.51	-0.1	0.45	0.18	0.31
Rn								
Bias	-0.02	0.04	-0.11	-0.11	-0.04	0.04	-	-
RMSE	19.74	15	37.47	35.87	48.39	49.88	-	-
r	0.5	0.51	-0.22	-0.22	0.56	0.57	-	-

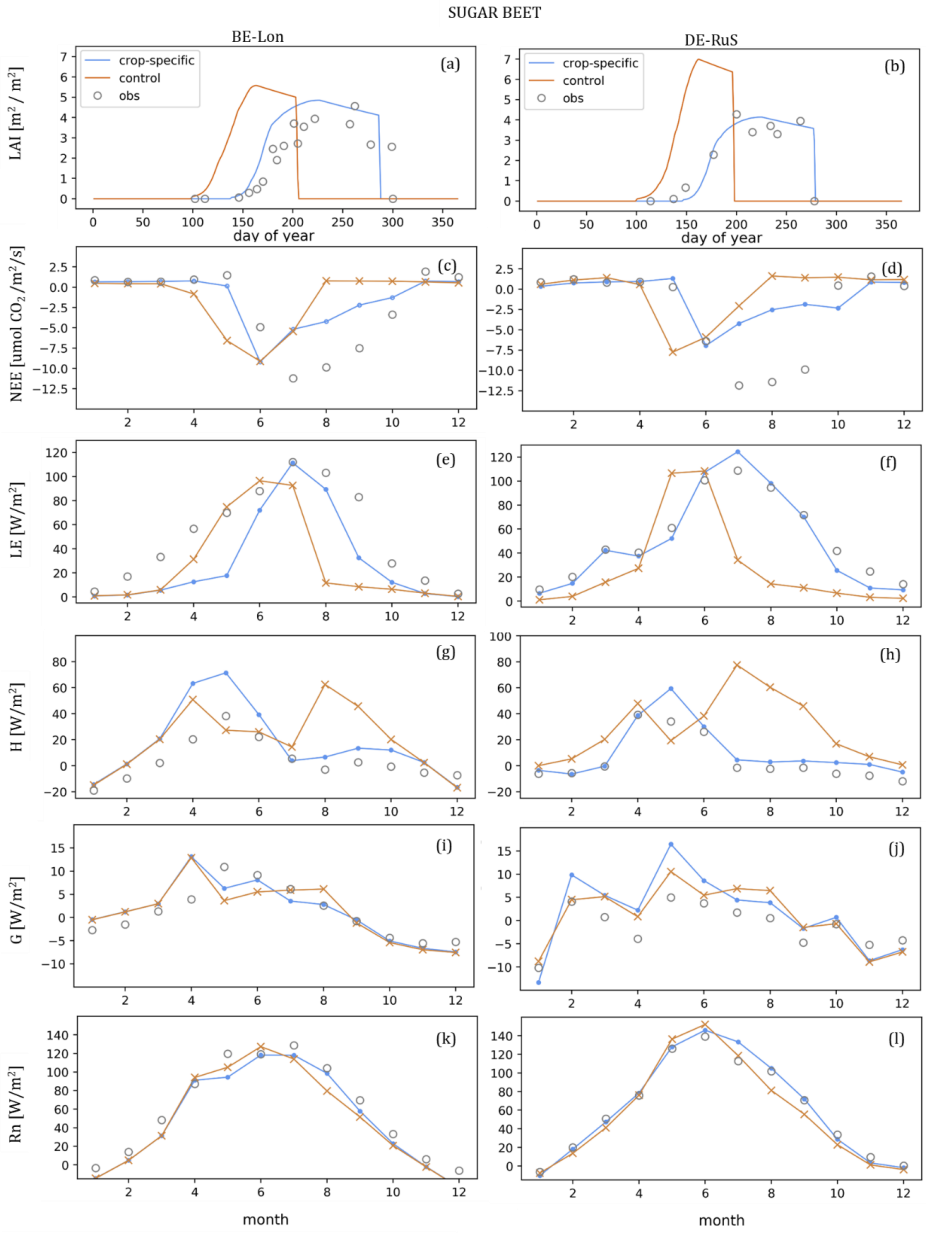

Figure 3.7: Simulation results of (**a-b**) LAI and monthly averaged simulation results of (**c-d**) NEE, (**e-f**) LE, (**g-h**) H, (**i-j**) G and (**k-l**) Rn for all sugar beet years (see Table 3.5) at the sites (left) BE-Lon and (right) DE-RuS. Simulation results for the control run (orange) and the crop specific parameter set (blue) are compared to available site observations (grey) of LAI (all available point observations plotted) and fluxes (averaged over all respective years). Corresponding performance statistics for daily simulation results are listed in Table 3.5.

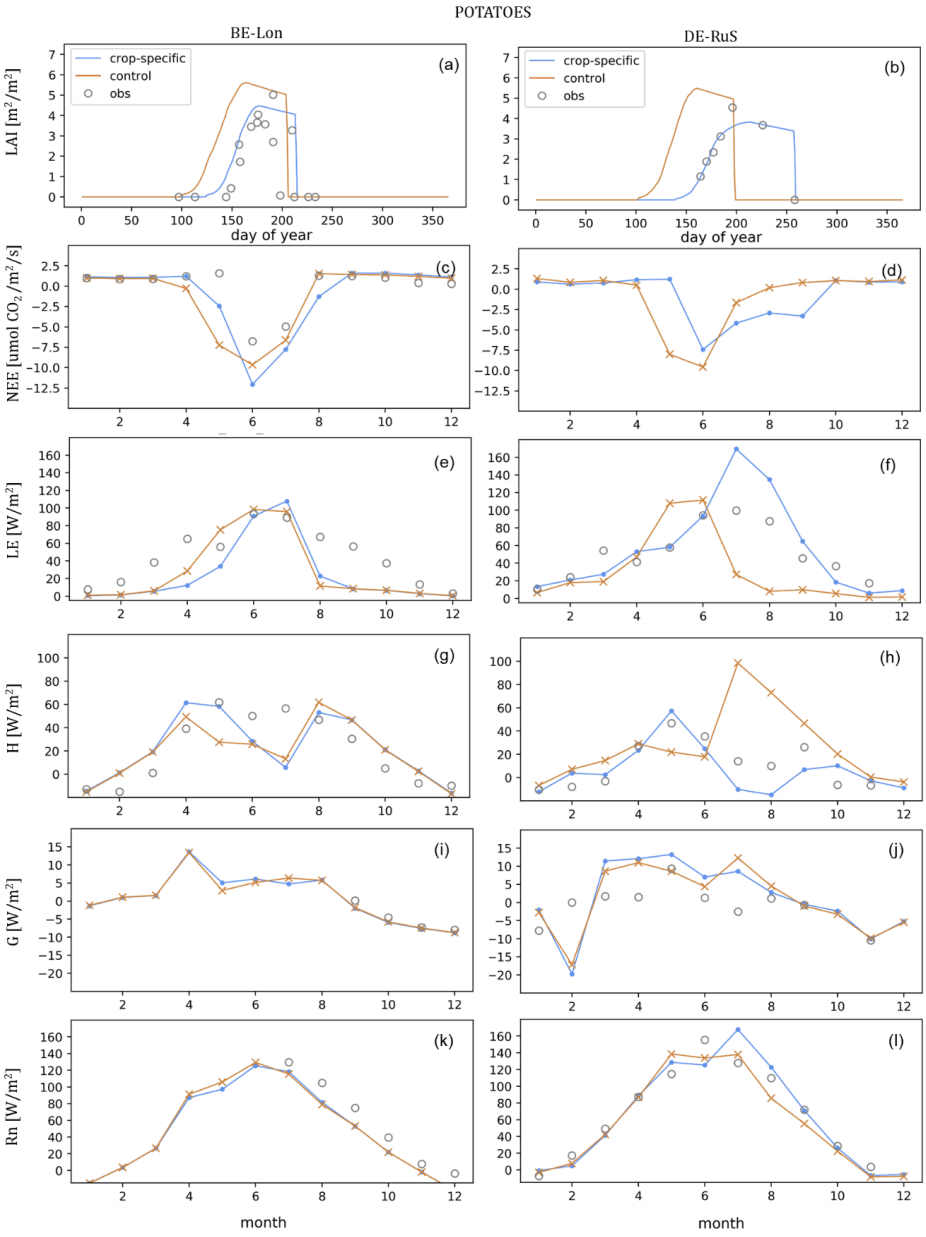

Figure 3.8: Simulation results of (**a-b**) LAI and monthly averaged simulation results of (**c-d**) NEE, (**e-f**) LE, (**g-h**) H, (**i-j**) G and (**k-l**) Rn for all potatoes years (see Table 3.5) at the sites (left) BE-Lon and (right) DE-RuS. Simulation results for the control run (orange) and the crop specific parameter set (blue) are compared to available site observations (grey) of LAI (all available observations plotted) and fluxes (averaged over all respective years). Corresponding performance statistics for daily simulation results are listed in Table 3.5.

3.4.3 Cover cropping and crop rotation scheme

The cover cropping scheme was tested for two fields of application: (1) simulation of a cover crop as a second crop growth onset within a single year, and (2) a more flexible crop rotation between different cash crops. In this step, simulations were run with the previously tested crop specific parameterizations for sugar beet, potatoes and winter wheat and results were again compared to a control simulation run, where a consecutive growth of spring wheat is simulated.

To test the first application of the cover cropping and crop rotation scheme, we simulated the cash crop and cover crop rotation cycle at DE-RuS from 2016 to 2017 (Figure 3.9). A greening mix was planted as a cover crop in between the cash crop rotation of barley (simulated using the spring wheat CFT) in 2016 and sugar beet in 2017. While only a consecutive growth cycle of spring wheat is simulated in the control run, the new routine was able to represent the crop rotation from barley to sugar beet in the following year as well as a cover crop in between the cash crop cycles. Both, the simulation of a cover crop and the rotation of cash crops strongly improved the representation of LAI in simulations with the new routine over multiple years, especially during winter months (Figure 3.9 and Figure 3.10). While in control simulations, the model assumed bare field conditions with no plant growth (LAI of 0) and very low latent heat flux, the new routine simulated the planting of a cover crop in autumn of 2016, which leads to an increase in latent heat flux related to increased transpiration. Statistical evaluation of the simulated latent heat flux for the time window after harvest of the first cash crop from August 2016 to April 2017 shows that with the new routine, the negative bias was reduced from 0.74 to 0.13 compared to control simulation results, resulting in an RMSE reduction by approximately 42 % (Figure 3.9).

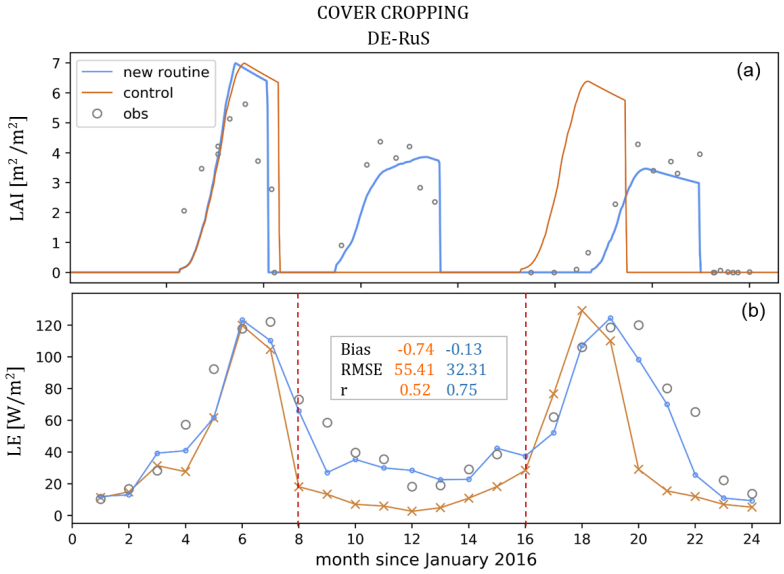

Figure 3.9: (**a**) Simulated LAI for cover cropping at DE-RuS with a barley (2016), greening mix cover crop (2016/2017) and sugar beet (2017) using the new cover cropping subroutine (blue) in comparison to control simulation results with the default phenology algorithm of CLM5 (orange). (**b**) Corresponding monthly averaged simulation results for the latent heat flux with

respective bias, RMSE and r for the time window between the red dashed lines (calculated using simulation output and observation data at daily time step). Available observation data are plotted in grey.

For the second case (DE-RuS), which represents a higher flexibility towards cash crop rotation, we simulated the years of 2017 to 2019. Here, the crop rotation switched from sugar beet in 2017 to winter wheat in 2017/2018 to potatoes in 2019 (Figure 3.10). In the control simulation, using the default CLM5 phenology algorithm, a consecutive cycle of spring wheat is simulated. The new routine was able to represent the rotation between different cash crops on the same field. This resulted in a much better correspondence of simulated LAI cycle and magnitudes with observations compared to control simulations. Statistical analysis of the latent heat flux showed an improvement of the RMSE (calculated for daily simulation output and observation data over these three years) from 43.74 to 32.94 and the correlation coefficient from 0.40 to 0.63 with the new routine. The improvement in simulated energy fluxes for each CFT individually is in accordance with the results presented in the previous chapters (0 and 0).

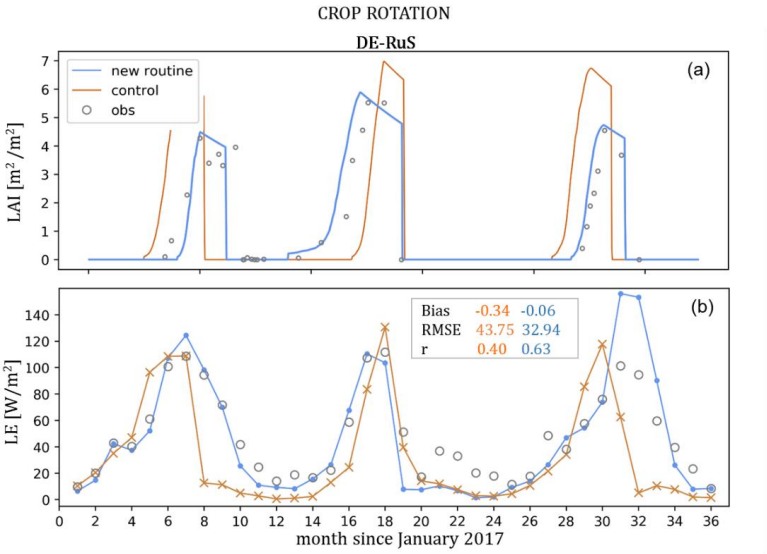

Figure 3.10: (**a**) Simulated LAI for crop rotation from sugar beet (2017) to winter wheat (2017/2018) and to potatoes (2019) at DE-RuS using the new cover cropping subroutine (blue) in comparison to control simulation results with the default phenology algorithm of CLM5 (orange). (**b**) Corresponding monthly averaged simulation results for the latent heat flux with respective bias, RMSE and r over the whole time interval (calculated using simulation output and observation data at daily time step). Available observation data are plotted in grey.

3.5 Discussion

All three modifications that were implemented in this study helped to improve the representation of cropland sites in CLM5. Similar to the findings of Lu et al. (2017) for CLM4.5, the implementation of their winter wheat routine resulted in a significant improvement in representing the seasonal LAI variations and surface energy fluxes during winter wheat growth. Next to maize and rice, wheat is one of the most important international food crops and among the most important cash crops in Germany (22.8 million tons winter wheat yield in 2019 nation-wide (Statista, 2020). In Germany and other western European countries, winter cereal varieties (e.g. winter rye, barley

and wheat) are more abundant than summer cereals due to climatic conditions (Palosuo et al., 2011; Semenov and Shewry, 2011; Thaler et al., 2012). With an average annual winter wheat yield of around 20 Mt/a for Germany, an improvement of 87 % in simulated yield with CLM_WW compared to the default model (as observed at the DE-RuS site in 2018) could result in a difference of several tens of millions of tons in total predicted annual yield on a nation-wide scale.

Despite the general improvement of winter wheat growth and yield simulated with the modified CLM_WW, there is still potential in further increasing the flexibility towards simulating different crop varieties and management practices. Due to the phenology algorithm of CLM5, a low simulated LAI can indicate a lower grain yield due to low biomass growth. Accordingly, the higher simulated LAI for the DE-RuS site was associated with a slightly higher simulated grain yield for DE-RuS compared to BE-Lon. However, this relationship is not reflected in the observations, as the measured grain yield is lower for DE-RuS compared to BE-Lon, although the observed LAI is higher for DE-RuS (Figure 3.5, Table 3.3).

In CLM, there are several variables that influence the simulated crop yield, such as LAI cycle and peak, length of the leaf emergence phase, harvest date, and water availability from the soil. Except for soil moisture, these variables are strongly correlated to the GDD scheme which suggests that the simulated crop yield profoundly depends on the GDD. The high sensitivity of simulated yield in CLM towards GDD is not reflected in actual field observation, where crop yield depends on a multitude of factor, environmental conditions (weather, nutrient availability, atmospheric CO_2) and management decisions. Underestimation of winter wheat yield at BE-Lon may be due to model deficiencies in representing the complex crop management practices, such as timing and type of fertilizer, ploughing crop varieties and the usage of different winter wheat varieties that can show different responses to water or heat stress, frost and have different grain productivities (White and Wilson, 2006; Bergkamp et al., 2018; Ceglar et al., 2019). In order to include different varieties of any crop, the list of CTFs could be extended with suitable plant parameterizations. However, this information is not readily available, due to a combination of measurement data scarcity and the complexity of the phenology algorithm and parameter scheme. The introduction of a phenology scheme based on plant physiological trait information in CLM could be a major improvement in this field (see Fisher et al., 2019), as plant trait information becomes more readily available (e.g. TRY Plant Trait Database, Kattge et al., 2011). Whether considering different varieties and cultivars of a crop is important for regional or global scale simulations remains to be evaluated. In general, as already noted by Lu et al. (2017), a more process based vernalization and cold tolerance routine would be useful to make this subroutine more applicable to other winter crops like rapeseed.

The early leaf onset and harvest for winter wheat simulated by CLM (both with the new routine and parameter set and the control run) could be met by adjusting the minimum date for planting within the CFT parameterization. This could be useful to easily improve the crop cycle representation in regional simulations, where planting patterns are similar for larger agricultural areas. However it would restrict the flexibility of the model to prognostically simulate planting dates.

In general, the simulated plant growth and resulting yield were highly sensitive to plant parameters that govern the growing degree calculation which in turn influence the phenological development and allocation of C and N. With only a limited number of CFTs in CLM, a discretization of plant parameters or varieties on a regional scale is not possible at this point. A potential solution, without introducing additional CFT´s, could be to account for key parameters for each CFT varying with climate and soil conditions for large scale simulations (e.g. by gridded

parameter sets). Furthermore, there is a need to evaluate and further discretise plant hydraulic properties (at this point one set of hydraulic parameters is applied to all types of crops) (Verhoef and Egea, 2014; Kennedy et al., 2019). Within the crop module of CLM5, the carbon allocation of crops is limited by soil water available to the plant. Thus, both an improved soil hydrology and an improved representation of plant hydraulics could play a major role in improving the quality of yield prediction by the model (Bassu et al., 2014; Kennedy et al., 2019). These plant hydraulic properties could be estimated by inverse modelling or data assimilation (e.g. by assimilating measurement data like NEE, LAI, soil moisture and/or energy fluxes using an augmented state-vector approach). In addition, data assimilation of e.g. in situ or remotely sensed soil moisture data and/or LAI could play a major role in increasing the accuracy of regional yield predictions (e.g. Guérif and Duke, 2000; Launay and Guerif, 2005; de Wit and van Diepen, 2007; Fang et al., 2008; Vazifedoust et al., 2009; Huang et al., 2015; Jin et al., 2018).

The default CLM5 does not account for the influence of weeds or cover crops and/or its litter on the carbon balance. There is a tool available for CLM5 that enables the simulation of transient land use and land cover changes (LULCC) (Lawrence et al., 2018). It was designed to simulate the effects of changing distributions of natural and crop vegetation, e.g. land use change from forest to agricultural fields and also allows for changes in crop type between years (Lawrence et al., 2018), but does not account for intra-annual changes of agricultural management on crop vegetated areas that happen in double and triple cropping scenarios. While this tool is useful to study general land use changes by changing the land cover type of individual land units, we found it lacks flexibility in accounting for changes within land units of the same land cover and does not account for all 64 CFTs. Furthermore, this tool changes the CFT of each column on the 1st of January every year according to prescribed values (customized). Thus, when using the CLM5 land-use change tool, for example to simulate the crop rotation from sugar beet in 2017 to winter wheat in 2017/2018 at DE-RuS, winter wheat would not be planted before autumn of 2018 (rather than in the same year as sugar beet is harvested) resulting in a long period of fallow field when switching from summer to winter crop (Figure 3.10). Here, the implementation of our cover cropping routine enabled a second onset of plant growth within a year (including the switch to another CFT). This resulted in a pronounced improvement in LAI curves and latent heat flux, especially during winter months, by simulating the growth of a cover crop. It also proved to be beneficial in representing realistic agricultural field conditions by allowing crop rotations with higher flexibility than the default model.

This new routine can be used to study cover cropping scenarios in future large-scale simulations. The effect of a cover crop during winter months on all crop land units where cash crops are grown in summer could be tested. This could also be tested for specific cash crops only. In addition, it is possible to simulate cover crop plantations based on harvest date thresholds. A defined maximum harvest date for any specific cash crop could define whether a cover crop such as winter wheat would be planted or not. For example, for all sugar beet land units with harvest dates before a certain threshold (e.g. day 290 of any given year) winter wheat could be planted as a cover crop during winter. If this harvest threshold were not reached and the summer crop is harvested late in the year, no cover crop would be planted. Alternatively, these harvest thresholds could define the type of cover crop, e.g. early harvest - winter wheat, late harvest – simple greening mix, etc. Also, historical land use information could be used to simulate realistic cover cropping and crop rotation scenarios. The succession of different crops from historical data could also be used to model the succession of crops for the future. In order to study large scale effects of cover cropping and common crop rotations, the CLM5 model would greatly benefit from further crop specific parameter sets for cover crops such as mustard, and further important cash crops.

In their approach, Lombardozzi et al. (2018) studied the effects of idealized cover crop scenarios by simulating winter crops in all crop regions throughout North America. They found that the effects of cover crops on winter temperatures is strongly related to plant height and LAI and emphasized the importance of biogeophysical effects and varietal selection when evaluating the climate mitigation potential of cover cropping (Lombardozzi et al., 2018). With our new routine, it is now possible to evaluate the biogeophysical effects of cover crops over longer time scales and in combination with typical cash crop rotations throughout agricultural areas. Also the ecological potential of different cover crop varieties could be evaluated. We anticipate that this modification will allow a more realistic representation of seasonal LAI in ecosystems where cover cropping and crop rotations are common management practices. The application of this routine is also of interest for areas with several cash crop cycles within a year like multiple annual crop cycles in India and China (Biradar and Xiao, 2011; Li et al., 2014; Sharma et al., 2015). We see further development potential for this routine and corresponding datasets to account for typical crop rotations and cover cropping scenarios for regional scale simulations (e.g. EU regulations and goals on the adoption of cover crops for climate change mitigation (Smit et al., 2019)).

3.6 Conclusion

The default CLM5 was extended by adopting the winter wheat representation of Lu et al. (2017), by including crop specific parameterization for winter wheat, sugar beet and potatoes and by the addition of a cover cropping subroutine that allows several growth cycles within one year. The model modifications were tested for the respective crops at four TERENO and ICOS cropland sites in Germany and Belgium, Selhausen (DE-RuS), Merzenhausen (DE-RuM), Klingenberg (DE-Kli) and Lonzée (BE-Lon), for multiple years. The main results drawn from this study are as follows:

- The implementation of the winter wheat subroutines led to a significant simulation improvement in terms of energy fluxes, leaf area index, net ecosystem exchange and crop yield (reduction of underestimation from 80 – 90 % to 18 – 36 % at test site BE-Lon, good match for the test sites DE-RuS and DE-Kli in 2016 and slight overestimation at test site DE-Kli in 2011)
- The model performance was strongly improved with the crop specific parameter sets for sugar beet and potatoes: seasonal variations and magnitudes of energy fluxes and LAI were better reproduced with RMSE reduction during the crop cycle by up to 57 % for latent and 59 % for sensible heat flux at test site DE-RuS.
- In most cases the modification of CLM5 led to better reproduction of measured NEE at the test sites. However, the model showed a general weakness in reasonably simulating the NEE on agricultural fields, especially the peak value and post-harvest conditions.
- The implementation of our cover cropping routine enabled a second onset of plant growth within a year and thus was able to better capture realistic field conditions after harvest. Winter time RMSE for latent heat flux was reduced by 42 %. Also, a higher flexibility in terms of crop rotations is now possible with CLM5.

We anticipate that our implementation of the winter wheat representation and specified parameterization will markedly improve yield predictions at regional scale for regions with a high abundance of winter cereal varieties. The cover cropping routine offers an improved basis on which to study the effects of large scale cover cropping on energy fluxes, soil water storage, soil carbon and nitrogen pools, as well as to investigate the role of different cover crops as natural fertilizer in future studies with CLM5. A more realistic representation of post-harvest field

conditions can play a crucial part in better representing the role of agriculture on regional and global energy and carbon fluxes and will be further developed and tested for regional scale simulations in future studies.

Despite our improvements, there is still a need to further develop certain functionalities and specific routines regarding the crop representation and land management in CLM5 in order to achieve better model performance for agricultural land. The applicability of the routines to large scale simulations would strongly benefit from additional crop specific parameterizations for important cash and cover crops. Also a better representation of ploughing and tillage needs be included in future model versions in order to better account for the effects of cover crops on the terrestrial carbon cycle and their biogeochemical benefits.

Further general examples for improvements include: (1) an improved representation of plant and soil hydrology that may be highly beneficial for yield predictions, (2) a more detailed representation of agricultural management practices (e.g. tillage, C/N turnover, post-harvest surface conditions, fertilizer types and applications), (3) tools to account for spatial variability in plant physiological parameters, and (4) the discretization of plant hydraulic properties as opposed to using one parametrization for all crops.

4 Seasonal soil moisture and crop yield predictions with fifth-generation seasonal forecasting system (SEAS5) long-range meteorological forecasts in a land surface modelling approach

Adapted from: Boas, T., Bogena, H. R., Ryu, D., Vereecken, H., Western, A., and Hendricks Franssen, H.-J.: Seasonal soil moisture and crop yield prediction with fifth-generation seasonal forecasting system (SEAS5) long-range meteorological forecasts in a land surface modelling approach, Hydrology and Earth System Sciences., 27, 3143–3167, https://doi.org/10.5194/hess-27-3143-2023, 2023.

4.1 Introduction

Reliable high-resolution seasonal weather forecasting systems can provide important information for a multitude of weather-sensitive sectors, especially for agricultural regions with high inter-annual variability of rainfall patterns that are strongly influenced by El Niño events (Ash et al., 2007; McIntosh et al., 2007; Troccoli, 2010). Information on seasonal rainfall and temperature development can influence agricultural management decisions at the beginning of the growing season and potentially mitigate yield losses related to droughts. However, the relevance and usability of such seasonal forecasts depend on the predicted variables, their accuracy and their lead time as well as whether they are supplied in a user-friendly and content-specific format, e.g. in combination with other model applications (e.g. crop or land surface models), to assess the expected benefits to the economy or natural resources (Cantelaube and Terres, 2005; Hansen et al., 2006; Ash et al., 2007; McIntosh et al., 2007; Meza et al., 2008). Sub-seasonal (1 to 3 months) and seasonal (up to 7-month lead times) forecasts bridge the gap between short-range weather forecasts and climate predictions and are the most important time periods for model applications and planning purposes, e.g. in agriculture or risk management (Monhart et al., 2018). In the last decade, substantial improvements have been made in numerical weather prediction, especially in short- and medium-range weather forecasts by further model development, data assimilation methods and the incorporation of ensemble prediction into seasonal forecasting systems (Coelho and Costa, 2010; Bauer et al., 2015; Monhart et al., 2018).

In spite of these substantial improvements, there are still considerable challenges in interfacing forecast information from climate to systems science (Coelho and Costa, 2010). For instance, deficiencies remain in the definition and communication of forecast uncertainties (e.g. due to discrepancies between the spatial and temporal resolutions of the global weather forecasting system and the regional or local land surface models) and in the lack of available tools, literature and experience for correct usage and data processing (Coelho and Costa, 2010). Seasonal and sub-seasonal forecasts do not reflect day-to-day weather statistics but rather project general weather trends of the predicted season. This leads to high-precipitation biases compared to observations, which is a major limitation for crop models that usually operate on sub-daily time steps in response to precipitation and corresponding soil moisture dynamics. In their study, Monhart et al. (2018) conducted a verification of sub-

seasonal forecasts (with a 1-month lead time) from the European Centre for Medium-Range Weather Forecasts (ECMWF) against ground-based observational time series of 20 years across Europe for precipitation and temperature and performed two different bias-correction techniques. They found generally better skill for temperature than precipitation and that the accuracy of both variables improved significantly after station-based bias correction (Monhart et al., 2018). However, McIntosh et al. (2007) evaluated the potential of different forecasting systems for wheat growth in Victoria, Australia, and concluded that even a perfect forecast of the total rainfall amount throughout the growing season is not enough to explain even half of the overall potential of an ideal forecasting system.

The major aim of this study was to evaluate the efficacy and applicability of this state-of-the-art forecasting product for physical and biogeochemical land surface responses and regional crop production in an ecosystem process model approach. To this end, we tested the combination of the Community Land Model version 5 (CLM5) (Lawrence et al., 2018; 2019) and seasonal forecasts from the ECMWF's latest seasonal forecasting system SEAS5 (Johnson et al., 2019). Regional simulations were conducted for two domains with different climate regimes and agricultural characteristics, one covering the state of North Rhine-Westphalia in Germany (DE-NRW), and one the state of Victoria in Australia (AUS-VIC), using sub-seasonal and seasonal forecasts with different lead times as input. In our evaluations we focused on (1) the model's sensitivity to seasonal changes in weather patterns and their effect on regional vegetation properties, e.g. leaf area index (LAI), evapotranspiration (ET), and crop yield; (2) the representation of the surface soil moisture content; and (3) the overall applicability and potential of seasonal weather forecasts for the prediction of regional agricultural production in model applications such as CLM5. In addition, we address the pre-processing steps required for the usage of the SEAS5 product in this model application and briefly discuss the importance of temporal downscaling.

The long-range forecast product generated by the ECMWF SEAS5 system, the fifth-generation seasonal forecast system that became operational in November 2017 (Johnson et al., 2019), represents one of the most sophisticated seasonal products available to date. Studies that evaluated the quality of the SEAS5 product globally and for specific regions concluded that it outperforms earlier versions of ECMWF forecast products and can provide useful information for regional agriculture (e.g. Johnson et al., 2019; Wang et al., 2019; Gubler et al., 2020). The prediction performance was found to be highest for maximum temperature over South America (with an up to 70% probability that the predictions will correctly capture the observed outcomes in the tropics during austral summer) (Gubler et al., 2020) and Australia (Wang et al., 2019). For precipitation, the performance was considerably lower and more variable (spatially and temporally) than for temperature (Wang et al., 2019; Gubler et al., 2020). The best forecast performance was observed over regions that are influenced by El Niño where SEAS5 outperformed predictions from statistical relationships at the seasonal scale (Gubler et al., 2020).

The relevance and value of meteorological forecasting systems for agriculture have been evaluated by a number of studies (e.g. Cantelaube and Terres, 2005; Marletto et al., 2007; McIntosh et al., 2007; Semenov and Doblas-Reyes, 2007). In their study, Semenov and Doblas-Reyes (2007) used a stochastic weather generator to obtain site-specific daily weather from seasonal DEMETER (European Development of a European Multimodel Ensemble system for seasonal to inTERannual climate prediction) predictions. They found that dynamical seasonal forecasts did not improve single-site yield predictions with the wheat simulation model compared to approaches based on historical climatology due to their low skill for latitudes higher than 30° for the Northern Hemisphere and Southern Hemisphere. Cantelaube and Terres (2005) evaluated an ensemble of seasonal weather forecasts from the

DEMETER project in a multi-model approach with a crop growth modelling system (CGMS), showing encouraging results for the usage of seasonal forecasts for weather-sensitive decision-making. Wang et al. (2020) investigated the impact of pre-season and early season El Niño-Southern Oscillation (ENSO)-related large-scale climate signals on wheat yields in Australia. They found that these ENSO signals can have a significant impact on wheat yields in the Australian wheat belt and could explain up to 21% of the yield variation. In another study by Potgieter et al. (2022), the lead time and skill of Australian wheat yield forecasts using seasonal climate forecasts derived from a statistical ENSO-analogue system were compared with using a dynamic general circulation model (GCM). They found that ENSO-derived forecasts showed higher skills at a longer lead time (6 months), with a higher correlation coefficient of 0.48 compared to 0.37 for GCM forecasts, while GCM forecasts provided higher skill at shorter lead times (1-3 months) with a higher correlation coefficient of 0.44 compared to 0.35 for ENSO-analogue forecasts.

Thus, although seasonal weather forecasts have immense potential for the agricultural sector, i.e. for individual farming decisions, risk management and adaptation strategies for increasing climate variability, and extreme weather events in the context of climate change (Calanca et al., 2011), they need to be combined with a measurable system response via e.g. crop models or Earth system models. Land surface models are our primary tools for simulating water, energy and nutrient fluxes in the terrestrial ecosystem and are broadly applied for different scientific purposes (e.g. Niu et al., 2011; Lawrence et al., 2018, 2019; Lombardozzi et al., 2020; Naz et al., 2019). CLM5 is the latest version of the land component in the Community Earth System Model and offers the possibility of prognostic vegetation state and yield prediction with its new biogeochemistry module (Lawrence et al., 2018; 2019). CLM5 includes a representation of crops and agricultural management (fertilization, irrigation, different crop types) essential for studying the impact of climate change on yield as well as the implications of agriculture for climate change (Lombardozzi et al., 2020). In CLM5, crop productivity is a dynamic non-linear interaction between meteorological conditions, crop phenology, nutrient dynamics, and water availability in the soil. Thus, a reliable prediction of the soil moisture regime is also essential for the relevance of land surface model applications for climate change research and is a major source of uncertainty for the simulation of the terrestrial carbon cycle (Trugman et al., 2018).

Another major limitation of the usage of seasonal and sub-seasonal forecasting products for crop or land surface modelling is their coarse spatial and temporal resolution. This problem can be addressed by disaggregating forecast variables using stochastic weather generators (e.g. Hansen et al. 2006), which has already been done for several crop model approaches (see the reviews in Cantelaube and Terres, 2005; Ash et al., 2007; Meza et al., 2008).

Despite their potential economic value for agricultural production systems, the quantitative adoption of seasonal climate forecasts by farmers is low, both in Victoria and NRW (e.g. Parton et al., 2019). The Australian Bureau of Meteorology attributed this to insufficient data and evidence about their value and conducted a series of studies of the potential value of a forecast based on a particular production system and for specific regions and timescales (Hansen, 2002; Hansen et al., 2006). Furthermore, the challenges highlighted above have hindered widespread application of such long-range forecasts for agriculture, particularly for larger (not site-specific) scales (Coelho and Costa, 2010; Calanca et al., 2011). The lack of user-friendly tools and services that can provide content-specific information based on seasonal forecasts and account for other economic factors (e.g. political choices, outlook for crop markets) represents another constraint.

A thorough review of the economic value of seasonal weather forecasts for agriculture can be found in Meza et al. (2008), Klemm and McPherson (2017), and references therein. For an improved understanding of the value of seasonal forecasts for the agricultural sector, more studies are needed that explore state-of-the-art forecast products and for a larger range of regions (i.e. high seasonal predictability, large areas of extensive management, rain-fed). Here, we provide a first feasibility study of the combination of seasonal forecasts from SEAS5 with CLM5, focusing on crop yield and soil moisture predictions on a regional scale.

4.2 Material and Methods

4.2.1 Regional domains and surface input data

The CLM5 simulations were carried out in two regional domains, one in western Europe covering the state of North Rhine-Westphalia in Germany (DE-NRW) and one that covers large parts of the state of Victoria in Australia (AUS-VIC) (Figure 4.1, Figure 4.2). The DE-NRW domain is characterized by a very diverse land cover with urban, natural and mixed agricultural areas that are mostly fed by rainwater. The agricultural land cover in DE-NRW is especially abundant in the northern and western parts of the domain along with natural vegetation and urban areas. Winter wheat, winter barley, corn, sugar beet and rape seed are the most important cash crops in DE-NRW, which are mostly rain-fed (Figure 4.2, BMEL, 2020, 2022). In the southern part of the domain over the Eifel region, forests and grasslands are the dominant land cover. Recently, agricultural yield in this area was impacted in 2018 and 2019, by a late cold spell (late February to early March 2018) and extreme heat and dry spells in both summers which led to an unusually high spatial variability of yield, especially for cereals (NRW Gov., 2020; BMEL, 2020, 2022). The AUS-VIC domain covers large parts of the Australian wheat belt in the state of Victoria (Figure 4.1). The land cover is dominated by rain-fed agricultural areas with large paddock sizes of mostly cereal cultivation, with winter wheat being the most important crop, followed by barley and canola (ABARES, 2020; Morse-McNabb et al., 2015), along with large patches of naturally vegetated areas (i.e. pasture, grasslands, and native woody cover) and woody horticulture and wood plantations. Unfavourable weather conditions for winter crop farming (i.e. the timing and intensity of early season rainfall events) are clearly reflected in the relatively low regional production and yield per area (ABARES, 2020).

For the DE-NRW domain, land cover information was derived from the crop and land cover dataset by Griffiths et al. (2019) that covers Germany at 30-m resolution. This dataset was generated from Sentinel-2A MultiSpectral Instrument and Landsat-8 Operational Land Imager observation data from the NASA Harmonized Landsat-Sentinel dataset for the year 2016 (Claverie et al., 2018). Comparison of the derived crop type and land cover map with agricultural reference data showed a very good overall accuracy of > 80%, especially for crop types with high abundances, e.g. cereals, maize and canola (Griffiths et al., 2019). For the AUS-VIC domain the 500 m resolution Moderate Resolution Imaging Spectroradiometer (MODIS) land cover product (Friedl and Sulla-Menashe, 2019) was aggregated to the coarser resolution of 1 km and masked with information from the latest Victorian Land Use Information System (VLUIS) product for the year 2016 (Morse-McNabb et al., 2015). The VLUIS dataset covers the whole state of Victoria and contains information on land use and land cover for each cadastral parcel. It is a product of time series analysis of remote-sensing data (MOD13Q1 or MYD13Q1 by NASA) and annually collected field data (Morse-McNabb et al., 2015).

For both domains, we used soil texture and soil organic matter information from the global SoilGrids database that provides soil information at seven depths (0, 0.05, 0.15, 0.30, 0.60, 1 and 2 m) at 250 m spatial resolution (Hengl

et al., 2017). Soil information from SoilGrids are publicly accessible via the International Soil Reference and Information Centre (ISRIC) – World Soil Information Data Hub (ISRIC, 2023).

Other soil parameters, such as the saturated hydraulic conductivity and soil retention parameters, were calculated within CLM5 with the pedotransfer function after Cosby et al. (1984). Additional properties of each of the sub-grid land fractions (e.g. properties of urban land cover) were derived from the global CLM5 surface dataset (see Lawrence et al., 2018).

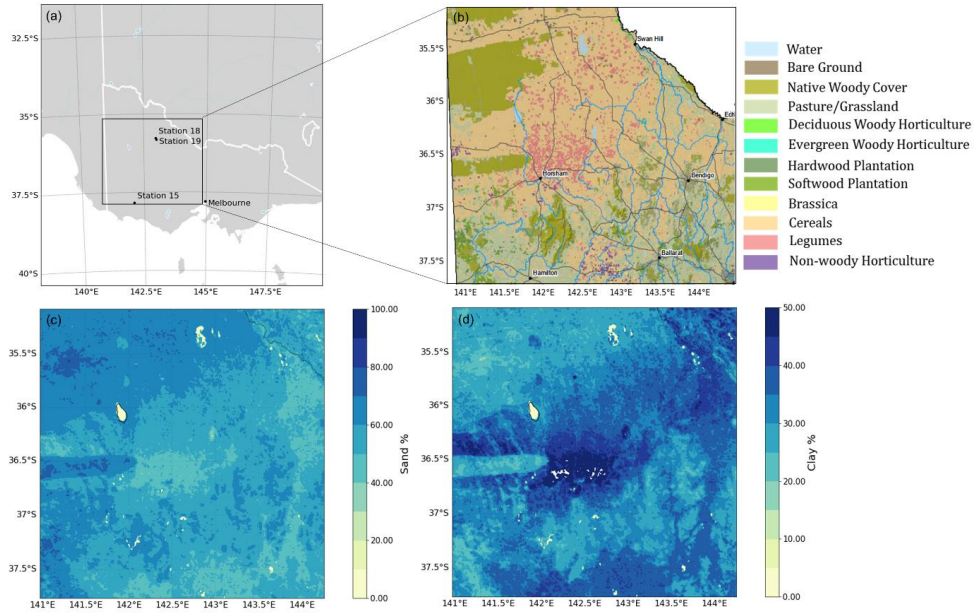

Figure 4.1: (**a**) AUS-VIC simulation domain extent. (**b**) Dominant land use type based on VLUIS data, modified after the Victorian Government Data Directory (2018). (**c**) Percentage of sand content (averaged throughout the soil profile) based on SoilGrids data. (**d**) Percentage of clay content (averaged throughout the soil profile) based on SoilGrids. The locations of CosmOz network (Hawdon et al., 2014) stations 15 (Hamilton), 18 (Bishes), and 19 (Bennets) are indicated in panel (a).

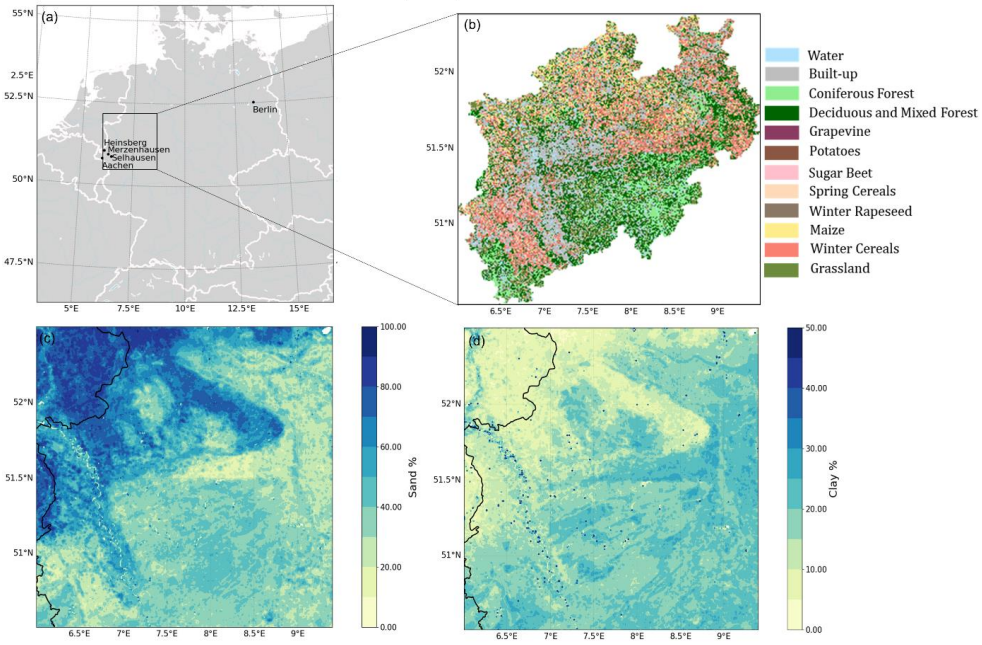

Figure 4.2: (**a**) DE-NRW simulation domain extent. (**b**) Dominant land use type based on Griffiths et al. (2018, 2019). (**c**) Percentage of sand content (averaged throughout the soil profile) based on SoilGrids data, and (**d**) percentage of clay content (averaged throughout the soil profile) based on SoilGrids. The locations of the COSMOS-Europe (Bogena et al., 2022) stations Merzenhausen, Heinsberg, Selhausen, and Aachen are indicated in panel (a).

4.2.2 Agricultural statistics

The mild climate in Victoria is favourable to a range of winter crops, especially cereals (wheat, barley, oats), oilseeds (canola) and pulses (lentils, beans, chickpeas) contributing to Australia's total annual winter crop yield of ~5 million tons on average. Most of the crop production in Victoria is from the western and northern regions, expanding to high-rainfall zones of southern Victoria. Wheat varieties represent the most commonly sown winter crop in Victoria, with an average operated area of 1.3 million hectares (2015 to 2019 average) (ABARES, 2020). The production of summer crops such as grain sorghum, cotton or rice in Victoria is negligible, with an average total production of 2000 t per year (2015 to 2021 average) (ABARES, 2020). The main cropping season in Victoria is from April to November. Regional average farming yield in the Victoria domain is highly influenced by seasonal rainfall patterns. In 2018, Victoria experienced substantial yield losses due to long dry spells and high temperatures after the first seasonal rainfalls, while record grain yields were recorded for the year 2020 (ABARES, 2020).

In the state of NRW, the most relevant cash crops are grain crops such as cereals (especially winter cereals) and corn, followed by canola, sugar beet and potatoes (BMEL, 2020, 2022). The main cropping season in Germany occurs during the spring and summer months until the beginning of autumn from April to the end of October. The European drought of 2018 led to local yield losses, especially for the crops corn, potatoes and sugar beet and slightly for canola, and to unusually high spatial wheat yield variability within the region. The spatial variability was strongly related to soil type (IT.NRW, 2019; NRW Gov., 2020). Regions with clay-rich soils that have high water-holding capacities, saw unexpectedly high wheat yields in 2019, while regions dominated by less fertile

sandy soils in the north-western part of the state experienced yield losses due to water deficits (NRW Gov., 2020). In general, the annual crop yield of the main cash crops varies more in Victoria than in NRW, where, on a regional average, there is only small variation between the annual yields of the respective crops (for a complete list of cropland area and production of major cash crops in Victoria and NRW, please see Table B6 and Table B7).

4.2.3 Land surface model

Land surface models such as CLM5 are essential tools for the study and prediction of terrestrial processes (e.g. energy, water and nutrient fluxes) and climate feedbacks in the terrestrial ecosystem and are broadly applied in different scientific disciplines (e.g. Baatz et al., 2017; Lu et al., 2017; Chang et al., 2018; Han et al., 2018; Lawrence et al., 2018, 2019; Naz et al., 2019; Lombardozzi et al., 2020). In this study, the land surface model simulations were carried out with the latest version of CLM5, which includes an adopted version of the prognostic crop module from the Agro-Ecosystem Integrated Biosphere Simulator (Kucharik and Brye, 2003; Lawrence et al., 2019). CLM5 is forced by atmospheric states at a given time step and simulates the exchange of water, energy, carbon and nitrogen between land and the atmosphere, their storage and transport on the land surface and in the sub-surface, as well as the biomass and respective yield of crops upon harvest (Lawrence et al., 2019; Lombardozzi et al., 2020). In CLM5, the plant hydraulic stress routine simulates water transport through the soil-root-stem-leaf system based on Darcy´s law for porous media flow and adapts the vegetation water potential according to the water supply with transpiration demand. Water stress for plants is based on leaf water potential which is used for the attenuation of photosynthesis in a transpiration loss function relative to maximum transpiration (Lawrence et al., 2018). The leaf stomatal conductance and leaf photosynthesis are modelled for sunlit and shaded leaves separately based on the approaches of Medlyn et al. (2011) and Farquhar et al. (1980) for C_3 plants and Collatz et al. (1992) for C_4 plants (Lawrence et al., 2018) respectively. Adapted from Medlyn et al. (2011), the leaf stomatal resistance is calculated using the net leaf photosynthesis, the vapour pressure deficit and the CO_2 concentration at the leaf surface with plant-specific slope parameters (Lawrence et al., 2018).

With its biogeochemistry module, CLM5 is fully prognostic regarding crop phenology (e.g. grain yield, leaf area index or crop height) as well as carbon and nitrogen in the soil, vegetation and litter. The crop module includes a total of 78 plant and crop functional types, including an irrigated and non-irrigated C3 crop and crops such as winter wheat, spring wheat, canola temperate and tropical corn, temperate and tropical soybean, cotton, rice and sugarcane (Lawrence et al., 2018). Fertilization dynamics and annual fertilizer amounts in CLM5 depend on the crop functional types and vary spatially and yearly based on the land use and land cover change time series from the Land Use Model Intercomparison Project (Lawrence et al., 2016). Mineral fertilizer application starts during the leaf emergence phase of crop growth and continues for 20 d, and manure nitrogen is applied at slower rates of 0.002 kg N m^{-2} per year. For a more detailed description of the features and formulations of CLM5, the reader is referred to the technical description and the latest literature (Lawrence et al., 2018, 2019).

Here, we used a modified version of CLM5 that includes a winter cereal representation, an updated parameter set for several cash crops (winter wheat, sugar beet and potatoes) and a new sub-routine that allows the simulation of cover cropping and a more flexible crop rotation (Boas et al., 2021). The modified CLM5 version led to significantly improved simulations of LAI, net ecosystem exchange, crop yield and energy fluxes at several central European sites (Boas et al., 2021).

4.2.4 Seasonal weather forecasts

In this study, we used long-range meteorological forecasts from the ECMWF's fifth-generation seasonal forecasting system, SEAS5, which has been operational since November 2017 (Johnson et al., 2019). The SEAS5 forecasts are based on a coupled atmosphere-ocean model and provide forecasts of numerous meteorological variables at either 6-hourly or daily time steps at a horizontal resolution of 1 degree. For the seasonal forecast, an ensemble of 51 members is initialized on the first day of a month and integrated for 7 months (Johnson et al., 2019). Furthermore, SEAS5 provides a set of retrospective seasonal hindcasts from 25 ensemble members for the years 1981 to 2016 that are used to calibrate and verify the forecasts compared to other datasets. While the whole period of hindcasts is used to verify the system, a subset from the years 1993 to 2016 is used in the calculation of forecast anomalies to avoid unreasonable effects from long-term climate trends on the forecast product (Johnson et al., 2019). A detailed description of the SEAS5 forecasting system and an overview of its performance are presented in Johnson et al. (2019). The SEAS5 forecasting product provides all the variables needed to force CLM5 at daily or 6-hourly time steps: accumulated daily precipitation amounts, daily short-wave and long-wave radiation fluxes, wind speed, air temperature, dew point temperature and mean sea level pressure. In this study, we used the years 2017 to 2020 for our simulation experiments, in accordance with the availability of the forecasting product.

We used different sets of SEAS5 forecast data, seasonal forecasts with a 7-month lead time and sub-seasonal forecasts with 3- and 4-month lead time. Those variables available at only a daily time step (incoming short-wave radiation and precipitation) were temporally disaggregated to a 6-hourly time step using the Meteorology Simulator (MetSim) (Bennett et al., 2020) to provide realistic information on atmospheric states. MetSim is based on algorithms from the Mountain Microclimate Simulation Model (MTCLIM) (Hungerford et al., 1989; Thornton and Running, 1999; Thornton et al., 2000; Bohn et al., 2013) and the Variable Infiltration Capacity (VIC) macroscale hydrologic model (Liang et al., 1994). MetSim can be used to either generate spatially distributed sub-daily time series of meteorological variables from a smaller number of input variables (daily minimum and maximum temperatures and elevation data) or to disaggregate meteorological data from a coarse temporal resolution to a finer one (Bennett et al., 2020).

In addition to the necessary meteorological input and calibration variables, MetSim also requires a grid description file that comprises information like spatial location (latitude and longitude), size of the grid cells and topography. Here, elevation data at a spatial resolution of 1 arc second from the ASTER Global Digital Elevation Model were used (NASA/METI/AIST/Japan Spacesystems and U.S./Japan ASTER Science Team, 2019).

The daily variables were disaggregated to sub-daily resolution. The total daily precipitation was split into four equal amounts of precipitation and then spread across the sub-daily time steps (6-hourly). Similar approaches were used for the National Centre for Environmental Prediction (NCEP) dataset (Viovy, 2018) and in Hudiburg et al. (2013). Unfortunately, this deterministic approach cannot characterize the diurnal cycle of precipitation properly. The incoming short-wave radiation is disaggregated by multiplying the total daily short-wave radiation by the fraction of radiation that is calculated by the solar geometry module of MetSim. The solar geometry module within MetSim computes the daily potential radiation, day length and transmittance of the atmosphere based on the algorithms from MTCLIM (Thornton and Running, 1999). The influence of the temporal resolution of forcing data on simulation results and the quality of MetSim-disaggregated data for the CLM5 model performance relative to hourly forcing data is illustrated and discussed for an example at point scale in Appendix B1.

4.2.5 Simulation experiments and performance metrics

We conducted simulation experiments using different sets of seasonal (up to a 7-month lead time) and sub-seasonal (up to a 4-month lead time) forecasts in order to assess a potential difference for the prediction of annual crop yields and general model system responses for different forecast lead times. For the seasonal experiments (CLM-S), forecasts with a lead time of 7 months covering the main growing season (1st of April to 31st of October) were used. The seasonal simulations started on 1st of April and continued for 7 months, until the end of October of the same year. The same timescale was used for the sub-seasonal experiments (CLM-SUB) that were forced with a combined set of forecasts with lead times of 3 and 4 months (from 1st of April until the end of June and from the 1st of July until 31st of October) (Figure 4.3). Seasonal and sub-seasonal experiments were conducted for the years 2017, 2018, 2019 and 2020 in order to assess the ability of the model to portray inter-annual differences in crop production for both domains. Furthermore, reference simulations (CLM-WFDE5) were conducted for the years 2017, 2018 and 2019 using the bias-adjusted global reanalysis dataset WFDE5 (Cucchi et al., 2020). The WFDE5 dataset was generated from the ERA5 reanalysis product (Hersbach et al., 2020) using the WATCH Forcing Data (WFD) methodology (Cucchi et al., 2020). It is provided at 0.5° spatial resolution and at an hourly time step for the period from 1979 to 2019.

An 850-year spin-up was performed prior to production runs for both domains in order to reach equilibrium conditions for soil carbon and nitrogen pools, soil water storage and other ecosystem variables. The global CRUNCEP atmospheric forcing dataset (Viovy, 2018) was used to force the spin-up simulations. The CRUNCEP dataset is a combination of the CRU TS3.2 0.5 x 0.5 degree monthly data covering the period 1901-2002 (Harris et al., 2014) and the NCEP reanalysis 2.5 x 2.5 degree 6-hourly data covering the period 1948-2016 (Kalnay et al., 1996).

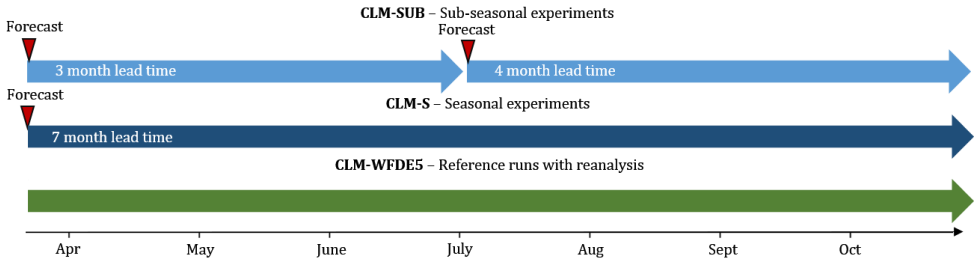

Figure 4.3: Overview of experimental simulation design. CLM-SUB and CLM-S were driven by SEAS5 forecasts at hourly timestep, with a spatial resolution of approximately 36 km. CLM-WFDE5 reference runs were forced with WFDE5 data, characterized by a spatial resolution of 0.5° at hourly timestep.

In order to evaluate the quality of the simulation results we used the root mean square error (RMSE), the mean bias error (MBE) and the squared correlation coefficient (R^2) as statistical validation metrics:

$$RMSE = \sqrt{\frac{1}{n}\sum_{i=1}^{n}(x_i - y_i)^2}, \quad (4.1)$$

$$MBE = \frac{\sum_{i=1}^{n}(x_i - y_i)}{n}, \quad (4.2)$$

$$R^2 = 1 - \frac{\sum_{i=1}^{n}(y_i - X_i)^2}{\sum_{i=1}^{n}(y_i - \overline{y})^2}, \quad (4.3)$$

where n is the total number of time steps, X_i and y_i are the simulated and the observed values of a given variable at every time step i, and the overbar represents the mean value.

4.2.6 Validation data

For the validation of CLM5-simulated surface soil moisture, we compared simulation results with the Soil Moisture Active Passive (SMAP) mission Enhanced Level-3 radiometer soil moisture product (SMAP L3) (Entekhabi et al., 2016) and with the Soil Moisture CCI combined dataset, version 05.2 (ESA-CCI), from the European Space Agency (ESA) Soil Moisture Essential Climate Variable (ECV) Climate Change Initiative (CCI) project (Dorigo et al., 2017; Gruber et al., 2017, 2019). The global SMAP L3 product comprises soil moisture retrievals at both 06:00 and 18:00 LT at a spatial resolution of 9 km (Entekhabi et al., 2016). The ESA-CCI soil moisture combined product provides global daily volumetric soil moisture data at a spatial resolution of 0.25 degrees from 1978 to 2019. It was created by merging multiple scatterometer and radiometer soil moisture products (from the AMI-WS, ASCAT, SMMR, SSM/I, TMI, AMSR-E, WindSat, AMSR2, SMOS and SMAP satellites) and covers the period from 1978 to 2019 (Dorigo et al., 2017; Gruber et al., 2017, 2019).

In addition, simulation results were compared to available soil moisture content (SMC) measurements from three cosmic-ray neutron sensor (CRNS) measurements. For AUS-VIC we used measurement data from the stations Hamilton (station 15), Bishes (station 18) and Bennets (station 19) that are part of the CosmOz network (Hawdon et al., 2014). For DE-NRW, CRNS measurements were obtained from the four COSMOS-Europe stations Selhausen, Merzenhausen, Aachen and Heinsberg (Bogena et al., 2022). For this comparison, simulation outputs from the closest grid point to the respective station were averaged with the weighting approach after Schrön et al. (2017).

In order to validate the regional LAI and ET simulation results, we used the latest MODIS satellite data product (MCD15A3H version 6). This includes the Combined Fraction of Photosynthetically Active Radiation (FPAR) and LAI product (Myneni et al., 2015) as well as the MODIS ET/Latent Heat Flux (LH) (MOD1A2 version 6) product (Running et al., 2017). The MODIS LAI product is a 4-day composite dataset (combined acquisitions of both MODIS sensors located on NASA's Terra and Aqua satellites) on a 500 m global grid (Myneni et al., 2015). The MODIS ET product is an 8-day composite at 500 m global resolution (Running et al., 2017). We compared simulated LAI and ET with monthly mean values from MODIS for cropland-dominated land units throughout both domains.

4.3 Results

4.3.1 Comparison of seasonal forecasts to recorded weather statistics

In a first step, the forecasts for both domains were compared to official weather statistics and trends.

In 2017, the weather in Victoria was generally slightly drier and warmer than average. However, the winter season was unusually cool, with record minimum temperatures in July and August (BOM, 2021). Annual rainfall was below average in most months, especially in June and July, which resulted in the driest winter season since 2006.

However, early growing season rainfall in April was more than 50% above average for large parts of the state (BOM, 2021). The year 2018 continued with drier and warmer-than-average weather, with the lowest annual rainfall amount since 2006 and an annual mean temperature of more than 1°C above average (reference period of 1980-2010) (BOM, 2021). In the south-west and south of Victoria, winter season rainfall was close to average, while below-average rainfall amounts were recorded across the north and east of the state (BOM, 2021). Similarly to the previous years, 2019 was generally warmer and drier than average. Winter season rainfall showed high variability throughout the state, it was below average for large parts of Victoria in the north and east and above average in the south (BOM, 2021). The year 2020 continued with close-to-average rainfall and temperatures (BOM, 2021). The recorded weather pattern in Victoria is to a certain extent represented in the SEAS5 seasonal forecast data. The predicted state-wide average rainfall amount was highest for the autumn and winter seasons (from April to October) of 2020 and 2017, where recorded early season rainfall was 50 % above average, and lowest for 2018, where extremely low winter season rainfall was predicted. In NRW, the weather in 2017 was slightly warmer than the 30-year average with close-to- average rainfall. The year 2018 was characterized by an exceptional heat and drought wave during summer (Graf et al., 2020; DWD, 2021). Overall summertime rainfall in 2018 was below average which, in combination with high temperatures, led to exceptional drought conditions in NRW and most of Europe that represent the largest annual soil moisture anomaly in the period 1979–2019 (Graf et al., 2020, and references therein). The same pattern, though less extreme, was observed in 2019, where a heat wave occurred during summer in combination with long dry spells. Total summertime rainfall was slightly below average. The year 2020 continued with above-average summertime temperatures and below-average rainfall, making it the third too dry and too warm year in a row (DWD, 2021). The trend of the recorded weather patterns is to a certain extent reflected in the SEAS5 forecasts for NRW. The predicted total rainfall over 7 months was lowest in the 2018 forecasts. The heat wave in 2018 is reflected in the forecasts of the predicted mean daily temperature, which is more than 1°C higher than in 2017, 2019 and 2020.

4.3.2 Model performance with long-range forecasts

4.3.2.1 Soil moisture content

In general, the SMAP L3 dataset depicts much stronger fluctuations in the SMC than the ESA-CCI product over both domains. Over the DE-NRW domain, SMAP L3 is drier in the early growing season and shows a slightly wetter trend towards the end of the season compared to ESA-CCI (Figure 4.4). Large differences in SMC can be observed for the AUS-VIC domain, where SMAP L3 shows much higher magnitudes of SMC compared to ESA-CCI, in July-September in particular. Overall, the simulated SMC shows lower fluctuations for the DE-NRW domain than for AUS-VIC. While the CLM5-simulated SMC for AUS-VIC corresponds better with the ESA-CCI product, for the DE-NRW domain, the CLM5-simulated SMC shows larger fluctuations and correlates better with

the SMAP L3 product. For AUS-VIC, the CLM5-simulated SMC shows a wet trend towards the end of the winter season (August, September, October), especially for 2018 and 2019, compared to ESA-CCI (Figure 4.4). The reference runs, CLM-WFDE5, generally correlated better with the ESA-CCI data ($R^2 > 0.8$) than the seasonal and sub-seasonal runs (R^2 values between 0.2 and 0.64) for AUS-VIC (Table 4.1). Overall, the fluctuations of the SMAP L3 product are not well represented in CLM5-simulated SMC over AUS-VIC. Both the forecast experiments and the reference simulations underestimated the SMC in comparison to SMAP L3 during the middle of the growing season for all the years, while overestimating early and late growing season SMCs (Figure 4.4).

A different trend can be observed for the DE-NRW domain (Figure 4.4). While simulation results from CLM-S and CLM-SUB show a slight overestimation of the surface SMC in the beginning of the growing season (April to June) of 2017 and 2019 compared to the ESA-CCI product, a clear negative bias can be observed over summer and towards the end of the growing season (July to October) of 2017 and 2020 compared to ESA-CCI (Figure 4.4). This is also true for the CLM-WFDE5 run in 2018 and 2019. For 2017, CLM-WFDE5 overestimated the early season surface SMC but captured it relatively well towards the end of the season in reference to ESA-CCI (Figure 4.4). Compared to the SMAP L3 product, CLM5 overestimated early growing season SMC for all the years except 2020, where a systematic underestimation of simulated SMC can be observed throughout the whole season. For the years 2018 and 2019, the SMAP L3 product seems to capture the recorded drought conditions in DE-NRW better compared to the ESA-CCI product, showing much lower SMCs. In the late growing season of 2019 (September and October), the SMAP L3 data and the ESA-CCI product show a prominent increase in SMC that is to a certain extent captured in the reference simulations, but not in the seasonal and sub-seasonal experiments. Overall, the CLM-WFDE5 simulations correlated better with both SMAP L3 and ESA-CCI ($R^2 > 0.54$ for all years) compared to forecast experiments (R^2 values between 0.12 and 0.42).

Only minor differences between the seasonal and sub-seasonal experiments can be observed for AUS-VIC, while for DE-NRW, the sub-seasonal experiment yielded lower mean soil moisture contents compared to the seasonal model runs in the late growing season, especially in August and September of 2017.

Because of the large differences between the two validation datasets ESA-CCI and SMAP L3 over AUS-VIC, we also compared the simulated SMC to available SMC measurements from three CRNS stations (station 15: Hamilton; station 18: Bishes; station 19: Bennets) (Hawdon et al., 2014) for the years 2017 and 2018 (Figure B4). A relatively good correlation is reached for Hamilton during the early growing seasons of 2017 and 2018, while later in the season the SMC is underestimated. The simulated SMC is relatively high at the Bennets and Bishes stations (Figure B4) compared to CRNS data. We note that this comparison can only serve as an impression to give a tendency of model performance as simulation results and measurements may differ in soil types. For instance, Bishes and Bennets have a very sandy soil composition while in the SoilGrids dataset the sand content is between 20 and 40 % (Figure 4.1). Station Hamilton is characterized by soils with a high water-holding capacity which explains the high SMCs in the middle and towards the end of the wet season (Figure B4) and which is not to the extent represented in the CLM5 simulations and underlying SoilGrids data. Single precipitation and/or flooding events that are reflected in the CRNS data are not represented in the forecasts and, thus, are naturally not captured in the simulation results. However, the reference simulations were also not able to represent these fluctuations (Figure B4). For DE-NRW, CLM5 simulations correspond better with SMAP L3 and show more fluctuations in day-to-day SMC. Here, the forecast experiments performed reasonably well in capturing the drought conditions, with very low soil moisture contents throughout summer and autumn in 2018 and 2019. We

compared CRNS measurements from four stations within DE-NRW (Selhausen, Merzenhause, Aachen and Heinsberg) (Bogena et al., 2022) to the simulated SMC at the closest grid point. The comparisons showed that the reference simulations forced with reanalysis generally produced higher SMCs than the forecast simulations and corresponded better with CRNS measurement in terms of fluctuation intensity and magnitudes than SMCs from forecast simulations for single sites (Figure B5).

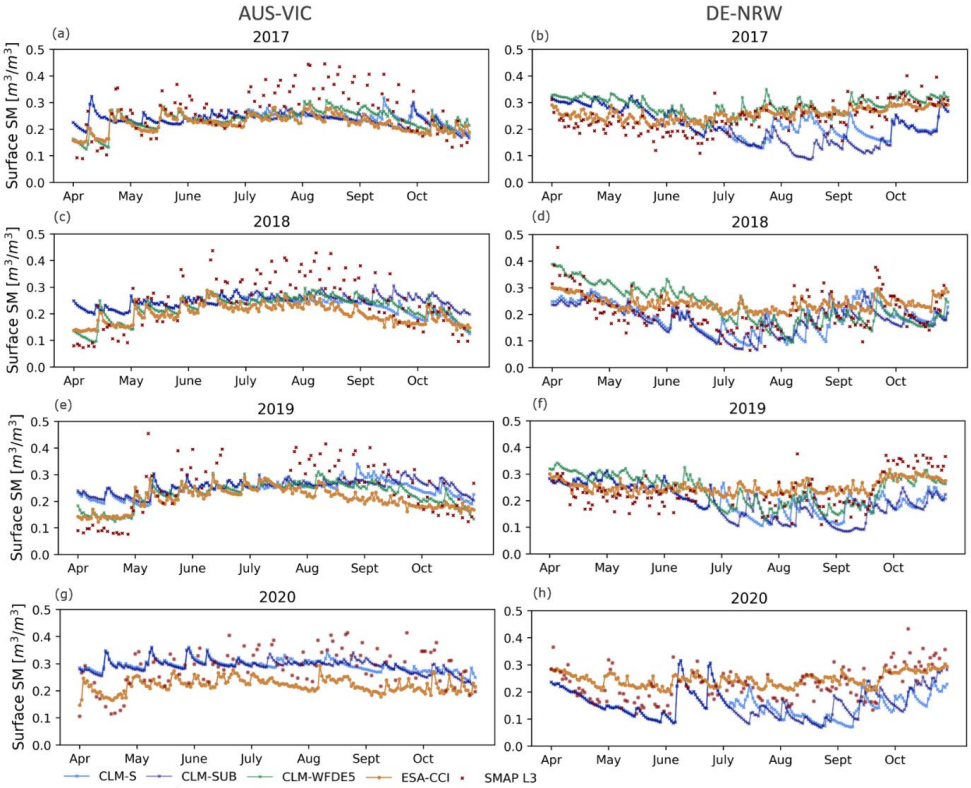

Figure 4.4: CLM-S, CLM-SUB and CLM-WFDE5 (for 2017, 2018 and 2019) simulated daily soil moisture content in the surface layer (0 – 0.05 m) from April to October of 2017, 2018, 2019 and 2020 averaged over (**a**, **c**, **e**, **g**) the AUS-VIC domain and (**b**, **d**, **f**, **h**) the DE-NRW domain, compared to the ESA-CCI surface soil moisture product and SMAP L3 data for the same time period and domain respectively. Corresponding statistics (RMSE and bias) are listed in Table 4.1.

Table 4.1: RMSE, MBE and R^2 of CLM-S-, CLM-SUB- and CLM-WFDE5-simulated surface soil moisture [m^3/m^3] (0 – 0.05 m) from the 1st of April to the 31st of October of 2017, 2018, 2019 and 2020, compared to the ESA-CCI and SMAP L3 soil moisture products for the AUS-VIC and the DE-NRW domains.

	2017			2018			2019			2020		
	RMSE	MBE	R^2	RMSE	MBE	R^2	RMSE	MBE	R^2	RMSE	MBE	R^2
AUS-VIC												
SMAP L3												
CLM-S	0.102	0.012	0.450	0.089	0.015	0.797	0.100	0.027	0.567	0.049	0.002	0.045
CLM-SUB	0.101	0.009	0.448	0.105	0.028	0.475	0.109	0.032	0.295	0.048	0.001	0.124
CLM-WFDE5	0.094	0.009	0.629	0.086	0.012	0.708	0.085	0.014	0.751	-	-	-
ESA-CCI												
CLM-S	0.038	0.018	0.233	0.043	0.031	0.635	0.054	0.038	0.452	0.079	0.074	0.226
CLM-SUB	0.036	0.014	0.288	0.058	0.048	0.477	0.059	0.045	0.392	0.077	0.071	0.200
CLM-WFDE5	0.022	0.014	0.886	0.033	0.023	0.846	0.029	0.019	0.881	-	-	-
DE-NRW												
SMAP L3												
CLM-S	0.068	-0.011	0.186	0.056	-0.010	0.420	0.065	-0.016	0.190	0.079	-0.047	0.123
CLM-SUB	0.083	-0.023	0.259	0.058	-0.016	0.412	0.071	-0.024	0.199	0.075	-0.044	0.404
CLM-WFDE5	0.053	0.030	0.521	0.057	0.014	0.523	0.053	0.009	0.473	-	-	-
ESA-CCI												
CLM-S	0.068	-0.033	0.161	0.071	-0.051	0.458	0.071	-0.046	0.164	0.079	-0.047	0.123
CLM-SUB	0.092	-0.053	0.266	0.076	-0.060	0.464	0.085	-0.057	0.174	0.075	-0.044	0.404
CLM-WFDE5	0.040	0.029	0.583	0.058	-0.010	0.621	0.049	-0.011	0.548	-	-	-

4.3.2.2 Leaf area index and evapotranspiration

For AUS-VIC, the simulated LAI from seasonal and sub-seasonal experiments corresponds well with MODIS data, especially for the years 2017 and 2018. Only minor differences can be observed for 2017 and 2018 between the seasonal and sub-seasonal experiments and reference simulations. For 2019, CLM-S and CLM-SUB performed better than the reanalysis run which shows a systematic underestimation of LAI compared to MODIS throughout most of the cropping season. This is also reflected in CLM-WFDE5-simulated ET, which is strongly underestimated for 2019 compared to MODIS. CLM5 simulation results for AUS-VIC generally show a systematic negative bias in simulated ET compared to MODIS data from April to August (Figure 4.5). The simulated inter-annual differences in LAI and ET are relatively small. For the DE-NRW domain, CLM5 overestimated the LAI compared to MODIS, in particular for the months June and July (Figure 4.6). For 2017 and 2018, CLM-WFDE5 resulted in very similar LAI values compared to CLM-S and CLM-SUB, while for 2019 the CLM-WFDE5-simulated LAI curve peaked later (highest LAI in August) compared to forecast simulations (highest LAI in July). Both CLM-S and CLM-SUB captured lower LAI magnitudes in August 2018 compared to the other years. In general, CLM-S and CLM-SUB show only minor differences in terms of LAI and ET. An exception is the year 2017, where CLM-SUB resulted in very similar LAI values compared to MODIS in September and October, while at the same time also resulting in a smaller underestimation of ET compared to CLM-S. Similarly to the results for the other domain, the simulated inter-annual differences in LAI and ET are relatively small.

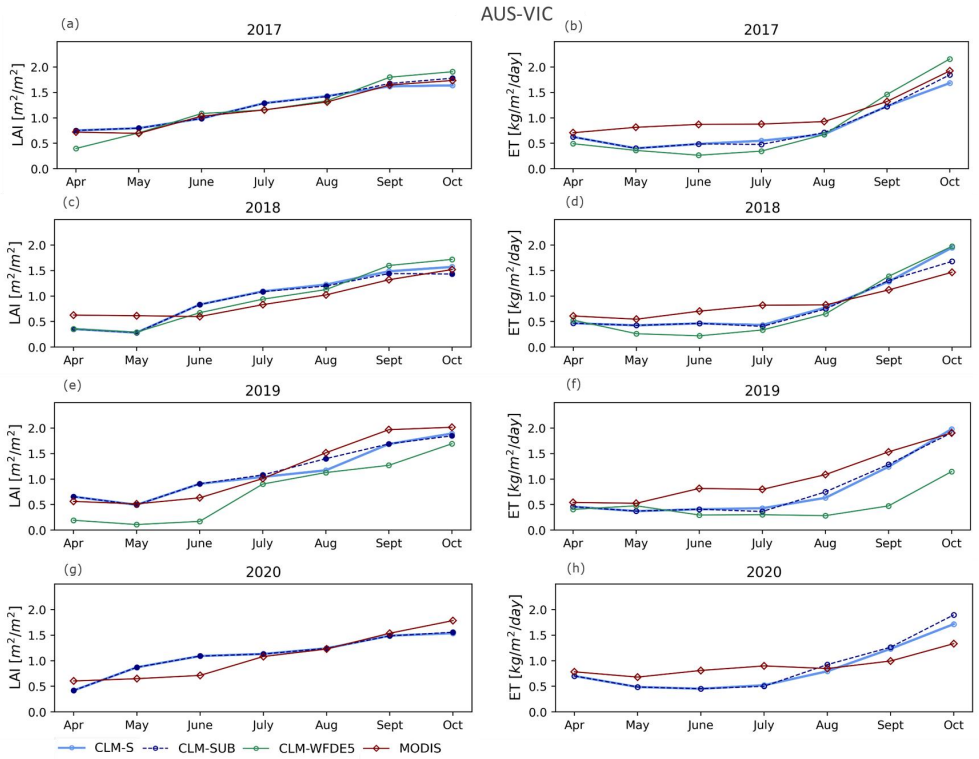

Figure 4.5: (**a**, **c**, **e**, **g**) Monthly mean LAI and (**b**, **d**, **f**, **h**) monthly mean ET derived from MODIS for April-October 2017-2020 compared to corresponding CLM-S and CLM-SUB simulation results, averaged over all land units with more than 70 % cropland within the AUS-VIC domain.

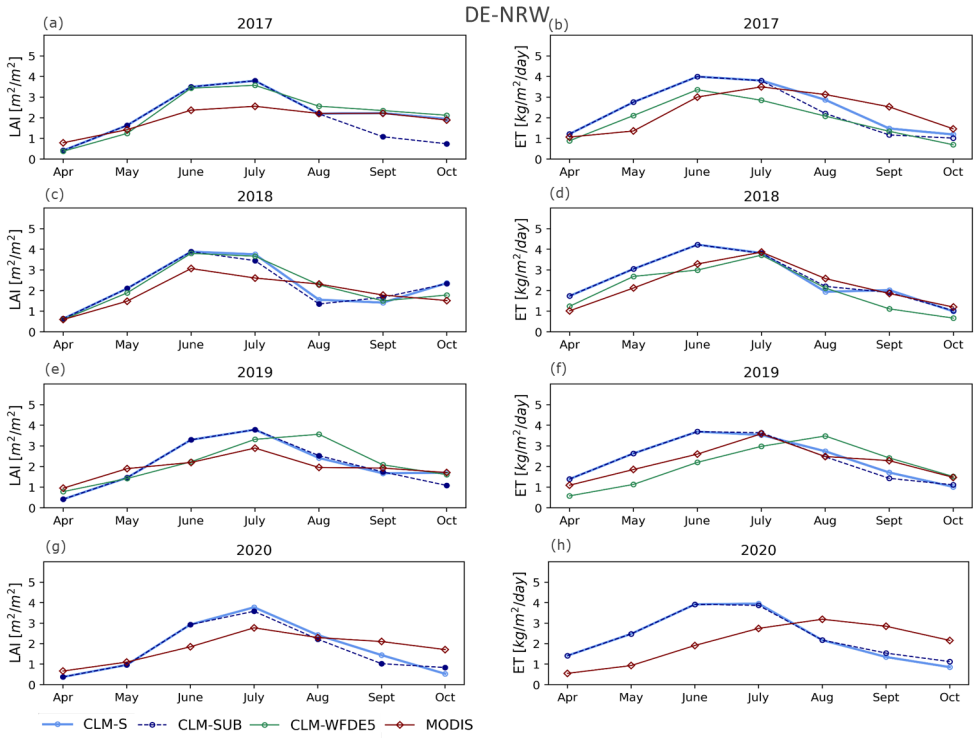

Figure 4.6: (**a**, **c**, **e**, **g**) Monthly mean LAI and (**b**, **d**, **f**, **h**) monthly mean ET derived from MODIS for April-October 2017-2020 compared to corresponding CLM-S and CLM-SUB simulation results, averaged over all land units with more than 70 % cropland within the DE-NRW domain.

4.3.2.3 Regional crop yield predictions

CLM5 was able to reproduce the higher annual total crop yield for the DE-NRW domain compared to AUS-VIC (Figure 4.7, Table 4.2). For AUS-VIC, the simulations resulted in similar magnitudes of overall annual yield compared to statistics from the Australian Department of Agriculture, Water and Environment (ABARES) (Figure 4.7, Table 4.2). CLM-S and CLM-SUB systematically underestimated the crop yield of all crops for the years 2017, 2019 and 2020 while overestimating crop yields for 2018 in comparison to official records. Still, the annual trends of recorded crop yield were to a certain extent captured in the simulations. CLM-S and CLM-SUB showed the lowest yields in 2018 and slightly higher yields in 2017, 2019 and 2020, with 2020 being the most productive year in terms of total crop yield (Figure 4.7). Thus, for AUS-VIC, both the high-yield year of 2020 and the low-yield year of 2017 are well captured in the simulations. However, both the forecast experiments as well as the reference simulations resulted in a slightly lower overall yield for 2019 compared to 2017, which is contrary to the records. CLM5 simulations generally showed lower inter-annual differences in crop yield compared to the records. While the recorded annual crop yield varies by up to 50 %, simulations resulted in differences of up to 17 % for the years 2017-2020. Inter-annual differences in the mean annual crop yield (averaged for the regarded crops) of up to 1.31 t/ha can be observed in the records, while crop yield simulated by CLM5 showed only differences of up to 0.30 t/ha in the forecast simulations (0.28 t/ha for CLM-SUB) and up to 0.24 t/ha in the reference simulations. In addition, we observed a difference in the spatial distribution of crop productivity between the forecast

experiments and reference simulations. While in the forecast experiments the highest crop productivity is simulated in the central and north-eastern parts of the domain, the highest crop productivity in the reference simulations is located in the southern part of the domain closer to the coastline (Figure 4.8).

For the DE-NRW domain, the simulated crop yields are relatively close to recorded yields in terms of magnitudes for all of the analyzed cash crops wheat, corn, and canola (Figure 4.7, Table 4.2). The seasonal experiments were able to capture the high-yield year of 2020 and the yield loss in 2018. In addition, the second- and third-highest yield years are captured in CLM-S and CLM-WFDE5 simulation results but not in CLM-SUB simulation which had higher yields in 2019 than in 2017 (Figure 4.7). CLM-S performed slightly better than CLM-SUB for all years in terms of total yields compared to records, except for 2018 where the CLM-SUB yield is lower and closer to records. CLM5 simulations resulted in smaller inter-annual differences in the total annual crop yield with up to 6 % variation, compared to a recorded inter-annual difference of up to 15 % from 2017 to 2020. While inter-annual differences in crop yield of up to 1.23 t/ha were observed in official records, CLM5 simulations resulted in smaller differences of up to 0.45 t/ha in CLM-S, 0.35 t/ha in CLM-SUB and 0.38 t/ha in reference simulations, on average for the regarded crops. There are no apparent spatial differences in simulated agricultural productivity between the different experiments (Figure 4.9). Despite earlier enhancements to the model code and parameterization scheme (see Boas et al., 2021), the crop module of CLM5 does not include a proper representation of root crops. Here, we focus on the analysis of simulation results for wheat, corn and canola (Figure 4.7). An evaluation of simulation results for root crops can be found in the Appendix B5: Regional crop yield predictions for root crops.

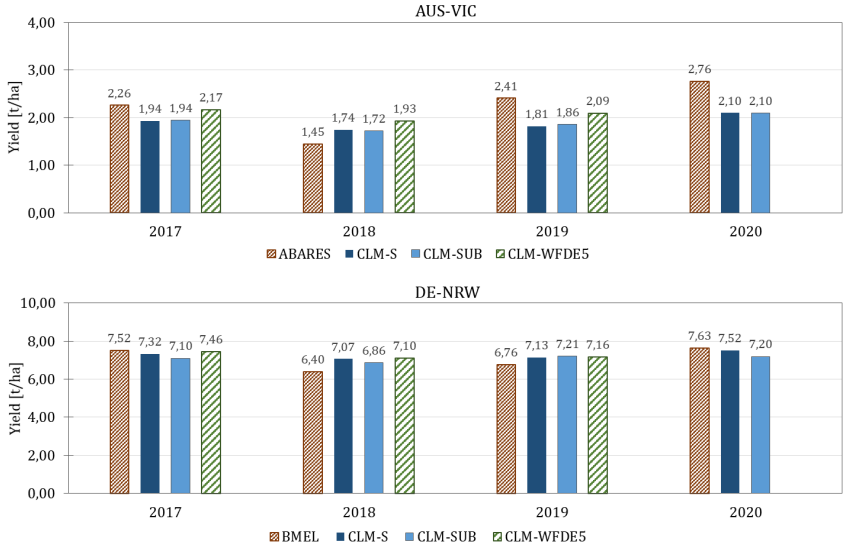

Figure 4.7: CLM-S-, CLM-SUB-, and CLM-WFDE5-simulated crop yield compared to corresponding official production records (**a**) from ABARES (2020), averaged for all analyzed winter crops (wheat, barley, and canola) within the AUS-VIC domain, and (**b**) from BMEL (2020, 2022), averaged for all analyzed crops (wheat, corn, and canola) within the DE-NRW domain, for the years 2017 to 2020. Corresponding data are listed in Table 4.2.

Table 4.2: Simulated crop yields [t/ha] for the main cash crops CLM-S, CLM-SUB and CLM-WFDE5 forcing data for the years 2017 to 2020, compared to official crop statistics from ABARES (2020) for the AUS-VIC domain and from BMEL (2020, 2022) for the DE-NRW domain. The lowest (italics) and highest (bold) yields amongst the respective years are indicated.

	AUS-VIC					DE-NRW			
	2017	2018	2019	2020		2017	2018	2019	2020
Wheat					Wheat				
ABARES	2.54	*1.62*	2.48	**2.98**	BMEL	7.92	*7.91*	8.14	**8.66**
CLM-S	2.15	*2.05*	2.15	**2.23**	CLM-S	7.96	*7.59*	7.61	**8.19**
CLM-SUB	2.15	*2.03*	2.19	**2.23**	CLM-SUB	7.57	*7.24*	**7.76**	7.67
CLM-WFDE5	2.48	2.12	2.26	-	CLM-WFDE5	8.04	7.41	7.67	-
Barley					Corn				
ABARES	2.50	*1.50*	3.05	**3.2**	BMEL	**10.74**	*7.80*	8.44	10.49
CLM-S	2.46	*2.15*	2.17	**2.47**	CLM-S	9.27	*9.12*	9.27	**9.68**
CLM-SUB	**2.47**	*2.12*	2.20	**2.47**	CLM-SUB	9.21	*9.06*	9.34	**9.29**
CLM-WFDE5	2.61	2.38	2.45	-	CLM-WFDE5	9.72	9.31	9.26	-
Canola					Canola				
ABARES	1.73	*1.23*	1.69	**2.11**	BMEL	**3.90**	*3.48*	3.69	3.74
CLM-S	1.20	*1.03*	1.13	**1.35**	CLM-S	**4.73**	*4.49*	4.52	4.69
CLM-SUB	1.21	*1.02*	1.18	**1.35**	CLM-SUB	4.53	*4.28*	4.54	**4.63**
CLM-WFDE5	1.42	1.29	1.56	-	CLM-WFDE5	4.62	4.59	4.46	-
Average					Average				
ABARES	2.26	*1.45*	2.41	**2.76**	BMEL	7.52	*6.40*	6.76	**7.63**
CLM-S	1.94	*1.74*	1.81	**2.02**	CLM-S	7.32	*7.07*	7.13	**7.52**
CLM-SUB	1.94	*1.72*	1.86	**2.02**	CLM-SUB	7.10	*6.86*	7.21	**7.20**
CLM-WFDE5	2.17	1.93	2.09	-	CLM-WFDE5	7.46	7.08	7.16	-

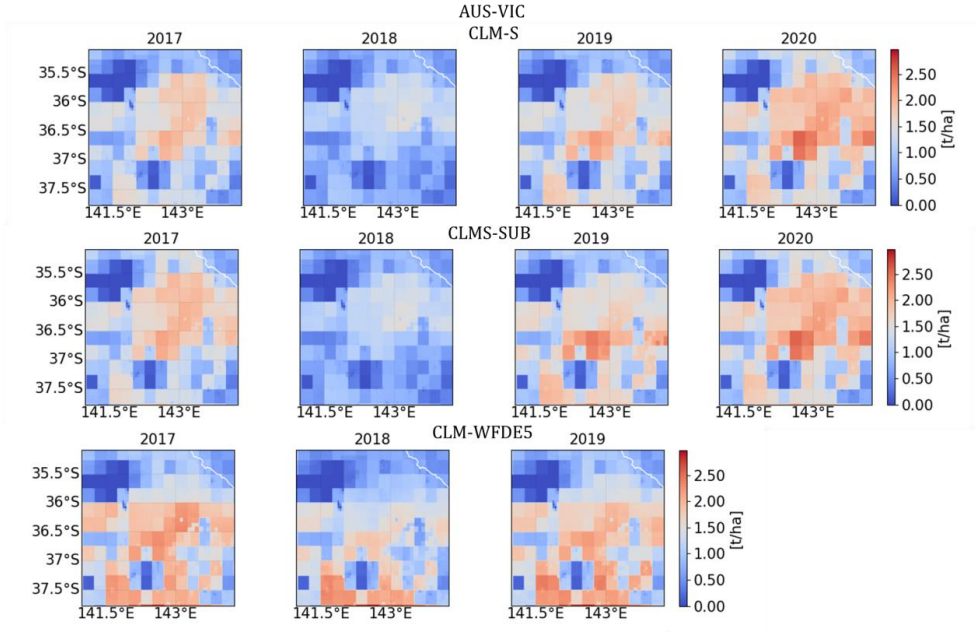

Figure 4.8: Spatial and inter-annual differences in the simulated annual crop yield (averaged) from (top) CLM-S, (middle) CLM-SUB and (bottom) CLM-WFDE5 simulations throughout the AUS-VIC domain for the years 2017 to 2020.

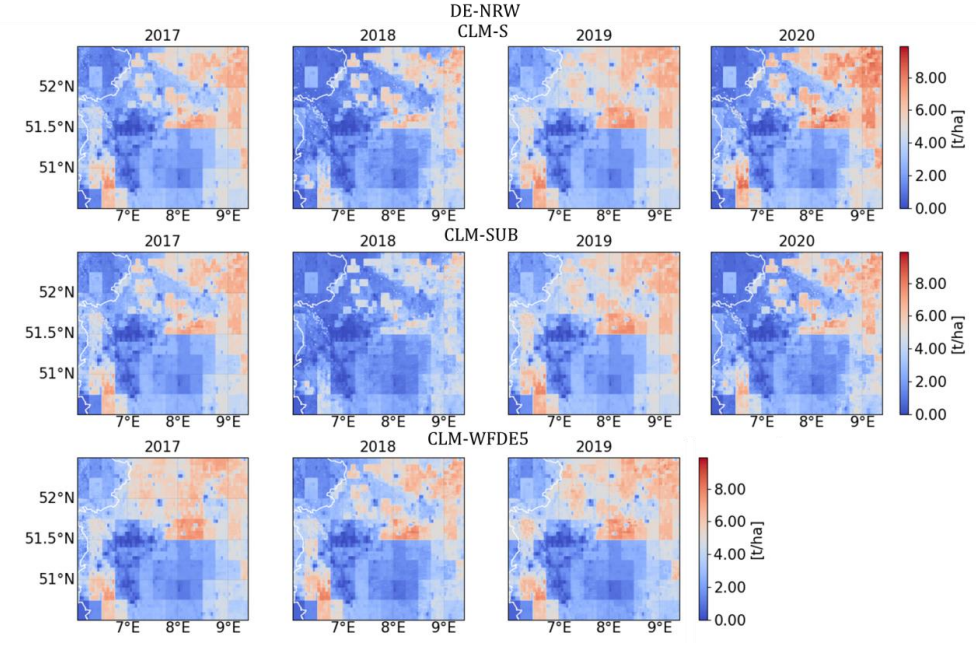

Figure 4.9: Spatial and inter-annual differences in the simulated annual crop yield (averaged) from (top) CLM-S, (middle) CLM-SUB and (bottom) CLM-WFDE5 simulations throughout the DE-NRW domain for the years 2017 to 2020.

4.4 Discussion

Overall, annual crop yield predictions from the forecast experiments were close to results from the reference simulations, with maximum differences between mean annual crop yield simulated with forecasts and with reanalysis of 0.28 and 0.36 t/ha for AUS-VIC and DE-NRW respectively. The forecast experiments were able to reproduce the recorded inter-annual trends of high-yield year (2020) and low-yield year (2018). In addition, the forecast experiments and the reference simulations were also able to reproduce the generally higher total values of annual crop yield for NRW compared to Victoria. The lower recorded crop yields in Victoria can be explained by less productive soils, limited water availability and different crop varieties. This is to a certain extent also represented in CLM5 by a different parameterization and classification of Northern Hemisphere and Southern Hemisphere crops. Furthermore, we used the CLM5 version and parameterization that were optimized for several European cropland sites and crops in an earlier study (Boas et al., 2021). The same study revealed a significant limitation of the default CLM5 phenology module and default crop parameterization in accurately representing European cropland sites, especially in terms of crop phenology (LAI magnitudes and seasonality), and grain yield (Boas et al., 2021). Still, the inter-annual differences are lower in the CLM5 simulations compared to official yield statistics. On the one hand this could be due to the limited resolution and quality of the forecasts that predict general meteorological trends rather than realistic weather patterns (especially for precipitation). Although seasonal and sub-seasonal forecasts correctly predicted drier and hotter trends (e.g. for 2018), the 2018 drought was less pronounced in the forecast than in the observations. In addition, we observed a difference in the spatial pattern of crop productivity over the AUS-VIC domain simulated with forecasts and reanalysis. Reference simulations resulted in a higher crop production in the southern part of the domain than forecast experiments (Figure 4.8). This is related to the influence of near-coastal precipitation events that are not well represented in the forecasts.

We found that the simulated LAI and ET corresponded reasonably well with data from MODIS in terms of magnitudes and fluctuations for the AUS-VIC domain, while for the DE-NRW simulations simulated LAI and ET were larger than the observed values, in particular for the months of May, June and July. The better correlation between the simulated LAI and ET with observed values in the AUS-VIC domain, compared to DE-NRW, can be partly attributed to the larger paddock sizes and more homogeneous land cover in Victoria. The land cover in the state of NRW is more diverse, with numerous urban areas and fallow lands between croplands that are not considered to the same extent by CLM5. Moreover, agricultural management practices and the variety of crop types and cultivars are more diverse in DE-NRW, which is more challenging to represent accurately in simulations due to limitations in the input data and model structure. Several studies over European forest sites found lower absolute LAI values for MODIS compared to ground-based measurements as well as different seasonal dynamics that were partly explained by understory or herbal-layer greening together with cryptophytes and microphytes in the understory that are not included in the measurements (e.g. Wang et al., 2005; Sprintsin et al., 2009). Earlier studies with CLM5 showed relatively good correspondence between CLM5-simulated LAI and field measurements for several crops (Boas et al., 2021). For 2018, the seasonal experiments showed a relatively steep decline in LAI towards the end of the growing season that occurred earlier than for other years. The decline in LAI reflects the early simulation onset of harvest. The early harvest in a large part of the cropland in 2018 is closely linked to the recorded yield losses in NRW (Reinermann et al., 2019).

In general, the inter-annual differences in simulated LAI and ET were relatively low in the forecast experiments and in the reference simulations. This is also reflected in low inter-annual differences in simulated crop yields. The seasonal experiments were able to reproduce the generally higher inter-annual differences in crop yield throughout the AUS-VIC domain (up to 50 % in records and 17 % in simulated yields) compared to the DE-NRW domain (up to 15 % in records and 5 % in simulated yields). After weather conditions, regional agriculture and crop yield are largely impacted by agricultural management decisions (e.g. on crop varieties, planting dates, irrigation, and fertilizer types and application techniques) and other environmental factors such as pests and crop damage from wildlife, which are not sufficiently well represented by CLM5. In addition, the crop module of CLM5 lacks parameterizations for most crop types and varieties, and the fertilizer application routine is highly simplified. These deficiencies in the model structure led to considerable uncertainties in the crop phenology simulated by CLM5.

Thus, the inter-annual variability in crop yield simulated by CLM5 is primarily influenced by the variability of model forcing data and soil moisture states, as it does not consider further anthropogenic or economic factors affecting crop yield, as discussed above. Consequently, the small inter-annual differences in simulated yield suggest that the CLM5 crop module has limited sensitivity to changes in climate conditions. Uncertainties in the simulated annual crop productivity and its low inter-annual differences can be partly explained by the observed systematic biases of the simulated soil moisture content compared to satellite-derived soil moisture products, i.e. ESA-CCI and SMAP L3, and CRNS measurements for both domains.

The reference simulations showed higher correlations between the simulated and observed surface soil moisture than the forecast experiments, which could be expected given the wrong timing of precipitation events in the seasonal weather predictions, while still showing similar systematic differences compared to all the products. Earlier studies with CLM3.5 (e.g. Zhao et al., 2021; Hung et al., 2022) and CLM5 (e.g. Strebel et al., 2022) found pronounced discrepancies in CLM-simulated soil moisture contents and field measurements. In this context, data assimilation has proven to be a valuable technique for reproducing better soil moisture dynamics (Strebel et al., 2022). While the assimilation of soil moisture and groundwater level data into the Terrestrial Systems Modeling Platform (TSMP), which includes an earlier version of CLM (version 3.5), significantly improved simulated soil moisture properties and groundwater levels, it had only limited effects on the resulting evapotranspiration (Hung et al., 2022). Whether a better representation of soil moisture within the model, i.e. through data assimilation, can significantly improve crop yield predictions with CLM5 remains to be evaluated.

The systematic uncertainties in the simulated soil moisture content as well as the low inter-annual differences in predicted crop yield and vegetation parameters (e.g. LAI and ET) show the need to improve the representation of these variables at the technical model level and to improve the model sensitivity to drought stress and other stressors (e.g. frost, pests, hail and wind). A sophisticated representation of crops and agricultural management in Earth system models is essential in order to better assess the impact of climate change on yield in land surface models and specifically CLM5 (Lombardozzi et al., 2020). This includes e.g. the consideration of different types of fertilizers and application strategies, as well as a more detailed representation of root crops. It is crucial for the model to be sensitive enough to respond to changes in seasonality, drought stress and extreme events and realistically reflect these in resulting crop yields in order to study future yield scenarios. A better characterization of plant physiological and hydraulic properties, e.g. via plant trait information, is one suggestion for future model

improvements. Studies over longer simulation periods are needed to confirm whether this low inter-annual difference in CLM5-simulated crop yield is a systematic problem.

One major challenge in applying long-range forecast products in land surface models stems from the extensive pre-processing that is needed, including the temporal downscaling of certain meteorological variables (especially incoming short-wave radiation and precipitation). Simplifications in physical model formulations and uncertainties in the forcing data (e.g. due to coarse spatial and temporal resolution) may have impacted the simulated states. A more sophisticated temporal downscaling of precipitation, e.g. through machine-learning techniques, could help improve the applicability of forecasting products for model applications and improve the quality of model system responses. This becomes especially relevant when studying the impact of extreme events on agricultural productivity and other land surface processes. However, more sophisticated downscaling approaches often require further datasets that are not readily available. A clearer statement about the SEAS5 seasonal forecasting product regarding its overall quality for land surface modelling can be made once it is available for longer timescales. A performance analysis of available hindcasts over longer timescales and for further domains could provide a further systematic evaluation of the accuracy of the products in combination with CLM5. This could also benefit the creation of appropriate tools for end-users in order to increase the user-friendliness of the respective products. For future studies, we additionally propose a benchmarking study of different forecasting products, e.g. from the German Weather Service (DWD), NCEP or CMCC (Centro Euro-Mediterraneo sui Cambiamenti Climatici) Seasonal Prediction System, in combination with different land surface models like CLM5 that can point towards the relative differences and limitations of each product in terms of applicability and overall skill. We believe that such a study, in addition to providing a better representation of the current state of the art in this field, will also benefit the exchange of knowledge at the interface between science and society.

4.5 Conclusion

The effects of climate change and the growing demand for food production entail vulnerability and challenges for regional agriculture and food security across all scales. Reliable high-resolution seasonal weather forecasting systems can provide important information for a multitude of weather-sensitive sectors when combined with a measurable model system response.

Here, we evaluated the quality and applicability of SEAS5 long-range meteorological forecasts in combination with CLM5 for two different regions. Our analysis illustrated that simulations forced with long-range forecasts were able to generate a model system response that was close to reference simulations which is an encouraging result for future studies. Both forecast- and reanalysis-forced models captured the inter-annual differences in yield, at least in sign (increase or decrease). The low-yield and high-yield seasons of 2018 and 2020 are clearly indicated for both simulated regions. The inter-annual differences in crop yield and other vegetation parameters (LAI and ET) were comparably low. Still, simulation results represented the higher inter-annual differences in crop yield across the AUS-VIC domain compared to the DE-NRW domain. While general trends of soil moisture such as the drought in 2018 were reproduced in the simulations, we found systematic overestimations and underestimations compared to different validation datasets and site observations in both the forecast and reference simulations that cannot be explained by uncertainties in the forecasting product alone. These systematic uncertainties in the simulated soil moisture and the low inter-annual differences in simulated vegetation parameters indicate the need for further technical model improvements.

Overall, this study provides a first impression of the utility and skill of the relatively new SEAS5 forecasting system for land surface models and provides an evaluation of the CLM5 crop module potential for regional-scale agricultural yield prediction in two different climate zones. Our evaluation and analysis of the CLM5 crop model performance set the stage for further model evaluation and improvements. A strong conclusion about the SEAS5 seasonal forecasting product regarding its overall quality for land surface modelling can be drawn once this is available for longer timescales. This research underlines the value of combining seasonal forecasts with land surface models such as CLM5 or similar model applications (i.e. crop models).

5 Multi-decadal soil moisture and crop yield variability – A case study with CLM5

Adapted from: Boas, T., Bogena, H., Ryu, D., Western, A., and Hendricks-Franssen, H.-J.: Multi-decadal soil moisture and crop yield variability – A case study with the Community Land Model (CLM5), Journal of Advances in Modeling Earth Systems, 16(9), http://dx.doi.org/10.1029/2023MS004023, 2024.

5.1 Introduction

Agricultural production and management are closely connected to weather and climate conditions and farming yields are significantly affected by inter-annual weather variability. In addition to changes in annual average temperatures and shifts in seasonality, recent climate projections also indicate an increasing number of extreme weather events and a higher intensity of such events, which poses a new challenge for agriculture (Urban et al., 2012; Challinor et al., 2014; Deryng et al., 2014; Rosenzweig et al., 2014; Tai et al., 2014; Levis et al., 2018). The impacts of climate change on food security and agricultural land are a research topic with high relevance to society. In addition, the fluxes of water, energy and carbon associated with agriculture (use of irrigation and fertilizer, timing of crop growth and fallow periods, etc.) can have implications for local and regional weather and climate, and biochemistry (Sacks et al., 2009).

Numerical modelling of Earth system components plays a vital role in assessing the impacts of climate change, exploring adaptation strategies and their impact on various parts of the terrestrial system. Land surface models (LSMs) such as the Community Land Model (CLM) are essential tools for studying changes in response to weather conditions and are particularly valuable for examining the effects of climate change on agricultural land at larger spatial scales. Prognostic simulations of land surface models (LSMs) and global crop models can be used to quantify the impact of climate change on agro-ecosystems and study the response of agricultural land to inter-annual weather variations. While both contribute to our understanding of Earth's systems, LSMs encompass a broader focus on land surface processes, including natural ecosystems, while global crop models specialize in simulating and analysing agricultural systems at a global scale. For example, results from the Global Gridded Crop Model Intercomparison (GGCMI; Franke et al., 2020; Jägermeyr et al., 2021) offer valuable insights into long-term productivity trends and the adaptive capacity of the agricultural system under different climate scenarios on a global scale and have been applied to investigate various questions, e.g. on challenges for food production, future crop yields and irrigation water demand (e.g. Wada et al., 2013; Müller et al., 2015; Blanchard et al., 2017; Jägermeyr et al., 2021). The Agricultural Model Intercomparison and Improvement Project (AgMIP) is another important example of a research initiative focused on improving agricultural models and enhancing our understanding of climate change impacts on food security and developing integrated assessment tools for decision-making in agriculture (e.g. White et al., 2013; Rosenzweig et al., 2013, 2014; Tumbo et al., 2020; Asseng et al., 2019; Cammarano et al., 2020; Kimball et al., 2019). Multiple studies have showcased assessments of AgMIP datasets at the regional scale and for a variety of crops, which revealed significant variations in climate change impacts on wheat yields across different regions, emphasizing the need for tailored adaptation strategies (e.g. Kimball et al., 2019; Rosenzweig et al., 2014; Cammarano et al., 2020; Asseng et al., 2019).

The impacts of climate change on food security have received considerable attention in recent years. Still, the consequences of altered weather patterns on yearly yield variations remains an important area of interest. The potential value of LSMs for these purposes largely depends on their ability to adequately simulate the crop productivity variability, which has not been tested rigorously for dryland and dominantly rain-fed cropping regions, where yield is vulnerable to drought and heat stresses. The inter-annual variability of model output is an important performance measure for land surface models (LSMs) as it reflects the ability of the model to capture the natural variability observed in the real world over multiple years. Assessing and understanding inter-annual variability of terrestrial fluxes is crucial for various applications, including climate projections, agricultural management, water resources management, and ecosystem dynamics. Reliable predictions of regional crop yield variability can help to design agricultural adaptation and mitigation strategies and can provide useful information for local stakeholders and policy makers.

In order to adequately represent inter-annual variability of crop growth, it is crucial for the model to sufficiently represent the soil moisture regime and corresponding vegetative drought stress in response to changes in precipitation amounts, specifically in dominantly rain-fed areas. While an increasing number of studies focus on incorporating irrigation and human water use in LSMs and hydrological models in general (e.g. Pokhrel et al., 2016, 2012; Shah et al., 2019; Yassin et al., 2019; Xia et al., 2022; McDermid et al., 2023), many challenges still remain in representing rain-water limited agricultural regimes in general circulation models and LSMs.

The realistic representation of many processes is still a challenge in LSMs. Major challenges arise from the complex representation of soil-plant-atmosphere feedbacks, root water uptake and plant responses to environmental stress, land use and land cover change, spatial heterogeneity in soil properties, vegetation cover and topography, and uncertainties in model parameterizations (Huntzinger et al., 2013; Franks et al., 2018; Trugman et al., 2018; Sulis et al., 2019a; Dagon et al., 2020; Fisher and Koven, 2020; Lombardozzi et al., 2020; Blyth et al., 2021; Sabot et al., 2022). The ability of LSMs to capture the impacts of land use change on biogeochemistry and hydrology is often limited by the oversimplification of human influences on land use and land cover, such as agricultural practices and management decisions. Additionally, multiple studies found that the representation of plant responses to environmental stress need to be improved in global LSMs (Sabot et al., 2022; De Kauwe et al., 2015b; Franks et al., 2018; Sulis et al., 2019b). In a recent study, Boas et al. (2023) highlighted the potential value of combining CLM5 with seasonal weather forecasts. They also identified limitations of the model in capturing inter-annual variations in agricultural characteristics over a short period of four cropping seasons.

Focussing on soil water, root water uptake plays an important role in rain-fed agricultural systems and is often simplified in LSMs, which can affect simulated vegetation growth, productivity and water use efficiency of the plants (De Kauwe et al., 2015b; Sulis et al., 2019a). Most LSMs, including earlier versions of CLM, utilize soil moisture stress parameterizations where water stress is based on a plant wilting factor (calculated with the soil water matric potential values corresponding to plant dependent parameters for fully open and fully closed stomata conditions) (Lawrence et al., 2019). In contrast to this physical representation, the active role of roots in redistributing water within the soil profile has been investigated by numerous studies and different formulations of root hydraulic redistribution have been included in LSMs, highlighting the relevance of atmospheric processes and carbon and nutrient cycling (e.g. Li et al., 2012; Tang et al., 2015; Ryel et al., 2002; Zheng and Wang, 2007; Yan and Dickinson, 2014; Sulis et al., 2019). CLM5 includes a plant hydraulic stress model that replaced the empirical soil moisture stress formulation from earlier model versions (Lawrence et al., 2019). This plant hydraulic

stress scheme simulates vegetation water potential for every segment in the soil-root-stem-leaf system and includes a stress formulation where leaf water potential is used to attenuate photosynthesis. This plant hydraulic framework provides a better physical basis for multiple processes represented in CLM, such as the attenuation of photosynthesis and transpiration during drought conditions (Lawrence et al., 2019). A similar approach has been presented in Sulis et al. (2019), where a macroscopic root water uptake model was introduced in CLM (version 4.0) that also explicitly simulated the leaf water potential at stomatal closure defining water stress conditions for the plants. They found that root hydraulic properties control transpiration during dry periods and that the roots distribution induced a larger variability in the hydraulic model response (Sulis et al., 2019a). Their modified model resulted in a good correlation of simulated and observed transpiration fluxes for a winter wheat test site and a more distinct response under water stress conditions compared to default model simulations (Sulis et al., 2019a). The subject of plant response to drought stress also encompasses the representation of stomatal conductance. In a recent study by Sabot et al. (2022), multiple empirical and optimization formulations for stomatal conductance were evaluated using a simplified LSM framework. They found that the selection of the stomatal conductance model could considerably influence the simulation of carbon and water exchange in global models. Further factors that can impact inter-annual variations in yield variability and that also need to be considered in the numerical representation of the system are changes in crop management practices in relation to technical advances, public policies, and farming techniques such as fertilization or double-cropping, as well as pests, diseases, and floods (Lombardozzi et al, 2020).

Furthermore, the accuracy of LSMs also heavily depends on their complex parameterizations that aim to account for a wide range of variability in soil and vegetation types. Uncertainties arise due to the limited availability of observational data for parameter estimation and validation as well as the complexity of the parameterizations themselves, leading to potential errors in model predictions (Huntzinger et al., 2013; Sulis et al., 2015; Lu et al., 2017; Lombardozzi et al., 2020; Boas et al., 2021). In addition to improvements in model parameterization (e.g. through new methods for parameter estimation and uncertainty quantification), the study by Fisher and Koven (2020) highlights the role of data assimilation techniques, including the use of remote sensing and machine learning, that can help improve the accuracy of LSM predictions (e.g. Dagon et al., 2020; Pinnington et al., 2020; 2021).

This study aims to analyse the model performance across two regions with different climates and dominated by rain-fed agriculture, for a period spanning multiple decades. Specifically, we assessed the ability of the CLM5 with its prognostic crop module to capture the inter-annual variability of crop yield, soil moisture and plant water stress over two simulation domains: one covering large parts of the south-east Australian wheat belt in the state of Victoria in Australia (AUS-VIC) and the other extending over the state of North Rhine-Westphalia in Germany (DE-NRW). Simulations were conducted over the two regional domains, which are in different climate zones, and forced with the global bias-adjusted reanalysis dataset WFDE5 (Cucchi et al., 2020). We compared our simulation results with recorded yields and examined which variables (i.e., seasonal rainfall, root zone soil moisture) dominantly drive changes in CLM5-predicted total yield and yield variability. Additionally, the simulated multi-decadal near-surface soil moisture was compared with two reference datasets, the combined ESA-CCI product (Dorigo et al., 2017) and the satellite-derived SMAP L3 soil moisture product (Entekhabi et al., 2016). In this study, we provide an overview on multi-decadal model performance across two model domains, both of which are dominated by rain-fed agriculture and with state-wide agricultural yield statistics available as validation data. The

results of this follow-up study provide valuable insights for the use of CLM5 in agricultural landscapes. We addressed both the model's skill and limitations in predicting long-term variations in annual crop productivity and soil moisture levels at the regional scale, which allowed us to highlight specific areas in need for further investigation.

5.2 Methodology

5.2.1 Land surface model

In this study, all simulation were carried out with CLM5, which is the first model version that includes a fully prognostic crop module (Lawrence et al., 2018, 2019; Lombardozzi et al., 2020). In CLM5, human management is represented by fertilization and irrigation. Other aspects of agricultural management, such as residue management and soil tillage, or ecological factors affecting crops, such as pests, diseases, or wildlife damage, are also not accounted for in CLM5 at this stage of development. Crop growth and phenology are simulated based on atmospheric factors (i.e. incoming shortwave and longwave radiation, atmospheric pressure, relative humidity, wind speed and temperature) and water availability from irrigation and precipitation (soil moisture). Besides, crop biomass and yield depend on nutrient availability in the soil. Fertilization is represented in a simplified scheme by adding prescribed amounts of nitrogen directly to the soil mineral pool. The possibility of simulating crop growth and development in CLM5 enables a broader and more accurate approach to address economic challenges and questions in land use change and agriculture (e.g. Lobell et al., 2006). Furthermore, a new plant hydraulic stress formulation was introduced in CLM5 that explicitly simulates the transport of water within the soil-root-leaf system, as well as the plant-mediated vertical hydraulic redistribution of soil water from wet to dry soil layers was implemented (Lawrence et al., 2018, 2019). While CLM5 does not explicitly model groundwater dynamics, it indirectly considers its effects on crop growth through its representation of soil moisture dynamics (redistribution within the soil column) and groundwater discharge and recharge. Groundwater is simulated with explicit representation of the saturated and unsaturated zone, using soil thickness and impermeable bedrock as a zero-flux boundary. Soil profile depths are based on a spatially explicit soil thickness data product by Pelletier et al. (2016). Additionally, the stomatal conductance scheme was updated in CLM5 to the approach proposed by Medlyn et al. (2011). The new model formulations led to better performance in simulating ecosystem water fluxes, vegetation water stress, and productivity, thus providing a basis for an improved plant water use and water stress simulation in future applications of the model (Lawrence et al., 2019).

The plant hydraulic stress routine simulates water transport in the soil-root-stem-leaf system by explicitly calculating water potential gradients based on Darcy´s Law for porous media flow (Lawrence et al., 2018, 2019 and references therein). The representation of either positive or negative soil-to-root fluxes depending on the water potential gradients allows for a plant-mediated vertical hydraulic redistribution of soil water from wet to dry soil layers through vegetation tissue (Lawrence et al., 2018, 2019).

Water potential gradients in the soil-root-stem-leaf system (water fluxes from soil to root, from root to stem and in between the plant segments) are modelled at each time step as follows (Lawrence et al., 2018, 2019):

$$q = kA\,(\psi_1 - \psi_2) \tag{5.1}$$

where q is the flux of water spanning the segment between ψ_1 and ψ_2 [mmH_2O/s], ψ_1 - ψ_2 is the gradient in water potential across the segments [mmH_2O], k is the hydraulic conductance [s^{-1}] and A is the area basis [m^2/m^2].

The segment's resistance to hydraulic stress is calculated with a sigmoidal curve function, where hydraulic conductance decreases as water potentials decrease. The maximum segment conductance is multiplied by a sigmoidal function that accounts for the percentage loss of conductivity using the water potential at 50% loss of conductivity (p_{50}) and a shape parameter (Lawrence et al., 2018):

$$k = k_{max} \cdot 2^{-\left(\frac{\psi_1}{p50}\right)^{c_k}} \tag{5.2}$$

where k_{max} is the maximum segment conductance [s^{-1}], p_{50} is the water potential at 50 % loss of conductivity [mmH_2O], ψ_1 is the water potential of the lower segment terminus [mmH_2O] and c_k is the vulnerability curve shape-fitting parameter [-]. Parameters such as k_{max}, p_{50} and c_k strongly control the modelled plant hydraulic stress routine and thus determine the capability of the plant to extract water from the soil and to resist hydraulic stress. These routines are physically constrained by the plant hydraulic parameterization after Kennedy et al. (2019) which until now contains the same parameters for all crops.

In this routine, the vegetation water potential responds to water supply and transpiration demand (i.e. plant water demand), and transpiration demand is dependent on stomatal conductance. The leaf stomatal conductance and leaf photosynthesis are modelled for sunlit and shaded leaves separately based on the approaches after Medlyn et al. (2011), and Farquhar et al. (1980) for C_3 plants and Collatz et al. (1992) for C_4 plants (Lawrence et al., 2018). Adapted from Medlyn et al. (2011), the leaf stomatal resistance is calculated using the net leaf photosynthesis, the vapor pressure deficit and the CO_2 concentration at the leaf surface with plant-specific slope parameters based on de Kauwe et al. (2015a) and Lin et al. (2015) as follows (Lawrence et al., 2018):

$$\frac{1}{r_s} = g_s = g_o + 1.6\left(1 + \frac{g_1}{\sqrt{D}}\right)\frac{A_n}{\frac{c_s}{P_{atm}}} \tag{5.3}$$

where r_s is leaf stomatal resistance [s m^2/µmol], g_o is the minimum stomatal conductance [µmol/m^2/s], A_n is leaf net photosynthesis [µmolCO_2/m^2/s], g_1 is the plant dependent slope parameter [-] (for a full parameter table see Lawrence et al. (2018)), c_s is the CO_2 partial pressure at the leaf surface [Pa] and P_{atm} is the atmospheric pressure [Pa] and D is the vapor pressure deficit at the leaf surface [kPa].

The leaf transpiration is regulated by the leaf water potential. It is calculated for shaded and sunlit leaves separately based on maximum transpiration multiplied by the percent of maximum transpiration as modelled by the sigmoidal loss function (Equation 2) (Lawrence et al., 2018). Plant water stress is then calculated for shaded and sunlit leaves separately as the ratio of stomatal conductance of the leaf transpiration relative to maximum stomatal conductance corresponding to maximum transpiration (Lawrence et al., 2018). Leaf transpiration and the transpiration water stress (transpiration beta) are calculated for sunlit and shaded leaves separately as follows:

$$E = E_{max} \cdot 2^{-\left(\frac{\psi}{p50_e}\right)^{c_k}}, \tag{5.4}$$

$$\beta_t = \frac{g_s}{g_{s,max}}, \tag{5.5}$$

where E is leaf transpiration [mm/s], E_{max} is the leaf transpiration in the absence of water stress [mm/s], β_t is the transpiration water stress [-], g_s is the stomatal conductance of water corresponding to leaf transpiration [µmol/m^2/s], and $g_{s,max}$ is the stomatal conductance of water corresponding to maximum transpiration [µmol/m^2/s]. The calculated transpiration water stress is then used for the attenuation of photosynthesis, where $\beta_t = 1$ is no water stress and $\beta_t < 1$ is the relative transpiration water stress.

For a more detailed description of the algorithms applied in CLM5, the reader is referred to the model technical description (Lawrence et al., 2018, 2019) and references therein.

In this study, all simulations were carried out with a modified version of CLM5 that was developed in an earlier study by Boas et al. (2021). This CLM5 version was extended with an adaptation of the winter cereal representation after Lu et al. (2017), a cover cropping and crop rotation routine, and crop phenology parameters for the northern hemisphere crop types winter wheat, sugar beet and potatoes. These modifications have proven to significantly improve the simulation of energy fluxes, vegetation states and carbon fluxes (e.g. leaf area index (LAI), net ecosystem exchange (NEE) and yield) at several Central European sites (Boas et al., 2021).

5.2.2 Study areas and input data

Simulations were conducted for two intensive cropping regions in different climate zones, spanning a two-decade period from 1999 to 2019 (Figure 5.1). The first domain covers large parts of the south-east Australian wheat belt in the state of Victoria in Australia (AUS-VIC) and is characterized by large rain-fed agricultural areas with large paddock sizes, primarily dedicated to cereal cultivation, and extensive naturally vegetated or woody areas (i.e., grasslands, native woody cover and woody horticulture). The agricultural parts of the domain are mostly characterized by deep groundwater tables. The main cash crop in this domain is winter wheat, followed by barley and canola. Land cover information for the AUS-VIC domain was based on the Victorian Land Use Information System (VLUIS) product for the year 2016 (Morse-McNabb et al., 2015; Victoria Government Data Directory, 2020). This dataset was generated through a combination of time series analysis of remote sensing data (MOD13Q1 or MYD13Q1 by NASA) and annually collected field data (Morse-McNabb et al., 2015), and provides detailed information on land use and land cover for the entire state of Victoria. Unfavourable weather conditions for winter crop farming can have profound impacts on regional grain production and yield per area (ABARES, 2020).

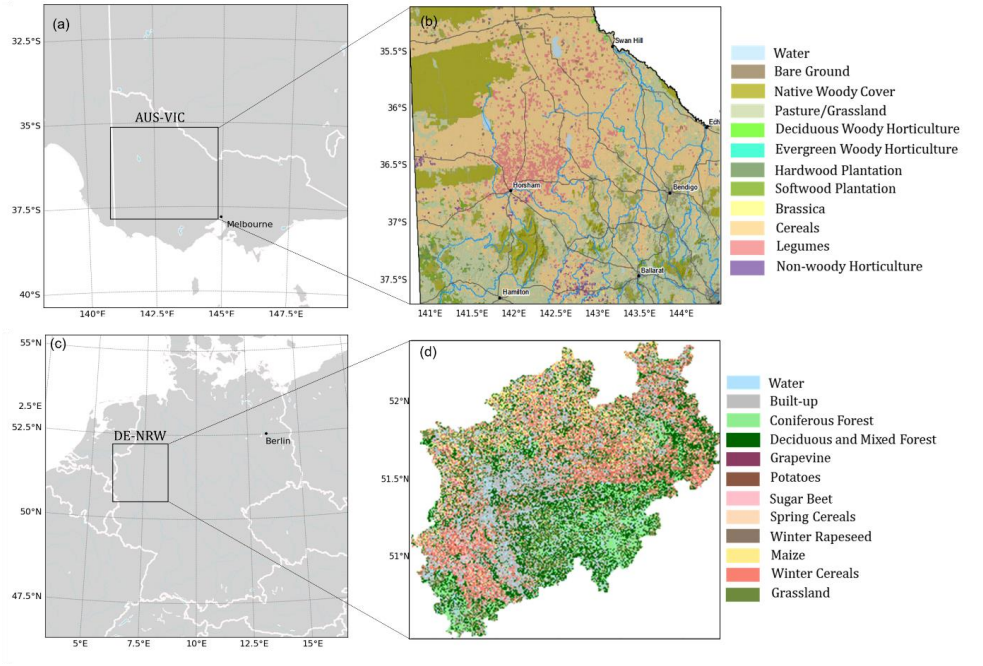

Figure 5.1: (**a**) AUS-VIC simulation domain extent and (**b**) dominant land use type based on VLUIS data, modified after (Victorian Government Data Directory, 2020; Morse-McNabb et al., 2015); (**c**) DE-NRW simulation domain extent and (**d**) dominant land use type based on Griffiths et al. (2018, 2019), modified from Boas et al. (2023).

The second domain covers the state of North Rhine-Westphalia in Germany (DE-NRW). It is characterized by a diverse landscape with urban, natural, and mixed agricultural areas that are mostly rain-fed. The groundwater regime in this domain is largely characterized by relatively shallow groundwater tables and a high degree of human influence due to intensive land use and urbanization. Land cover information for the DE-NRW domain was based on the 30-m resolution land cover dataset by Griffiths et al. (2019). This dataset was generated from Sentinel-2A MSI and Landsat-8 OLI observation data from the NASA Harmonized Landsat-Sentinel dataset for the year 2016 (Claverie et al., 2018). Compared to agricultural reference data, the derived crop type and land cover map showed a high overall accuracy of over 80%, particularly for crop types with high abundances such as cereals, maize, and canola (Griffiths et al., 2019). The agricultural land cover in DE-NRW is primarily concentrated in the northern and western part of the domain, alongside natural vegetation and urban areas. The main cash crops in this region are winter wheat, winter barley, corn, sugar beet and rape seed (Figure 1, BMEL, 2020, 2022). In the southern part of the domain, which includes the Eifel, Bergisches Land and Sauerland regions, forests and grassland are the dominant land cover. Due to a late cold spell in late February/early March, agricultural yields in the area were significantly impacted in 2018. In addition, extreme heat and dry spells during both summers of 2018 and 2019 resulted in unusually high spatial variability of yield, particularly for cereals (NRW State Government, 2020; BMEL, 2020, 2022).

For both domains, soil variables such as clay, sand and organic matter content were derived from the global SoilGrids database (Hengl et al., 2017). SoilGrids provides soil information at seven depths (0, 0.05, 0.15, 0.30, 0.60, 1 and 2 m) at 250 m, 500 m and 1 km spatial resolution. Further soil properties, such as the saturated hydraulic

conductivity and soil retention parameters are calculated within CLM5 based on the pedotransfer function after Cosby et al. (1984). Irrigation demand is dynamically calculated based on simulated soil moisture conditions. For irrigated croplands, the model assesses daily whether irrigation is needed. Irrigation is triggered when the crop leaf area index is greater than zero and available soil water drops below a specified threshold.

The amount of fertilizer is prescribed by crop functional types and varies spatially based on the LUMIP land use and land cover change time series (Lawrence et al., 2016). The LUMIP time series (1999-2019) provides land use and land cover data for prescribing fertilizer rates in the CLM5 model. Fertilizer application is adjusted spatially based on crop type and regional agricultural intensity, representing average historical rates. While spatial variability is accounted for, temporal changes in fertilization practices are not simulated beyond a repeated annual cycle, with nitrogen from industrial fertilizer applied consistently over 20 consecutive days each year. Manure nitrogen is uniformly applied at 0.002 kg N/m²/year across all crop types.

5.2.3 Forcing and validation data

The simulations were forced with the bias-adjusted global reanalysis dataset WFDE5 (Cucchi et al., 2020). The WFDE5 dataset provides all meteorological variables that are needed to force CLM5 (i.e., precipitation, incoming shortwave and longwave radiation, atmospheric pressure, relative humidity, wind speed and temperature) at hourly time step for the period from 1979 to 2019, and at a 0.5° spatial resolution. The dataset was generated using the WATCH Forcing Data (WFD) methodology (Cucchi et al., 2020) based on the ERA5 reanalysis product (Hersbach et al., 2020).

In order to validate and compare model results for crop yields, we used state-wide agricultural statistics. For Victoria, official records of annual crop yields are available for all simulated years from the database of the Australian Bureau of Agricultural and Resources Economics and Sciences (ABARES). The Australian crop report contains both realised and forecast growing area, production and yield for the major winter and summer crops on the Australian state level. The reports are produced with the participation of industry contacts and are released quarterly with the most recent estimates and updated forecasts.

For the DE-NRW domain, official agricultural records are available for 2005-2019 from IT.NRW (2022). The yield statistics are compiled for selected agricultural crops at the state and municipal levels in Germany. This information is gathered through an annual crop reporting process, where industry contacts with local expertise for the reporting areas, typically a municipality, provide harvest information and yield estimates for the year. Acknowledging the inherent uncertainties in these agricultural datasets, i.e. stemming from variations in reporting methods, they provide valuable insights into the overall magnitudes and yearly trends of crop yield. As such, they serve as suitable validation datasets to assess the general quality of yield predictions in terms of magnitudes and inter-annual variations.

For validating simulated soil moisture contents in the top soil layers (up to 0.06 m depth), we used the CCI Soil Moisture-Combined dataset, version 07.1 (ESA-CCI), from the European Space Agency's (ESA) Soil Moisture Essential Climate Variable (ECV) Climate Change Initiative (CCI) project (Dorigo et al., 2017; Gruber et al., 2017, 2019; Preimesberger et al., 2021). The ESA-CCI-SM combined product provides global daily volumetric soil moisture data at a spatial resolution of 0.25 degrees from 1978 to 2021 (Dorigo et al., 2017; Gruber et al., 2017, 2019; Preimesberger et al., 2021). Additionally, we compared simulation results to the Soil Moisture Active Passive (SMAP) mission Enhanced Level-3 radiometer soil moisture product (SMAP L3) that is available since

March 2015 and comprises soil moisture retrievals at a spatial resolution of 36 and 9 km (Entekhabi et al., 2016). When comparing daily simulation results with satellite-derived soil moisture retrievals, it is important to acknowledge the inherent uncertainties of these products, e.g. due the impact of vegetation cover and surface characteristics, variations in satellite sensor characteristics, algorithm and model uncertainties etc., which may result in a distorted representation of daily soil moisture dynamics (Seo and Dirmeyer, 2022). Furthermore, it is crucial to recognize that these products represent near-surface soil moisture and can only serve as an indication for the conditions over the entire root zone.

5.2.4 Simulation experiments and performance metrics

Table 5.1: Overview of conducted simulation experiments, used forcing and simulation period, for each domain.

	Description	Forcing	Simulation period
I	Spin-up	CRUNCEP	1901-2016, loop
II	Realistic land cover simulations	WFDE5	1999-2019
III	Winter wheat monoculture experiments	WFDE5	1999-2019
IV	Winter wheat monoculture experiments with reduced precipitation	modified WFDE5 with 50% reduced precipitation	1999-2019

As a first step, a model spin-up of more than 850 simulation years was conducted for each simulation domain so that the model ecosystem variables reach equilibrium prior to production simulations (experiment I in Table 5.1). This spin-up process comprised an initial phase under accelerated decomposition conditions lasting more than 300 years, followed by a final phase in normal mode lasting over 500 years. The spin-up is essential to attain equilibrium in ecosystem carbon and nitrogen pools, gross primary production, and total water storage. Notably, achieving equilibrium is particularly time-intensive for the slow carbon and nitrogen pools. For the spin-up, the combined global CRUNCEP atmospheric forcing dataset (Viovy, 2018) was used, which consists of the CRU TS3.2 0.5 x 0.5 degree dataset covering the period from 1901-2002 (Harris et al., 2014) and the NCEP reanalysis 2.5 x 2.5 degree 6-hourly dataset available for 1948-2016 (Kalnay et al., 1996).

Then, simulations were conducted for both study domains with high resolution land cover information as described above for the period 1999-2019, forced with WFDE5 data (experiment II in Table 5.1) (Cucchi et al., 2020). In the following step, the land cover was modified by setting the CFTs on all cropland land units within the domain to winter wheat. This synthetic winter wheat monoculture was simulated for both domains with the WFDE5 forcing data set, and for the years 1999-2019 (experiment III in Table 5.1). Additionally, the same set of simulations was conducted for the synthetic winter wheat monocultures with 50 % reduced WFDE5 precipitation to synthetically create more drought stress for the crop (experiment IV in Table 5.1).

The model performance was statistically evaluated using the root mean square error (RMSE), the Pearson correlation coefficient (r), the squared correlation coefficient (R^2), and the mean bias error (MBE):

$$RMSE = \sqrt{\frac{1}{n}\sum_{i=1}^{n}(x_i - y_i)^2}, \tag{5.6}$$

$$r = \frac{\sum(x_i - \bar{x})(y_i - \bar{y})}{(n-1)\cdot\sigma_x\sigma_y}, \tag{5.7}$$

$$R^2 = 1 - \frac{\sum_{i=1}^{n}(y_i - x_i)^2}{\sum_{i=1}^{n}(y_i - \bar{y})^2}, \tag{5.8}$$

$$MBE = \frac{\sum_{i=1}^{n}(x_i - y_i)}{n}, \tag{5.9}$$

where n is the total number of time steps (days or years), x_i and y_i are the simulated and the observed values of a given variable at every time step i, overbar represents the mean value, and σ_x and σ_y are the standard deviations of the simulated and observed data respectively.

In order to quantify the inter-annual variability of annual crop yields and daily soil moisture contents, the mean absolute anomaly (MAA [%]), the mean absolute deviation (MAD) and mean absolute deviation ratio (MAD_r [-]) were defined as follows:

$$MAA = \frac{\sum_{i=1}^{n}\left(\left|\frac{Y_i - \bar{Y}}{\bar{Y}}\right| \cdot 100\right)}{n}, \tag{5.10}$$

$$MAD = \frac{\sum_{i=1}^{n}(|Y_i - \bar{Y}|)}{n}, \tag{5.11}$$

$$MAD_r = \frac{MAD_X}{MAD_y}, \tag{5.12}$$

where i is time step (days or years) and n the total number of time steps, Y_i is the respective variable [t/ha] at every time step i, $\bar{Y}$ is the 1999-2019 average of that variable [t/ha], MAD_X and MAD_y are the mean absolute deviation [t/ha] for the simulations and the reference dataset respectively.

The absolute anomaly (AA) and the absolute deviation (AD) provide the percentage difference and the average absolute difference, respectively, between observations at the respective time step and the long-term average. Their mean values MAA and MAD provide insight into overall variability. Lower values in both metrics indicate less variability and a closer alignment to the long-term average. The MAD_r compares the calculated variability (MAD) between simulations and the reference dataset, with values nearing one indicating greater similarity.

5.3 Results

5.3.1 Soil moisture regime

We compared the simulated surface soil moisture content (SMC) of the top soil layers (0 – 0.06 m depth) with data from the combined ESA-CCI product (Dorigo et al., 2017; Gruber et al., 2017, 2019) and the satellite derived SMAP L3 data (Entekhabi et al., 2016).

For AUS-VIC, the simulated SMC is systematically higher than ESA-CCI during the main cropping season (May - October) and lower during the austral summer months (December - February), resulting in a R^2 value of approximately 0.7 (Figure 5.2). The SMAP L3 product generally showed larger day-to-day fluctuations compared to the ESA-CCI data, with higher values during the main cropping season (May - October) and lower values during the summer months (December - February) than ESA-CCI. The simulations resulted in SMC very close to the SMAP L3 product during the first quarter of the year, while underestimating maximum values in the SMAP L3 data set during the growing season (May - October).

For the DE-NRW domain, comparison against ESA-CCI revealed large deviations compared to the simulated surface SMC, resulting in an R^2 value of approximately 0.4. For DE-NRW, the simulated winter season (December – February) and early growing season (March, April) SMC were significantly overestimated for all years, while

late summer SMCs (August, September) were systematically underestimated with respect to ESA-CCI (Figure 5.3). The SMAP L3 product showed smaller values compared to ESA-CCI and was largely overestimated by CLM5 results for the majority of years and months, particularly during the main growing season (April-August) (Figure 5.3). The drought years of 2018 and 2019 are reflected in lower simulated SMC compared to the 1999 - 2019 average, particularly in (late) summer, where CLM5 showed lower values than SMAP L3 in 2019 (Figure 5.3i). Simulated soil moisture by CLM5 showed a smaller inter-annual variability than SMAP, but a larger inter-annual variability than ESA-CCI. For the AUS-VIC domain, the mean absolute anomaly (MAA) for simulated soil moisture was approximately 30% (0.063 m³/m³ MAD), while it was 19% (0.036 m³/m³ MAD) for ESA-CCI and 48% (0.097 m³/m³ MAD) for SMAP (Table 5.2). Similarly, for the DE-NRW domain, the simulated soil moisture showed an MAA of approximately 17% (0.058 m³/m³ MAD), while ESA-CCI showed 7% MAA (0.02 m³/m³ MAD) and SMAP L3 had 23% MAA (0.058 m³/m³ MAD). The correlations between the simulated daily surface soil moisture and the reference datasets were generally higher for the AUS-VIC domain compared to DE-NRW. The correlation coefficient between simulated soil moisture and both reference datasets in AUS-VIC was approximately 0.85, whereas it was approximately 0.6 for both SMAP and ESA-CCI in DE-NRW.

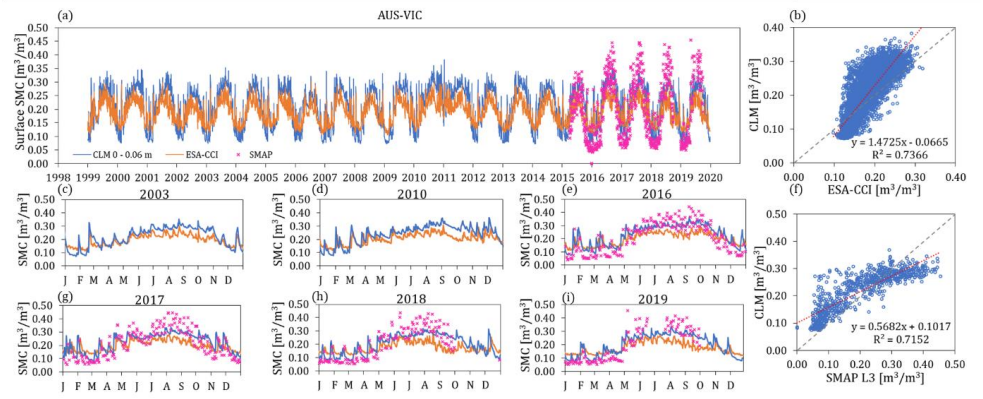

Figure 5.2: Simulated daily surface soil moisture (0 - 0.06 m depth) throughout the AUS-VIC domain (**a**) from 1999 – 2019, and (**c**, **d**, **e**, **g**, **h**, **i**) for individual years, compared to the ESA-CCI product and available SMAP L3 data. Scatterplots show the correlation between simulated SMC and (**b**) ESA-CCI, and (**f**) SMAP L3, with the respective regression equations.

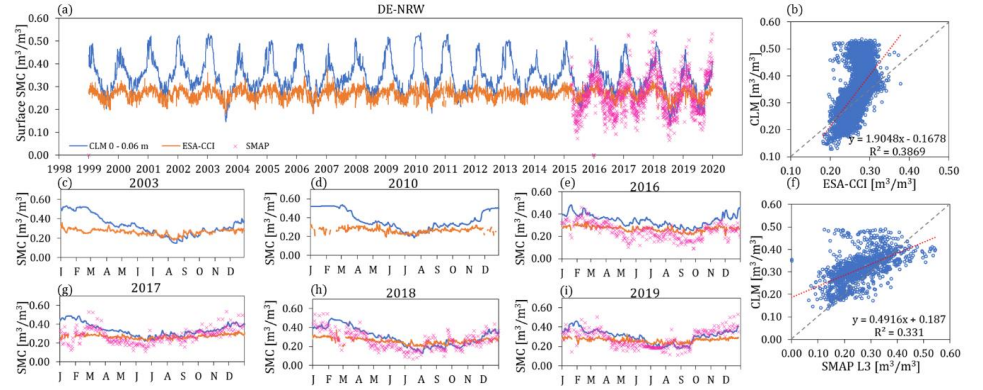

Figure 5.3: Simulated daily surface soil moisture (0 - 0.06 m depth) throughout the DE-NRW domain (**a**) from 1999 – 2019, and (**c**, **d**, **e**, **g**, **h**, **i**) for individual years, compared to the ESA-CCI product and available SMAP L3 data. Scatterplots show the correlation between simulated SMC and (**b**) ESA-CCI, and (**f**) SMAP L3, with the respective regression equations.

Table 5.2: Mean annual SMC, mean absolute anomaly (MAA), mean absolute deviation (MAD) and mean absolute deviation ratio (MAD_r) for simulated daily soil moisture content, and daily soil moisture data from ESA-CCI and SMAP L3 from 1999 – 2019, for AUS-VIC and DE-NRW respectively. Corresponding performance parameters *r*, RMSE and MBE were calculated with respect to the validation datasets ESA-CCI and SMAP L3

	Mean SMC [m^3/m^3]	MAA [%]	MAD [m^3/m^3]	MADr [-]	*r* [-]	RMSE [m^3/m^3]	MBE [m^3/m^3]
AUS-VIC							
CLM	0.21	29.927	0.063	-	-	-	-
ESA-CCI	0.188	19.012	0.036	1.757	0.858	0.032	0.01
SMAP L3	0.203	48.038	0.097	0.645	0.846	0.014	0.001
DE-NRW							
CLM	0.344	16.869	0.058	-	-	-	-
ESA-CCI	0.267	7.041	0.019	3.087	0.622	0.064	0.033
SMAP L3	0.262	26.306	0.069	0.843	0.574	0.024	0.004

5.3.2 Regional crop productivity

For the multi-decadal simulation runs we compared the simulated annual crop yields for DE-NRW and AUS-VIC to available yield records. We calculated yield variability as mean absolute deviation (MAD) and mean absolute anomaly (MAA) both for simulations and yield records, as well as the ratio of MAD from simulations and records (MAD_r) as explained in chapter 5.2.4 (Table 5.3).

In general, the simulations produced mean annual crop yields that are comparable to the mean observed yields across both domains and for all considered crop types in terms of overall magnitudes (Figure 5.4a and 5.4c). For AUS-VIC, the average simulated mean annual crop yield (excluding sorghum) was 1.57 t/ha, compared to 1.75 t/ha in records. In DE-NRW, the simulated mean yield averaged for all considered crops was 6.7 t/ha, while the official records reported approximately 7 t/ha. Additionally, there were differences in the simulated yield amounts and inter-annual yield variability between the two domains (Figure 5.4b and 5.4d). The simulated annual yield amounts were significantly higher in DE-NRW than in AUS-VIC for all crops, which is consistent with official yield statistics (Table 5.3). Additionally, the simulated inter-annual variability was lower for DE-NRW than for AUS-VIC, which is also the case in the official records (Figure 5.4b and 5.4d, Table 5.2)

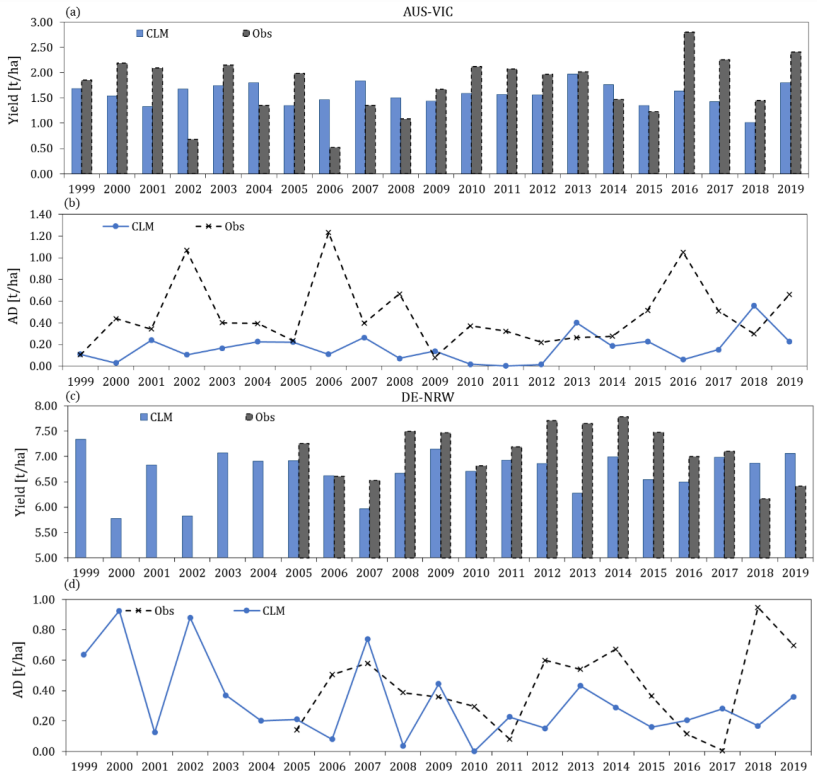

Figure 5.4: Simulated mean annual crop yield (CLM) and recorded mean annual yield (Obs), and corresponding absolute deviation from the 1999 – 2019 mean for each year (AD), averaged for all regarded crops, for (**a-b**) the AUS-VIC domain (winter wheat, barley, canola, sorghum) and (**c-d**) the DE-NRW domain (winter wheat, spring wheat, canola, corn).

For AUS-VIC, profound differences were observed in the inter-annual yield variability between the simulation results and crop survey records, with the absolute deviation (AD) being more than 3 times lower on average in simulation results compared to records (Figure 5.4b, Table 5.3). Specifically, the mean absolute anomaly was approximately 5% (0.12 t/ha MAD) for winter wheat in the simulations and 29 % in the records. Similarly, the MAA and MAD values for sorghum were substantially underestimated, with 9% and 0.2 t/ha for simulations, compared to 59 % and 1.3 t/ha for yield records. Overall, the lowest MAD ratios were reached for sorghum and winter wheat, with 0.15 and 0.2 respectively, while simulation results for canola and barley had ratios of 0.95 and 0.5 respectively (Table 5.3). The crop functional types (CFTs) for barley and canola are both derived from the spring wheat CFT (with adjusted values for several phenological parameters such as maximum LAI, maximum crop height, etc.), which explains the very similar yield predictions and inter-annual fluctuations for these two crops (Figure 5.5c and 5.5e). The drought year of 2018 and the reduction in recorded yields compare to previous years was only captured in the simulations for barley and canola (Figure 5.5c and 5.5e).

For the DE-NRW domain, the simulated total annual crop yield was close to official records, especially for winter wheat (Figure 5.6a, Table 5.3). However, simulated inter-annual yield variability was considerably lower than in the yield records for winter wheat (with a MAA of 2.6% and MAD of 0.3 t/ha in the simulations compared to 5.4%

and 0.5 t/ha in the records) and corn (MAA of 3.4% and MAD of 0.3 t/ha in the simulations, and 7.9% and 0.8 t/ha in the records, approximately), resulting in low MAD ratios of 0.6 and 0.4, respectively (see Figure 5.6, Table 5.3). Similar to the results for AUS-VIC, the influence of the shared crop parameterization between canola and spring wheat was evident in the simulation results for D-NRW. While the inter-annual yield variations for spring wheat were reasonably well-captured in the simulations, with a MAD ratio of approximately 0.8, the inter-annual yield variations for canola were overestimated in comparison to records, resulting in a very high MAD ratio of 2.5.

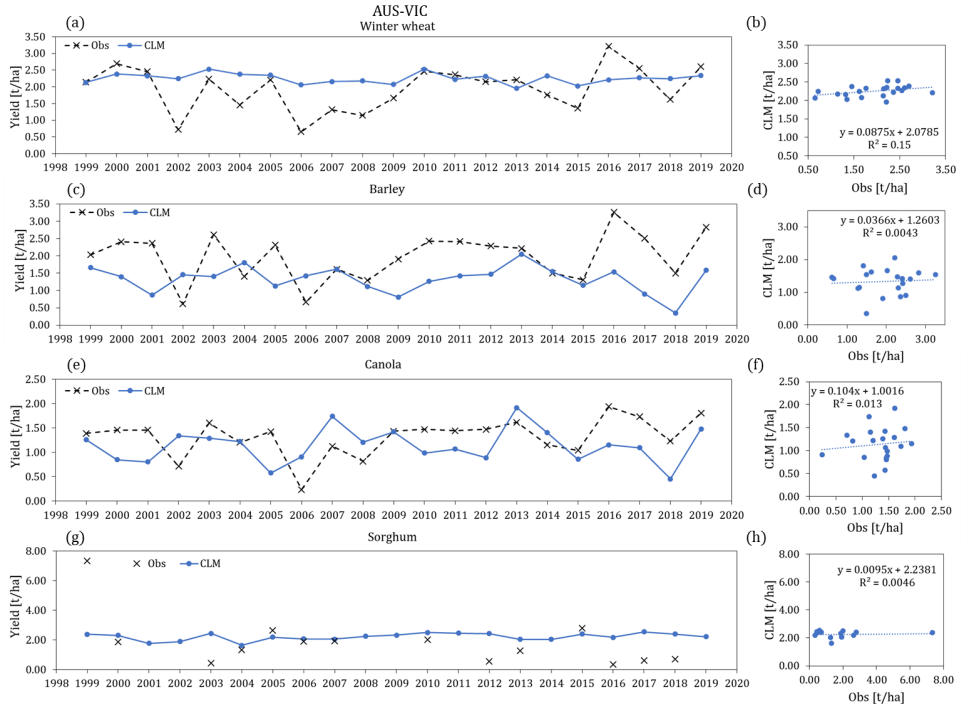

Figure 5.5: (left) Simulated mean annual crop yields for (**a**) winter wheat, (**c**) barley, (**e**) canola and (**g**) sorghum from 1999 – 2019 throughout the AUS-VIC domain compared to available records from ABARES (2020) with (right) corresponding correlations between simulated and observed values, with the respective R^2 values and regression equations. The corresponding data is also shown in Table C1.

Throughout AUS-VIC, crop yield is strongly correlated with the total amount of rainfall throughout the cropping season (May – October), as demonstrated by the positive correlation of total growing season rainfall and recorded grain yields (Figure 5.7). This relationship was not evident in the CLM simulation results. In addition, a weak correlation could be observed between the simulated annual yield and the simulated root zone soil moisture (0.02 - 0.32 m depth) (Figure 5.8a).

For DE-NRW, the correlation between total growing season rainfall and recorded or simulated crop yields is not significant, reflecting the energy-limited regime in the area. This is demonstrated by the weak correlation between recorded yields and seasonal rainfall amounts. For spring wheat, the influence of precipitation is reflected in the correlation with recorded yields (wetter years resulted in higher grain yield), while for other crops the constraining

effects of water availability and energy are more in balance. The simulation results showed a slightly negative correlation of yield, particularly pronounced for spring wheat and canola, with seasonal rainfall (and root zone soil moisture), which might be related to less energy input (smaller global radiation) for growing seasons with higher precipitation amounts (Figure 5.8b). With this negative correlation the simulation results overestimated the effects of energy limitation for the domain.

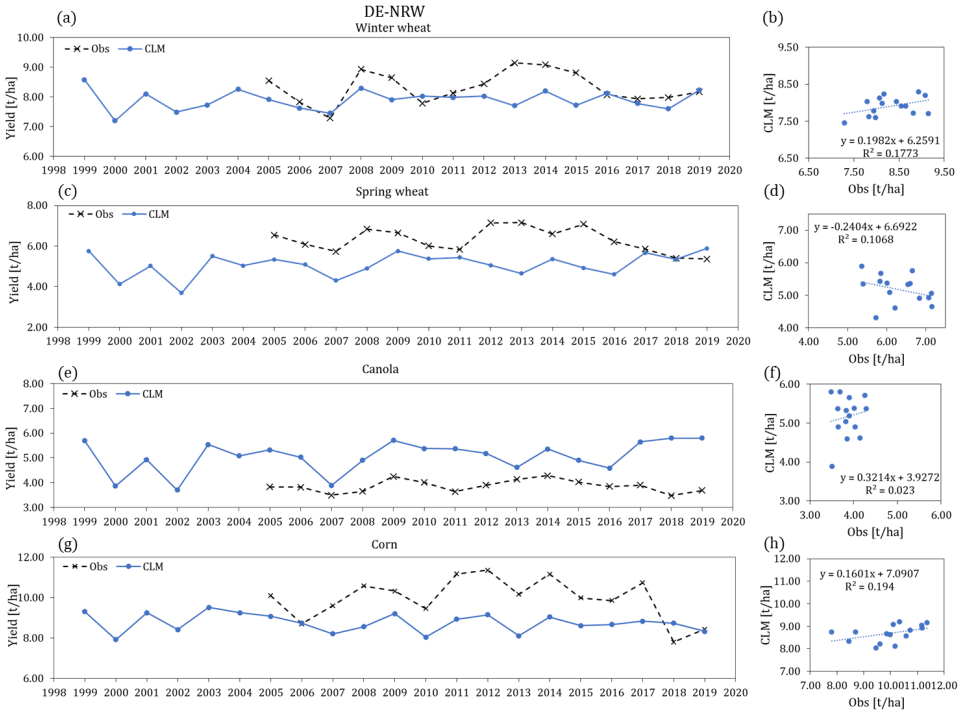

Figure 5.6: (left) Simulated mean annual crop yields for Simulated mean annual crop yields for (**a**) winter wheat, (**c**) spring wheat, (**e**) canola and (**g**) corn from 1999 – 2019 in the entire DE-NRW domain compared to available records from 2005 – 2019 (IT.NRW, 2022) and (right) corresponding correlations between simulated and observed values, with the respective R^2 values and regression equations. The corresponding data is also shown in Table C2.

Table 5.3: Mean annual crop yield, mean absolute anomaly (MAA), mean absolute deviation (MAD) and mean absolute deviation ratio (MAD_r) for simulated and recorded yields for 1999 – 2019, averaged for winter wheat, barley, canola and sorghum for AUS-VIC, and for winter wheat, spring wheat, canola and corn for DE-NRW. Corresponding performance parameters *r*, RMSE and MBE were calculated for the annual mean yield from 1999-2019 for AUS-VIC and 2005-2019 for DE-NRW with respect to available observations.

	Mean yield [t/ha]		MAA [%]		MAD [t/ha]		MAD_r [-]	*r* [-]	RMSE [t/ha]	MBE [t/ha]
	Obs	CLM	Obs	CLM	Obs	CLM				
AUS-VIC										
Winter wheat	1.95	2.25	28.65	5.26	0.56	0.12	0.21	0.39	0.68	0.30
Barley	1.97	1.31	28.75	22.62	0.57	0.29	0.51	0.07	0.98	-0.64
Canola	1.32	1.15	21.99	24.03	0.29	0.28	0.95	0.11	0.52	-0.18
Sorghum	1.84	2.20	59.21	9.05	1.34	0.20	0.15	0.07	1.76	0.42
DE-NRW										
Winter wheat	8.32	7.90	5.39	2.63	0.45	0.27	0.60	0.42	0.61	-0.40
Spring wheat	6.30	5.09	8.29	7.27	0.52	0.43	0.83	0.11	1.40	-1.12
Canola	3.87	5.07	5.05	8.49	0.20	0.49	2.51	0.22	1.39	1.28
Corn	9.97	8.76	7.93	3.43	0.79	0.30	0.38	0.13	1.58	-1.29

In order to better isolate the impact of soil moisture and precipitation on simulated crop yield, we additionally performed a multiple regression analysis, taking global (shortwave) radiation into account. We examined two different models to explain the simulated mean annual crop yield using (1) the simulated mean seasonal root zone soil moisture and the mean seasonal global radiation, and (2) the seasonal precipitation amount and the mean seasonal global radiation as independent variables. For DE-NRW, the model showed a moderate relationship between the variation in crop yield and changes in root zone soil moisture and global radiation with a R^2 of 0.38, and a slightly lower correlation of seasonal precipitation amount and global radiation with crop yield with a R^2 of 0.35 (Table C3). For DE-NRW, global radiation exhibited a positive relationship, implying that increased radiation was associated with higher crop yields, while both the root zone soil moisture and seasonal rainfall amount exhibited negative relationships (not showing any statistical relevance with p-values > 0.05) (Table C3). For the AUS-VIC domain, the model showed a weaker relationship between variations in crop yield and changes in root zone soil moisture and global radiation than in DE-NRW, with an R^2 of 0.16. Both the root zone soil moisture (p-value of 0.09) and global radiation (p-value of 0.26) were not statistically significant predictors in this case. The correlation of seasonal precipitation amount and global radiation with crop yield was slightly higher with an R^2 of 0.34, with both showing a positive relationship with crop yield (Table C3).

Analysis of the simulated transpiration beta factor, which represents plant water stress in CLM5, did not show any apparent correlation with the simulated yield in both domains (Figure 5.9). The transpiration water stress (βt =1 indicates absence of water stress; declining values indicate growing water stress) is utilized in CLM5 to regulate plant photosynthesis. The lack of a correlation for AUS-VIC suggests that the simulated crop yield was not influenced by transpiration water stress (Figure 5.9a). In DE-NRW, even a slightly negative correlation could be observed for simulated crop yield and transpiration beta (Figure 5.9b). This is consistent with the results regarding the correlation of simulated yield with both root zone soil moisture and precipitation as discussed above (Figure 5.6 and 5.7).

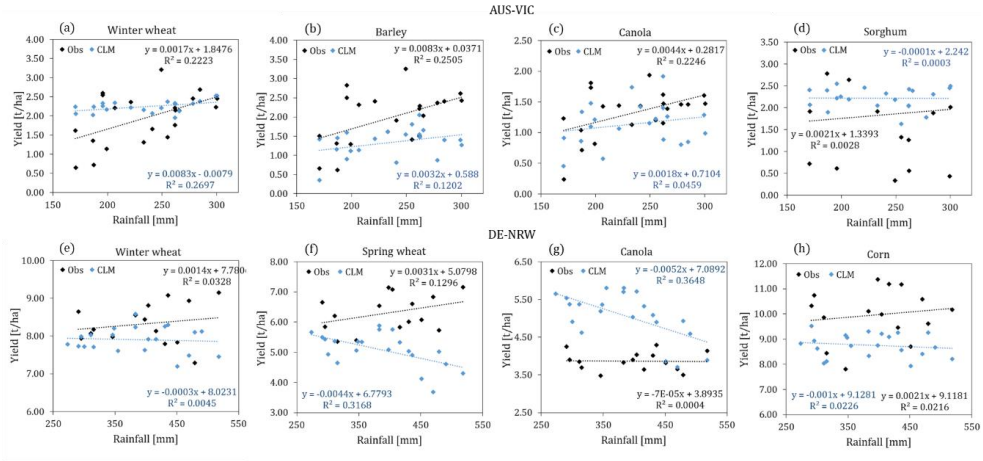

Figure 5.7: Relationship between mean annual crop yield (simulated (CLM) and recorded (Obs)) and WFDE5 cropping season rainfall amounts (May – October for AUS-VIC, and April – September for DE-NRW) for the period of 1999 – 2019. Average crop yields are given for (top) AUS-VIC and (bottom) DE-NRW. The yields of the following individual crops are given: (**a**) winter wheat; (**b**) barley; (**c**) canola; (**d**) sorghum; (**e**) winter wheat; (**f**) spring wheat; (**g**) canola; (**h**) corn. The respective R^2 values and regression equations are given for (blue) simulation results and (black) records.

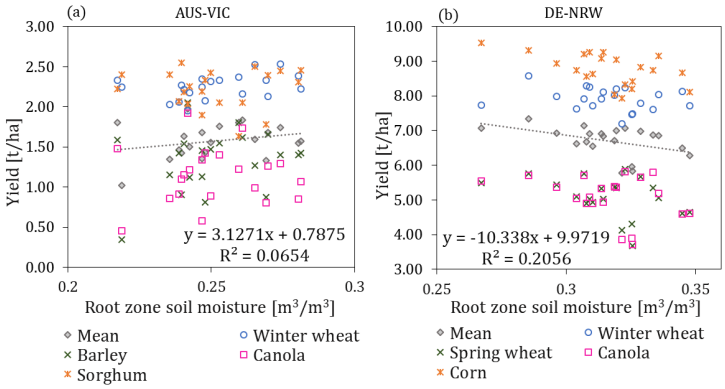

Figure 5.8: Relationship between mean annual crop yield (CLM) and the mean simulated root zone soil moisture (0.02 - 0.32 m depth) for the cropping seasons from 1999 - 2019, averaged for (**a**) AUS-VIC (May - October) and (**b**) DE-NRW (April - September), and for the respective crops. The respective R^2 values and regression equations for the mean yield are indicated in black.

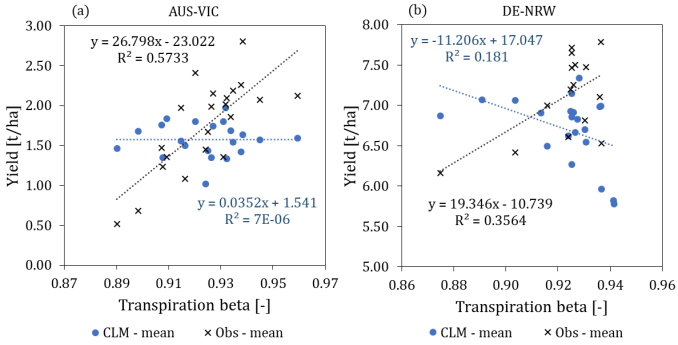

Figure 5.9: Relationship between simulated mean annual transpiration beta and simulated mean annual crop yield (CLM - mean), and recorded mean annual yield (Obs - mean) respectively, averaged for all regarded crops, for (**a**) the AUS-VIC domain (winter wheat, barley, canola, sorghum) and (**b**) the DE-NRW domain (winter wheat, spring wheat, canola, corn). The respective R^2 values and regression equations for (blue) simulations and (black) records are also given.

5.3.3 Winter wheat monoculture experiments with reduced precipitation

In a subsequent step, we conducted synthetic monoculture experiments where winter wheat cultivation was implemented exclusively across all crop land units. These experiments were performed using two different forcings: the default WFDE5 dataset (CLM_WFDE5) and the WFDE5 dataset with 50% reduction in precipitation (CLM_LowP). The reduction in rainfall synthetically increased the plant water stress for both domains, as represented by the transpiration beta factor.

In the AUS-VIC domain, the simulations with reduced precipitation not only led to decreased mean yield amounts, introducing a larger negative bias in overall yield results, but also increased inter-annual variability compared to the WFDE5 simulations with unchanged precipitation. The recorded winter wheat yields exhibited a mean absolute anomaly of 28.7% (0.56 t/ha MAD), which was underestimated in the default CLM_WFDE5 runs with a mean absolute anomaly of 8.4% (0.16 t/ha MAD). In the reduced precipitation runs this underestimation was less pronounced with a mean absolute anomaly of 13.5% (0.18 t/ha MAD) (Figure 5.10b, Table 5.4). In the rain-fed and water-limited regions of the AUS-VIC domain, we expect a positive correlation between seasonal rainfall amounts and crop productivity. CLM results were able to capture this relationship only with the reduced precipitation, indicating an underestimation of plant water stress in the scenario with the default WFDE5 forcing (Figure 5.11a).

In the DE-NRW domain, the reduced precipitation runs consistently underestimated the total annual winter wheat yield for all years, except 2007 (Figure 5.10c, Table 5.4). The variability of yield increased from 3.3% (0.25 t/ha MAD) in default WFDE5 simulations to 7.5% (0.55 t/ha MAD) with reduced precipitation amounts (CLM_LowP), which was even higher than the recorded yield variability with 5.39 % MAA (0.45 t/ha MAD). The overestimation of yield variability in the CLM_LowP runs was also reflected in the high MAD_r value of 1.2. By reducing precipitation amounts, we artificially created a more water-limited regime in the DE-NRW domain, resulting in a positive linear correlation between seasonal rainfall amounts and yield, which was even more pronounced than for the official yield records (Figure 5.11d).

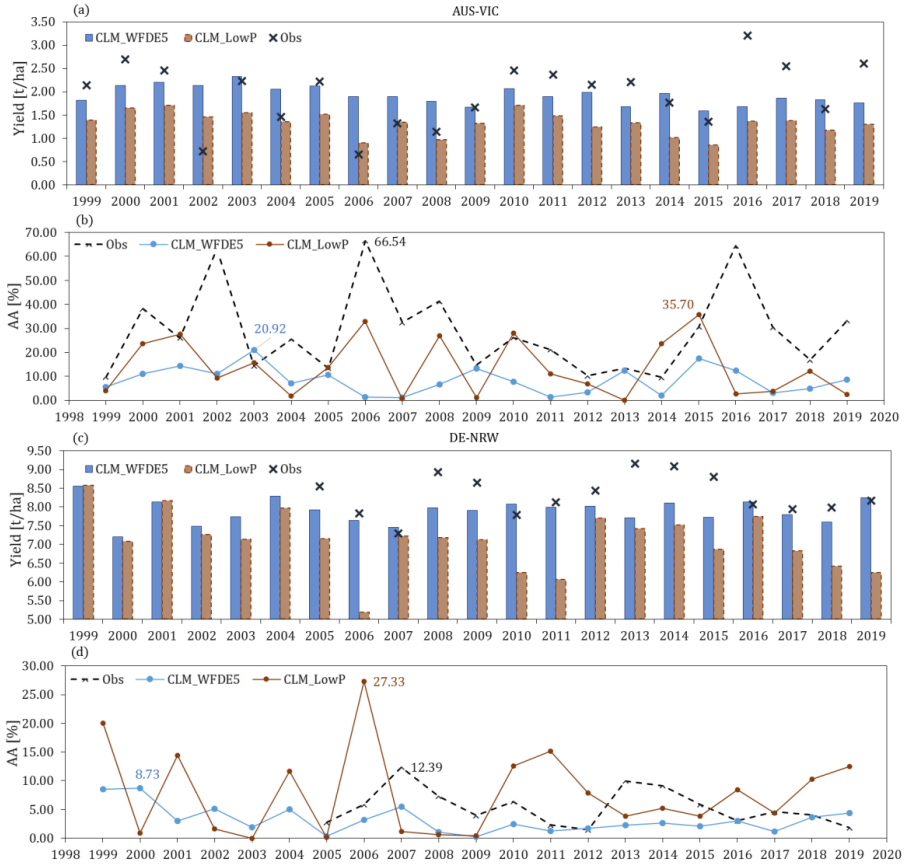

Figure 5.10: Mean annual crop yield from simulations forced with WFDE5 (CLM_WFDE5) and 50 % reduced WFDE5 precipitation (CLM_LowP), and recorded mean annual yield (Obs) for (**a**) the AUS-VIC domain and (**c**) the DE-NRW domain, with (**b**, **d**) the corresponding annual absolute yield anomaly (AA) for each simulation scenario and domain. The corresponding data is also shown in Table C1 and Table C2.

Table 5.4: Mean annual crop yield, mean absolute anomaly (MAA), mean absolute deviation (MAD) and mean absolute deviation ratio (MAD_r) for available records and results from winter wheat monoculture experiments, forced with WFDE5 precipitation (CLM_WFDE5) and 50 % reduced WFDE5 precipitation (CLM_LowP), averaged for 1999 – 2019, for both domains. Corresponding performance parameters *r*, RMSE and MBE were calculated for the annual mean yield from 1999-2019 for AUS-VIC and 2005-2019 for DE-NRW with respect to available observations.

	Mean yield [t/ha]	MAA [%]	MAD [t/ha]	MADr [-]	*r* [-]	RMSE [t/ha]	MBE [t/ha]
AUS-VIC							
Obs	1.95	28.65	0.56				
CLM_WFDE5	1.92	8.41	0.16	0.29	0.05	0.67	-0.03
CLM_LowP	1.33	13.51	0.18	0.32	0.59	0.83	-0.62
DE-NRW							
Obs	8.32	5.39	0.45				
CLM_WFDE5	7.89	3.20	0.25	0.56	0.29	0.64	-0.43
CLM_LowP	7.14	7.48	0.55	1.22	0.45	1.60	-1.46

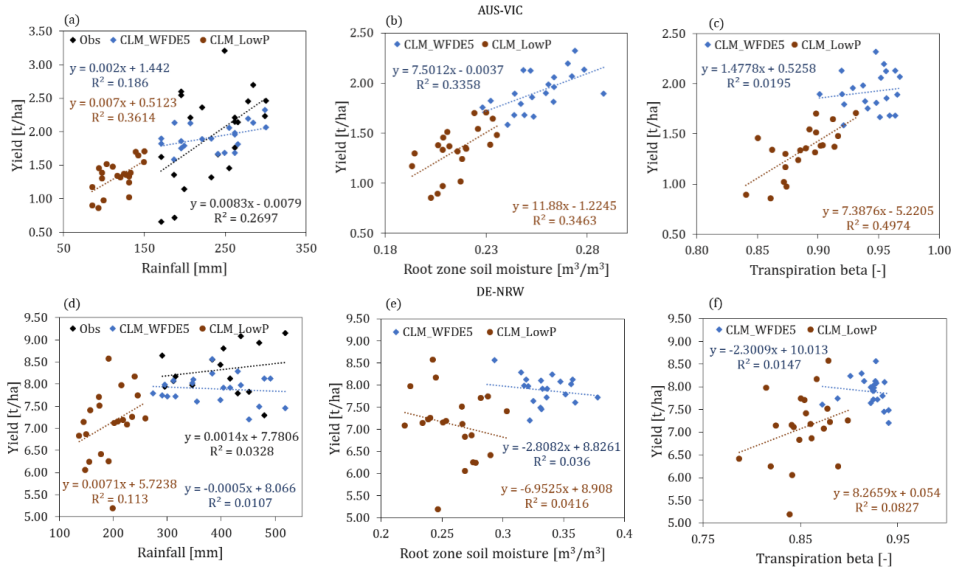

Figure 5.11: : Relationship between mean annual winter wheat yield (either WFDE5 precipitation simulations (CLM_WFDE5), 50 % reduced WFDE5 precipitation simulations (CLM_LowP) or records (Obs)) and the corresponding rainfall amounts for the cropping seasons of 1999 – 2019 (**a**, **d**), the simulated root zone soil moisture (**b**, **e**) and the simulated transpiration beta factor (**c**, **f**). Results are provided for the AUS-VIC domain (May - October) (**a**-**c**) and the DE-NRW domain (April - September) (**d**-**f**). The corresponding regression equations are indicated and color coded. The recorded yield is compared to WFDE5 annual precipitation.

The synthetic winter wheat monoculture experiments additionally offer the possibility to study simulated spatial differences as well as the effects of soil properties on simulated crop productivity in more detail (Figure 5.12). The highest variability of simulated annual crop yield is reached for regions with high sand contents, while in regions with relatively high clay contents, the inter-annual variability of yield is comparably low. This observed pattern suggests a link between the simulated yield and the higher water-retaining capabilities of clay-rich soils. In summary, the reduced precipitation amounts illustrate a more realistic water stress response from the crops, leading to a more realistic correlation of yield and rainfall amounts for the water-limited regime in AUS-VIC and higher

inter-annual yield variabilities. However, the reduced precipitation lead to an underestimation of annual yield amounts for both domains compared to records (Table C1 and Table C2).

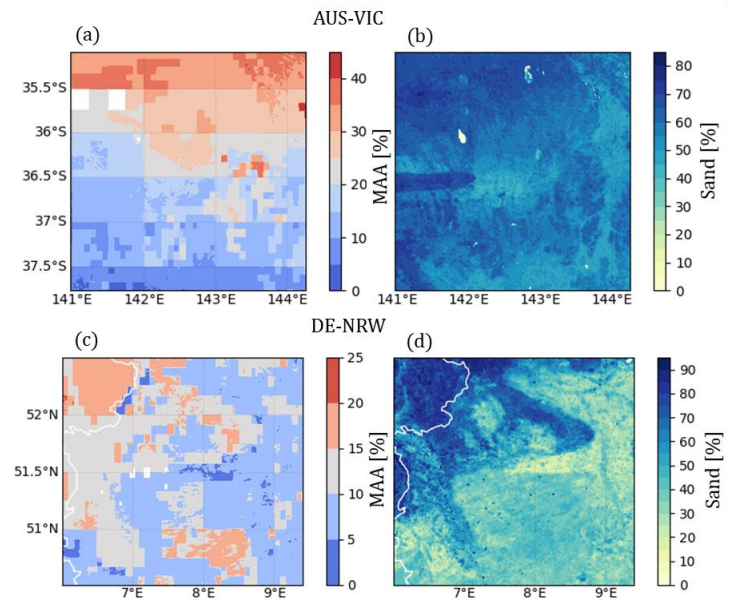

Figure 5.12: Spatial mean absolute yield anomaly (MAA) for winter wheat monoculture simulations (1999-2019) throughout (**a**) AUS-VIC and (**c**) DE-NRW, and (**b**, **d**) the sand content in the root zone throughout the respective domains, based on SoilGrids (Hengl et al., 2017).

5.4 Discussion

During the growing season, the vast majority of agricultural land is under water-limited conditions (Papagiannopoulou et al., 2017; Koster et al., 2009; Nemani et al., 2003). Studies indicate a widespread trend of ecosystems moving from energy to water limited due to climate change (Denissen et al., 2022; Orth et al., 2023). Unsustainable water use in large parts of the world additionally increases the ecosystem vulnerability to drought with depleting groundwater and surface water resources (Samaniego et al., 2018; Taylor et al., 2013; Wada et al., 2012, 2010). Thus, a reliable representation of the plant water stress regime and drought responses of vegetation are essential for the relevance of LSM applications for climate change research. The representation of vegetation responses to changes in available water is a major issue for studying the impact of climate change on ecosystems and food security.

In this study, we assessed the skill of CLM5 in portraying inter-annual variations of crop yield in response to weather patterns recorded in the bias corrected reanalysis product WFDE5. Validation of simulated crop yields against state-wide statistics demonstrated that the model was able to estimate the total crop yield for both domains reasonably well, while underestimating the inter-annual variability of annual crop yield. A relatively good match of simulated total annual yield amounts for winter wheat in the DE-NRW domain, compared to yield records, was achieved which reflects the modifications and enhancements validated for winter wheat at several European sites in Boas et al. (2021). The model's ability to portray inter-annual yield variability was better for the CFTs related

to or derived from spring wheat, i.e. spring wheat, barley and canola, which show very similar magnitudes and fluctuations of annual yield. The summer wheat CFT has been widely tested at global scale and its parameterization calibrated for CLM5 (Lombardozzi et al., 2020). In general, CLM5 is tuned to replicate average crop yields through parameter adjustments. Theoretically, well-calibrated parameters have the potential to offset the impacts of environmental factors such as pests, diseases, wildlife damage or pollutants. Previous studies showed that including crop-specific physiological parameters had a significant effect on the quantification of the diurnal energy partitioning and resulting grain yields (e.g. Lu et al., 2017; Sulis et al., 2015; Boas et al., 2021). Further improving the parameterization within the crop phenology module of CLM5 for the individual crops could help to alleviate model limitations. Another example of recent CLM5 model improvement is the incorporation of externally-specified crop planting dates and maturity requirements, as highlighted in a recent study by Rabin et al. (2023). By utilizing planting and maturity inputs derived from observations, biases in the simulated global yield of sugarcane and cotton were reduced, although an increased bias was observed for corn, wheat, and particularly rice. These inputs also led to a 15% reduction in the simulated global irrigation demand, with significant effects observed in regions where corn and rice are extensively cultivated. Lombardozzi et al. (2020) highlight that advancements in data availability and the development of new parameterizations enable further model developments for improved representation of arable land in LSMs (e.g. McDermid et al., 2017, 2023; Pongratz et al., 2018). Further specific areas for improvement as proposed by Lombardozzi et al. (2020) include enhancing the connection and expansion of phenological triggers to address water availability and heat stress, improving the representation of agricultural management (through the representations for residue management and soil tillage, allowing fertilizer and manure application to be more flexible, and including more complexity in the irrigation scheme) and accounting for major technological advancements related to recent intensification (e.g. higher planting densities, earlier sowing dates, and genetic improvements).

Analysis of the correlation between simulated annual yield and recorded rainfall amounts, as well as simulated root zone soil moisture contents, revealed model limitations in representing the water-limited regime in AUS-VIC. Throughout Victoria, crop growth and yield is highly influenced by rainfall patterns and amounts (French and Schultz, 1984a, b) which is also reflected in a strong positive correlation between total growing season rainfall amounts from reanalysis and observed total yields (Figures 5.7a - d). This relationship is not reflected in CLM5 simulations. Only in reduced precipitation experiments for winter wheat, did we observe a positive linear relationship between yield and rainfall amounts; and yield and soil moisture for AUS-VIC (Figure 5.11a - c). In the DE-NRW domain, the shallower groundwater tables and better water storing properties of soils lead to an absence of positive correlation between rainfall and overall annual yield compared to AUS-VIC. In addition, due to the high annual precipitation in general, soil water does not represent the main limiting factor for state-wide agricultural yields throughout DE-NRW, and global radiation is the most limiting factor. Even during the drought year of 2018, the state-wide yield statistics for DE-NRW do not show a strong declining trend (Figure 5.4c). While severe yield losses were recorded in specific regions within the state NRW, other regions with shallower groundwater tables and soils with higher water-storing capacities experienced record yields due to more sunshine hours (which is also represented in the negative correlation between seasonal rainfall and yield, Figure 5.7e - h). The slightly negative correlation between simulated crop yield and seasonal rainfall, as well as root zone soil moisture, in DE-NRW (which can be attributed to the reduction in sunshine hours caused by cloud cover associated with increased rainfall) suggests an exaggeration of the energy-limited regime by the land surface model and thus, a failure to correctly reproduce the effects of soil water stress on crop yield. The simulation results do not reflect

the differences in the water-limited and energy-limited regimes between the two domains, except for a weak positive correlation between yield and rainfall in AUS-VIC, which indicates an inaccurate representation of the water-limited regime in AUS-VIC and a systematic model insensitivity towards drought stress. This is also underlined by the results from the multiple regression analysis (i.e. root zone soil moisture, precipitation and global radiation) that did not identify seasonal soil moisture as a relevant predictor for simulated crop yield in the AUS-VIC domain.

Our results are consistent with other studies that indicate systematic issues across LSMs in simulating vegetation responses under drought conditions (e.g. Ukkola et al., 2016; Trugman et al., 2018; De Kauwe et al., 2015b). Especially in water-limited agricultural regions, the selection of crop varieties is largely influenced by their resilience to prolonged dry periods. While plant physiological properties play an important role in the energy partitioning at the land surface and carbon fixation and drought sensitivity varies considerably among plants, state-of-the-art LSMs currently assume the same drought sensitivity for all crop types. The studies by Trugman et al. (2018) and Sulis et al. (2019) emphasize the importance of including mechanistic water limitation algorithms in LSMs to improve the representation of plant hydraulics and thus projections of the land carbon sink. Trugman et al. (2018) found that soil moisture-limited productivity and its uncertainties significantly influenced carbon cycle simulations and thus concluded that the representation of soil moisture represents a major source of uncertainty in land surface models.

In CLM5, the empirical soil moisture stress formulation from earlier model versions was replaced with a plant hydraulic stress model (Lawrence et al., 2019). However, one of the main challenges for the application of plant hydraulic models for different biomes is the parameterization. In CLM5, plant hydraulics are physically constrained by plant-dependent parameters, such as the conductivities of the soil-root interface and at the interfaces between each of the plant elements (Kennedy et al., 2019). Due to a lack of readily available data for these parameters, they do not vary for the different crops and represent first estimates, which is a challenge the model developers are well aware of (Kennedy et al., 2019; Lawrence et al., 2019). The simulated plant water states in CLM5 are physical properties that can be validated against field observations (e.g. Konings et al., 2017; Li et al., 2017) which could facilitate the estimation of specific hydraulic parameters for the individual plants.

Our analysis of the transpiration beta factor that represents water stress in CLM5 revealed a lack of correlation between transpiration beta and the simulated annual yield. Reducing the precipitation in the forcing data sets generally had an effect on the transpiration beta factor, which reflects the induced water stress at lower precipitation rates. It appears that the threshold for plant water stress induced yield loss is not reached in the simulations with unchanged WFDE5 precipitation amounts or its effects on overall grain yield remain too small. The small range of transpiration water stress in simulation results implies that the modelled system experienced a relatively uniform degree of water stress, possibly due to low variations in soil moisture conditions or other factors influencing water availability for transpiration, such as the water-retaining capacities of the soil or irrigation. While the effects of irrigation can be considered negligible in our predominantly rain-fed simulation domains, this small range of beta serves as an indication for inconsistencies in the representation of the soil moisture regime. In addition to limitations in representing crop yield variability, we also observed profound differences of the simulated soil moisture contents throughout the decades compared to the ESA-CCI and the SMAP L3 products. For DE-NRW, the simulated surface soil moisture was systematically overestimated compared to both ESA-CCI and SMAP L3 during the early growing season. The same was observed for the AUS-VIC simulation results

compared to ESA-CCI, where CLM5 simulations resulted in higher daily SMCs. Compared to SMAP L3, however, the simulated SMC fitted well during the early stages of the year, while daily values of SMAP L3 during the growing season were underestimated in the simulation results. The observed differences in error between the simulated soil moisture content (SMC) by CLM5 and satellite-derived data (ESA-CCI and SMAP L3) at different growth stages can be attributed to several factors specific to each region. Overall, these discrepancies in error between simulated and satellite-derived SMC at different growth stages could stem from variations in soil properties, precipitation patterns, and uncertainties associated with satellite-derived data retrieval algorithms and spatial resolution, all of which interact differently in each region and influence soil moisture dynamics throughout the year. The discrepancy during winter months may be due to greater biases in satellite-derived products related to frozen soil and snow cover. Moreover, the higher SMC in CLM5 simulations outside of the main cropping season in DE-NRW could also result from a misrepresentation of post-harvest field conditions, where large fields of cropland are simulated as bare soil while, in reality, cover crops or weeds are growing on these fields. A misrepresentation of the soil moisture regime with overly high soil moisture contents could potentially dampen the potential benefits of the new plant hydraulic stress routine in CLM5. In earlier studies, data assimilation has been applied to address discrepancies between CLM simulated soil moisture and data derived from satellite and field observations (e.g. Zhao et al., 2021; Hung et al., 2022; Strebel et al., 2022; Naz et al., 2019). However, data assimilation of soil moisture and groundwater level observations had only limited effects on simulated evapotranspiration (Hung et al., 2022). Another way to improve the predictions of hydrologic states and fluxes with LSMs is the coupling with subsurface or groundwater models, such as ParFlow (Kollet and Maxwell, 2008; Kuffour et al., 2020), in integrated modelling approaches (e.g. Kollet and Maxwell, 2008; Yuan et al., 2008; Maxwell et al., 2011; Tian et al., 2012; Soltani et al., 2022; Naz et al., 2023). These studies have shown that coupled models can simulate complex processes more realistically than uncoupled models (e.g. Yuan et al., 2008; Maxwell et al., 2011; Tian et al., 2012). In addition, it is crucial to acknowledge the uncertainties in the satellite-derived data sets. Studies evaluating the quality of SMAP in Europe found local errors of 0.056 cm^3/cm^3 for a catchment in the state of NRW, Germany (Zhao et al., 2021), and comparable error magnitudes close to 0.06 cm^3/cm^3 for a region in the Netherlands (van der Velde et al., 2021). Addressing these uncertainties is crucial for interpreting satellite-derived soil moisture data accurately, with ongoing research and technological advancements contributing to improvements in reliability. For example, Seo and Dirmeyer (2022) propose an adjustment of ESA-CCI soil moisture achieved through Fourier transform time-filtering, which led to improved subseasonal variability, increased temporal correlation, and enhanced skill across various land cover classes.

Moreover, the simulation of soil water fluxes is intricately linked to the hydraulic properties of the soil, which are in CLM5 estimated from soil texture information using pedotransfer functions after Clapp and Hornberger (1978) or Cosby et al. (1984). In addition, the use of different pedotransfer functions for specific soil types can introduce substantial variability in the numerical modelling results of water fluxes, as demonstrated by Weihermüller et al. (2021) and Boas and Mallants (2022). One approach to improve the simulation of soil moisture in CLM5 may therefore involve the numerical implementation of various pedotransfer functions tailored to different soil types. Alternatively, the soil hydraulic information could be acquired through machine learning techniques or by utilizing suitable pedotransfer functions, similar to the approach outlined by Montzka et al. (2017), and incorporated via input files similar to the other surface input data. The inherent uncertainty in simulation results due to input data extends also to meteorological information. Bodjrenou et al. (2023) assessed multiple reanalysis products, including WFDE5, in West Africa from 1981 to 2019. While WFDE5 provided accurate estimates for annual

precipitation, it exhibited an excess of small rainfall events compared to observations. These uncertainties in commonly used reanalysis products for land surface modelling add an additional layer of complexity when examining the inter-annual variability of simulated variables influenced by precipitation.

While the adequate simulation of plant water stress is crucial to simulate crop productivity in response to changing weather conditions, it is also important to address additional processes that influence the yield variability of rain-fed agriculture. Crop management practices (e.g. fertilization, double cropping) and the selection of cultivars specifically bred for high grain yields under local climate conditions have significant impacts on agricultural production and are currently not accounted for in CLM5. Allowing for a broader range of yields (maximum productivity) for specific crops through changes in the physiological parameters that constrain the simulation of crop growth and development in CLM5 could be another approach to allow for a higher inter-annual variability of yield. Whether structural modifications to the phenology module or systematic adjustments in the crop-specific parameterization can effectively allow for a broader range of yield magnitudes for the respective crops remains to be evaluated through model evaluation and parameter sensitivity studies.

In summary, we argue that the limitations of model performance presented and discussed in this study arise from three main sources. Firstly, despite the incorporation of the new plant hydraulic stress routine in CLM5, there is a lack of sensitivity of crop yield towards drought stress and soil water availability. This may arise from the simplified parameterization of plant hydraulics which is unified for all plant functional types in CLM5. Secondly, CLM5 simulated soil moisture exhibited higher values during the cropping season, particularly in the early stage, than both ESA-CCI and SMAP products, which may have contributed to the weaker inter annual variability of yield. Thirdly, while CLM5 already incorporates a complex representation of crop growth and phenology compared with other state-of-the-art LSMs, there are several significant factors that contribute to inter-annual yield variability that are currently not adequately accounted for. Some examples include human crop management practices in response to technological advancements and public policies, diverse farming techniques such as varying fertilization amounts and types, double cropping, as well as environmental factors such as pests, diseases, and floods. Additionally, the crop–specific parameterizations in the crop phenology module, as well as the limited availability of data representing a wide range of crop varieties and geographic regions, represent substantial areas for improvement.

To overcome these challenges, the plant specific hydraulic parameterization needs to be improved, which can be achieved with the help of high-resolution field observations combined with parameter estimation methods. For a better representation of crop growth and yield, there is a need for further model developments, representing the influence of frost, pests, hail and wind on crop growth, different fertilizer types and application techniques and a more detailed representation of root crops. Finally, we propose to use state and parameter updating techniques, such as data assimilation, when studying global climate change impacts on agriculture with CLM5 to better account for model and parameter uncertainties (e.g. Strebel et al, 2022).

5.6 Summary and conclusions

Rapid changes in atmospheric conditions and land use over recent decades have made the fate of our terrestrial biosphere, depletion of natural water resources, food security, and the impact of anthropogenic carbon emissions major global research topics. Land surface models (LSMs), such as CLM5, are the primary tools used to study changes in our terrestrial surface in response to climate projections. With predicted changes in regional and global

climate, and a potential increase in drought risk, it is vital for the LSMs used in coupled climate models to realistically portray the drought responses of the land surface, and vegetation in particular. Reliable predictions of crop yield variability can contribute to discussions on climate change impacts and mitigation strategies.

In this study, we evaluated the performance of the land surface model CLM5 forced with reanalysis data in representing inter-annual variability of crop yield in multi-decadal simulations for two regions, AUS-VIC and DE-NRW, in different climate zones and with different soil moisture regimes. Evaluation studies for different ecosystems, such as the one presented here, are essential to improve our understanding of model performance and to identify the key challenges towards reliable projections of LSMs in climate change research.

Our analysis showed that CLM5 was able to capture the overall magnitudes of yields for individual crops, as well as regional differences for the same crops in the two domains (i.e., lower overall yield magnitudes for AUS-VIC than for DE-NRW for the same crop type). Overall, the lower annual yields per area over AUS-VIC can be attributed to differences in climate, crop varieties grown, soil characteristics, fertilizer rates and management techniques (e.g. larger paddock sizes with less dense plantations). Previous studies showed that the yield magnitudes for winter cereals specifically were too low at multiple European test sites (Boas et al., 2021). Hence, modifications and enhancements were introduced and validated for several European sites by Boas et al. (2021). These modifications were also used in our study, contributing to the reasonable yield magnitudes observed for DE-NRW. These factors collectively contribute to the disparities observed in simulation results between the two domains. However, the inter-annual fluctuations of yield in response to differences in weather patterns, such as seasonal rainfall amounts, were underestimated for both domains. Interestingly, the higher variability throughout the AUS-VIC domain compared to DE-NRW was reflected in the simulation results. Analysis of the plant water stress regime and correlations between seasonal rainfall amounts and crop yields revealed a misrepresentation of the more water-limited regime in AUS-VIC.

Experiments with reduced precipitation amounts that synthetically increased the plant water stress in simulations were able to better capture inter-annual variations of crop yield but underestimated crop yield. CLM5 is typically fine-tuned to replicate average crop yields through parameter adjustments. Theoretically, well-calibrated parameters have the potential to offset the impacts environmental factors such as pests, diseases, wildlife damage or pollutants.

Possible explanations for the underestimation of inter-annual variability of crop yields include: (1) a lack of sensitivity within the vegetation and crop module towards changes in soil moisture contents and soil water available for plants, possibly due to the parameterization of plant hydraulics; (2) systematic wet bias in simulated soil moisture content that may have dampened the potential benefit of the new plant water stress representation in CLM5; and (3) general uncertainties in the simulation of crop growth and yield due to inaccurate parameterizations and underrepresentation of environmental factors (e.g. pests, diseases) and human influences (e.g. agricultural management decisions, fertilizer type and application, cultivar selection). To remedy those effects, model enhancements are necessary, particularly in the field of plant hydraulic and physiological parameterizations. In addition, integrated approaches with subsurface or groundwater models (e.g. ParFlow) along with data assimilation offer potential for enhancing the simulation accuracy of soil moisture and other variables in future studies.

6 Summary and discussion

A sophisticated representation of agricultural land cover in Earth system models is essential to enhance our understanding and the predictability of feedback mechanisms between climate change and agriculture, a research area of great importance to society. Land surface models like CLM5 are our primary tool to study changes of the terrestrial surface in response to weather conditions and are essential for exploring the impacts of climate change on agricultural land at larger spatial scales. The potential value of land surface models for these purposes largely depends on their ability to adequately simulate the soil moisture regime, crop phenology and the variability of crop productivity in response to changes in weather patterns. Despite being the focus of many studies, accurately simulating agricultural land remains a persistent challenge due to the intricacy of agricultural management practices and the diverse range of crop types and biomes. In addition, with the majority of global cropland being water limited, an accurate prediction of the soil moisture states, the plant water stress regime and drought responses of vegetation is imperative for the relevance of LSM applications for climate change research. The recent inclusion of a crop module for prognostic calculation of crop phenology and the integration of a plant hydraulic stress model in CLM5 are significant advancements (Lawrence et al., 2019; Lombardozzi et al., 2020), positioning CLM5 as one of the most advanced and sophisticated LSMs currently available.

This cumulative thesis aimed to systematically evaluate and enhance the new prognostic crop representation of CLM5 across different spatial scales using input and validation datasets from various data sources. Point-scale simulations were conducted at several European cropland sites to identify any model limitations and to improve the model performance through new parameterizations and technical model development. The availability of high-resolution observation data on meteorological variables, surface energy fluxes, vegetation parameters and detailed information on agricultural management practices at the selected sites offer an excellent opportunity for in-depth validation of simulation results, model parameterizations and technical model developments. These model enhancements were then ported to the regional scale and tested in combination with reanalysis data in multi-decadal simulation scenarios and with seasonal weather forecasts over multiple cropping seasons. Information on agricultural practices and crop yield from official sources are typically provided at the state or administrative level, thus, regional scale simulations for two states with contrasting climate conditions and agricultural practices allowed for a comprehensive evaluation of model performance at the regional scale. The simulation domains DE-NRW and AUS-VIC were selected due to the availability of high-resolution input data on land cover and land use and meaningful validation data on crop yield and soil moisture. In addition, these two regions are characterized by agricultural land that is largely rain-fed, which minimized the impact of irrigation both in the simulation results and the official yield statistics. The regional studies allowed a comprehensive evaluation of the model's long-term performance (1999 - 2019), utilizing the bias-adjusted WFDE5 reanalysis dataset, and provided initial insights into the utility and skill of one of the most sophisticated seasonal forecasting products from the latest European Centre for Medium-Range Weather Forecasts (ECMWF) seasonal forecasting system (SEAS5) in combination with CLM5.

The main evaluation focus was placed on the representation of crop phenology, the inter-annual variability of crop yield, and the representation of surface soil moisture. Several key aspects were extensively explored throughout

this body of work: (1) The parameterization of crop phenology within CLM5; (2) technical advancements in the model that have the potential to significantly augment the crop module's performance; (3) the accurate representation of plant hydraulics and the model's sensitivity to drought stress, reflected in the simulated inter-annual variability of crop yield; (4) addressing biases in simulation outcomes pertaining to regional surface soil moisture; and (5) exploring the combination of CLM5 with seasonal forecasts for the prediction of regional crop yield.

In a first step, several limitations in the crop module were identified, including the absence of crop-specific parameters for abundant European cash crops and an oversimplified representation of winter cereal varieties (e.g. winter rye, barley and wheat). Winter cereals are more frequently planted than summer cereals in Germany and other western European countries (Palosuo et al., 2011; Semenov and Shewry, 2011; Thaler et al., 2012). In CLM5, there are several variables that influence simulated plant growth and resulting yield, such as LAI cycle and peak, length of the leaf emergence phase, harvest date, and water availability from the soil. With the exception of soil moisture, these variables are particularly responsive to plant-related parameters that guide the computation of growing degree days. This, in turn, significantly affects the calculation of the phenological progression and the allocation of carbon and nitrogen. However, within the crop phenology parameterization of CLM5, specific parameters for a majority of crop types and varieties, although present in the model's infrastructure, remain uncalibrated. To address these issues, crop-specific parameters for sugar beet, potatoes, and winter wheat were incorporated into the crop phenology parameterization scheme (Chapter 3). At point scale, an improved performance in simulating energy fluxes, leaf area index, net ecosystem exchange, and crop yield, with a RMSE reduction of up to 57% and 59% for latent and sensible heat could be attributed to the added crop-specific parameterization (Chapter 3). The role of parameterization effects were also noticeable in regional simulations (Chapter 4 and 5). The model performed better in portraying the inter-annual yield variability for the CFTs related to or derived from spring wheat, i.e. spring wheat, barley and canola, which has been widely tested at global scale and its parameterization calibrated for CLM5 (Lombardozzi et al., 2020). Consistent with previous studies (Sulis et al., 2015; Lu et al., 2017; Rabin et al., 2023), this emphasized the significant impact of including crop-specific physiological parameters on the representation of diurnal energy distribution and resulting grain yields in simulation results. In general, this indicates the potential benefits of expanding CLM5's parameter range to cover a wider range of crop varieties for improving simulation results for agricultural areas. However, the extension of the parameter scheme for more crop varieties poses challenges due to limited available measurement data and the complexity of the phenology algorithm and parameter framework. In their study, Rabin et al. (2023) highlighted that incorporating externally-specified crop planting dates and maturity requirements derived from observations could mitigate biases in the simulated global yield of sugarcane and cotton, and result in a 15% decrease in the simulated global irrigation demand. Another potential approach, without introducing additional Crop Functional Types (CFTs), might involve incorporating key parameters for each CFT that vary with climate and soil conditions, particularly for large-scale simulations, through gridded parameter sets. In addition, the integration of a phenology scheme based on plant physiological traits in CLM could be a significant advancement in this field (Fisher et al., 2019), as plant trait information becomes increasingly accessible (e.g., TRY Plant Trait Database, Kattge et al., 2011).

In addition to an extension of the crop parameter scheme, technical model developments were implemented to improve the performance over arable land. A winter cereal representation based on Lu et al. (2017) was introduced,

incorporating the cumulative effects of vernalization and cold tolerance of winter crops, and a quantitative representation of frost damage. In combination with the new parameterization for winter wheat, the incorporation of the winter cereal representation in CLM5 resulted in improved crop yield predictions for winter wheat by up to 87% compared to default model results at European cropland sites (Chapter 3). This could potentially translate to a substantial difference, possibly amounting to tens of millions of tons in the projected annual yield (average annual winter wheat yield of around 20 Mt/a throughout Germany), in simulation results compared to default model simulations on a nation-wide scale. A relatively good match of simulated total annual yield amounts was also found for winter wheat in the regional DE-NRW domain, compared to yield records, which reflected the antecedent modifications and enhancements validated for winter wheat at several European sites (Chapter 5).

Another major development derived from this study is the integration of a cover cropping and crop rotation subroutine. In CLM5, the crop phenology simulation is limited to a single crop type and phenological cycle per column within a year. This limitation fails to account for common agricultural practices, such as cover cropping, crop rotations from summer crops to winter crops, and multiple intra-annual cropping cycles, which are prevalent in various regions across the globe. Incorporating these practices into LSMs is pivotal for accurately simulating terrestrial fluxes (i.e. water and energy fluxes, carbon and nitrogen cycles) in agricultural areas, in particular over extended time scales. With the newly introduced subroutine, CLM5 has gained enhanced flexibility for crop rotations, enabling the simulation of multiple cropping cycles within a year and the representation of cover cropping. In addition, organic fertilization through cover crops can now be simulated with CLM5. These technical developments led to a better representation of field conditions after harvest for several sites, significantly reducing model bias during the winter season as indicated by the seasonal cycle of LAI magnitudes, and a 42% reduction in the RMSE of winter season latent heat flux compared to default model simulations. The specific implementation of the routine allows the simulation of cover crop plantations based on the CFT specified for the regarded land unit and customizable harvest date thresholds. Specifically, a defined maximum harvest date for any cash crop could define whether a cover crop is planted or not, and which type of cover crop is planted. With the modified model version, a more flexible land cover transition could be simulated based on the succession of different crops from historical data. It can furthermore be used to evaluate the biogeophysical effects of cover crops in combination with typical cash crop rotations throughout agricultural areas over longer time scales. For instance, the effect of cover crops during winter months on all crop land units designated for cash crop cultivation during summer could be tested on a larger scale. A similar study was presented by Lombardozzi et al. (2018), who studied the effects of idealized cover crop scenarios by simulating winter crops in all crop regions throughout North America. Their results indicate that cover crops can increase winter temperatures by up to 3°C in these regions. These findings highlight the importance of accurately implementing agricultural management options that can influence land-climate feedbacks over large regions. Accurately representing these biogeophysical impacts of anthropogenic land use in LSMs, which are used in GCMs, can enhance global climate projections and aid in developing climate mitigation strategies. With the new routine, a more systematic methodology could be pursued to study this, allowing for continuous simulations over longer timescales and considering the effects of organic fertilization through ploughing cover crops residuals into the soil.

Furthermore, the utilization of this routine holds significant promise for regions characterized by multiple cropping cycles within a single year, as seen in the context of monsoon-influenced cropping seasons in regions of India and China (e.g. Biradar and Xiao, 2011; Li et al., 2014; Sharma et al., 2015). Without its incorporation, CLM5 fails to

accurately depict key variables related to crop phenology, including the cycle of LAI, ET and nutrient fluxes. Similar to the approach by Rabin et al. (2023), who defined planting and maturity dates based on observations, the crop phenology algorithm of CLM5 could be reinitialized multiple times within one year with the new subroutine based on prescribed planting and harvest threshold in order to simulate multiple cropping cycles in those regions.

Combining this routine with an expanded parameter scheme designed to encompass a wider range of cover crop varieties would allow the evaluation of ecological potentials associated with various cover crop options. Next to the challenges arising from parameterization of new crop varieties in CLM5 as discussed above, there is additional development potential for this routine. This includes the technical incorporation of spatially varying crop rotations and cover cropping practices. The underlying structure of CLM5 inherently supports geospatial input data sets, as the input files for atmospheric forcing and surface information are sourced from gridded and georeferenced files. Exploiting the existing model infrastructure could entail the incorporation of spatially varying crop rotation schemes, linked to individual land units rather than being contingent upon specific crop types and harvest date thresholds. This development could synergize with the previously discussed regionally varying plant parameterizations through gridded input datasets.

The accurate representation of regional land surface fluxes and understanding their inter-annual variability is crucial for a range of applications, including climate projections, agricultural management, water resources management, and understanding ecosystem dynamics. Furthermore, reliable predictions of regional crop yield can help to design agricultural adaptation and mitigation strategies. Overall, the simulation results were able to reproduce annual magnitudes of simulated yields for winter wheat, barley, canola, and sorghum in AUS-VIC and winter wheat, spring wheat, canola, and corn in DE-NRW, which were comparable to official yield records. Interestingly, the simulation results also reflected the general difference in yield magnitudes between the two regional domains (lower mean crop yield in AUS-VIC in simulation results and records). However, the model showed limitations in capturing inter-annual variations of crop yield, showing profound differences in the inter-annual variability of crop productivity compared to official statistics. Specifically, the mean absolute deviation of mean regional yield from 1999-2019 was, on average, more than three times lower in simulation results compared to records for the regarded crops in AUS-VIC, and more than 1.5 times lower on average in DE-NRW (except for canola) (Chapters 4 and 5).

With regard to the simulation of inter-annual variations in crop growth and yield prediction, the representation of vegetative drought stress as well as the accurate simulation of soil moisture (available water for root uptake) play a crucial role. Analysis of the multi-decadal simulation results indicated that the simulations were not able to accurately represent the correlation between the annual crop yield and seasonal rainfall amounts or seasonal root zone soil moisture. This was also highlighted in synthetic regional simulation experiments with reduced precipitation rates. Particularly for AUS-VIC, the lack of a positive correlation between simulated crop yield and water available from precipitation and root zone soil moisture indicated a misrepresentation of the water-limited regime. Together with the low inter-annual variability in simulated crop yields, this indicated a limited sensitivity towards drought stress in spite of the new representation of plant hydraulics in CLM5. This plant hydraulic scheme provides a better physical basis for multiple processes represented in the model, such as the attenuation of photosynthesis and transpiration during drought conditions (Lawrence et al., 2019). Incorporating root water uptake formulations into LSMs has demonstrated significant potential for achieving more accurate simulations of transpiration fluxes compared to the soil moisture stress functions commonly found in LSMs (Kennedy et al.,

2019; Lawrence et al., 2019; Sulis et al., 2019). The primary challenge in applying plant hydraulic models across different biomes is the parameterization due to limited data availability. In CLM5, the plant-specific parameters that constrain the calculation of plant hydraulics remain uniform across all CFTs. Nevertheless, CLM5's simulated plant water states hold physical significance and can therefore be estimated and validated against field observations for individual plants (e.g., Konings et al., 2017; Li et al., 2017). However, achieving a satisfactory representation of global-scale agricultural fields can be an extensive and time-consuming endeavour, heavily dependent on the availability of observational data and extensive field measurements. An alternative approach to estimating new plant-specific parameters is the use of state and parameter updating techniques, such as data assimilation, to address model and parameter uncertainties (e.g., Strebel et al., 2022).

The simulation of inter-annual yield variations in LSMs is also closely linked to the representation of soil moisture, specifically, an accurate representation of changes in the soil moisture regime in response to changes in weather patterns. In addition, a misrepresentation of the soil moisture regime can potentially dampen the potential benefits of the new plant hydraulic stress routine in CLM5. In the course of this work, systematic differences of the simulated soil moisture contents compared to various validation data sets were identified. At the regional scale, the simulated surface soil moisture was systematically overestimated compared to both ESA-CCI and SMAP L3 during the early growing season for DE-NRW. The same was observed for the AUS-VIC simulation results, where CLM5 simulations resulted in higher daily SMCs compared to ESA-CCI, while, compared to SMAP L3, the daily soil moisture contents were underestimated during the growing season (Chapter 4 and 5). The multi decadal regional simulations resulted in RMSE of 0.032 m^3/m^3 and 0.014 m^3/m^3 with respect to ESA-CCI and SMAP L3, with moderate correlations of approximately 0.86 and 0.85 respectively. For DE-NRW, correlations were lower with values of approximately 0.62 and 0.57 compared to ESA-CCI and SMAP L3, with higher RMSE of 0.064 m^3/m^3 and 0.024 m^3/m^3 respectively (Chapter 5).

These challenges in correctly simulating soil moisture contents can be addressed by applying data assimilation techniques using data from remote sensing or field observations (e.g., Zhao et al., 2021; Hung et al., 2022; Strebel et al., 2022; Naz et al., 2019). However, the gained skill by data assimilation would only be effective for historic, real-time or short-term forecasting simulations, and could not be applied for long-term projections. Another established approach to improve the predictions of hydrologic states and fluxes with LSMs is the coupling with subsurface or groundwater models such as ParFlow (Kollet and Maxwell, 2008; Kuffour et al., 2020), in integrated modelling approaches (e.g., Kollet and Maxwell, 2008; Yuan et al., 2008; Maxwell et al., 2011; Tian et al., 2012; Soltani et al., 2022; Naz et al., 2023). While these approaches can be good measures to improve simulations of the hydrological cycle and soil moisture regime, both data assimilation and integrated modelling approaches, or a combination of both, can be computationally expensive, depending on the scale and resolution of simulations. Moreover, they may not effectively address the processes that could be responsible for these errors on the technical model level. The simulation of soil water fluxes is intricately linked to the hydraulic properties of the soil. In CLM5, soil hydraulic properties are estimated using pedotransfer functions after Clapp and Hornberger (1978) or Cosby et al. (1984). The utilization of different pedotransfer functions for specific soil types can introduce substantial variability in the numerical modelling results of water fluxes, as demonstrated by Weihermüller et al. (2021) and Boas and Mallants (2022). An approach to improve the simulation of soil moisture in CLM5 could therefore involve the numerical implementation of various pedotransfer functions tailored to different soil types, which vary based on textural fractions (i.e. sand, clay and organic matter content) provided in the input data.

Alternatively, the soil hydraulic information could be obtained through machine learning techniques or by utilizing appropriate pedotransfer functions, similar to the approach outlined by Montzka et al. (2017), and incorporated via input files, comparable to the other surface input data.

When assessing the applicability and significance of LSMs for agricultural planning purposes, a promising avenue of research involves integrating LSMs with weather data on time scales pertinent to agriculture. Next to the thorough evaluation of simulation results obtained with bias corrected reanalysis, this study also assessed the effectiveness and practicality of combining CLM5 with SEAS5 seasonal weather forecasts for regional crop yield prediction. Despite their potential to enhance agricultural production systems, the use of seasonal forecasting products by farmers remains low, which can be partly attributed to a lack of sufficient data and evidence supporting their value, as well as to the absence of user-friendly tools and services that provide relevant information on crop yield for specific crop varieties based on seasonal forecasts. Furthermore, there is often a resolution mismatch of forecasting products and modelling applications which has hindered their widespread use in this field.

After extensive pre-processing of the forecasting product that specifically involved temporal downscaling of precipitation and incoming shortwave radiation, the forecasts produced model output closely matched the reference simulation results forced by reanalysis. Over the four simulated cropping seasons (2017-2020), the forecast simulations successfully captured both the highest and lowest yield years and replicated the generally larger year-to-year variations and lower annual yield magnitudes in crop yield across the AUS-VIC region compared to the DE-NRW region. The limitations in adequately representing the inter-annual variations in crop yield, as previously discussed, were evident in both the forecast and reanalysis simulations. This was also observed for the simulated LAI and ET, which showed lower inter-annual variabilities in comparison to MODIS data. The simulated LAI and ET from both forecast and reanalysis simulations corresponded reasonably well with data from MODIS in terms of magnitudes and fluctuations for AUS-VIC, while for the DE-NRW simulated LAI and ET were larger than the observed values, in particular in early summer (May, June and July). Still, CLM5 was able to reproduce the generally higher inter-annual differences in crop yield throughout the AUS-VIC domain (up to 50 % in records and 17 % in simulated yields) compared to the DE-NRW domain (up to 15 % in records and 5 % in simulated yields), which can be attributed to the more diverse land cover in DE-NRW (i.e. larger variety of cultivated crops, more urban areas and fallow land between croplands, smaller paddock sizes) that is more challenging to represent in CLM5.

A noteworthy limitation in the forecast quality stems from the large uncertainties in the prediction of precipitation amounts and patterns. This became evident in the higher crop production in the southern region of the AUS-VIC domain attributed to near-coastal precipitation events that was evident in the reference simulations with reanalysis, but not represented in the forecast simulations. Advanced temporal downscaling methods, like machine learning techniques, could help to improve the usability of forecasting products in model applications. This topic has been gaining increasing attention in research due to its growing significance and the recent developments in the field of machine learning (e.g. Hwang et al., 2019; Xu et al., 2019; Pakdaman et al., 2022; Jin et al., 2023). Performance analyses over extended periods and multiple regions, including benchmarking with other forecasting products and LSMs, are needed, that can provide valuable insights into uncertainties of the respective models and advance our understanding and the applicability of forecasting products. Conducting research for agricultural regions influenced by El Niño events, e.g. soybean cropping in Brazil, can shed more light on the effectiveness of seasonal forecasts, which exhibit higher predictive accuracy in El Niño-affected regions, in combination with CLM5 and

other model applications. Interestingly, the seasonal experiments revealed an early decline in LAI in DE-NRW during the 2018 growing season, reflecting the early onset of harvest. During the European drought of 2018, a large part of the cropland in Germany was harvested earlier than usual which was closely linked to the recorded yield losses in NRW (Reinermann et al., 2019). This indicates a certain level of skill in this model combination that warrants further exploration, and, in light of improving forecast quality, suggests potential for using seasonal forecasts in model applications like CLM5.

While the adequate simulation of plant phenology, plant water stress and the soil moisture regime are crucial to simulate crop productivity in response to changing weather conditions, it is also important to address additional processes that influence the yield variability of rain-fed agriculture. Beyond weather conditions, regional agriculture and crop yield are largely impacted by agricultural management decisions such as the selection of crop varieties, planting schedules, irrigation, and fertilizer types and application techniques (White and Wilson, 2006; Bergkamp et al., 2018; Ceglar et al., 2019). Furthermore, other environmental factors such as soil quality and nutrient availability, atmospheric CO_2, pests and crop damage from wildlife play a role in some regions, which are not sufficiently well represented by CLM5.

One approach to improve crop yield predictions with CLM5 and to allow for a higher inter-annual variability of yield is by expanding the permissible yield range for specific crops through changes in the physiological parameters, and by parameterizing more crop types and crop cultivars that are specifically bred for high grain yields under local climate conditions. In addition, a sophisticated representation of root crops could potentially enhance yield forecasts and improve the simulation of C and N cycling, particularly in regions with extensive cultivation of root crops (EU production of sugar beet accounts for about half of the global production (Eurostat, 2018). Incorporating a broader range of crop types into CLM5 represents a pivotal objective for advancing the model and is the aim of many studies (e.g. Lu et al., 2017; Cheng et al., 2020; Dombrowski et al., 2022). Further specific areas for enhancing the representation of agricultural management in CLM5 include improvements in residue management and soil tillage representations, allowing greater flexibility in fertilizer and manure application. In addition, there is a need for increased complexity in the irrigation scheme (Zhu et al., 2020; Brogi et al., 2022; Yang et al., 2022; McDermid et al., 2023; Rabin et al., 2023) and the incorporation of major technological advancements associated with recent agricultural intensification, such as higher planting densities, earlier sowing dates, and genetic improvements (Lombardozzi et al., 2020; McDermid et al., 2023).

Whether structural modifications to the phenology module or systematic adjustments in the crop-specific parameterization can effectively allow for a broader range of yield magnitudes for the respective crops requires rigorous evaluation through further model assessments and parameter sensitivity studies. Further studies should be prioritized in regions known for significant crop-yield variability, like the Corn Belt regions in the United States. These areas are prone to weather anomalies, including late frosts, excessive rainfall, and heatwaves during the growing season, resulting in substantial yield fluctuations. Utilizing the dataset provided by global and regional networks of eddy-covariance towers, such as FLUXNET (FLUXNET, 2023), can facilitate comprehensive investigations in these regions. Exploring the model performance in regions impacted by monsoon timing and intensity, such as rice plantations in Southeast Asia or cotton plantations in India, also hold opportunity to study inter-annual yield variability in particular, provided sufficient data is accessible for both model input and result validation.

While there is a need for more process complexity and representation of land surface heterogeneity, further technical advancements of already complex LSMS also encompasses growing uncertainties in understanding parameter dynamics, process interactions within the model code and differences between LSMs predictions. Modularization of model code in LSMs, allowing for more effective testing and validation of model code and more flexibility for different scientific interests via alternate configurations and parameterizations as proposed by Fisher and Koven (2020), is one approach for this issue. Considering the increasing availability of data and a growing number of open source data providers, along with the expanding field of machine learning for dataset generation, another proposed solution to tackle these structural issues is the integration of a technical framework for incorporating supplementary input datasets. Specifically, this could involve modifying the model to accommodate georeferenced information on soil hydraulic properties and plant parameters derived from plant traits (e.g. TRY Plant Trait Database, Kattge et al., 2011).

Overall, there is a need for further comprehensive model evaluation studies such as the ones presented in this cumulative thesis, for other regions, ecosystems and biomes. These investigations should focus on consistently addressing the significant gaps and challenges that persist in current land surface modelling, in particular in the representation of arable land and anthropogenic influences. As we move forward, a collective effort to systematically improve our understanding of Earth's land surface dynamics remains imperative for advancing environmental research and predicting the impacts of global climate change.

7 Final conclusions and outlook

The accurate representation of agricultural land cover within Earth system models is pivotal for enhancing our understanding of the intricate feedback mechanisms between climate change and agriculture. While this field of research is of paramount importance to society, it remains challenging due to the complexity of agricultural management practices and the diversity of crop types and ecosystems. LSMs such as CLM5 represent our primary tool to study terrestrial surface fluxes in response to changing weather conditions. Evaluation studies for different ecosystems are essential to improve our understanding of model performance and to identify the key challenges towards reliable projections of LSMs in climate change research.

This cumulative thesis systematically evaluated the performance of CLM5 to accurately represent agricultural land at different scales and identified some key limitations in the representation of crop phenology and model responses to drought stress. Significant progress has been made throughout this cumulative work in enhancing and evaluating the representation of crops within the CLM5 model across various spatial scales. This work has involved refining crop phenology parameterization, introducing technical advancements, addressing plant hydraulics and drought sensitivity, and exploring the combination of CLM5 with seasonal weather forecasts for crop yield prediction.

The technical developments and novel parameterizations developed in the course of this work, i.e., the introduction of winter cereal representation, new crop-specific parameterizations for multiple cash crops, and the incorporation of a new cover cropping and crop rotation subroutine, led to significant improvements of the simulation results over arable land. The improved model can provide better predictions of the carbon cycle, vegetation phenology and terrestrial fluxes for arable land, which is crucial for understanding and managing agricultural productivity. The promising outcomes achieved with model developments in the crop module of CLM5 will greatly benefit the land surface modelling community in better representing the role of agriculture on regional and global energy and carbon fluxes, in particular for regions with high abundance of winter cereal varieties and multiple cropping cycles per year.

This cumulative work furthermore emphasized the significance of accurately representing plant hydraulic responses to water stress and the importance of a reliable representation of soil moisture in land surface models. The implementation of the new plant hydraulic stress model in CLM5 marks a significant advancement in the field of plant hydraulics within land surface models that remains to be evaluated for a larger number of climate zones and biomes (Kennedy et al., 2019; Lawrence et al., 2019). Multi-decadal regional simulations revealed systematic limitations of CLM5 in adequately representing inter-annual variations of crop productivity for certain cash crops and a lack of model sensitivity to drought conditions. The new plant hydraulic scheme in CLM5 allows for further refinement through the use of physical plant hydraulic parameters that constrain the new algorithms, which can be validated with field measurements. However, the lack of available plant-specific parameters is a current limitation that must be addressed through the calibration of parameters for different biomes in future studies to fully utilize its potential. Whether the simulation of inter-annual crop variability and more sensitivity of the model towards drought stress can be obtained through parameter estimation for plant hydraulics remains to be evaluated in future studies. In addition, the validation of soil moisture simulations in CLM5 against satellite data and field

observations revealed systematic biases, which could lead to inaccurate representation of the environmental stress regime and biased simulations of vegetation responses to drought stress.

This thesis furthermore highlights the promising prospects of combining land surface models with seasonal weather forecasts for agricultural forecasting. By assessing the feasibility of combining seasonal weather forecasts with CLM5, a first study of this scope of application is provided. Overall, results from forecast simulations were able to give a first indication of the annual crop productivity trends, generating similar results to reference simulations forced with reanalysis, which is an encouraging result for future applications. However, next to the uncertainties in the forecasting products, challenges in data handling, which includes the temporal downscaling of certain meteorological variables, need to be addressed for widespread adoption. Benchmarking studies of different forecasting products in combination with different modelling applications can provide better representation of the current state of the art in this field and can also help to increase the adaptation of forecasting products in agriculture and politics. In light of the predicted global climate change and the growing number of skilful seasonal forecast products, this combination is of great interest for science and society.

Insights from this work serve as a basis for future analysis of CLM5 simulations over agriculturally managed land and can guide future technical and empirical model enhancements. Despite the advancements made throughout this thesis, there remain challenges in simulating the full range of agricultural management practices, soil types, and crop varieties. Some of the suggested model improvements to the crop module of CLM5 include a more comprehensive representation of human management impacts such as different fertilizer types and application strategies, including residue management and soil tillage, a more sophisticated irrigation scheme, a representation of technological advancements, as well as the addition of other environmental factors such as pests and wildlife damage. Moreover, incorporating a larger number of crop types and cultivars, as well as a sophisticated representation of root crops, should be a priority. These efforts will require rigorous evaluations and parameter sensitivity studies. Alternatively, the integration of supplementary input datasets, particularly for soil hydraulic properties and plant phenology, e.g. from plant trait information, present promising avenues to address growing uncertainties in land surface models. By systematically enhancing the models' capabilities and refining the parameterizations, we can continue to improve our understanding of the complex interactions between climate change and agriculture, ultimately supporting more informed decision-making in agricultural adaptation and mitigation strategies.

Overall, the outcomes of this research hold significant potential to greatly benefit the scientific community, especially in enhancing the representation of arable land in global land surface and earth systems models - an essential area that currently presents a key gap in land surface modelling.

Appendix

A SI: Improving the representation of cropland sites in the Community Land Model (CLM) version 5.0

Table A1: Sowing and harvest dates at the ICOS and TERENO cropland study sites.

Site code	Site	Years	Crop	Sowing	Harvest/plowing
DE-RuS	Selhausen	2015-2016	Winter barley	29.09.2015	10.07.2016
		2016	Greening mix cover crop	22.08.2016	06.01.2017
		2017	Sugar beet	31.03.2017	05.10.2017
		2017-2018	Winter wheat	25.10.2017	16.07.2018
		2019	Potato	26.04.2019	03.10.2019
DE-RuM	Merzenhausen	2016	Potato	12.04.2016	24.08.2016
		2016-2017	Winter wheat	17.10.2016	22.07.2017
		2017-2018	Rapeseed	30.08.2017	16.07.2018
DE-Kli	Klingenberg	2003-2004	Winter barley	06.09.2003	31.07.2004
		2004-2005	Rapeseed	18.08.2004	02.08.2005
		2005-2006	Winter wheat	25.09.2005	06.09.2006
		2007	Corn	23.04.2007	02.10.2007
		2008-2009	Winter barley	25.04.2008	27.08.2008
				12.09.2008	22.07.2009
		2009-2010	Rapeseed	25.08.2009	24.08.2010
		2010-2011	Winter wheat	02.10.2010	22.08.2011
		2012	Corn	25.04.2012	18.09.2012
		2013-2014	Winter barley	17.04.2013	24.08.2013
				01.10.2013	20.07.2014
		2014-2015	Rapeseed	21.08.2014	08.08.2015
		2015-2016	Winter wheat	18.09.2015	24.08.2016
		2016-2017	Radish and Brassica cover crop	01.09.2016	15.03.2017
		2017-2018	Winter barley	02.04.2017	25.08.2017
		2016-2017	Radish and Brassica cover crop	13.09.2017	13.04.2018
		2018	Corn	02.05.2018	04.09.2018
		2019	Bean	23.03.2019	18.08.2019
BE-Lon	Lonzée	2006-2007	Winter wheat	13.10.2006	05.08.2007
		2008	Sugar beet	22.04.2008	04.11.2008
		2008-2009	Winter wheat	13.11.2008	07.08.2009
		2009	Mustard	01.09.2009	01.12.2009
		2010	Potato	25.04.2010	05.09.2010
		2010-2011	Winter wheat	14.10.2010	16.08.2011
		2012	Corn	14.05.2012	13.10.2012
		2012-2013	Winter wheat	25.10.2012	12.08.2013
		2013	Mustard	05.09.2013	15.11.2013
		2014	Potato	07.04.2014	22.08.2014
		2014-2015	Winter wheat	15.10.2014	02.08.2015
		2015	Mustard	26.08.2015	09.12.2015
		2016	Sugar beet	12.04.2016	27.10.2016
		2016-2017	Winter wheat	29.10.2016	30.07.2017
		2017	Mustard	07.09.2017	08.12.2017
		2018	Potato	23.04.2018	11.09.2018
		2018-2019	Winter wheat	10.10.2018	01.08.2019

Table A2: Default (*control*) and new crop specific (*new*) phenology and CN allocation parameters for the CFTs sugar beet and potatoes (control parameters are those for the CFT spring wheat) and winter wheat.

CFT		Sugar beet		Potatoes		Winter wheat	
Parameter set		*control*	*new*	*control*	*new*	*control*	*new*
Variable	Units	*Phenology*					
min_NH_planting_date	MMDD	401	401	401	401	901	901
max_NH_planting_date	MMDD	615	530	615	530	1130	1130
planting_temp	K	280.15	280.15	280.15	277.15	1000	1000
min_planting_temp	K	272.15	272.15	272.15	272.15	283.15	283.15
gddmin	°days	50	60	50	60	50	100
mxmat	days	150	180	150	180	330	400
baset	°days	0	0	0	0	0	0
mxtmp	°C	26	30	26	30	26	26
hybgdd	-	1700	2000	1700	2000	1700	2000
lfemerg	%	0.05	0.05	0.05	0.05	0.03	0.03
grnfill	%	0.6	0.65	0.6	0.65	0.4	0.6
ztopmx	m	1.2	0.5	1.2	0.5	1.2	1.2
laimx	m^2/m^2	7	6	7	6	7	7
slatop	m^2/gC	0.035	0.02	0.035	0.02	0.035	0.028
Variable	Units	*CN ratios and allocation*					
leafcn	gC/gN	20	11	20	11	20	20
leafcn_min	gC/gN	15	8	15	8	15	15
leafcn_max	gC/gN	35	20	35	20	35	35
frootcn	gC/gN	42	42	42	42	42	43
graincn	gC/gN	50	50	50	50	50	15
flnr	fraction/gNm^{-2}	0.41	0.15	0.41	0.15	0.41	0.3

Table A3: Textural fractions (sand, silt and clay percentages) for the ICOS and TERENO cropland study sites averaged for the upper soil layers (up to 50 cm) with corresponding reference.

Site/ID	Sand [%]	Silt [%]	Clay [%]	Ref.
Selhausen/DE-RuS	16.4	63.4	14.9	Brogi et al. (2019)
Merzenhausen/DE-RuM	16.4*	63.4*	14.9*	-
Klingenberg/DE-Kli	21.5	22.8	55.7	Grünwald (personal communication, 2020)
Lonzée/BE-Lon	5-10	68-77	18-22	Moureaux et al. (2006)

*adopted from the DE-RuS site

A1: Winter cereal representation (extended)

The temperature at the crown of the plant (T_{crown}) is assumed to be slightly higher than the 2-m air temperature (T_{2m}) in winter when covered by snow, and the same as the 2-m air temperature without snow cover. Within CLM5, it is calculated separately for temperatures below and above the freezing temperature (T_{frz}):

$$T_{crown} = 2 + \left(T_{2m} - T_{frz}\right) * (0.4 + 0.0018 * (min(D_{snow} * 100, 15) - 15)^2$$

$$for\ T_{2m} < T_{frz} \quad \text{(A.1)}$$

$$T_{crown} = T_{2m} - T_{frz}$$

$$for\ T_{2m} > T_{frz} \quad \text{(A.2)}$$

where T_{crown} [K] is the calculated crown temperature, T_{2m} [K] is the 2-m air temperature, T_{frz} [K] is the freezing point and D_{snow} [m] is the snow height.

The temperature at which 50 % of the plant is damaged (LT_{50}) is calculated interactively at each time step (LT_{50t}) depending on the previous time step (LT_{50t-1}) and on several accumulative parameters. These parameters are the exposure to near-lethal temperatures ($rate_s$), the stress due to respiration under snow ($rate_r$), the cold hardening or low temperature acclimation (contribution of hardening – $rate_h$) and the loss of hardening due to the exposure to a period of higher temperatures (dehardening – $rate_d$) that are each functions of the crown temperature (Lu et al., 2017 and references therein):

$$LT_{50t} = LT_{50t-1} - rate_h + rate_d + rate_s + rate_r \quad \text{(A.3)}$$

The exposure to near-lethal temperatures is based on the winter survival model after (Fowler et al., 1999) and is calculated as follows:

$$rate_s = \frac{LT_{50t-1} - T_{crown}}{e^{-1.9(LT_{50t-1} - T_{crown})-3.74}} \quad \text{(A.4)}$$

The stress due to respiration under snow is calculated as a function of snow depth (dsnow) that ranges from 0 to 1 for snow cover up to 12.5 cm (equal to 1 for all snow depth higher than 12.5), and a specific respiration factor (RE):

$$rate_r = R\ x\ RE\ x\ f(dsnow)$$

$$R = 0.54\ f(dsnow) = min(dsnow, 12.5)\ /12.5$$

$$RE = \frac{e^{0.84+0.051\,T_{crown}-2}}{1.85} \quad \text{(A.5)}$$

The contribution of hardening and dehardening are calculated within certain temperature ranges as follows:

$$For\ T_{crown} < 10°C$$

$$rate_h = 0.0093(10 - max(T_{crown}, 0))(LT_{50t-1} - LT_{50c}) \quad \text{(A.6)}$$

For $T_{crown} \geq 10°C$ when $vf < 1$ (not fully vernalized),

and $T_{crown} \geq -4°C$ when $vf = 1$ (fully vernalized)

$$rate_d = 2.7\ x\ 10^{-5}(LT_{50i} - LT_{50t-1})(T_{crown} + 4)^3 \quad \text{(A.7)}$$

where LT_{50c} is the maximum frost tolerance of -23 °C and LT_{50i} represents the LT_{50} for an unacclimated plant (LT_{50i} = -0.6+0.142 LT_{50c}).

The survival rate (f_{surv}) is then calculated as a function of LT_{50} and the crown temperature. The probability of survival is a function of T_{crown} in time (t). It increases once T_{crown} is higher than LT_{50} or decreases when it is lower (Vico et al., 2014):

$$f_{surv}(T_{crown}, t) = 2^{-\frac{T_{crown}}{LT_{50}}^{\alpha_{surv}}} \quad \text{(A.8)}$$

where α_{surv} is a shape parameter of 4.

The winter killing degree day (WDD) is calculated as a function of crown temperature and survival probability, where the maximum function limits the integration to the potentially damaging periods, when the air temperature (T) is lower than the base temperature (T_{base}) of 0°C (Vico et al., 2014):

$$WDD = \int_{winter} max\ [(T_{base} - T_{crown}),0]\ [1 - f_{surv}(T_{crown}, t)]dt \quad \text{(A.9)}$$

Lower LT_{50} indicate a higher frost tolerance and would result in higher survival rates, smaller WDD and less cold damage to the plant. Thus, when the survival probability and crown temperature are low, the WDD will be high (Vico et al., 2014).

The survival probability and the WDD are then used to estimate instant and accumulated frost damage to the crop during the leaf emergence phase (Lu et al., 2017). Instant frost damage is assumed to happen at the beginning of the growing season when the plants are not fully vernalized (vf < 0.9) when the growth of leaves (especially new leaves or small seedlings) due to an exposure to low temperatures. It is simulated by reducing the leaf carbon at low survival probabilities (whenever f_{surv} is below 1). The leaf carbon is reduced by an amount of 5 gC m^{-2} scaled by a factor of 1-f_{surv} that is moved to the carbon litter pool, up to a minimum value of 10 gC m^{-2} leaf carbon:

$$leafc_t = leafc_{t-1} - leafc_{damage}(1 - f_{surv})$$

for $vf < 0.9$, $WDD > 0$, $f_{surv} < 1$, and $leafc_t > 10$ (A.10)

where $leafc_t$ is the simulated leaf carbon of the current time step, $leafc_{t-1}$ is the leaf carbon of the previous step and $leafc_{damage}$ is equivalent to 5 gC m^{-2}.

When the plant is close to vernalization towards the end of the leaf emergence phase, it is not as susceptible to suffer from instantaneous frost damage as in the beginning of this phase. Still, an extended period of freezing temperatures can potentially induce damage to the plant (Lu et al., 2017). This accumulated frost damage is simulated based on the accumulated WDD and average survival probability. When the accumulated WDD reaches

a value higher than 1° days, the leaf carbon from the previous time step (leafc$_{t-1}$), scaled by the average f_{surv}, is moved to the soil carbon litter pool:

$$leafc_t = leafc_{t-1}(1 - average\ f_{surv})$$

$$for\ vf \geq 0.9\ and\ WDD > 1 \quad \text{(A.11)}$$

Once this has occurred, the accumulated WDD is reset to 0 and the tracking of the average f_{surv} is restated. Corresponding to the leaf carbon reduction, the leaf nitrogen is reduced from the leaf nitrogen pool to the soil nitrogen litter pool scaled with the parameterized leaf C/N ratio for winter wheat of 20.

A2: Evaluation of default parameterization for temperate corn

There is already a specific set of parameters available for the CFT temperate corn. This parameterization was tested for the site DE-Kli, where it resulted in a reasonable representation of seasonal LAI variation and magnitude (Figure A1). A moderate correlation was obtained for latent heat flux (0.56), with underestimation of latent heat flux during the early growing cycle of corn, as well as for sensible heat flux (0.41). Similar to winter wheat at BE-Lon and DE-RuS, the simulated NEE shows a negative bias with an underestimation of peak NEE (Figure A1).

Table A4: Bias, RMSE and *r* for the simulated daily NEE [µmol CO_2 W m^{-2} s^{-1}], LE [W m^{-2}], H [W m^{-2}] and Rn [W m^{-2}]) using the default parameterization for the CFT temperate corn at DE-Kli for the year 2007. Values were calculated for the time between recorded planting and harvest dates using simulation output and observation data at daily time step.

CFT	CORN
Site	DE-Kli
Year(s)	2007
Parameter set	*default*
NEE	
Bias	-1
RMSE	2.59
r	0.46
LE	
Bias	-0.33
RMSE	37.82
r	0.56
H	
Bias	-0.01
RMSE	39.21
r	0.41
Rn	
Bias	-0.12
RMSE	52.33
r	0.51

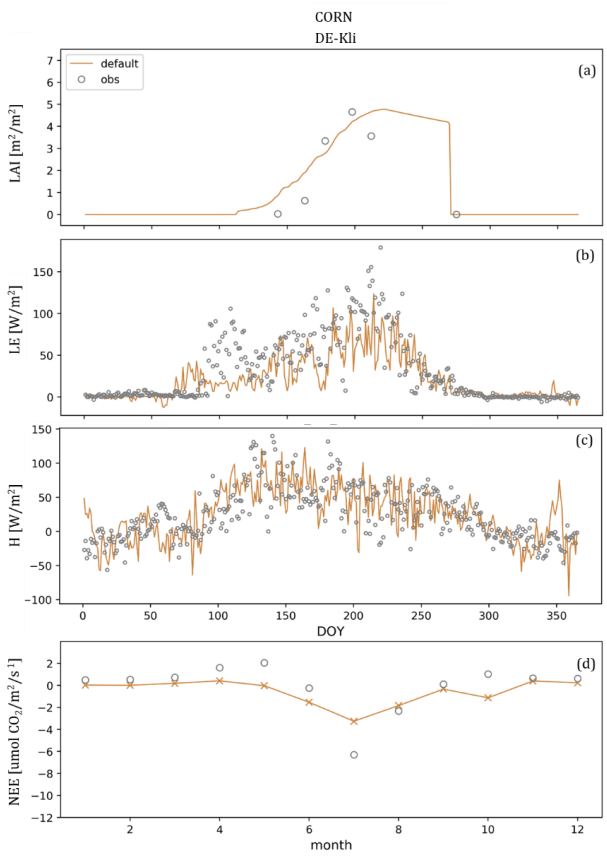

Figure A1: Daily simulation results of (**a**) LAI, (**b**) LE, (**c**) H, and (**d**) monthly averaged NEE rates over all corn years at DE-Kli using the default parameterization (orange). Site observation data on LAI (all available observations plotted) and fluxes (averaged over all respective years) are indicated in grey. Corresponding statistical analysis is listed in Table A4.

A3: Annual metrics for winter wheat, temperate corn, sugar beet and potatoes simulation runs

Table A5: Bias, RMSE and *r* of the simulated daily NEE [umol $CO_2/m^2/s$], LE [W/m^2], H [W/m^2] and Rn [W/m^2] averaged for all winter wheat years at the sites BE-Lon, DE-RuS, DE-RuM and DE-Kli respectively, simulated with CLM_WW and the control configuration.

CFT	Winterwheat							
Site	BE-Lon		DE-RuS		DE-RuM		DE-Kli	
Year(s)	2010/2011 2012/2013 2014/2015 2016/2017		2017/2018		2016/2017		2010/2011 2015/2016	
Model	*control*	*CLM_WW*	*control*	*CLM_WW*	*control*	*CLM_WW*	*control*	*CLM_WW*
NEE								
Bias	-0.9	-0.36	-1.06	-0.41	-	-	-0.48	0.97
RMSE	5.52	4.96	5.61	5.03	-	-	2.5	6.82
r	-0.03	0.43	0.26	0.46	-	-	0.56	0. 28
LE								
Bias	-0.73	-0.34	-0.40	-0.30	-55.55	-27.83	-0.48	-0.10
RMSE	52.24	44.37	38.40	36.53	53.07	44.02	37.01	35.73
r	0.44	0.52	0.45	0.72	0.47	0.57	0.61	0.71
H								
Bias	2.50	1.20	0.96	0.79	-28.00	-16.72	1.83	0.42
RMSE	41.30	31.49	30.19	25.64	37.79	32.23	32.33	30.83
r	0.48	0.53	0.68	0.78	0.47	0.53	0.47	0.63
Rn								
Bias	-0.21	-0.11	-0.09	-0.05	-11.29	-0.06	-0.08	-0.04
RMSE	34.77	35.49	35.17	35.95	16.05	39.23	38.76	38.21
r	0.78	0.79	0.79	0.79	0.82	0.78	0.78	0.80

Table A6: Bias, RMSE and *r* for the simulated daily NEE [µmol CO_2 W m^{-2} s^{-1}], LE [W m^{-2}], H [W m^{-2}] and Rn [W m^{-2}]) using the crop-specific parameterization (*specific*) for the CFTs sugar beet and potatoes at the sites BE-Lon and DE-RuS respectively. Results are compared to those from the control simulation runs (*control*). Values were calculated over the whole year (averaged over all respective CFT years at each site) using simulation output and observation data at daily time step.

CFT	Corn	Sugarbeet				Potatoes			
Site	DE-Kli	DE-RuS		BE-Lon		DE-RuS		BE-Lon	
Year(s)	2007	2017		2004 2008 2016		2019		2006 2010 2014 2018	
Parameter set	*control*	*control*	*crop-specific*	*control*	*crop-specific*	*control*	*crop-specific*	*control*	*crop-specific*
NEE									
Bias	-0.99	-0.81	-0.73	-0.41	-0.39	-	-	6.96	6.03
RMSE	2.59	7.31	6.21	5.83	4.41	-	-	3.73	3.54
r	0.26	0.05	0.31	0.16	0.56	-	-	0.43	0.55
LE									
Bias	-0.93	-0.45	-0.07	-0.46	-0.41	-0.37	0.16	-0.98	-0.47
RMSE	51.65	47.84	20.43	49.39	39.88	48.9	40.59	53.14	38.54
r	0.24	0.38	0.61	0.43	0.65	0.23	0.55	0.2	0.39
H									
Bias	0.04	4.89	1.45	4.15	3.37	1.57	-0.29	0.1	0.14
RMSE	35.12	35.43	14.37	33.39	27.85	42.14	27.11	30.06	30.09
r	0.58	0.32	0.83	0.31	0.59	0.17	0.41	0.44	0.47
Rn									
Bias	-0.22	-0.08	0.01	-0.2	-0.18	-0.08	0.02	-	-
RMSE	43.09	15.75	11.7	32.01	30.83	39.86	40.82	-	-
r	0.79	0.81	0.82	0.63	0.64	0.69	0.7	-	-

B. SI: Seasonal crop yield predictions with SEAS5 long-range meteorological forecasts in a land surface modelling approach

B1: Effect of temporal forcing data resolution – a synthetic experiment

In a first step, we analyzed the performance of MetSim as a disaggregation tool for solar radiation by using MetSim to disaggregate the daily averaged variables to an hourly time step and comparing the output to the hourly observations (Figure B1, Table B1). Comparing the time series of disaggregated shortwave radiation at hourly time step with the initial hourly measurement data, we see that the disaggregated dataset has slightly higher monthly sums of solar radiation and a higher mean value over the entire time series of 7 years (Figure B1a), while underestimating the peak daily value compared to the initial observations (Figure B1b). The disaggregated dataset represents a realistic diurnal cycle with reasonable magnitudes of solar incoming radiation.

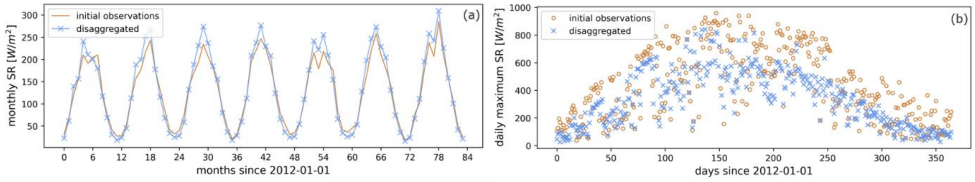

Figure B1: Comparison of MetSim disaggregated data with initial observations of incoming shortwave radiation (SR): (**a**) averaged for each months over 7 years, and (**b**) the respective daily maximum values for one selected year.

Table B1: Comparison of MetSim disaggregated incoming shortwave radiation [W m^{-2}] at hourly time step with the original hourly observation data over the time period of 7 years.

Data	Min	Max	Mean	Total (7-year sum)	Bias	RMSE
Initial observation	0.00	988.24	127.81	7843522.00	0.04	41.23
Disaggregated	0.00	867.26	132.42	8126221.50		

For statistical evaluation of the results, the root mean square error (RMSE) and the bias were chosen as performance metrics:

$$bias = \sum_{i=1}^{n}(X_i - X_{obs,i}) / \sum_{i=1}^{n}(X_{obs,i}), \quad \text{(B.1)}$$

where i is time step and n the total number of time steps, X_i and $X_{obs,i}$ are the simulated and the observed values at every time step.

The statistical evaluation was conducted against the reference simulation results that were generated from the original hourly observation forcing for multiple simulated variables: leaf are index (LAI), latent heat flux (LH), sensible heat flux (SH), evapotranspiration (ET), ground evaporation (Qsoil), transpiration (QVegT), soil water content at different depths (SWC) and surface runoff (Qover). In general, the 6 hourly disaggregated data, both for single forcing variables as well as for combined forcing datasets performed better for all individual output variables than the daily data in terms of RMSE and bias (Figure B2). The daily forcing dataset with all variables at daily time step performed the most poorly compared to the reference forcing, thus resulting in high RMSE and high biases for all output variables that were analyzed. The effect is especially prominent for the soil water content and the surface runoff. For the individual forcing variables, the temporal resolution of incoming shortwave radiation had slightly higher effects on simulation results than the resolution of precipitation for most of the analyzed output, such as leaf area index, soil water content at different depths of the soil profile, ground evaporation, evapotranspiration and energy fluxes, except for surface runoff, where daily precipitation data resulted in a higher bias than daily shortwave radiation (Figure B2). The simulated grain yield was the model output variable least affected by the temporal resolution of forcing data (Table B2). Here, most of the forcing dataset combinations resulted in similar or slightly higher grain yields compared to the reference dataset, except for the all daily and all 6 hourly forcings and the 6 hourly precipitation dataset (Table B2).

Table B2: Simulation results for grain yield [t/ha] calculated with different forcing datasets at different temporal resolutions; all forcing variables (Incoming shortwave and longwave radiation, precipitation, temperature, relative humidity, wind speed and pressure) at either daily or 6 hourly disaggregated resolution, and only shortwave or precipitation as well as a combination of both shortwave and precipitation at daily and 6 hourly resolution with all other forcing variables at hourly time step.

Temporal resolution	Grain yield [t/ha]
Hourly forcing	4.90
All - 6h	4.71
All - daily	4.13
SW+Precip - 6h	5.41
SW+Precip - daily	5.75
SW - 6h	5.40
SW - daily	5.66
Precip - 6h	4.74
Precip - daily	5.13

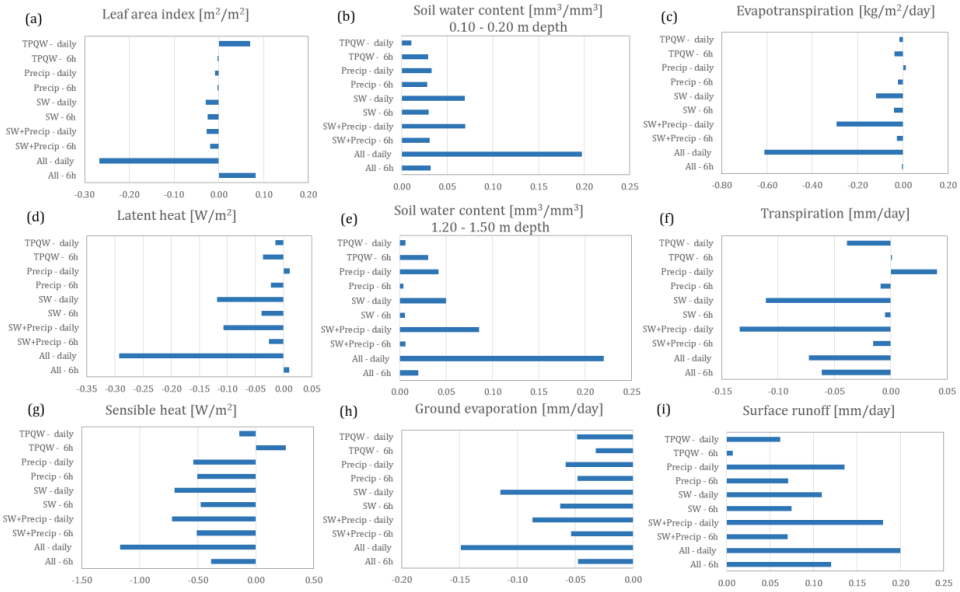

Figure B2: Biases introduced by different temporal forcing data resolutions and combinations on various output variables. TPQW refers to temperature, pressure, relative humidity and wind speed, Precip to precipitation, and SW to shortwave radiation.

In order to analyse the overall effect of temporal forcing data resolution on model outputs and to assess the general need for temporal disaggregation from daily variables for CLM5 simulations, we performed a synthetic simulation experiment for a high-resolution dataset at the point scale. We used a continuous measurement dataset at an hourly time step for 5 consecutive years from the cropland study site Selhausen (DE-RuS) located in the western part of Germany. Selhausen (50.86589°N, 6.44712°E) is part of the TERENO (TERrestrial Environment Obervatories) Rur Hydrological Observatory (Bogena at al., 2018), the TERENO Eifel/Lower Rhine Valley Observatory (Zacharias et al., 2011) and the Integrated Carbon Observation System (ICOS, 2020). Continuous measurements of meteorological variables and land-atmosphere exchange fluxes are available via the respective data portals (Kunkel et al., 2013; ICOS, 2020; TERENO, 2020). The original measurement data were first averaged to daily values and then temporally disaggregated to a 6-hourly time step using MetSim. Hence, simulations for a consecutive cycle of spring wheat over 5 years (hypothetical) were conducted with the reference observation data

at an hourly time step, with daily averaged observations, and with the disaggregated 6-hourly forcing dataset. A spin-up was conducted prior to this trial in order to balance ecosystem carbon and nitrogen pools, gross primary production and total water storage in the system (see Lawrence et al., 2018). As expected, the 6-hourly disaggregated data performed significantly better for all individual output variables than the daily data, which performed poorly compared to the reference forcing. The effect is especially prominent for the soil water content and the surface runoff. Here, the 6-hourly disaggregated forcing was able to capture more realistic magnitudes of both soil moisture content and runoff, resulting in only a small wet bias compared to the reference forcing (Table B3). The 6-hourly forcing resulted in a grain yield of 4.71 t/ha, which is relatively close to the grain yield simulated with an hourly forcing of 4.9 t/ha, while the grain yield simulated with a daily forcing of 4.12 t/ha is slightly lower. The soil moisture content (in the surface layers and the root zone) plays an important role in the simulation of reasonable crop productivity, especially when trying to simulate inter-annual differences in crop yield and crop growth in response to e.g. drought conditions. However, in the given simulation example for the DE-RuS site, water availability in the root zone does not represent the main limiting factor for plant growth for the simulated years. This explains the small variations of simulated grain yield and LAI with the different forcing datasets despite the profound differences in simulated soil water contents. The results from this trial underline the importance of an adequate temporal resolution for forcing data. For the seasonal weather forecast data, the temporal disaggregation of the product to an adequate temporal resolution is crucial in order to make the data suitable for comparable model applications.

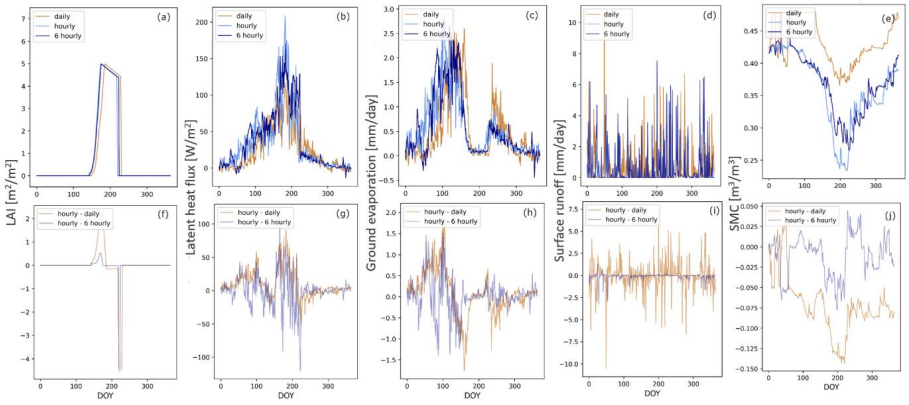

Figure B3: (Top) Comparison of simulation results for a cycle of (hypothetical) spring wheat cropping (averaged over 5 years) at DE-RuS with different temporal resolutions of the forcing data: reference simulations forced with hourly observation data (light blue), daily averaged forcing data at a 24 h time step (orange) and disaggregated forcing data at 6-hourly resolution (navy) for (**a**) LAI, (**b**) latent heat flux, (**c**) ground evaporation, (**d**) surface runoff and (**e**) SMC (in an upper soil layer of 0.12 to 0.20 m depth). (Bottom) The difference in the simulation results for each variable. Results from the reference simulation forced with hourly data minus the daily forcing (orange) and 6-hourly disaggregated forcing (blue) respectively. Corresponding statistics are listed in Table B3.

Table B3: Bias and RMSE calculation for model output produced with different sets of forcing data at different temporal resolutions; all forcing variables (Incoming shortwave and longwave radiation, precipitation, temperature, relative humidity, wind speed and pressure) at either daily or 6 hourly disaggregated resolution, a combination of both shortwave and precipitation, as well as only shortwave or precipitation and TPQW at daily and 6 hourly resolution with all other forcing variables at hourly time step respectively. The bias and RMSE were calculated with the model output produced with hourly forcings as validation data set.

Output varibales	LAI [m^2/m^2]		LH [W/m^2]		SH [W/m^2]		SWC [mm^3/mm^3]		SWC [mm^3/mm^3]		ET [$kg/m^2/day$]		Qsoil [mm/day]		Qover [mm/day]		QVegT [mm/day]	
	RMSE	Bias	RMSE	bias	RMSE	bias	RMSE	bias	RMSE	bias	RMSE	bias	RMSE	bias	RMSE	bias	RMSE	bias
All forcing variables																		
6 hourly	0.65	0.08	24.57	0.01	18.62	-0.38	0.03	0.02	0.03	0.03	0.85	0.00	0.42	-0.05	0.41	0.20	0.42	-0.06
daily	0.62	-0.27	23.96	-0.29	29.89	-1.17	0.08	0.22	0.29	0.20	0.83	-0.61	0.54	-0.15	1.70	0.12	0.89	-0.07
Shortwave and Precipitation																		
6 hourly	0.06	-0.02	17.32	-0.03	16.83	-0.51	0.03	0.01	0.02	0.03	0.60	-0.03	0.46	-0.05	0.49	0.07	0.31	-0.02
daily	0.38	-0.03	24.59	-0.11	25.87	-0.72	0.06	0.09	0.04	0.07	0.85	-0.29	0.57	-0.09	1.61	0.18	0.68	-0.13
Shortwave																		
6 hourly	0.10	-0.02	16.14	-0.04	16.02	-0.47	0.03	0.01	0.02	0.03	0.56	-0.04	0.43	-0.06	0.33	0.07	0.32	-0.01
daily	0.38	-0.03	24.99	-0.12	25.29	-0.70	0.05	0.05	0.03	0.07	0.86	-0.12	0.56	-0.11	0.82	0.11	0.64	-0.11
Precipitation																		
6 hourly	0.40	0.00	16.12	-0.02	14.27	-0.51	0.03	0.00	0.02	0.03	0.56	-0.02	0.44	-0.05	0.49	0.07	0.06	-0.01
daily	0.34	-0.01	19.96	0.01	16.18	-0.54	0.02	0.04	0.02	0.03	0.69	0.01	0.42	-0.06	1.63	0.14	0.32	0.04
TPQW																		
6 hourly	0.07	0.00	8.63	-0.04	7.60	0.26	0.02	0.03	0.01	0.03	0.30	-0.04	0.14	-0.03	0.29	0.01	0.40	0.00
daily	0.50	0.07	13.43	-0.01	15.43	-0.14	0.02	0.01	0.02	0.01	0.46	-0.02	0.26	-0.05	0.83	0.06	0.28	-0.04

B2: Comparison with CRNS data

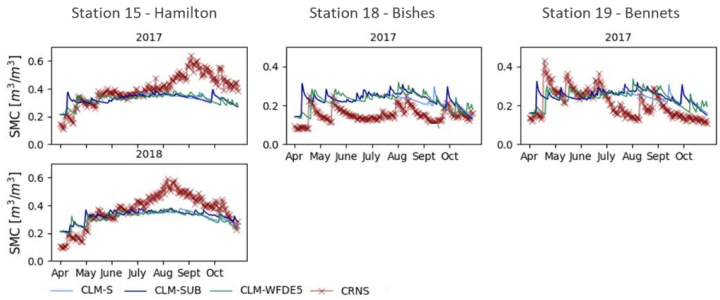

Figure B4: Comparison of CRNS data (level 4) from the stations 15 (Hamilton), 18 (Bishes) and 19 (Bennets) available from the CosmOz network (Hawdon et al., 2014) with simulated SMCs at the closest grid point for the years 2017 and 2018. Corresponding statistics Corresponding statistics can be found in Table B4.

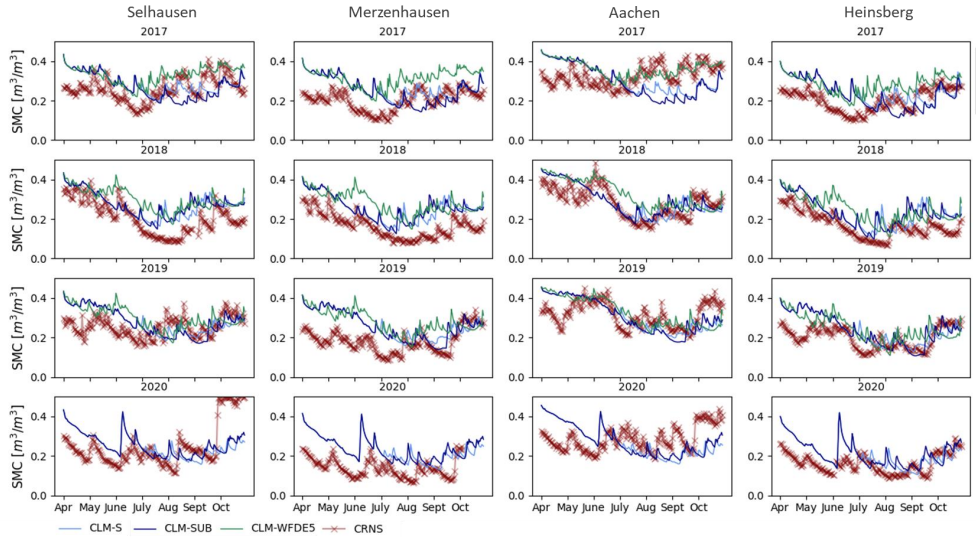

Figure B5: Comparison of CRNS data from the COSMOS-Europe sites Selhausen, Merzenhausen, Aachen and Heinsberg (Bogena et al., 2022) with simulated SMCs at the closest grid point for the years 2017-2020. Corresponding statistics can be found in Table B5.

Table B4: RMSE, MBE and R^2 for CLM-S-, CLM-SUB- and CLM-WFDE5-simulated surface soil moisture moisture from the 1st of April to the 31st of October of 2017 and 2018 compared to daily averaged CRNS measurements (Level 4) from the CosmOZ sites Hamilton, Bishes and Bennets respectively. The simulation outputs were averaged using a physically based weighting approach after Schrön et al. (2017).

AUS-VIC						
	2017			2018		
	RMSE	MBE	R^2	RMSE	MBE	R^2
Station 15 - Hamilton						
CLM-S	0.12	-0.07	0.48	0.10	-0.05	0.81
CLM-SUB	0.12	-0.07	0.43	0.09	-0.04	0.83
CLM-WFDE5	0.11	-0.07	0.63	0.10	-0.06	0.82
Station 18 - Bishes						
CLM-S	0.09	0.08	0.14	-	-	-
CLM-SUB	0.10	0.09	0.30	-	-	-
CLM-WFDE5	0.09	0.08	0.58	-	-	-
Station 19 - Bennets						
CLM-S	0.08	0.03	0.29	-	-	-
CLM-SUB	0.08	0.04	0.25	-	-	-
CLM-WFDE5	0.08	0.03	0.34	-	-	-

Table B5: RMSE, MBE and R^2 for CLM-S-, CLM-SUB- and CLM-WFDE5-simulated surface soil moisture from the 1st of April to the 31st of October of 2017, 2018, 2019 and 2020, compared to daily averaged CRNS measurements from the COSMOS-Europe sites Selhausen, Merzenhausen, Aachen and Heinsberg respectively. The simulation outputs were averaged using a physically based weighting approach after Schrön et al. (2017).

DE-NRW												
	2017			2018			2019			2020		
	RMSE	MBE	R^2	RMSE	MBE	R^2	RMSE	MBE	R^2	RMSE	MBE	R^2
Selhausen												
CLM-S	0.08	0.03	0.10	0.08	0.06	0.80	0.08	0.03	0.16	0.12	0.00	0.08
CLM-SUB	0.09	0.01	-0.01	0.08	0.06	0.79	0.08	0.03	0.22	0.11	0.01	0.17
CLM-WFDE5	0.08	0.07	0.69	0.10	0.09	0.82	0.09	0.05	-0.03	-	-	-
Merzenhausen												
CLM-S	0.09	0.06	0.27	0.10	0.09	0.78	0.11	0.08	0.34	0.10	0.08	0.45
CLM-SUB	0.09	0.05	0.11	0.10	0.09	0.75	0.10	0.08	0.42	0.10	0.08	0.45
CLM-WFDE5	0.11	0.11	0.81	0.12	0.11	0.85	0.12	0.10	0.25	-	-	-
Aachen												
CLM-S	0.10	-0.01	-0.31	0.06	0.01	0.70	0.08	0.00	0.42	0.11	-0.01	-0.18
CLM-SUB	0.11	-0.03	-0.36	0.06	0.01	0.72	0.08	0.00	0.50	0.10	-0.01	-0.13
CLM-WFDE5	0.07	0.03	0.22	0.07	0.05	0.75	0.08	0.01	0.34	-	-	-
Heinsberg												
CLM-S	0.08	0.04	0.34	0.08	0.06	0.78	0.08	0.04	0.53	0.08	0.05	0.50
CLM-SUB	0.08	0.03	0.30	0.07	0.06	0.81	0.07	0.04	0.60	0.08	0.05	0.49
CLM-WFDE5	0.08	0.08	0.87	0.08	0.08	0.84	0.08	0.04	0.45	-	-	-

B3: State-wide agricultural statistics

Table B6: Cropping area and production of major cash crops in Victoria, Australia, from 2014/15 to 2020/21, and six year average (Source: ABARES, 2020).

Year	Area ("000 ha)	Production (kt)	Yield (t/ha)
Wheat			
2014-15 to 2020-21 average	1455.43	3348.24	2.30
2014-15	1492.66	2631.30	1.76
2015–16	1,342	1,815	1.35
2016–17	1,454	4,665	3.21
2017–18	1,447	3,682	2.54
2018–19	1,403	2,277	1.62
2019–20 *	1,450	3,600	2.48
2020–21 *	1,600	4,768	
Barley			
2014-15 to 2020-21 average	876.17	2042.15	2.33
2014-15	916.08	1373.83	1.50
2015–16	844	1,107	1.31
2016–17	946	3,083	3.26
2017–18	844	2,110	2.50
2018–19	893	1,337	1.50
2019–20 *	820	2,500	3.05
2020–21 *	870	2,784	3.20
Canola			
2014-15 to 2020-21 average	411.12	646.71	1.57
2014-15	483.27	558.68	1.16
2015–16	277	287	1.04
2016–17	327	633	1.94
2017–18	542	938	1.73
2018–19	414	511	1.23
2019–20 *	385	650	1.69
2020–21 *	450	950	
Oats			
2014-15 to 2020-21 average	128.84	250.15	1.94
2014-15	133.21	179.47	1.35
2015–16	140	185	1.32
2016–17	162	493	3.05
2017–18	97	188	1.94
2018–19	134	165	1.23
2019–20 *	100	175	1.75
2020–21 *	135	365	2.70

*ABARES estimate

Table B7: Cropping area and production of main cash crops (grain crops, wheat, corn, canola, potatoes and sugar beet) in North Rhine-Westphalia, Germany, from 2016 to 2020, and five year average (Source: BMEL, 2022).

Year	Area ("000 ha)	Production (kt)	Yield (t/ha)
Grain crops (without corn)			
2013 to 2018 average	610.9	4036.4	7.87
2016	514.2	3852.6	7.49
2017	502.4	3694.6	7.35
2018	485.5	3534.1	7.28
2019	498.6	3826	7.67
2020	490.00	3700.30	7.55
Wheat (winter and summer wheat)			
2013 to 2018 average	270	2292.5	8.49
2016	268.6	2161.3	8.05
2017	265	2098.3	7.92
2018	247.2	1955.5	7.91
2019	253.5	2063.7	8.14
2020	230.60	1996.56	8.66
Corn			
2013 to 2018 average	98.3	984.2	10.01
2016	88.6	873.7	9.86
2017	99.8	1071.1	10.74
2018	88.5	690.2	7.8
2019	85.8	724.5	8.44
2020	79.73	836.60	10.49
Canola			
2013 to 2018 average	60.8	240.8	3.96
2016	58.7	226.0	3.85
2017	56.7	221.2	3.9
2018	57.2	198.8	3.48
2019	40.3	148.6	3.69
2020	42,3	158,5	3.74
Potatoes			
2013 to 2018 average	31.1	1502.7	48.28
2016	31	1457.2	46.95
2017	31.1	1627.0	52.26
2018	33.2	1322.8	39.83
2019	40.5	1885.7	46.53
2020	36.7	1694.9	46.16
Sugar beet			
2013 to 2018 average	-	-	-
2016	-	-	-
2017	61	5411.5	88.7
2018	61.7	3958.1	64.2
2019	59.3	4450	75.1
2020	52.7	4183.9	79.3

B4: Processing and analysis of seasonal forecasts - precipitation bias

We compared the ECMWF SEAS5 seasonal precipitation forecasts initialized on the first of April with 7 month lead time for the years 2017 and 2018 to corresponding data from the bias-adjusted global reanalysis dataset WFDE5 (Cucchi et al., 2020).

For the AUS-VIC domain, both the seasonal and sub-seasonal forecasts were not able to capture the wet period in August 2017. A slightly better correspondence was reached for the late growing season of 2018 (August, September and October) both in the seasonal and sub-seasonal forecasts (Figure B6). No systematic or consistent improvement in terms of total predicted precipitation amounts respective to the WFDE5 data can be observed in the sub-seasonal forecasts starting on the 1st of July of the respective years compared to the seasonal forecasts that are initialized on the 1st of April (Figure B6).

For the DE-NRW domain the predicted rainfall amounts in the seasonal forecasts are too large compared to WFDE5, especially in the beginning of the growing season (April, May, June) of 2017, and towards the end of the growing season of 2018 (especially September and October), where the forecasts were not able to capture the dry spell that corresponds to the 2018 European drought. The sub-seasonal forecasts performed better for September 2018, while still overestimating the overall rainfall amounts of the second half of the growing season (July, August and October). Both the seasonal and sub-seasonal forecast predicted a generally dry year in 2018 (with the exception being September 2018 in the seasonal forecasts), but did not reflect the extreme drought conditions that were recorded in 2018 (Figure B6).

In general, the correspondence of predicted total monthly rainfall amounts in seasonal and sub-seasonal forecasts with the WFDE5 reanalysis is better for the AUS-VIC domain than for the DE-NRW domain. The bias is much smaller over the Australian continent, with a maximum of +/- 0.90 mm/day, than for Germany (and Europe), where a maximum bias of up to 2.70 mm/day (local maximum, 2018) can be observed (Figure B6, Figure B7).

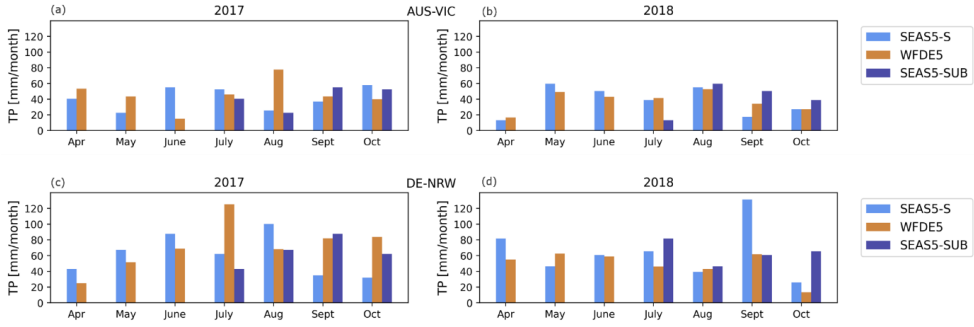

Figure B6: SEAS5 total monthly precipitation amounts from seasonal forecasts starting on the 1st of April (SEAS5-S) and sub-seasonal forecasts starting on the 1st of July (SEAS5-SUB) for the years 2017 and 2018, for (**a**, **b**) the AUS-VIC domain and (**c**, **d**) the DE-NRW domain, compared to WFDE5 data for the respective domains.

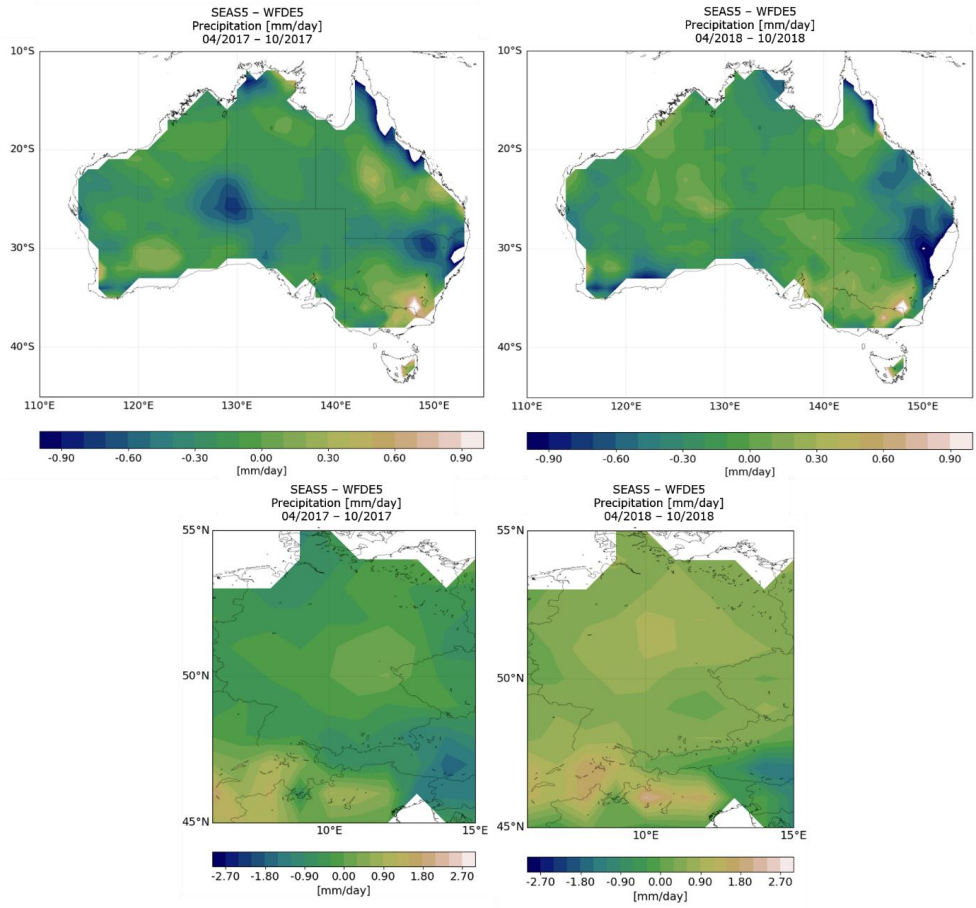

Figure B7: Bias (forecast – reference data) for ECMWF SEAS5 mean daily rainfall amount [mm/day] with 51 ensemble members for (top) Australia and (bottom) Germany. Forecast period initialized on the 1st of April until the 31st of October of (left) 2017 and (right) 2018 respectively. The bias was computed with respect to the WFDE5 dataset.

B5: Regional crop yield predictions for root crops

Despite earlier enhancements to the model code and parameterization scheme, the crop module of CLM5 does not include a proper representation of root crops. The harvesting scheme of root crops in CLM5 crop module is adapted to the one for grain crops. This resulted in large discrepancies between simulated and recorded crop yields for potatoes and sugar beet with recorded yields being up to 10 times larger (Table B8).

Table B8: Simulated crop yields [t/ha] for potatoes and sugar beet with seasonal (CLM-S), sub-seasonal (CLM-SUB) and reanalysis (CLM-WFDE5) forcing data for the years 2017 to 2020, compared to official crop statistics from (BMEL, 2022) for the DE-NRW domain. The lowest (italics) and highest (bold) yields amongst the respective years are indicated.

	DE-NRW			
	2017	2018	2019	2020
Potatoes				
BMEL	**52.26**	*39.83*	46.53	46.16
CLM-S	**7.50**	*6.95*	6.97	7.29
CLM-SUB	**7.11**	*6.63*	7.03	6.94
CLM-WFDE5	7.37	6.79	7.03	-
Sugarbeet				
BMEL	**88.7**	*64.2*	75.1	79.3
CLM-S	**7.35**	*6.82*	6.83	7.34
CLM-SUB	6.87	*6.50*	6.84	**6.97**
CLM-WFDE5	7.22	6.65	6.89	-

C. SI: On the predictability of multi-decadal soil moisture and crop yield variability with CLM5

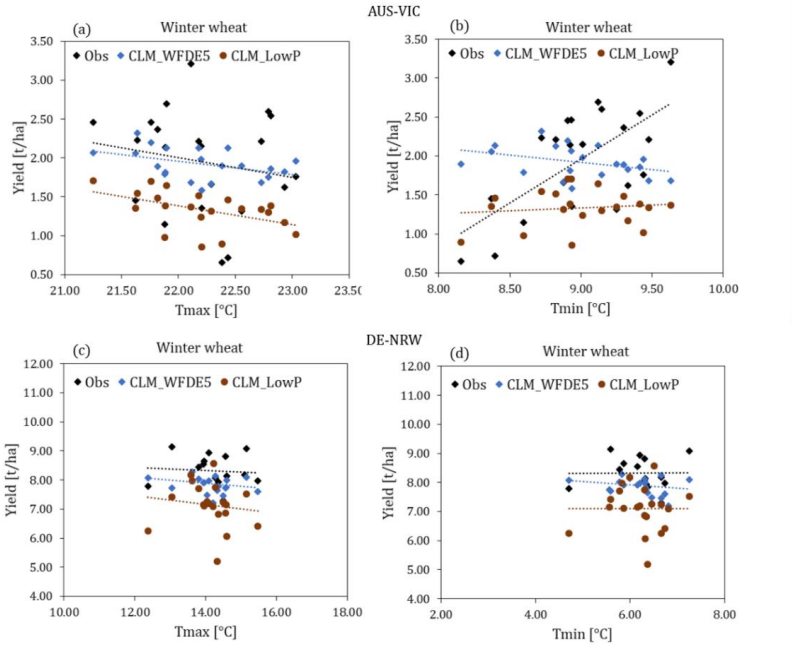

Figure C1: Correlation of mean annual winter wheat yield (simulated (CLM_WFDE5), simulated with reduced precipitation (CLM_LowP) and from records (Obs)) with the corresponding mean daily maximum and minimum temperatures from 1999 – 2019 for (**a**-**b**) the AUS-VIC domain and (**c**-**d**) the DE-NRW domain respectively.

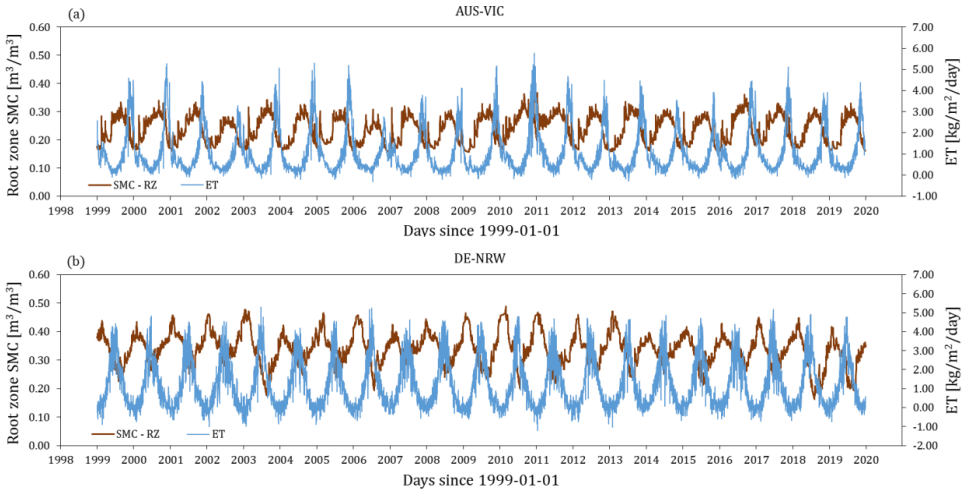

Figure C2: Simulated daily evapotranspiration and root zone soil moisture (0 - 0.32 m depth) throughout (**a**) the AUS-VIC domain and (**b**) the DE-NRW domain from 1999 – 2019.

Table C1: Total annual crop yield (t/ha) and corresponding yield anomaly (%) from simulation results (*CLM*) for winter wheat, winter wheat monoculture with unchanged WFDE5 precipitation (*CLM-WFDE5*) and reduced precipitation (*CLM_LowP*), barley, canola and sorghum throughout the AUS-VIC domain for the years 1999 – 2019, compared to available records (*Obs*) from ABARES (2020).

	1999	2000	2001	2002	2003	2004	2005	2006	2007	2008	2009	2010	2011	2012	2013	2014	2015	2016	2017	2018	2019
Yield [t/ha]																					
Obs																					
Winter wheat	2.14	2.70	2.46	0.72	2.23	1.45	2.21	0.65	1.32	1.14	1.66	2.46	2.36	2.15	2.21	1.76	1.35	3.21	2.54	1.62	2.60
Barley	2.03	2.41	2.36	0.62	2.61	1.41	2.31	0.66	1.62	1.29	1.91	2.43	2.41	2.29	2.22	1.50	1.31	3.26	2.50	1.50	2.83
Canola	1.39	1.46	1.46	0.71	1.61	1.21	1.43	0.24	1.13	0.82	1.43	1.47	1.44	1.47	1.62	1.16	1.04	1.94	1.73	1.23	1.81
Sorghum	7.32	1.88	-	-	0.43	1.32	2.64	1.91	1.92	-	-	2.01	-	0.56	1.27	-	2.78	0.34	0.61	0.72	-
Mean	1.85	2.19	2.09	0.68	2.15	1.36	1.98	0.52	1.35	1.08	1.67	2.12	2.07	1.97	2.01	1.47	1.23	2.80	2.26	1.45	2.41
CLM																					
Winter wheat	2.13	2.38	2.33	2.24	2.53	2.37	2.35	2.06	2.16	2.18	2.07	2.53	2.22	2.31	1.95	2.33	2.03	2.21	2.27	2.24	2.33
Barley	1.66	1.40	0.87	1.46	1.40	1.81	1.13	1.42	1.62	1.12	0.81	1.27	1.43	1.47	2.05	1.55	1.15	1.54	0.90	0.35	1.59
Canola	1.26	0.85	0.80	1.34	1.29	1.22	0.58	0.91	1.74	1.21	1.42	0.99	1.07	0.89	1.92	1.40	0.86	1.15	1.10	0.46	1.48
Sorghum	2.39	2.31	1.78	1.90	2.45	1.63	2.19	2.07	2.05	2.25	2.33	2.50	2.46	2.42	2.04	2.05	2.40	2.18	2.55	2.40	2.22
Mean	1.68	1.54	1.33	1.68	1.74	1.80	1.35	1.46	1.84	1.50	1.43	1.59	1.57	1.56	1.98	1.76	1.35	1.63	1.42	1.02	1.80
Winter wheat monoculture																					
CLM_WFDE5	1.81	2.13	2.20	2.13	2.32	2.06	2.13	1.90	1.90	1.79	1.67	2.07	1.89	1.98	1.68	1.96	1.59	1.68	1.86	1.82	1.76
CLM_LowP	1.39	1.65	1.70	1.46	1.54	1.36	1.51	0.90	1.34	0.97	1.32	1.71	1.48	1.24	1.33	1.02	0.86	1.37	1.38	1.17	1.30
Yield anomaly [%]																					
Obs																					
Winter wheat	9.72	38.18	25.93	-63.16	14.44	-25.55	13.44	-66.54	-32.43	-41.31	-14.75	26.16	21.13	10.23	13.36	-9.62	-30.64	64.46	30.48	-16.80	33.27
Barley	2.91	22.04	19.77	-68.84	32.15	-28.49	17.10	-66.47	-18.14	-34.86	-3.29	22.87	22.16	15.75	12.23	-24.05	-33.59	65.01	26.64	-24.14	43.26
Canola	5.25	10.16	10.14	-46.09	21.38	-8.88	7.92	-82.20	-14.80	-38.07	8.40	11.31	9.06	11.15	22.18	-12.59	-21.45	46.47	30.86	-6.82	36.61
Sorghum	298.88	2.25	-	-	-76.59	-27.98	43.82	4.14	4.41	-	-	9.35	-	-69.48	-31.07	-	51.60	-81.67	-66.66	-61.01	-
Mean	6.03	25.04	19.63	-60.99	22.85	-22.46	13.43	-70.46	-22.61	-38.07	-4.60	21.18	18.48	12.54	15.16	-15.80	-29.44	60.13	29.13	-17.05	37.87
CLM																					
Winter wheat	-5.34	5.99	3.58	-0.20	12.47	5.53	4.34	-8.46	-4.01	-3.27	-7.88	12.28	-1.22	2.86	-13.10	3.64	-9.93	-1.66	0.84	-0.20	3.75
Barley	26.55	6.73	-33.71	11.01	6.87	37.71	-13.76	8.43	23.28	-14.80	-38.31	-3.52	8.73	11.97	56.44	17.80	-12.18	17.44	-31.23	-73.38	21.21
Canola	9.76	-25.96	-30.04	16.56	12.23	6.51	-49.76	-20.72	51.37	5.48	23.73	-14.13	-7.17	-22.57	67.17	22.19	-25.27	0.42	-4.58	-60.27	28.84
Sorghum	8.48	4.85	-19.29	-13.95	11.01	-25.97	-0.44	-6.24	-6.96	2.17	5.67	13.39	11.61	9.97	-7.52	-7.02	8.94	-0.95	15.76	8.99	0.82
Mean	6.95	-1.84	-15.22	6.74	10.57	14.44	-14.11	-6.98	16.80	-4.59	-8.88	1.19	-0.15	-1.05	25.52	11.82	-14.51	3.90	-9.64	-35.39	14.44
Winter wheat monoculture																					
CLM_WFDE5	-5.65	11.04	14.35	10.97	20.92	7.19	10.72	-1.28	-1.14	-6.61	-13.23	7.70	-1.42	3.35	-12.47	2.06	-17.38	-12.37	-3.23	-4.95	-8.58
CLM_LowP	3.98	23.52	27.64	9.34	15.71	1.73	13.60	-32.81	0.75	-26.92	-1.12	27.93	11.07	-6.96	0.11	-23.62	-35.70	2.74	3.70	-12.26	-2.44

Table C2: Total annual crop yield (t/ha) and corresponding yield anomaly (%) from simulation results (*CLM*) for winter wheat, winter wheat monoculture with unchanged WFDE5 precipitation (*CLM-WFDE5*) and reduced precipitation (*CLM_LowP*), spring wheat, canola and corn throughout the DE-NRW domain for the years 1999 – 2019, compared to available records (*Obs*) from IT.NRW (2022).

	1999	2000	2001	2002	2003	2004	2005	2006	2007	2008	2009	2010	2011	2012	2013	2014	2015	2016	2017	2018	2019
Yield [t/ha]																					
Obs																					
Winter wheat	-	-	-	-	-	-	8.55	7.83	7.29	8.93	8.65	7.79	8.13	8.44	9.15	9.08	8.81	8.07	7.94	7.98	8.17
Spring wheat	-	-	-	-	-	-	6.54	6.08	5.73	6.84	6.65	6.01	5.83	7.14	7.15	6.60	7.08	6.21	5.85	5.40	5.36
Canola	-	-	-	-	-	-	3.83	3.82	3.50	3.65	4.25	4.01	3.64	3.90	4.14	4.29	4.03	3.85	3.90	3.48	3.69
Corn	-	-	-	-	-	-	10.10	8.70	9.61	10.58	10.33	9.46	11.18	11.37	10.17	11.17	9.99	9.86	10.74	7.80	8.44
Mean	-	-	-	-	-	-	7.26	6.61	6.53	7.50	7.47	6.82	7.20	7.71	7.65	7.79	7.48	7.00	7.11	6.17	6.42
CLM																					
Winter wheat	8.58	7.20	8.11	7.49	7.73	8.26	7.92	7.62	7.46	8.30	7.91	8.03	7.98	8.03	7.71	8.20	7.72	8.13	7.79	7.60	8.23
Spring wheat	5.76	4.12	5.02	3.68	5.50	5.03	5.34	5.09	4.30	4.90	5.76	5.37	5.43	5.05	4.65	5.36	4.93	4.61	5.67	5.34	5.89
Canola	5.71	3.86	4.93	3.71	5.54	5.08	5.32	5.03	3.89	4.90	5.71	5.38	5.37	5.18	4.62	5.37	4.91	4.59	5.65	5.80	5.80
Corn	9.31	7.93	9.25	8.42	9.52	9.25	9.08	8.74	8.21	8.57	9.21	8.04	8.93	9.15	8.11	9.05	8.62	8.67	8.83	8.74	8.33
Mean	7.34	5.78	6.83	5.82	7.07	6.91	6.91	6.62	5.96	6.67	7.15	6.70	6.93	6.86	6.27	6.99	6.54	6.50	6.98	6.87	7.06
Winter wheat monoculture																					
CLM_WFDE5	8.56	7.20	8.13	7.49	7.74	8.29	7.92	7.64	7.46	7.97	7.91	8.08	7.99	8.03	7.72	8.10	7.73	8.13	7.80	7.60	8.24
CLM_LowP	8.58	7.08	8.17	7.26	7.14	7.98	7.15	5.19	7.23	7.19	7.12	6.25	6.06	7.71	7.42	7.52	6.87	7.75	6.83	6.41	6.25
Yield anomaly [%]																					
Obs																					
Winter wheat	-	-	-	-	-	-	2.76	-5.90	-12.39	7.32	3.96	-6.38	-2.29	1.43	9.97	9.13	5.88	-3.01	-4.57	-4.09	-1.81
Spring wheat	-	-	-	-	-	-	3.84	-3.46	-9.02	8.61	5.59	-4.57	-7.43	13.37	13.53	4.80	12.42	-1.40	-7.11	-14.26	-14.89
Canola	-	-	-	-	-	-	-0.91	-1.17	-9.45	-5.57	9.95	3.74	-5.83	0.90	7.11	10.99	4.26	-0.40	0.90	-9.97	-4.54
Corn	-	-	-	-	-	-	1.34	-12.71	-3.58	6.15	3.65	-5.08	12.17	14.08	2.04	12.07	0.23	-1.07	7.76	-21.74	-15.32
Mean	-	-	-	-	-	-	2.00	-7.10	-8.16	5.45	5.02	-4.15	1.16	8.43	7.59	9.45	5.13	-1.62	-0.07	-13.32	-9.81
CLM																					
Winter wheat	8.58	-8.92	2.54	-5.27	-2.19	4.47	0.17	-3.54	-5.68	4.97	0.10	1.56	1.02	1.59	-2.45	3.73	-2.31	2.80	-1.51	-3.81	4.14
Spring wheat	13.22	-18.91	-1.21	-27.58	8.11	-1.09	4.92	0.11	-15.43	-3.62	13.20	5.60	6.84	-0.59	-8.60	5.32	-3.13	-9.44	11.47	5.06	15.76
Canola	12.63	-23.74	-2.64	-26.76	9.35	0.30	5.08	-0.62	-23.14	-3.20	12.81	6.15	6.03	2.36	-8.80	5.94	-3.16	-9.33	11.58	14.53	14.60
Corn	6.28	-9.51	5.62	-3.93	8.72	5.62	3.67	-0.20	-6.33	-2.21	5.09	-8.21	1.99	4.47	-7.43	3.31	-1.58	-1.01	0.81	-0.25	-4.92
Mean	9.47	-13.81	1.86	-13.12	5.50	3.00	3.14	-1.20	-11.04	-0.55	6.62	0.00	3.38	2.26	-6.44	4.31	-2.39	-3.06	4.18	2.50	5.36
Winter wheat monoculture																					
CLM_WFDE5	8.51	-8.73	3.02	-5.10	-1.90	5.05	0.32	-3.22	-5.51	1.05	0.27	2.43	1.23	1.70	-2.22	2.65	-2.11	2.99	-1.20	-3.65	4.41
CLM_LowP	20.76	-0.26	15.06	2.20	0.60	12.29	0.74	-26.89	1.73	1.19	0.22	-12.01	-14.67	8.53	4.41	5.81	-3.26	9.09	-3.84	-9.70	-11.99

Table C3: Multiple correlation coefficient (multiple *r*), R^2, adjusted R^2 (R^2 adjusted for the complexity of the model), standard error and corresponding t-statistics and probability values (p-values) resulting from multiple regression analysis for simulated annual mean crop yield (averaged for all regarded crops, dependent variable), explained with the simulated mean seasonal root zone soil moisture and the mean seasonal WFDE5 global radiation as independent variables, and with the seasonal WFDE5 precipitation amount and mean seasonal WFDE5 global radiation as independent variables, for the DE-NRW and AUS-VIC domain, respectively.

Annual mean crop yield - mean seasonal root zone soil moisture and mean seasonal global radiation						
DE-NRW						
Multiple *r*	0.6146		Coefficients	Standard error	t-statistics	P-value
R^2	0.3777	Intercept	4.5111	2.7914	1.6161	0.1235
Adjusted R^2	0.3086	Root zone soil moisture	-6.9219	4.5068	-1.5359	0.1420
Standard error	0.3563	Global radiation	0.0356	0.0159	2.2312	0.0386
AUS-VIC						
Multiple r	0.4081		Coefficients	Standard error	t-statistics	P-value
R^2	0.1665	Intercept	-3.3872	2.9009	-1.1676	0.2582
Adjusted R^2	0.0739	Root zone soil moisture	5.5062	3.0850	1.7849	0.0911
Standard error	0.2102	Global radiation	0.0182	0.0123	1.4782	0.1566
Annual mean crop yield - seasonal precipitation amount and mean seasonal global radiation						
DE-NRW						
Multiple r	0.5945		Coefficients	Standard error	t-statistics	P-value
R^2	0.3534	Intercept	3.1432	2.3843	1.3183	0.2039
Adjusted R^2	0.2816	Seasonal rainfall	-0.0016	0.0013	-1.2625	0.2229
Standard error	0.3631	Global radiation	0.0339	0.0172	1.9677	0.0647
AUS-VIC						
Multiple r	0.5864		Coefficients	Standard error	t-statistics	P-value
R^2	0.3439	Intercept	-3.6735	2.2545	-1.6294	0.1206
Adjusted R^2	0.2710	Seasonal rainfall	0.0034	0.0012	2.9854	0.0079
Standard error	0.1865	Global radiation	0.0226	0.0107	2.1063	0.0495

References

Aaheim, A., Amundsen, H., Dokken, T., and Wei, T.: Impacts and adaptation to climate change in European economies, Glob. Environ. Change, 22, 959–968, https://doi.org/10.1016/j.gloenvcha.2012.06.005, 2012.

Aase, J. K. and Siddoway, F. H.: Crown-Depth Soil Temperatures and Winter Protection for Winter Wheat Survival, Soil Sci. Soc. Am. J., 43, 1229–1233, https://doi.org/10.2136/sssaj1979.03615995004300060036x, 1979.

ABARES – Australian Bureau of Agricultural and Resource Economics and Sciences: Australian Crop Report, February 2021, Canberra, https://doi.org/10.25814/xqy3-sx57, 2020.

Ali, A. A., C. Xu, A. Rogers, R. A. Fisher, S. D. Wullschleger, E. Massoud, J. A. Vrugt, J. D. Muss, N. McDowell, and J. Fisher: A global scale mechanistic model of photosynthetic capacity (LUNA V1. 0). Geosci. Mod. Dev., 9:587-606, 2016.

Ash, A., McIntosh, P., Cullen, B., Carberry, P., and Smith, M. S.: Constraints and opportunities in applying seasonal climate forecasts in agriculture, Aust. J. Agric. Res., 58, 952–965, https://doi.org/10.1071/AR06188, 2007.

Baatz, R., Hendricks Franssen, H.-J., Han, X., Hoar, T., Bogena, H. R., and Vereecken, H.: Evaluation of a cosmic-ray neutron sensor network for improved land surface model prediction, Hydrol. Earth Syst. Sci., 21, 2509–2530, https://doi.org/10.5194/hess-21-2509-2017, 2017.

Barlow, K. M., Christy, B. P., O'Leary, G. J., Riffkin, P. A., and Nuttall, J. G.: Simulating the impact of extreme heat and frost events on wheat crop production: A review, Field Crops Res., 171, 109–119, https://doi.org/10.1016/j.fcr.2014.11.010, 2015.

Basche, Miguez, F. E., Kaspar, T. C., and Castellano, M. J.: Do cover crops increase or decrease nitrous oxide emissions? A meta-analysis, J. Soil Water Conserv., 69, 471–482, https://doi.org/10.2489/jswc.69.6.471, 2014.

Basche, Archontoulis, S. V., Kaspar, T. C., Jaynes, D. B., Parkin, T. B., and Miguez, F. E.: Simulating long-term impacts of cover crops and climate change on crop production and environmental outcomes in the Midwestern United States, Agric. Ecosyst. Environ., 218, 95–106, https://doi.org/10.1016/j.agee.2015.11.011, 2016.

Bassu, S., Brisson, N., Durand, J. L., Boote, K., Lizaso, J., Jones, J. W., Rosenzweig, C., Ruane, A. C., Adam, M., Baron, C., Basso, B., Biernath, C., Boogaard, H., Conijn, S., Corbeels, M., Deryng, D., Sanctis, G. D., Gayler, S., Grassini, P., Hatfield, J., Hoek, S., Izaurralde, C., Jongschaap, R., Kemanian, A. R., Kersebaum, K. C., Kim, S. H., Kumar, N. S., Makowski, D., Müller, C., Nendel, C., Priesack, E., Pravia, M. V., Sau, F., Shcherbak, I., Tao, F., Teixeira, E., Timlin, D., and Waha, K.: How do various maize crop models vary in their responses to climate change factors?, Glob. Change Biol., 20, 2301–2320, https://doi.org/10.1111/gcb.12520, 2014.

Bauer, P., Thorpe, A., and Brunet, G.: The quiet revolution of numerical weather prediction, Nature, 525, 47–55, https://doi.org/10.1038/nature14956, 2015.

Bennett, A., Hamman, J., and Nijssen, B.: MetSim: A Python package for estimation and disaggregation of meteorological data, J. Open Source Softw., 5, 2042, https://doi.org/10.21105/joss.02042, 2020.

Bergjord, A. K., Bonesmo, H., and Skjelvåg, A. O.: Modelling the course of frost tolerance in winter wheat: I. Model development, Eur. J. Agron., 28, 321–330, https://doi.org/10.1016/j.eja.2007.10.002, 2008.

Bergkamp, B., Impa, S. M., Asebedo, A. R., Fritz, A. K., and Jagadish, S. V. K.: Prominent winter wheat varieties response to post-flowering heat stress under controlled chambers and field based heat tents, Field Crops Res., 222, 143–152, https://doi.org/10.1016/j.fcr.2018.03.009, 2018.

Betts, R. A.: Integrated approaches to climate–crop modelling: needs and challenges, Philos. Trans. R. Soc. B Biol. Sci., 360, 2049–2065, https://doi.org/10.1098/rstb.2005.1739, 2005.

Beven, K. J. and Kirkby, M. J.: A physically based, variable contributing area model of basin hydrology / Un modèle à base physique de zone d'appel variable de l'hydrologie du bassin versant, Hydrol. Sci. Bull., 24, 43–69, https://doi.org/10.1080/02626667909491834, 1979.

Biradar, C. M. and Xiao, X.: Quantifying the area and spatial distribution of double- and triple-cropping croplands in India with multi-temporal MODIS imagery in 2005, Int. J. Remote Sens., 32, 367–386, https://doi.org/10.1080/01431160903464179, 2011.

Blanchard, J. L., Watson, R. A., Fulton, E. A., Cottrell, R. S., Nash, K. L., Bryndum-Buchholz, A., Büchner, M., Carozza, D. A., Cheung, W. W. L., Elliott, J., Davidson, L. N. K., Dulvy, N. K., Dunne, J. P., Eddy, T. D., Galbraith, E., Lotze, H. K., Maury, O., Müller, C., Tittensor, D. P., and Jennings, S.: Linked sustainability challenges and trade-offs among fisheries, aquaculture and agriculture, Nat. Ecol. Evol., 1, 1240–1249, https://doi.org/10.1038/s41559-017-0258-8, 2017.

Blyth, E. M., Arora, V. K., Clark, D. B., Dadson, S. J., De Kauwe, M. G., Lawrence, D. M., Melton, J. R., Pongratz, J., Turton, R. H., Yoshimura, K., and Yuan, H.: Advances in Land Surface Modelling, Curr. Clim. Change Rep., 7, 45–71, https://doi.org/10.1007/s40641-021-00171-5, 2021.

BMEL: Besondere Ernte- und Qualitätsermittlung (BEE) 2019, agricultural yield and quality assessment, https://www.bmel-statistik.de/landwirtschaft/ernte-und-qualitaet/archiv-ernte-und-qualitaet-bee (last access: 15 March 2023), 2020.

BMEL: Besondere Ernte- und Qualitätsermittlung (BEE) 2021, agricultural yield and quality assessment, https://www.bmel-statistik.de/landwirtschaft/ernte-und-qualitaet/archiv-ernte-und-qualitaet-bee (last access: 15 March 2023), 2022.

Boas, T., Bogena, H., Grünwald, T., Heinesch, B., Ryu, D., Schmidt, M., Vereecken, H., Western, A., and Hendricks Franssen, H.-J.: Improving the representation of cropland sites in the Community Land Model (CLM) version 5.0, Geosci. Model Dev., 14, 573–601, https://doi.org/10.5194/gmd-14-573-2021, 2021.

Boas, T., Mallants, D.: Episodic extreme rainfall events drive groundwater recharge in arid zone environments of central Australia. Journal of Hydrology: Regional Studies, 40, 101005, https://doi.org/10.1016/j.ejrh.2022.101005, 2022.

Boas, T., Bogena, H., Ryu, D., Vereecken, H., Western, A., and Hendricks-Franssen, H.-J.: Seasonal crop yield prediction with SEAS5 long-range meteorological forecasts in a land surface modelling approach, Hydrol. Earth Syst. Sci. Discuss., 1–30, https://doi.org/10.5194/hess-2023-28, 2023.

Bogena, H. R., Huisman, J. A., Baatz, R., Franssen, H.-J. H., and Vereecken, H.: Accuracy of the cosmic-ray soil water content probe in humid forest ecosystems: The worst case scenario, Water Resour. Res., 49, 5778–5791, https://doi.org/10.1002/wrcr.20463, 2013.

Bogena, H. R., Montzka, C., Huisman, J. A., Graf, A., Schmidt, M., Stockinger, M., von Hebel, C., Hendricks-Franssen, H. J., van der Kruk, J., Tappe, W., Lücke, A., Baatz, R., Bol, R., Groh, J., Pütz, T., Jakobi, J., Kunkel, R., Sorg, J., and Vereecken, H.: The TERENO-Rur Hydrological Observatory: A Multiscale Multi-Compartment Research Platform for the Advancement of Hydrological Science, Vadose Zone J., 17, https://doi.org/10.2136/vzj2018.03.0055, 2018.

Bogena, H. R., Schrön, M., Jakobi, J., Ney, P., Zacharias, S., Andreasen, M., Baatz, R., Boorman, D., Duygu, M. B., Eguibar-Galán, M. A., Fersch, B., Franke, T., Geris, J., González Sanchis, M., Kerr, Y., Korf, T., Mengistu, Z., Mialon, A., Nasta, P., Nitychoruk, J., Pisinaras, V., Rasche, D., Rosolem, R., Said, H., Schattan, P., Zreda, M., Achleitner, S., Albentosa-Hernández, E., Akyürek, Z., Blume, T., del Campo, A., Canone, D., Dimitrova-Petrova, K., Evans, J. G., Ferraris, S., Frances, F., Gisolo, D., Güntner, A., Herrmann, F., Iwema, J., Jensen, K. H., Kunstmann, H., Lidón, A., Looms, M. C., Oswald, S., Panagopoulos, A., Patil, A., Power, D., Rebmann, C., Romano, N., Scheiffele, L., Seneviratne, S., Weltin, G., and Vereecken, H.: COSMOS-Europe: a European network of cosmic-ray neutron soil moisture sensors, Earth Syst. Sci. Data, 14, 1125–1151, https://doi.org/10.5194/essd-14-1125-2022, 2022.

Bohn, T. J., Livneh, B., Oyler, J. W., Running, S. W., Nijssen, B., and Lettenmaier, D. P.: Global evaluation of MTCLIM and related algorithms for forcing of ecological and hydrological models, Agric. For. Meteorol., 176, 38–49, https://doi.org/10.1016/j.agrformet.2013.03.003, 2013.

BOM: Australian Government: Climate summaries archive, http://www.bom.gov.au/climate/current/statement_archives.shtml (last access: 10 June 2023), 2021.

Bonan, G. B., Williams, M., Fisher, R. A., and Oleson, K. W.: Modeling stomatal conductance in the earth system: linking leaf water-use efficiency and water transport along the soil–plant–atmosphere continuum, Geosci. Model Dev., 7, 2193–2222, https://doi.org/10.5194/gmd-7-2193-2014, 2014.

Brogi, C., Huisman, J. A., Pätzold, S., von Hebel, C., Weihermüller, L., Kaufmann, M. S., van der Kruk, J., and Vereecken, H.: Large-scale soil mapping using multi-configuration EMI and supervised image classification, Geoderma, 335, 133–148, https://doi.org/10.1016/j.geoderma.2018.08.001, 2019.

Buysse, P., Manise, Bodson, Alain, Debacq, De, A., Ligne, Bernard, Heinesch, Tanguy, Manise, Christine, Moureaux, Marc, and Aubinet: Carbon budget measurement over 12 years at a crop production site in the silty-loam region in Belgium, Agric. For. Meteorol., 2017.

Calanca, P., Bolius, D., Weigel, A. P., and Liniger, M. A.: Application of long-range weather forecasts to agricultural decision problems in Europe, J. Agric. Sci., 149, 15–22, https://doi.org/10.1017/S0021859610000729, 2011.

Cantelaube, P. and Terres, J.-M.: Seasonal weather forecasts for crop yield modelling in Europe, Tellus A, 57, 476–487, https://doi.org/10.1111/j.1600-0870.2005.00125.x, 2005.

Carrer, D., Pique, G., Ferlicoq, M., Ceamanos, X., and Ceschia, E.: What is the potential of cropland albedo management in the fight against global warming? A case study based on the use of cover crops, Environ. Res. Lett., 13, 044030, https://doi.org/10.1088/1748-9326/aab650, 2018.

Ceglar, A., van der Wijngaart, R., de Wit, A., Lecerf, R., Boogaard, H., Seguini, L., van den Berg, M., Toreti, A., Zampieri, M., Fumagalli, D., and Baruth, B.: Improving WOFOST model to simulate winter wheat phenology in Europe: Evaluation and effects on yield, Agric. Syst., 168, 168–180, https://doi.org/10.1016/j.agsy.2018.05.002, 2019.

Challinor, A. J., Watson, J., Lobell, D. B., Howden, S. M., Smith, D. R., and Chhetri, N.: A meta-analysis of crop yield under climate change and adaptation, Nat. Clim. Change, 4, 287–291, https://doi.org/10.1038/nclimate2153, 2014.

Chang, L.-L., Dwivedi, R., Knowles, J. F., Fang, Y.-H., Niu, G.-Y., Pelletier, J. D., Rasmussen, C., Durcik, M., Barron-Gafford, G. A., and Meixner, T.: Why Do Large-Scale Land Surface Models Produce a Low Ratio of Transpiration to Evapotranspiration?, J. Geophys. Res. Atmospheres, 123, 9109–9130, https://doi.org/10.1029/2018JD029159, 2018.

Chen, M., Griffis, T. J., Baker, J., Wood, J. D., and Xiao, K.: Simulating crop phenology in the Community Land Model and its impact on energy and carbon fluxes: Evaluation of CLM crop simulations, J. Geophys. Res. Biogeosciences, 120, 310–325, https://doi.org/10.1002/2014JG002780, 2015.

Chen, M., Griffis, T. J., Baker, J. M., Wood, J. D., Meyers, T., and Suyker, A.: Comparing crop growth and carbon budgets simulated across AmeriFlux agricultural sites using the Community Land Model (CLM), Agric. For. Meteorol., 256–257, 315–333, https://doi.org/10.1016/j.agrformet.2018.03.012, 2018.

Cheng, Y., Huang, M., Chen, M., Guan, K., Bernacchi, C., Peng, B., and Tan, Z.: Parameterizing Perennial Bioenergy Crops in Version 5 of the Community Land Model Based on Site-Level Observations in the Central Midwestern United States, J. Adv. Model. Earth Syst., 12, e2019MS001719, https://doi.org/10.1029/2019MS001719, 2020.

Chouard, P.: Vernalization and its Relations to Dormancy, Annu. Rev. Plant Physiol., 11, 191–238, https://doi.org/10.1146/annurev.pp.11.060160.001203, 1960.

Chuang, Y.-L., Oren, R., Bertozzi, A. L., Phillips, N., and Katul, G. G.: The porous media model for the hydraulic system of a conifer tree: Linking sap flux data to transpiration rate, Ecol. Model., 191, 447–468, https://doi.org/10.1016/j.ecolmodel.2005.03.027, 2006.

Clapp, R. B. and Hornberger, G. M.: Empirical equations for some soil hydraulic properties, Water Resour. Res., 14, 601–604, https://doi.org/10.1029/WR014i004p00601, 1978.

Claverie, M., Ju, J., Masek, J. G., Dungan, J. L., Vermote, E. F., Roger, J.-C., Skakun, S. V., and Justice, C.: The Harmonized Landsat and Sentinel-2 surface reflectance dataset, Remote Sens. Environ., 219, 145–161, https://doi.org/10.1016/j.rse.2018.09.002, 2018.

Coelho, C. A. and Costa, S. M.: Challenges for integrating seasonal climate forecasts in user applications, Curr. Opin. Environ. Sustain., 2, 317–325, https://doi.org/10.1016/j.cosust.2010.09.002, 2010.

Collatz, G. J., Ribas-Carbo, M., and Berry, J. A.: Coupled Photosynthesis-Stomatal Conductance Model for Leaves of C4 Plants, Funct. Plant Biol., 19, 519–538, https://doi.org/10.1071/pp9920519, 1992.

Copernicus Climate Change Service, Climate Data Store: Seasonal forecast daily and subdaily data on single levels, Copernicus Climate Change Service (C3S) Climate Data Store (CDS) [data set], https://doi.org/10.24381/cds.181d637e, 2018.

Cosby, B. J., Hornberger, G. M., Clapp, R. B., and Ginn, T. R.: A Statistical Exploration of the Relationships of Soil Moisture Characteristics to the Physical Properties of Soils, Water Resour. Res., 20, 682–690, https://doi.org/10.1029/WR020i006p00682, 1984.

Cucchi, M., Weedon, G. P., Amici, A., Bellouin, N., Lange, S., Müller Schmied, H., Hersbach, H., and Buontempo, C.: WFDE5: bias-adjusted ERA5 reanalysis data for impact studies, Earth Syst. Sci. Data, 12, 2097–2120, https://doi.org/10.5194/essd-12-2097-2020, 2020.

Dagon, K., Sanderson, B. M., Fisher, R. A., and Lawrence, D. M.: A machine learning approach to emulation and biophysical parameter estimation with the Community Land Model, version 5, Adv. Stat. Climatol. Meteorol. Oceanogr., 6, 223–244, https://doi.org/10.5194/ascmo-6-223-2020, 2020.

De Kauwe, M. G., Kala, J., Lin, Y.-S., Pitman, A. J., Medlyn, B. E., Duursma, R. A., Abramowitz, G., Wang, Y.-P., and Miralles, D. G.: A test of an optimal stomatal conductance scheme within the CABLE land surface model, Geosci. Model Dev., 8, 431–452, https://doi.org/10.5194/gmd-8-431-2015, 2015a.

De Kauwe, M. G., Zhou, S.-X., Medlyn, B. E., Pitman, A. J., Wang, Y.-P., Duursma, R. A., and Prentice, I. C.: Do land surface models need to include differential plant species responses to drought? Examining model predictions across a mesic-xeric gradient in Europe, Biogeosciences, 12, 7503–7518, https://doi.org/10.5194/bg-12-7503-2015, 2015b.

Denissen, J. M. C., Teuling, A. J., Pitman, A. J., Koirala, S., Migliavacca, M., Li, W., Reichstein, M., Winkler, A. J., Zhan, C., and Orth, R.: Widespread shift from ecosystem energy to water limitation with climate change, Nat. Clim. Change, 12, 677–684, https://doi.org/10.1038/s41558-022-01403-8, 2022.

Deryng, D., Conway, D., Ramankutty, N., Price, J., and Warren, R.: Global crop yield response to extreme heat stress under multiple climate change futures, Environ. Res. Lett., 9, 034011, https://doi.org/10.1088/1748-9326/9/3/034011, 2014.

Dombrowski, O., Brogi, C., Hendricks Franssen, H.-J., Zanotelli, D., and Bogena, H.: CLM5-FruitTree: a new sub-model for deciduous fruit trees in the Community Land Model (CLM5), Geosci. Model Dev., 15, 5167–5193, https://doi.org/10.5194/gmd-15-5167-2022, 2022.

Dorigo, W., Wagner, W., Albergel, C., Albrecht, F., Balsamo, G., Brocca, L., Chung, D., Ertl, M., Forkel, M., Gruber, A., Haas, E., Hamer, P. D., Hirschi, M., Ikonen, J., de Jeu, R., Kidd, R., Lahoz, W., Liu, Y. Y., Miralles, D., Mistelbauer, T., Nicolai-Shaw, N., Parinussa, R., Pratola, C., Reimer, C., van der Schalie, R., Seneviratne, S. I., Smolander, T., and Lecomte, P.: ESA CCI Soil Moisture for improved Earth system

understanding: State-of-the art and future directions, Remote Sens. Environ., 203, 185–215, https://doi.org/10.1016/j.rse.2017.07.001, 2017.

DWD – Deutscher Wetter Dienst: German weather archive, https://www.dwd.de/DE/leistungen/klimadatendeutschland/klarchivtagmonat.html (last access: 15 March 2023), 2021.

Eder, F., Schmidt, M., Damian, T., Träumner, K., and Mauder, M.: Mesoscale Eddies Affect Near-Surface Turbulent Exchange: Evidence from Lidar and Tower Measurements, J. Appl. Meteorol. Climatol., 54, 189–206, https://doi.org/10.1175/JAMC-D-14-0140.1, 2015.

Elliott, J., Müller, C., Deryng, D., Chryssanthacopoulos, J., Boote, K. J., Büchner, M., Foster, I., Glotter, M., Heinke, J., Iizumi, T., Izaurralde, R. C., Mueller, N. D., Ray, D. K., Rosenzweig, C., Ruane, A. C., and Sheffield, J.: The Global Gridded Crop Model Intercomparison: data and modeling protocols for Phase 1 (v1.0), Geosci. Model Dev., 8, 261–277, https://doi.org/10.5194/gmd-8-261-2015, 2015.

Entekhabi, Dara, Das, Narendra, Njoku, Eni, Johnson, Joel, and Shi, Jiancheng: SMAP L3 Radar/Radiometer Global Daily 9 km EASE-Grid Soil Moisture, Version 3, https://doi.org/10.5067/7KKNQ5UURM2W, 2016.

Eurostat: Agriculture, forestry and fishery statistics, 2018 edition, European Union, https://doi.org/doi:10.2785/340432, (last access: 15 August 2019), 2018.

Fang, H., Liang, S., Hoogenboom, G., Teasdale, J., and Cavigelli, M.: Corn-yield estimation through assimilation of remotely sensed data into the CSM-CERES-Maize model, Int. J. Remote Sens., 29, 3011–3032, https://doi.org/10.1080/01431160701408386, 2008.

Farquhar, G. D., von Caemmerer, S., and Berry, J. A.: A biochemical model of photosynthetic CO2 assimilation in leaves of C3 species, Planta, 149, 78–90, https://doi.org/10.1007/BF00386231, 1980.

Fisher, R. A. and Koven, C. D.: Perspectives on the Future of Land Surface Models and the Challenges of Representing Complex Terrestrial Systems, J. Adv. Model. Earth Syst., 12, e2018MS001453, https://doi.org/10.1029/2018MS001453, 2020.

Fisher, R. A., Wieder, W. R., Sanderson, B. M., Koven, C. D., Oleson, K. W., Xu, C., Fisher, J. B., Shi, M., Walker, A. P., and Lawrence, D. M.: Parametric Controls on Vegetation Responses to Biogeochemical Forcing in the CLM5, J. Adv. Model. Earth Syst., 11, 2879–2895, https://doi.org/10.1029/2019MS001609, 2019.

FLUXNET - A Global Network of Eddy Covariance Flux Towers, available online at: https://fluxnet.org/, (last access: 15 August 2023).

Fowler, D. B., Limin, A. E., and Ritchie, J. T.: Low-Temperature Tolerance in Cereals: Model and Genetic Interpretation, Crop Sci., 39, cropsci1999.0011183X003900020002x, https://doi.org/10.2135/cropsci1999.0011183X003900020002x, 1999.

Franke, J. A., Müller, C., Elliott, J., Ruane, A. C., Jägermeyr, J., Balkovic, J., Ciais, P., Dury, M., Falloon, P. D., Folberth, C., François, L., Hank, T., Hoffmann, M., Izaurralde, R. C., Jacquemin, I., Jones, C., Khabarov, N., Koch, M., Li, M., Liu, W., Olin, S., Phillips, M., Pugh, T. A. M., Reddy, A., Wang, X., Williams, K.,

Zabel, F., and Moyer, E. J.: The GGCMI Phase 2 experiment: global gridded crop model simulations under uniform changes in CO2, temperature, water, and nitrogen levels (protocol version 1.0), Geosci. Model Dev., 13, 2315–2336, https://doi.org/10.5194/gmd-13-2315-2020, 2020.

Franks, P. J., Bonan, G. B., Berry, J. A., Lombardozzi, D. L., Holbrook, N. M., Herold, N., and Oleson, K. W.: Comparing optimal and empirical stomatal conductance models for application in Earth system models, Glob. Change Biol., 24, 5708–5723, https://doi.org/10.1111/gcb.14445, 2018.

French, R. J. and Schultz, J. E.: Water use efficiency of wheat in a Mediterranean-type environment. I. The relation between yield, water use and climate, Aust. J. Agric. Res., 35, 743–764, https://doi.org/10.1071/ar9840743, 1984a.

French, R. J. and Schultz, J. E.: Water use efficiency of wheat in a Mediterranean-type environment. II. some limitations to efficiency, Aust. J. Agric. Res., 35, 765–775, https://doi.org/10.1071/ar9840765, 1984b.

Friedl, M. and Sulla-Menashe, D.: MCD12Q1 MODIS/Terra+Aqua Land Cover Type Yearly L3 Global 500m SIN Grid V006 [data set], NASA EOSDIS Land Processes DAAC., https://doi.org/Accessed 2020-07-02 from https://doi.org/10.5067/MODIS/MCD12Q1.006, 2019.

Gan, Y. T., Liang, B. C., Liu, L. P., Wang, X. Y., and McDonald, C. L.: C:N ratios and carbon distribution profile across rooting zones in oilseed and pulse crops, Crop Pasture Sci., 62, 496, https://doi.org/10.1071/CP10360, 2011.

Gosling, S. N.: The likelihood and potential impact of future change in the large-scale climate-earth system on ecosystem services, Environ. Sci. Policy, 27, S15–S31, https://doi.org/10.1016/j.envsci.2012.03.011, 2013.

Graf, A.: Gap-filling meteorological variables with Empirical Orthogonal Functions, Conference Name: EGU General Assembly Conference Abstracts, 19, 8491, 2017.

Graf, A., Klosterhalfen, A., Arriga, N., Bernhofer, C., Bogena, H., Bornet, F., Brüggemann, N., Brümmer, C., Buchmann, N., Chi, J., Chipeaux, C., Cremonese, E., Cuntz, M., Dušek, J., El-Madany, T. S., Fares, S., Fischer, M., Foltýnová, L., Gharun, M., Ghiasi, S., Gielen, B., Gottschalk, P., Grünwald, T., Heinemann, G., Heinesch, B., Heliasz, M., Holst, J., Hörtnagl, L., Ibrom, A., Ingwersen, J., Jurasinski, G., Klatt, J., Knohl, A., Koebsch, F., Konopka, J., Korkiakoski, M., Kowalska, N., Kremer, P., Kruijt, B., Lafont, S., Léonard, J., De Ligne, A., Longdoz, B., Loustau, D., Magliulo, V., Mammarella, I., Manca, G., Mauder, M., Migliavacca, M., Mölder, M., Neirynck, J., Ney, P., Nilsson, M., Paul-Limoges, E., Peichl, M., Pitacco, A., Poyda, A., Rebmann, C., Roland, M., Sachs, T., Schmidt, M., Schrader, F., Siebicke, L., Šigut, L., Tuittila, E.-S., Varlagin, A., Vendrame, N., Vincke, C., Völksch, I., Weber, S., Wille, C., Wizemann, H.-D., Zeeman, M., and Vereecken, H.: Altered energy partitioning across terrestrial ecosystems in the European drought year 2018, Philos. Trans. R. Soc. B Biol. Sci., 375, 20190524, https://doi.org/10.1098/rstb.2019.0524, 2020.

Griffiths, P., Nendel, C., and Hostert, P: National-scale crop- and land-cover map of Germany (2016) based on imagery acquired by Sentinel-2A MSI and Landsat-8 OLI, PANGAEA [data set], https://doi.org/10.1594/PANGAEA.893195, 2018.

Griffiths, P., Nendel, C., and Hostert, P.: Intra-annual reflectance composites from Sentinel-2 and Landsat for national-scale crop and land cover mapping, Remote Sens. Environ., 220, 135–151, https://doi.org/10.1016/j.rse.2018.10.031, 2019.

Groff, S.: The past, present, and future of the cover crop industry, J. Soil Water Conserv., 70, 130A-133A, https://doi.org/10.2489/jswc.70.6.130A, 2015.

Gruber, A., Dorigo, W. A., Crow, W., and Wagner, W.: Triple Collocation-Based Merging of Satellite Soil Moisture Retrievals, IEEE Trans. Geosci. Remote Sens., 55, 6780–6792, https://doi.org/10.1109/TGRS.2017.2734070, 2017.

Gruber, A., Scanlon, T., van der Schalie, R., Wagner, W., and Dorigo, W.: Evolution of the ESA CCI Soil Moisture climate data records and their underlying merging methodology, Earth Syst. Sci. Data, 11, 717–739, https://doi.org/10.5194/essd-11-717-2019, 2019.

Gubler, S., Sedlmeier, K., Bhend, J., Avalos, G., Coelho, C. a. S., Escajadillo, Y., Jacques-Coper, M., Martinez, R., Schwierz, C., Skansi, M. de, and Spirig, C.: Assessment of ECMWF SEAS5 Seasonal Forecast Performance over South America, Weather Forecast., 35, 561–584, https://doi.org/10.1175/WAF-D-19-0106.1, 2020.

Guérif, M. and Duke, C. L.: Adjustment procedures of a crop model to the site specific characteristics of soil and crop using remote sensing data assimilation, Agric. Ecosyst. Environ., 81, 57–69, https://doi.org/10.1016/S0167-8809(00)00168-7, 2000.

Han, X., Franssen, H.-J. H., Montzka, C., and Vereecken, H.: Soil moisture and soil properties estimation in the Community Land Model with synthetic brightness temperature observations, Water Resour. Res., 6081–6105, https://doi.org/10.1002/2013WR014586@10.1002/(ISSN)1944-7973.SVASYST1, 2018.

Hansen, J. W.: Realizing the potential benefits of climate prediction to agriculture: issues, approaches, challenges, Agric. Syst., 74, 309–330, 2002.

Hansen, J. W., Challinor, A., Ines, A., Wheeler, T., and Moron, V.: Translating climate forecasts into agricultural terms: advances and challenges, Clim. Res., 33, 27–41, https://doi.org/10.3354/cr033027, 2006.

Harris, I., Jones, P. d., Osborn, T. j., and Lister, D. h.: Updated high-resolution grids of monthly climatic observations – the CRU TS3.10 Dataset, Int. J. Climatol., 34, 623–642, https://doi.org/10.1002/joc.3711, 2014.

Hawdon, A., McJannet, D., and Wallace, J.: Calibration and correction procedures for cosmic-ray neutron soil moisture probes located across Australia, Water Resour. Res., 50, 5029–5043, https://doi.org/10.1002/2013WR015138, 2014.

Hengl, T., Jesus, J. M. de, Heuvelink, G. B. M., Gonzalez, M. R., Kilibarda, M., Blagotić, A., Shangguan, W., Wright, M. N., Geng, X., Bauer-Marschallinger, B., Guevara, M. A., Vargas, R., MacMillan, R. A., Batjes, N. H., Leenaars, J. G. B., Ribeiro, E., Wheeler, I., Mantel, S., and Kempen, B.: SoilGrids250m: Global gridded soil information based on machine learning, PLOS ONE, 12, e0169748, https://doi.org/10.1371/journal.pone.0169748, 2017.

Hersbach, H., Bell, B., Berrisford, P., Hirahara, S., Horányi, A., Muñoz-Sabater, J., Nicolas, J., Peubey, C., Radu, R., Schepers, D., Simmons, A., Soci, C., Abdalla, S., Abellan, X., Balsamo, G., Bechtold, P., Biavati, G., Bidlot, J., Bonavita, M., Chiara, G. D., Dahlgren, P., Dee, D., Diamantakis, M., Dragani, R., Flemming, J., Forbes, R., Fuentes, M., Geer, A., Haimberger, L., Healy, S., Hogan, R. J., Hólm, E., Janisková, M., Keeley, S., Laloyaux, P., Lopez, P., Lupu, C., Radnoti, G., Rosnay, P. de, Rozum, I., Vamborg, F., Villaume, S., and Thépaut, J.-N.: The ERA5 global reanalysis, Q. J. R. Meteorol. Soc., 146, 1999–2049, https://doi.org/10.1002/qj.3803, 2020.

Huang, J., Tian, L., Liang, S., Ma, H., Becker-Reshef, I., Huang, Y., Su, W., Zhang, X., Zhu, D., and Wu, W.: Improving winter wheat yield estimation by assimilation of the leaf area index from Landsat TM and MODIS data into the WOFOST model, Agric. For. Meteorol., 204, 106–121, https://doi.org/10.1016/j.agrformet.2015.02.001, 2015.

Hudiburg, T. W., Law, B. E., and Thornton, P. E.: Evaluation and improvement of the Community Land Model (CLM4) in Oregon forests, Biogeosciences, 10, 453–470, https://doi.org/10.5194/bg-10-453-2013, 2013.

Hung, C. P., Schalge, B., Baroni, G., Vereecken, H., and Hendricks Franssen, H.-J.: Assimilation of Groundwater Level and Soil Moisture Data in an Integrated Land Surface-Subsurface Model for Southwestern Germany, Water Resour. Res., 58, e2021WR031549, https://doi.org/10.1029/2021WR031549, 2022.

Hungerford, R. D., Nemani, R. R., Running, S. W., and Coughlan, J. C.: MTCLIM: a mountain microclimate simulation model, U.S. Department of Agriculture, Forest Service, Intermountain Forest and Range Experiment Station, Ogden, UT, https://doi.org/10.2737/INT-RP-414, 1989.

Hunter, M. C., White, C. M., Kaye, J. P., and Kemanian, A. R.: Ground-Truthing a Recent Report of Cover Crop–Induced Winter Warming, Agric. Environ. Lett., 4, https://doi.org/10.2134/ael2019.03.0007, 2019.

Huntzinger, D. N., Schwalm, C., Michalak, A. M., Schaefer, K., King, A. W., Wei, Y., Jacobson, A., Liu, S., Cook, R. B., Post, W. M., Berthier, G., Hayes, D., Huang, M., Ito, A., Lei, H., Lu, C., Mao, J., Peng, C. H., Peng, S., Poulter, B., Riccuito, D., Shi, X., Tian, H., Wang, W., Zeng, N., Zhao, F., and Zhu, Q.: The North American Carbon Program Multi-Scale Synthesis and Terrestrial Model Intercomparison Project – Part 1: Overview and experimental design, Geosci. Model Dev., 6, 2121–2133, https://doi.org/10.5194/gmd-6-2121-2013, 2013.

ICOS: Integrated Carbon Observation System Carbon Portal, https://www.icos-cp.eu/ (last access: 15 May 2020), 2020.

International Soil Reference and Information Centre (ISRIC) – World Soil Information data hub: SoilGrids, [data set], https://www.isric.org/explore/soilgrids (last access: 10 November 2022), 2023.

IT.NRW: Ernte ausgewählter landwirtschaftlicher Feldfrüchte, yield statistics for certain cash crops, Landesbetrieb ITNRW, Düsseldorf, https://www.it.nrw/statistik/eckdaten/ernte-von-ausgewaehlten-landwirtschaftlichen-feldfruechten-und-gruenland-767 (last access: 5 August 2022), 2019.

IT.NRW: Erntebericht: Hektarerträge, Gesamterträge und Anbaufläche nach ausgewählten Fruchtarten (39) - Regierungsbezirke - Jahr, Landesbetrieb ITNRW, Düsseldorf, https://www.it.nrw/statistik/eckdaten/ernte-von-ausgewaehlten-landwirtschaftlichen-feldfruechten-und-gruenland-767 (last access: 5 May 2023), 2022.

Jägermeyr, J., Müller, C., Ruane, A. C., Elliott, J., Balkovic, J., Castillo, O., Faye, B., Foster, I., Folberth, C., Franke, J. A., Fuchs, K., Guarin, J. R., Heinke, J., Hoogenboom, G., Iizumi, T., Jain, A. K., Kelly, D., Khabarov, N., Lange, S., Lin, T.-S., Liu, W., Mialyk, O., Minoli, S., Moyer, E. J., Okada, M., Phillips, M., Porter, C., Rabin, S. S., Scheer, C., Schneider, J. M., Schyns, J. F., Skalsky, R., Smerald, A., Stella, T., Stephens, H., Webber, H., Zabel, F., and Rosenzweig, C.: Climate impacts on global agriculture emerge earlier in new generation of climate and crop models, Nat. Food, 2, 873–885, https://doi.org/10.1038/s43016-021-00400-y, 2021.

Jin, X., Kumar, L., Li, Z., Feng, H., Xu, X., Yang, G., and Wang, J.: A review of data assimilation of remote sensing and crop models, Eur. J. Agron., 92, 141–152, https://doi.org/10.1016/j.eja.2017.11.002, 2018.

Johnson, S. J., Stockdale, T. N., Ferranti, L., Balmaseda, M. A., Molteni, F., Magnusson, L., Tietsche, S., Decremer, D., Weisheimer, A., Balsamo, G., Keeley, S. P. E., Mogensen, K., Zuo, H., and Monge-Sanz, B. M.: SEAS5: the new ECMWF seasonal forecast system, Geosci. Model Dev., 12, 2019.

Kalnay, E., Kanamitsu, M., Kistler, R., Collins, W., Deaven, D., Gandin, L., Iredell, M., Saha, S., White, G., Woollen, J., Zhu, Y., Leetmaa, A., Reynolds, R., Chelliah, M., Ebisuzaki, W., Higgins, W., Janowiak, J., Mo, K. C., Ropelewski, C., Wang, J., Jenne, R., and Joseph, D.: The NCEP/NCAR 40-Year Reanalysis Project, 124, 1996.

Kattge, J., Díaz, S., Lavorel, S., Prentice, I. C., Leadley, P., Bönisch, G., Garnier, E., Westoby, M., Reich, P. B., Wright, I. J., Cornelissen, J. H. C., Violle, C., Harrison, S. P., Bodegom, P. M. V., Reichstein, M., Enquist, B. J., Soudzilovskaia, N. A., Ackerly, D. D., Anand, M., Atkin, O., Bahn, M., Baker, T. R., Baldocchi, D., Bekker, R., Blanco, C. C., Blonder, B., Bond, W. J., Bradstock, R., Bunker, D. E., Casanoves, F., Cavender-Bares, J., Chambers, J. Q., Iii, F. S. C., Chave, J., Coomes, D., Cornwell, W. K., Craine, J. M., Dobrin, B. H., Duarte, L., Durka, W., Elser, J., Esser, G., Estiarte, M., Fagan, W. F., Fang, J., Fernández-Méndez, F., Fidelis, A., Finegan, B., Flores, O., Ford, H., Frank, D., Freschet, G. T., Fyllas, N. M., Gallagher, R. V., Green, W. A., Gutierrez, A. G., Hickler, T., Higgins, S. I., Hodgson, J. G., Jalili, A., Jansen, S., Joly, C. A., Kerkhoff, A. J., Kirkup, D., Kitajima, K., Kleyer, M., Klotz, S., Knops, J. M. H., Kramer, K., Kühn, I., Kurokawa, H., Laughlin, D., Lee, T. D., Leishman, M., Lens, F., Lenz, T., Lewis, S. L., Lloyd, J., Llusià, J., Louault, F., Ma, S., Mahecha, M. D., Manning, P., Massad, T., Medlyn, B. E., Messier, J., Moles, A. T., Müller, S. C., Nadrowski, K., Naeem, S., Niinemets, Ü., Nöllert, S., Nüske, A., Ogaya, R., Oleksyn, J., Onipchenko, V. G., Onoda, Y., Ordoñez, J., Overbeck, G., et al.: TRY – a global database of plant traits, Glob. Change Biol., 17, 2905–2935, https://doi.org/10.1111/j.1365-2486.2011.02451.x, 2011.

Kaye, J. P. and Quemada, M.: Using cover crops to mitigate and adapt to climate change. A review, Agron. Sustain. Dev., 37, 4, https://doi.org/10.1007/s13593-016-0410-x, 2017.

Kennedy, D., Swenson, S., Oleson, K. W., Lawrence, D. M., Fisher, R., Costa, A. C. L. da, and Gentine, P.: Implementing Plant Hydraulics in the Community Land Model, Version 5, J. Adv. Model. Earth Syst., 11, 485–513, https://doi.org/10.1029/2018MS001500, 2019.

Klemm, T. and McPherson, R. A.: The development of seasonal climate forecasting for agricultural producers, Agric. For. Meteorol., 232, 384–399, https://doi.org/10.1016/j.agrformet.2016.09.005, 2017.

Kollas, C., Kersebaum, K. C., Nendel, C., Manevski, K., Müller, C., Palosuo, T., Armas-Herrera, C. M., Beaudoin, N., Bindi, M., Charfeddine, M., Conradt, T., Constantin, J., Eitzinger, J., Ewert, F., Ferrise, R., Gaiser, T., Cortazar-Atauri, I. G. de, Giglio, L., Hlavinka, P., Hoffmann, H., Hoffmann, M. P., Launay, M., Manderscheid, R., Mary, B., Mirschel, W., Moriondo, M., Olesen, J. E., Öztürk, I., Pacholski, A., Ripoche-Wachter, D., Roggero, P. P., Roncossek, S., Rötter, R. P., Ruget, F., Sharif, B., Trnka, M., Ventrella, D., Waha, K., Wegehenkel, M., Weigel, H.-J., and Wu, L.: Crop rotation modelling—A European model intercomparison, Eur. J. Agron., 70, 98–111, https://doi.org/10.1016/j.eja.2015.06.007, 2015.

Kollet, S. J. and Maxwell, R. M.: Capturing the influence of groundwater dynamics on land surface processes using an integrated, distributed watershed model, Water Resour. Res., 44, https://doi.org/10.1029/2007WR006004, 2008.

Konings, A. G., Yu, Y., Xu, L., Yang, Y., Schimel, D. S., and Saatchi, S. S.: Active microwave observations of diurnal and seasonal variations of canopy water content across the humid African tropical forests, Geophys. Res. Lett., 44, 2290–2299, https://doi.org/10.1002/2016GL072388, 2017.

Koster, R. D., Schubert, S. D., and Suarez, M. J.: Analyzing the Concurrence of Meteorological Droughts and Warm Periods, with Implications for the Determination of Evaporative Regime, J. Clim., 22, 3331–3341, https://doi.org/10.1175/2008JCLI2718.1, 2009.

Kucharik, C. J.: Evaluation of a Process-Based Agro-Ecosystem Model (Agro-IBIS) across the U.S. Corn Belt: Simulations of the Interannual Variability in Maize Yield, Earth Interact., 7, 1–33, https://doi.org/10.1175/1087-3562(2003)007<0001:EOAPAM>2.0.CO;2, 2003.

Kucharik, C. J. and Brye, K. R.: Integrated BIosphere Simulator (IBIS) Yield and Nitrate Loss Predictions for Wisconsin Maize Receiving Varied Amounts of Nitrogen Fertilizer, J. Environ. Qual., 32, 247–268, https://doi.org/10.2134/jeq2003.2470, 2003.

Kuffour, B. N. O., Engdahl, N. B., Woodward, C. S., Condon, L. E., Kollet, S., and Maxwell, R. M.: Simulating coupled surface–subsurface flows with ParFlow v3.5.0: capabilities, applications, and ongoing development of an open-source, massively parallel, integrated hydrologic model, Geosci. Model Dev., 13, 1373–1397, https://doi.org/10.5194/gmd-13-1373-2020, 2020.

Kunkel, R., Sorg, J., Eckardt, R., Kolditz, O., Rink, K., and Vereecken, H.: TEODOOR: a distributed geodata infrastructure for terrestrial observation data, Environ. Earth Sci., 69, 507–521, https://doi.org/10.1007/s12665-013-2370-7, 2013.

Kutsch, W. L., Aubinet, M., Buchmann, N., Smith, P., Osborne, B., Eugster, W., Wattenbach, M., Schrumpf, M., Schulze, E. D., Tomelleri, E., Ceschia, E., Bernhofer, C., Béziat, P., Carrara, A., Di Tommasi, P., Grünwald, T., Jones, M., Magliulo, V., Marloie, O., Moureaux, C., Olioso, A., Sanz, M. J., Saunders, M., Søgaard, H., and Ziegler, W.: The net biome production of full crop rotations in Europe, Agric. Ecosyst. Environ., 139, 336–345, https://doi.org/10.1016/j.agee.2010.07.016, 2010.

Launay, M. and Guerif, M.: Assimilating remote sensing data into a crop model to improve predictive performance for spatial applications, Agric. Ecosyst. Environ., 111, 321–339, https://doi.org/10.1016/j.agee.2005.06.005, 2005.

Lawrence, D. M., Hurtt, G. C., Arneth, A., Brovkin, V., Calvin, K. V., Jones, A. D., Jones, C. D., Lawrence, P. J., de Noblet-Ducoudré, N., Pongratz, J., Seneviratne, S. I., and Shevliakova, E.: The Land Use Model Intercomparison Project (LUMIP) contribution to CMIP6: rationale and experimental design, Geosci. Model Dev., 9, 2973–2998, https://doi.org/10.5194/gmd-9-2973-2016, 2016.

Lawrence, D. M., Fisher, R., Koven, C., Oleson, K., Svenson, S., Vertenstein, M., Andre, B., Bonan, G., Ghimire, B., van Kampenhout, L., Kennedy, D., Kluzek, E., Knox, R., Lawrence, P., Li, F., Li, H., Lombardozzi, D., Lu, Y., Perket, J., Riley,W., Sacks,W., Shi, M.,Wieder,W., Xu, C. (lead authors), Ali, A., Badger, A., Bisht, G., Broxton, P., Brunke, M., Buzan, J., Clark, M., Craig, T., Dahlin, K., Drewniak, B., Emmons, L., Fisher, J., Flanner, M., Gentine, P., Lenaerts, J., Levis, S., Leung, L. R., Lipscomb, W., Pelletier, J., Ricciuto, D. M., Sanderson, B., Shuman, J., Slater, A., Subin, Z., Tang, J., Tawfik, A., Thomas, Q., Tilmes, S., Vitt, F., and Zeng, X.: Technical Description of version 5.0 of the Community Land Model (CLM), Natl. Cent. Atmospheric Res. (NCAR), http://www.cesm.ucar.edu/models/cesm2/land/CLM50_Tech_Note.pdf (last access: 1 June 2023), 2018.

Lawrence, D. M., Fisher, R. A., Koven, C. D., Oleson, K. W., Swenson, S. C., Bonan, G., Collier, N., Ghimire, B., Kampenhout, L. van, Kennedy, D., Kluzek, E., Lawrence, P. J., Li, F., Li, H., Lombardozzi, D., Riley, W. J., Sacks, W. J., Shi, M., Vertenstein, M., Wieder, W. R., Xu, C., Ali, A. A., Badger, A. M., Bisht, G., Broeke, M. van den, Brunke, M. A., Burns, S. P., Buzan, J., Clark, M., Craig, A., Dahlin, K., Drewniak, B., Fisher, J. B., Flanner, M., Fox, A. M., Gentine, P., Hoffman, F., Keppel-Aleks, G., Knox, R., Kumar, S., Lenaerts, J., Leung, L. R., Lipscomb, W. H., Lu, Y., Pandey, A., Pelletier, J. D., Perket, J., Randerson, J. T., Ricciuto, D. M., Sanderson, B. M., Slater, A., Subin, Z. M., Tang, J., Thomas, R. Q., Martin, M. V., and Zeng, X.: The Community Land Model Version 5: Description of New Features, Benchmarking, and Impact of Forcing Uncertainty, J. Adv. Model. Earth Sy., 11, 4245–4287, https://doi.org/10.1029/2018MS001583, 2019.

Lawrence, M. and Slater, G.: Incorporating organic soil into a global climate model, Clim. Dyn., 145–160, https://doi.org/10.1007/s00382-007-0278-1, 2008.

Leng, G., Huang, M., Tang, Q., Sacks, W. J., Lei, H., and Leung, L. R.: Modeling the effects of irrigation on land surface fluxes and states over the conterminous United States: Sensitivity to input data and model parameters, J. Geophys. Res. Atmospheres, 118, 9789–9803, https://doi.org/10.1002/jgrd.50792, 2013.

Levis, S., Bonan, G. B., Kluzek, E., Thornton, P. E., Jones, A., Sacks, W. J., and Kucharik, C. J.: Interactive Crop Management in the Community Earth System Model (CESM1): Seasonal Influences on Land–Atmosphere Fluxes, J. Clim., 25, 4839–4859, https://doi.org/10.1175/JCLI-D-11-00446.1, 2012.

Levis, S., Badger, A., Drewniak, B., Nevison, C., and Ren, X.: CLMcrop yields and water requirements: avoided impacts by choosing RCP 4.5 over 8.5, Clim. Change, 146, 501–515, https://doi.org/10.1007/s10584-016-1654-9, 2018.

Li, L., Wang, Y.-P., Yu, Q., Pak, B., Eamus, D., Yan, J., van Gorsel, E., and Baker, I. T.: Improving the responses of the Australian community land surface model (CABLE) to seasonal drought, J. Geophys. Res. Biogeosciences, 117, https://doi.org/10.1029/2012JG002038, 2012.

Li, L., Friedl, M. A., Xin, Q., Gray, J., Pan, Y., and Frolking, S.: Mapping Crop Cycles in China Using MODIS-EVI Time Series, Remote Sens., 6, 2473–2493, https://doi.org/10.3390/rs6032473, 2014.

Li, Y., Guan, K., Gentine, P., Konings, A. G., Meinzer, F. C., Kimball, J. S., Xu, X., Anderegg, W. R. L., McDowell, N. G., Martinez-Vilalta, J., Long, D. G., and Good, S. P.: Estimating Global Ecosystem Isohydry/Anisohydry Using Active and Passive Microwave Satellite Data, J. Geophys. Res. Biogeosciences, 122, 3306–3321, https://doi.org/10.1002/2017JG003958, 2017.

Liang, X., Lettenmaier, D. P., Wood, E. F., and Burges, S. J.: A simple hydrologically based model of land surface water and energy fluxes for general circulation models, J. Geophys. Res. Atmospheres, 99, 14415–14428, https://doi.org/10.1029/94JD00483, 1994.

Lin, Y.-S., Medlyn, B. E., Duursma, R. A., Prentice, I. C., Wang, H., Baig, S., Eamus, D., de Dios, V. R., Mitchell, P., Ellsworth, D. S., de Beeck, M. O., Wallin, G., Uddling, J., Tarvainen, L., Linderson, M.-L., Cernusak, L. A., Nippert, J. B., Ocheltree, T. W., Tissue, D. T., Martin-StPaul, N. K., Rogers, A., Warren, J. M., De Angelis, P., Hikosaka, K., Han, Q., Onoda, Y., Gimeno, T. E., Barton, C. V. M., Bennie, J., Bonal, D., Bosc, A., Löw, M., Macinins-Ng, C., Rey, A., Rowland, L., Setterfield, S. A., Tausz-Posch, S., Zaragoza-Castells, J., Broadmeadow, M. S. J., Drake, J. E., Freeman, M., Ghannoum, O., Hutley, L. B., Kelly, J. W., Kikuzawa, K., Kolari, P., Koyama, K., Limousin, J.-M., Meir, P., Lola da Costa, A. C., Mikkelsen, T. N., Salinas, N., Sun, W., and Wingate, L.: Optimal stomatal behaviour around the world, Nat. Clim. Change, 5, 459–464, https://doi.org/10.1038/nclimate2550, 2015.

Lobell, Bala, G., and Duffy, P. B.: Biogeophysical impacts of cropland management changes on climate, Geophys. Res. Lett., 33, https://doi.org/10.1029/2005GL025492, 2006.

Lobell, Schlenker, W., and Costa-Roberts, J.: Climate Trends and Global Crop Production Since 1980, Science, 333, 616–620, https://doi.org/10.1126/science.1204531, 2011.

Lokupitiya, E., Denning, S., Paustian, K., Baker, I., Schaefer, K., Verma, S., Meyers, T., Bernacchi, C. J., Suyker, A., and Fischer, M.: Incorporation of crop phenology in Simple Biosphere Model (SiBcrop) to improve land-atmosphere carbon exchanges from croplands, Biogeosciences, 6, 969–986, https://doi.org/10.5194/bg-6-969-2009, 2009.

Lombardozzi, D. L., Bonan, G. B., Wieder, W., Grandy, A. S., Morris, C., and Lawrence, D. L.: Cover Crops May Cause Winter Warming in Snow-Covered Regions, Geophys. Res. Lett., 45, 9889–9897, https://doi.org/10.1029/2018GL079000, 2018.

Lombardozzi, D. L., Lu, Y., Lawrence, P. J., Lawrence, D. M., Swenson, S., Oleson, K. W., Wieder, W. R., and Ainsworth, E. A.: Simulating Agriculture in the Community Land Model Version 5, J. Geophys. Res. Biogeosciences, 125, e2019JG005529, https://doi.org/10.1029/2019JG005529, 2020.

Lu, Y., Williams, I. N., Bagley, J. E., Torn, M. S., and Kueppers, L. M.: Representing winter wheat in the Community Land Model (version 4.5), Geosci. Model Dev., 10, 1873–1888, https://doi.org/10.5194/gmd-10-1873-2017, 2017.

Ma, S., Churkina, G., and Trusilova, K.: Investigating the impact of climate change on crop phenological events in Europe with a phenology model, Int. J. Biometeorol., 56, 749–763, https://doi.org/10.1007/s00484-011-0478-6, 2012.

Marletto, V., Ventura, F., Fontana, G., and Tomei, F.: Wheat growth simulation and yield prediction with seasonal forecasts and a numerical model, Agric. For. Meteorol., 147, 71–79, https://doi.org/10.1016/j.agrformet.2007.07.003, 2007.

McDermid, S. S., Mearns, L. O., and Ruane, A. C.: Representing agriculture in Earth System Models: Approaches and priorities for development, J. Adv. Model. Earth Syst., 9, 2230–2265, https://doi.org/10.1002/2016MS000749, 2017.

McDermid, S., Nocco, M., Lawston-Parker, P., Keune, J., Pokhrel, Y., Jain, M., Jägermeyr, J., Brocca, L., Massari, C., Jones, A. D., Vahmani, P., Thiery, W., Yao, Y., Bell, A., Chen, L., Dorigo, W., Hanasaki, N., Jasechko, S., Lo, M.-H., Mahmood, R., Mishra, V., Mueller, N. D., Niyogi, D., Rabin, S. S., Sloat, L., Wada, Y., Zappa, L., Chen, F., Cook, B. I., Kim, H., Lombardozzi, D., Polcher, J., Ryu, D., Santanello, J., Satoh, Y., Seneviratne, S., Singh, D., and Yokohata, T.: Irrigation in the Earth system, Nat. Rev. Earth Environ., 1–19, https://doi.org/10.1038/s43017-023-00438-5, 2023.

McIntosh, P. C., Pook, M. J., Risbey, J. S., Lisson, S. N., and Rebbeck, M.: Seasonal climate forecasts for agriculture: Towards better understanding and value, Field Crops Res., 104, 130–138, https://doi.org/10.1016/j.fcr.2007.03.019, 2007.

Medlyn, B. E., Duursma, R. A., Eamus, D., Ellsworth, D. S., Prentice, I. C., Barton, C. V. M., Crous, K. Y., De Angelis, P., Freeman, M., and Wingate, L.: Reconciling the optimal and empirical approaches to modelling stomatal conductance, Glob. Change Biol., 17, 2134–2144, https://doi.org/10.1111/j.1365-2486.2010.02375.x, 2011.

Meza, F. J., Hansen, J. W., and Osgood, D.: Economic Value of Seasonal Climate Forecasts for Agriculture: Review of Ex-Ante Assessments and Recommendations for Future Research, J. Appl. Meteorol. Climatol., 47, 1269–1286, https://doi.org/10.1175/2007JAMC1540.1, 2008.

Möller, K. and Reents, H.-J.: Effects of various cover crops after peas on nitrate leaching and nitrogen supply to succeeding winter wheat or potato crops, J. Plant Nutr. Soil Sci., 172, 277–287, https://doi.org/10.1002/jpln.200700336, 2009.

Monhart, S., Spirig, C., Bhend, J., Bogner, K., Schär, C., and Liniger, M. A.: Skill of Subseasonal Forecasts in Europe: Effect of Bias Correction and Downscaling Using Surface Observations, J. Geophys. Res. Atmospheres, 123, 7999–8016, https://doi.org/10.1029/2017JD027923, 2018.

Montzka, C., Herbst, M., Weihermüller, L., Verhoef, A., and Vereecken, H.: A global data set of soil hydraulic properties and sub-grid variability of soil water retention and hydraulic conductivity curves, Earth Syst. Sci. Data, 9, 529–543, https://doi.org/10.5194/essd-9-529-2017, 2017.

Morse-McNabb, E., Sheffield, K., Clark, R., Lewis, H., Robson, S., Cherry, D., and Williams, S.: VLUIS, a land use data product for Victoria, Australia, covering 2006 to 2013, Sci. Data, 2, 150070, https://doi.org/10.1038/sdata.2015.70, 2015.

Moureaux, C., Debacq, A., Bodson, B., Heinesch, B., and Aubinet, M.: Annual net ecosystem carbon exchange by a sugar beet crop, Agric. For. Meteorol., 139, 25–39, https://doi.org/10.1016/j.agrformet.2006.05.009, 2006.

Moureaux, C., Debacq, A., Hoyaux, J., Suleau, M., Tourneur, D., Vancutsem, F., Bodson, B., and Aubinet, M.: Carbon balance assessment of a Belgian winter wheat crop (Triticum aestivum L.), Glob. Change Biol., 14, 1353–1366, https://doi.org/10.1111/j.1365-2486.2008.01560.x, 2008.

Müller, C., Elliott, J., Chryssanthacopoulos, J., Deryng, D., Folberth, C., Pugh, T. A. M., and Schmid, E.: Implications of climate mitigation for future agricultural production, Environ. Res. Lett., 10, 125004, https://doi.org/10.1088/1748-9326/10/12/125004, 2015.

Myneni, R., Knyazikhin, Y., and Park, T.: MOD15A2H MODIS/Terra Leaf Area Index/FPAR 8-Day L4 Global 500m SIN Grid V006. NASA EOSDIS Land Processes DAAC., https://doi.org/10.5067/MODIS/MOD15A2H.006, 2015.

NASA/METI/AIST/Japan Spacesystems And U.S./Japan ASTER Science Team: ASTER Global Digital Elevation Model V003, https://doi.org/10.5067/ASTER/ASTGTM.003, 2019.

Naz, B. S., Kurtz, W., Montzka, C., Sharples, W., Goergen, K., Keune, J., Gao, H., Springer, A., Hendricks Franssen, H.-J., and Kollet, S.: Improving soil moisture and runoff simulations at 3 km over Europe using land surface data assimilation, Hydrol. Earth Syst. Sci., 23, 277–301, https://doi.org/10.5194/hess-23-277-2019, 2019.

Naz, B. S., Sharples, W., Ma, Y., Goergen, K., and Kollet, S.: Continental-scale evaluation of a fully distributed coupled land surface and groundwater model, ParFlow-CLM (v3.6.0), over Europe, Geosci. Model Dev., 16, 1617–1639, https://doi.org/10.5194/gmd-16-1617-2023, 2023.

Nemani, R. R., Keeling, C. D., Hashimoto, H., Jolly, W. M., Piper, S. C., Tucker, C. J., Myneni, R. B., and Running, S. W.: Climate-Driven Increases in Global Terrestrial Net Primary Production from 1982 to 1999, Science, 300, 1560–1563, https://doi.org/10.1126/science.1082750, 2003.

Ney, P. and Graf, A.: High-Resolution Vertical Profile Measurements for Carbon Dioxide and Water Vapour Concentrations Within and Above Crop Canopies, Bound.-Layer Meteorol., 166, 449–473, https://doi.org/10.1007/s10546-017-0316-4, 2018.

Niu, G.-Y., Yang, Z.-L., Dickinson, R. E., and Gulden, L. E.: A simple TOPMODEL-based runoff parameterization (SIMTOP) for use in global climate models, J. Geophys. Res. Atmospheres, 110, https://doi.org/10.1029/2005JD006111, 2005.

Niu, G.-Y., Yang, Z.-L., Mitchell, K. E., Chen, F., Ek, M. B., Barlage, M., Kumar, A., Manning, K., Niyogi, D., Rosero, E., Tewari, M., and Xia, Y.: The community Noah land surface model with multiparameterization options (Noah-MP): 1. Model description and evaluation with local-scale measurements, J. Geophys. Res. Atmospheres, 116, https://doi.org/10.1029/2010JD015139, 2011.

NRW (North Rhine-Westphalia) state government: Preliminary data on cereal grain harvest balance in 2020, https://www.land.nrw/pressemitteilung/nordrhein-westfalen-legt-erntebilanz-2020-vor, (last access: 20 June 2022), 2020.

Olesen, J. E., Trnka, M., Kersebaum, K. C., Skjelvåg, A. O., Seguin, B., Peltonen-Sainio, P., Rossi, F., Kozyra, J., and Micale, F.: Impacts and adaptation of European crop production systems to climate change, Eur. J. Agron., 34, 96–112, https://doi.org/10.1016/j.eja.2010.11.003, 2011.

Oleson, K. W., Lawrence, D. M., B, G., Flanner, M. G., Kluzek, E., J, P., Levis, S., Swenson, S. C., Thornton, E., Feddema, J., Heald, C. L., Lamarque, J., Niu, G., Qian, T., Running, S., Sakaguchi, K., Yang, L., Zeng, X., Zeng, X., and Decker, M.: Technical Description of version 4.0 of the Community Land Model (CLM), 2010.

Orth, R., Denissen, J. M. C., Li, W., and Oh, S.: Increasing water limitation of global ecosystems in a changing climate , Copernicus Meetings, https://doi.org/10.5194/egusphere-egu23-1422, 2023.

Osborne, T., Gornall, J. L., Hooker, J., Williams, K., Wiltshire, A., Betts, R. A., and Wheeler, T.: JULES-crop: a parametrisation of crops in the Joint UK Land Environment Simulator, Geosci. Model Dev., 8, 1139–1155, 2015.

Ozdogan, M., Rodell, M., Beaudoing, H. K., and Toll, D. L.: Simulating the Effects of Irrigation over the United States in a Land Surface Model Based on Satellite-Derived Agricultural Data, J. Hydrometeorol., 11, 171–184, https://doi.org/10.1175/2009JHM1116.1, 2010.

Palosuo, T., Kersebaum, K. C., Angulo, C., Hlavinka, P., Moriondo, M., Olesen, J. E., Patil, R. H., Ruget, F., Rumbaur, C., Takáč, J., Trnka, M., Bindi, M., Çaldağ, B., Ewert, F., Ferrise, R., Mirschel, W., Şaylan, L., Šiška, B., and Rötter, R.: Simulation of winter wheat yield and its variability in different climates of Europe: A comparison of eight crop growth models, Eur. J. Agron., 35, 103–114, https://doi.org/10.1016/j.eja.2011.05.001, 2011.

Papagiannopoulou, C., Miralles, D. G., Decubber, S., Demuzere, M., Verhoest, N. E. C., Dorigo, W. A., and Waegeman, W.: A non-linear Granger-causality framework to investigate climate–vegetation dynamics, Geosci. Model Dev., 10, 1945–1960, https://doi.org/10.5194/gmd-10-1945-2017, 2017.

Parton, K. A., Crean, J., and Hayman, P.: The value of seasonal climate forecasts for Australian agriculture, Agric. Syst., 174, 1–10, https://doi.org/10.1016/j.agsy.2019.04.005, 2019.

Peel, M. C., Finlayson, B. L., and Mcmahin, T. A.: Updated world map of the Köppen-Geiger climate classification, Hydrol. Earth Syst. Sci. Discuss. Eur. Geosci. Union, 4, 439–473, 2007.

Pelletier, J. D., P. D. Broxton, P. Hazenberg, X. Zeng, P. A. Troch, G. Y. Niu, Z. Williams, M. A. Brunke, and D. Gochis: A gridded global data set of soil, intact regolith, and sedimentary deposit thicknesses for regional and global land surface modeling. J. Adv. Mod. Earth Sys., 8:41-65, https://doi.org/10.1002/2015MS000526, 2016.

Plaza-Bonilla, D., Nolot, J.-M., Raffaillac, D., and Justes, E.: Cover crops mitigate nitrate leaching in cropping systems including grain legumes: Field evidence and model simulations, Agric. Ecosyst. Environ., 212, 1–12, https://doi.org/10.1016/j.agee.2015.06.014, 2015.

Pokhrel, Y., Hanasaki, N., Koirala, S., Cho, J., Yeh, P. J.-F., Kim, H., Kanae, S., and Oki, T.: Incorporating Anthropogenic Water Regulation Modules into a Land Surface Model, J. Hydrometeorol., 13, 255–269, https://doi.org/10.1175/JHM-D-11-013.1, 2012.

Pokhrel, Y. N., Hanasaki, N., Wada, Y., and Kim, H.: Recent progresses in incorporating human land–water management into global land surface models toward their integration into Earth system models, WIREs Water, 3, 548–574, https://doi.org/10.1002/wat2.1150, 2016.

Pongratz, J., Dolman, H., Don, A., Erb, K. H., Fuchs, R., Herold, M., Jones, C., Kuemmerle, T., Luyssaert, S., Meyfroidt, P. & Naudts, K.: Models meet data: Challenges and opportunities in implementing land management in Earth system models. *Global change biology*, *24*(4), 1470-1487, https://doi.org/10.1111/gcb.13988, 2018.

Post, H., Vrugt, J. A., Fox, A., Vereecken, H., and Hendricks-Franssen, H.-J.: Estimation of Community Land Model parameters for an improved assessment of net carbon fluxes at European sites, J. Geophys. Res. Biogeosciences, 122, 661–689, https://doi.org/10.1002/2015JG003297, 2017.

Potgieter, A. B., Schepen, A., Brider, J., and Hammer, G. L.: Lead time and skill of Australian wheat yield forecasts based on ENSO-analogue or GCM-derived seasonal climate forecasts – A comparative analysis, Agr. Forest Meteorol., 324, 109116, https://doi.org/10.1016/j.agrformet.2022.109116, 2022.

Preimesberger, W., Scanlon, T., Su, C.-H., Gruber, A., and Dorigo, W.: Homogenization of Structural Breaks in the Global ESA CCI Soil Moisture Multisatellite Climate Data Record, IEEE Trans. Geosci. Remote Sens., 59, 2845–2862, https://doi.org/10.1109/TGRS.2020.3012896, 2021.

Prescher, A.-K., Grünwald, T., and Bernhofer, C.: Land use regulates carbon budgets in eastern Germany: from NEE to NBP, Agric. For. Meteorol., 150, 1016–1025, https://doi.org/10.1016/j.agrformet.2010.03.008, 2010.

Quintarelli, V., Radicetti, E., Allevato, E., Stazi, S. R., Haider, G., Abideen, Z., Bibi, S., Jamal, A., and Mancinelli, R.: Cover Crops for Sustainable Cropping Systems: A Review, Agriculture, 12, 2076, https://doi.org/10.3390/agriculture12122076, 2022.

Reichenau, T. G., Korres, W., Schmidt, M., Graf, A., Welp, G., Meyer, N., Stadler, A., Brogi, C., and Schneider, K.: A comprehensive dataset of vegetation states, fluxes of matter and energy, weather, agricultural management, and soil properties from intensively monitored crop sites in Western Germany, Earth Syst. Sci. Data Discuss., 1–59, https://doi.org/10.5194/essd-2019-193, 2020.

Reinermann, S., Gessner, U., Asam, S., Kuenzer, C., and Dech, S.: The Effect of Droughts on Vegetation Condition in Germany: An Analysis Based on Two Decades of Satellite Earth Observation Time Series and Crop Yield Statistics, Remote Sens., 11, 1783, https://doi.org/10.3390/rs11151783, 2019.

Rosenzweig, C., Elliott, J., Deryng, D., Ruane, A. C., Müller, C., Arneth, A., Boote, K. J., Folberth, C., Glotter, M., Khabarov, N., Neumann, K., Piontek, F., Pugh, T. A. M., Schmid, E., Stehfest, E., Yang, H., and Jones, J. W.: Assessing agricultural risks of climate change in the 21st century in a global gridded crop model intercomparison, Proc. Natl. Acad. Sci., 111, 3268–3273, https://doi.org/10.1073/pnas.1222463110, 2014.

Running, S., Mu, Q., and Zhao, M.: MOD16A2 MODIS/Terra Net Evapotranspiration 8-Day L4 Global 500 m SIN Grid V006, USGS, https://doi.org/10.5067/MODIS/MOD16A2.006, 2017.

Ryel, R. J., Caldwell, M. M., Yoder, C. K., Or, D., and Leffler, A. J.: Hydraulic Redistribution in a Stand of Artemisia tridentata: Evaluation of Benefits to Transpiration Assessed with a Simulation Model, Oecologia, 130, 173–184, 2002.

Sabot, M. E. B., De Kauwe, M. G., Pitman, A. J., Medlyn, B. E., Ellsworth, D. S., Martin-StPaul, N. K., Wu, J., Choat, B., Limousin, J.-M., Mitchell, P. J., Rogers, A., and Serbin, S. P.: One Stomatal Model to Rule

Them All? Toward Improved Representation of Carbon and Water Exchange in Global Models, J. Adv. Model. Earth Syst., 14, e2021MS002761, https://doi.org/10.1029/2021MS002761, 2022.

Sacks, W. J., Cook, B. I., Buenning, N., Levis, S., and Helkowski, J. H.: Effects of global irrigation on the near-surface climate, Clim. Dyn., 33, 159–175, https://doi.org/10.1007/s00382-008-0445-z, 2009.

Sainju, U. M., Whitehead, W. F., and Singh, B. P.: Cover crops and nitrogen fertilization effects on soil aggregation and carbon and nitrogen pools, Can. J. Soil Sci., 83, 155–165, https://doi.org/10.4141/S02-056, 2003.

Samaniego, L., Thober, S., Kumar, R., Wanders, N., Rakovec, O., Pan, M., Zink, M., Sheffield, J., Wood, E. F., and Marx, A.: Anthropogenic warming exacerbates European soil moisture droughts, Nat. Clim. Change, 8, 421–426, https://doi.org/10.1038/s41558-018-0138-5, 2018.

Sánchez-Sastre, L. F., Martín-Ramos, P., Navas-Gracia, L. M., Hernández-Navarro, S., and Martín-Gil, J.: Impact of Climatic Variables on Carbon Content in Sugar Beet Root, Agronomy, 8, 147, https://doi.org/10.3390/agronomy8080147, 2018.

Schrön, M., Köhli, M., Scheiffele, L., Iwema, J., Bogena, H. R., Lv, L., Martini, E., Baroni, G., Rosolem, R., Weimar, J., Mai, J., Cuntz, M., Rebmann, C., Oswald, S. E., Dietrich, P., Schmidt, U., and Zacharias, S.: Improving calibration and validation of cosmic-ray neutron sensors in the light of spatial sensitivity, Hydrol. Earth Syst. Sci., 21, 5009–5030, https://doi.org/10.5194/hess-21-5009-2017, 2017.

Semenov, M. A. and Doblas-Reyes, F. J.: Utility of dynamical seasonal forecasts in predicting crop yield, Clim. Res., 34, 71–81, https://doi.org/10.3354/cr034071, 2007.

Semenov, M. A. and Shewry, P. R.: Modelling predicts that heat stress, not drought, will increase vulnerability of wheat in Europe, Sci. Rep., 1, 1–5, https://doi.org/10.1038/srep00066, 2011.

Shah, H. L., Zhou, T., Huang, M., and Mishra, V.: Strong Influence of Irrigation on Water Budget and Land Surface Temperature in Indian Subcontinental River Basins, J. Geophys. Res. Atmospheres, 124, 1449–1462, https://doi.org/10.1029/2018JD029132, 2019.

Sharma, S. D., Kumar, P., Bhardwaj, S. K., and Chandel, A.: Agronomic performance, nutrient cycling and microbial biomass in soil as affected by pomegranate based multiple crop sequencing, Sci. Hortic., 197, 504–515, https://doi.org/10.1016/j.scienta.2015.10.013, 2015.

Sheng, M., Liu, J., Zhu, A.-X., Rossiter, D. G., Zhu, L., and Peng, G.: Evaluation of CLM-Crop for maize growth simulation over Northeast China, Ecol. Model., 377, 26–34, https://doi.org/10.1016/j.ecolmodel.2018.03.005, 2018.

Smit, B., Janssens, B., Haagsma, W., Hennen, W., Adrados Jose, L., and Kathage, J.: Adoption of cover crops for climate change mitigation in the EU, Publications Office of the European Union, 2019.

Soltani, S. S., Fahs, M., Bitar, A. A., and Ataie-Ashtiani, B.: Improvement of soil moisture and groundwater level estimations using a scale-consistent river parameterization for the coupled ParFlow-CLM hydrological model: A case study of the Upper Rhine Basin, J. Hydrol., 610, 127991, https://doi.org/10.1016/j.jhydrol.2022.127991, 2022.

Sperry, J. S. and Love, D. M.: What plant hydraulics can tell us about responses to climate-change droughts, New Phytol., 207, 14–27, https://doi.org/10.1111/nph.13354, 2015.

Sperry, J. S., Adler, F. R., Campbell, G. S., and Comstock, J. P.: Limitation of plant water use by rhizosphere and xylem conductance: results from a model, Plant Cell Environ., 21, 347–359, https://doi.org/10.1046/j.1365-3040.1998.00287.x, 1998.

Sprintsin, M., Karnieli, A., Berliner, P., Rotenberg, E., Yakir, D., Cohen, S., and Rotenberg, P.: Evaluating the performance of the MODIS Leaf Area Index (LAI) product over a Mediterranean dryland planted forest, Int. J. Remote Sens., 30, https://doi.org/10.1080/01431160903032885, 2009.

Statista: Yield statistics of winter wheat for Germany from 2006 to 2019, available at: https://de.statista.com/statistik/daten/studie/262303/umfrage/erntemenge-von-weizen-in-deutschland/, (last access: 1 June 2020).

Stehfest, E., Heistermann, M., Priess, J. A., Ojima, D. S., and Alcamo, J.: Simulation of global crop production with the ecosystem model DayCent, Ecol. Model., 209, 203–219, https://doi.org/10.1016/j.ecolmodel.2007.06.028, 2007.

Strebel, L., Bogena, H. R., Vereecken, H., and Hendricks Franssen, H.-J.: Coupling the Community Land Model version 5.0 to the parallel data assimilation framework PDAF: description and applications, Geosci. Model Dev., 15, 395–411, https://doi.org/10.5194/gmd-15-395-2022, 2022.

Streck, N. A., Weiss, A., and Baenziger, P. S.: A Generalized Vernalization Response Function for Winter Wheat, Agron. J., 95, 155–159, https://doi.org/10.2134/agronj2003.1550, 2003.

Sulis, M., Langensiepen, M., Shrestha, P., Schickling, A., Simmer, C., and Kollet, S. J.: Evaluating the Influence of Plant-Specific Physiological Parameterizations on the Partitioning of Land Surface Energy Fluxes, J. Hydrometeorol., 16, 517–533, https://doi.org/10.1175/JHM-D-14-0153.1, 2015.

Sulis, M., Couvreur, V., Keune, J., Cai, G., Trebs, I., Junk, J., Shrestha, P., Simmer, C., Kollet, S. J., Vereecken, H., and Vanderborght, J.: Incorporating a root water uptake model based on the hydraulic architecture approach in terrestrial systems simulations, Agric. For. Meteorol., 269–270, 28–45, https://doi.org/10.1016/j.agrformet.2019.01.034, 2019.

Tai, A. P. K., Martin, M. V., and Heald, C. L.: Threat to future global food security from climate change and ozone air pollution, Nat. Clim. Change, 4, 817–821, https://doi.org/10.1038/nclimate2317, 2014.

Tang, J., Riley, W. J., and Niu, J.: Incorporating root hydraulic redistribution in CLM4.5: Effects on predicted site and global evapotranspiration, soil moisture, and water storage, J. Adv. Model. Earth Syst., 7, 1828–1848, https://doi.org/10.1002/2015MS000484, 2015.

Taylor, R. G., Scanlon, B., Döll, P., Rodell, M., van Beek, R., Wada, Y., Longuevergne, L., Leblanc, M., Famiglietti, J. S., Edmunds, M., Konikow, L., Green, T. R., Chen, J., Taniguchi, M., Bierkens, M. F. P., MacDonald, A., Fan, Y., Maxwell, R. M., Yechieli, Y., Gurdak, J. J., Allen, D. M., Shamsudduha, M., Hiscock, K., Yeh, P. J.-F., Holman, I., and Treidel, H.: Ground water and climate change, Nat. Clim. Change, 3, 322–329, https://doi.org/10.1038/nclimate1744, 2013.

TERENO – TERrestrial ENvironment Observatories data portal: http://www.tereno.net/ddp/ (last access: 31 December 2020), 2020.

Thaler, S., Eitzinger, J., Trnka, M., and Dubrovsky, M.: Impacts of climate change and alternative adaptation options on winter wheat yield and water productivity in a dry climate in Central Europe, J. Agric. Sci., 150, 537–555, https://doi.org/10.1017/S0021859612000093, 2012.

Thornton, P. E. and Rosenbloom, N. A.: Ecosystem model spin-up: Estimating steady state conditions in a coupled terrestrial carbon and nitrogen cycle model, Ecol. Model., 189, 25–48, https://doi.org/10.1016/j.ecolmodel.2005.04.008, 2005.

Thornton, P. E. and Running, S. W.: An improved algorithm for estimating incident daily solar radiation from measurements of temperature, humidity, and precipitation, Agric. For. Meteorol., 93, 211–228, https://doi.org/10.1016/S0168-1923(98)00126-9, 1999.

Thornton, P. E., Hasenauer, H., and White, M. A.: Simultaneous estimation of daily solar radiation and humidity from observed temperature and precipitation: an application over complex terrain in Austria, Agric. For. Meteorol., 104, 255–271, https://doi.org/10.1016/S0168-1923(00)00170-2, 2000.

Tian, W., Li, X., Cheng, G.-D., Wang, X.-S., and Hu, B. X.: Coupling a groundwater model with a land surface model to improve water and energy cycle simulation, Hydrol. Earth Syst. Sci., 16, 4707–4723, https://doi.org/10.5194/hess-16-4707-2012, 2012.

Tiemann, L. K., Grandy, A. S., Atkinson, E. E., Marin-Spiotta, E., and McDaniel, M. D.: Crop rotational diversity enhances belowground communities and functions in an agroecosystem, Ecol. Lett., 18, 761–771, https://doi.org/10.1111/ele.12453, 2015.

Troccoli, A.: Seasonal climate forecasting, Meteorol. Appl., 17, 251–268, https://doi.org/10.1002/met.184, 2010.

Trugman, A. T., Medvigy, D., Mankin, J. S., and Anderegg, W. R. L.: Soil Moisture Stress as a Major Driver of Carbon Cycle Uncertainty, Geophys. Res. Lett., 45, 6495–6503, https://doi.org/10.1029/2018GL078131, 2018.

Twine, T. E. and Kucharik, C. J.: Climate impacts on net primary productivity trends in natural and managed ecosystems of the central and eastern United States, Agric. For. Meteorol., 149, 2143–2161, https://doi.org/10.1016/j.agrformet.2009.05.012, 2009.

Ukkola, A. M., Kauwe, M. G. D., Pitman, A. J., Best, M. J., Abramowitz, G., Haverd, V., Decker, M., and Haughton, N.: Land surface models systematically overestimate the intensity, duration and magnitude of seasonal-scale evaporative droughts, Environ. Res. Lett., 11, 104012, https://doi.org/10.1088/1748-9326/11/10/104012, 2016.

Urban, D., Roberts, M. J., Schlenker, W., and Lobell, D. B.: Projected temperature changes indicate significant increase in interannual variability of U.S. maize yields, Clim. Change, 112, 525–533, https://doi.org/10.1007/s10584-012-0428-2, 2012.

Van den Hoof, C., Hanert, E., and Vidale, P. L.: Simulating dynamic crop growth with an adapted land surface model – JULES-SUCROS: Model development and validation, Agric. For. Meteorol., 151, 137–153, https://doi.org/10.1016/j.agrformet.2010.09.011, 2011.

Van der Velde, R., Colliander, A., Pezij, M., Benninga, H.-J. F., Bindlish, R., Chan, S. K., Jackson, T. J., Hendriks, D. M. D., Augustijn, D. C. M., Su, Z.: Validation of SMAP L2 passive-only soil moisture products using

upscaled in situ measurements collected in Twente, the Netherlands. *Hydrology and Earth System Sciences*, 25, 473–495. https://doi.org/10.5194/hess-25-473-2021, 2021.

Vazifedoust, M., Dam, J. C. van, Bastiaanssen, W. G. M., and Feddes, R. A.: Assimilation of satellite data into agrohydrological models to improve crop yield forecasts, Int. J. Remote Sens., 30, 2523–2545, https://doi.org/10.1080/01431160802552769, 2009.

Verhoef, A. and Egea, G.: Modeling plant transpiration under limited soil water: Comparison of different plant and soil hydraulic parameterizations and preliminary implications for their use in land surface models, Agric. For. Meteorol., 191, 22–32, https://doi.org/10.1016/j.agrformet.2014.02.009, 2014.

Vermeulen, S. J., Campbell, B. M., and Ingram, J. S. I.: Climate Change and Food Systems, Annu. Rev. Environ. Resour., 37, 195–222, https://doi.org/10.1146/annurev-environ-020411-130608, 2012.

Vico, G., Hurry, V., and Weih, M.: Snowed in for survival: Quantifying the risk of winter damage to overwintering field crops in northern temperate latitudes, Agric. For. Meteorol., 197, 65–75, https://doi.org/10.1016/j.agrformet.2014.06.003, 2014.

Victorian Government Data Directory, Agriculture Victoria Research Division in the Department of Economic Development, Jobs, Transport, and Resources, Spatial Sciences Group: Victorian Land Use Information System 2016, Victorian Government Data Directory [data set], https://doi.org/10.4226/92/590abbe6ea3f1, 2018.

Viovy, N.: CRUNCEP Version 7 - Atmospheric Forcing Data for the Community Land Model, https://doi.org/10.5065/PZ8F-F017, 2018.

Wada, Y., van Beek, L. P. H., van Kempen, C. M., Reckman, J. W. T. M., Vasak, S., and Bierkens, M. F. P.: Global depletion of groundwater resources, Geophys. Res. Lett., 37, https://doi.org/10.1029/2010GL044571, 2010.

Wada, Y., van Beek, L. P. H., and Bierkens, M. F. P.: Nonsustainable groundwater sustaining irrigation: A global assessment, Water Resour. Res., 48, https://doi.org/10.1029/2011WR010562, 2012.

Wada, Y., Wisser, D., Eisner, S., Flörke, M., Gerten, D., Haddeland, I., Hanasaki, N., Masaki, Y., Portmann, F. T., Stacke, T., Tessler, Z., and Schewe, J.: Multimodel projections and uncertainties of irrigation water demand under climate change, Geophys. Res. Lett., 40, 4626–4632, https://doi.org/10.1002/grl.50686, 2013.

Wang, B., Feng, P., Waters, C., Cleverly, J., Liu, D. L., and Yu, Q.: Quantifying the impacts of pre-occurred ENSO signals on wheat yield variation using machine learning in Australia, Agr. Forest Meteorol., 291, 108043, https://doi.org/10.1016/j.agrformet.2020.108043, 2020.

Wang, Q., Tenhunen, J., Dinh, N., Reichstein, M., Otieno, D., Granier, A., and Pilegaard, K.: Evaluation of seasonal variation of MODIS derived leaf area index at two European deciduous broadleaf forest sites, Remote Sens. Environ., 96, 475–484, https://doi.org/10.1016/j.rse.2005.04.003, 2005.

Wang, Q. J., Shao, Y., Song, Y., Schepen, A., Robertson, D. E., Ryu, D., and Pappenberger, F.: An evaluation of ECMWF SEAS5 seasonal climate forecasts for Australia using a new forecast calibration algorithm, Environ. Model. Softw., 122, 104550, https://doi.org/10.1016/j.envsoft.2019.104550, 2019.

Webler, G., Roberti, D. R., Cuadra, S. V., Moreira, V. S., and Costa, M. H.: Evaluation of a Dynamic Agroecosystem Model (Agro-IBIS) for Soybean in Southern Brazil, Earth Interact., 16, 1–15, https://doi.org/10.1175/2012EI000452.1, 2012.

Weihermüller, L., Lehmann, P., Herbst, M., Rahmati, M., Verhoef, A., Or, D., Jacques, D. and Vereecken, H.: Choice of pedotransfer functions matters when simulating soil water balance fluxes. Journal of Advances in Modeling Earth Systems, 13(3), e2020MS002404, https://doi.org/10.1029/2020MS002404, 2021.

White, E. M. and Wilson, F. E. A.: Responses of Grain Yield, Biomass and Harvest Index and Their Rates of Genetic Progress to Nitrogen Availability in Ten Winter Wheat Varieties, Ir. J. Agric. Food Res., 45, 85–101, 2006.

Whitmore, A. P. and Groot, J. J. R.: The decomposition of sugar beet residues: mineralization versus immobilization in contrasting soil types, Plant Soil, 192, 237–247, https://doi.org/10.1023/A:1004288828793, 1997.

Williams, M., Rastetter, E. B., Fernandes, D. N., Goulden, M. L., Wofsy, S. C., Shaver, G. R., Melillo, J. M., Munger, J. W., Fan, S. M., and Nadelhoffer, K. J.: Modelling the soil-plant-atmosphere continuum in a Quercus-Acer stand at Harvard forest: The regulation of stomatal conductance by light, nitrogen and soil/plant hydraulic properties, Plant Cell Environ., 19, 911–927, 1996.

de Wit, A. J. W. and van Diepen, C. A.: Crop model data assimilation with the Ensemble Kalman filter for improving regional crop yield forecasts, Agric. For. Meteorol., 146, 38–56, https://doi.org/10.1016/j.agrformet.2007.05.004, 2007.

Wutzler, T., Lucas-Moffat, A., Migliavacca, M., Knauer, J., Sickel, K., Šigut, L., Menzer, O., and Reichstein, M.: Basic and extensible post-processing of eddy covariance flux data with REddyProc, Biogeosciences, 15, 5015–5030, https://doi.org/10.5194/bg-15-5015-2018, 2018.

Xia, Q., Liu, P., Fan, Y., Cheng, L., An, R., Xie, K., and Zhou, L.: Representing Irrigation Processes in the Land Surface-Hydrological Model and a Case Study in the Yangtze River Basin, China, J. Adv. Model. Earth Syst., 14, e2021MS002653, https://doi.org/10.1029/2021MS002653, 2022.

Xu, H., Twine, T. E., and Girvetz, E.: Climate Change and Maize Yield in Iowa, PLOS ONE, 11, e0156083, https://doi.org/10.1371/journal.pone.0156083, 2016.

Yan, B. and Dickinson, R. E.: Modeling hydraulic redistribution and ecosystem response to droughts over the Amazon basin using Community Land Model 4.0 (CLM4), J. Geophys. Res. Biogeosciences, 119, 2130–2143, https://doi.org/10.1002/2014JG002694, 2014.

Yassin, F., Razavi, S., Elshamy, M., Davison, B., Sapriza-Azuri, G., and Wheater, H.: Representation and improved parameterization of reservoir operation in hydrological and land-surface models, Hydrol. Earth Syst. Sci., 23, 3735–3764, https://doi.org/10.5194/hess-23-3735-2019, 2019.

Zacharias, S., Bogena, H., Samaniego, L., Mauder, M., Fuß, R., Pütz, T., Frenzel, M., Schwank, M., Baessler, C., Butterbach-Bahl, K., Bens, O., Borg, E., Brauer, A., Dietrich, P., Hajnsek, I., Helle, G., Kiese, R., Kunstmann, H., Klotz, S., Munch, J. C., Papen, H., Priesack, E., Schmid, H. P., Steinbrecher, R.,

Rosenbaum, U., Teutsch, G., and Vereecken, H.: A Network of Terrestrial Environmental Observatories in Germany, Vadose Zone J., 10, 955–973, https://doi.org/10.2136/vzj2010.0139, 2011.

Zhao, H., Montzka, C., Baatz, R., Vereecken, H., and Franssen, H.-J. H.: The Importance of Subsurface Processes in Land Surface Modeling over a Temperate Region: An Analysis with SMAP, Cosmic Ray Neutron Sensing and Triple Collocation Analysis, Remote Sens., 13, 3068, https://doi.org/10.3390/rs13163068, 2021.

Zheng, H., Wang, Y., Zhao, J., Shi, X., Ma, Z., and Fan, M.: Tuber formation as influenced by the C : N ratio in potato plants, J. Plant Nutr. Soil Sci., 181, 686–693, https://doi.org/10.1002/jpln.201700571, 2018.

Zheng, Z. and Wang, G.: Modeling the dynamic root water uptake and its hydrological impact at the Reserva Jaru site in Amazonia, J. Geophys. Res. Biogeosciences, 112, https://doi.org/10.1029/2007JG000413, 2007.

Band / Volume 629
Structure and properties of electrochemical interfaces from first principles simulations
R. Tesch (2024), xvi, 161 pp
ISBN: 978-3-95806-753-0

Band / Volume 630
Elucidation of Barocaloric Effect in Spin Crossover Compounds
H. Shahed (2024), x, 261 pp
ISBN: 978-3-95806-758-5

Band / Volume 631
Computational Investigation of Solvation Phenomena at Metal-Electrolyte Interfaces
O. Cheong (2024), xvii, 142 pp
ISBN: 978-3-95806-759-2

Band / Volume 632
Senkung zukünftiger Stickoxid- und Partikelemissionen in Nordrhein-Westfalen durch den Einsatz alternativer Energieträger und Antriebe
J. L. Breuer (2024), vii, 339 pp
ISBN: 978-3-95806-760-8

Band / Volume 633
Development of Model-Based Correction Methods for Temperature-Dependent Electromagnetic Induction (EMI) Measurement Errors in Soil Conductivity Estimations
T. M. Tchantcho Amin (2024), xx, 100 pp
ISBN: 978-3-95806-761-5

Band / Volume 634
Investigation and implementation of improved and degradation-tolerant fuel electrodes for solid oxide cells
A. Schwiers (2024), VI, 163, XIII pp
ISBN: 978-3-95806-762-2

Band / Volume 635
In Situ Time Calibration for Stationary Multichannel GPR Monitoring Systems
L. Steinbeck (2024), xvi, 98, xxxi pp
ISBN: 978-3-95806-767-7

Schriften des Forschungszentrums Jülich
Reihe Energie & Umwelt / Energy & Environment

Band / Volume 636
Erneuerbares Methanol als Ausgangsstoff für die Bereitstellung von flüssigen Kraftstoffen für den Transportsektor
F. Schorn (2024), VI, 275 pp
ISBN: 978-3-95806-769-1

Band / Volume 637
Investigation of Lower Boundary Conditions of Brominated Very Short-lived Species (VSLS)
S. Zheng (2024), 2, iii, 160 pp
ISBN: 978-3-95806-770-7

Band / Volume 638
Modellgestützte Analyse zukünftigen Mobilitätsverhaltens
J. P. Reul (2024), XVI, 291 pp
ISBN: 978-3-95806-771-4

Band / Volume 639
Insights into Mechanisms of Secondary Organic Aerosol Formation: Approaching Atmospherically Relevant Conditions in an Atmospheric Reaction Chamber
Y. Baker (2024), XVII, 122 pp
ISBN: 978-3-95806-776-9

Band / Volume 640
Advancing the representation of agricultural systems in Land Surface Models: systematic model evaluations and technical model developments
T. S. Boas (2024), xxi, 145 pp
ISBN: 978-3-95806-777-6

Energie & Umwelt / Energy & Environment
Band / Volume 640
ISBN 978-3-95806-777-6

Mitglied der Helmholtz-Gemeinschaft

JÜLICH
Forschungszentrum